UNIVERSIDADE FEDERAL DO ESPÍRITO SANTO

CENTRO TECNOLÓGICO

PROGRAMA DE PÓS-GRADUAÇÃO EM ENGENHARIA AMBIENTAL

ELSON SILVA GALVÃO

CHEMICAL CHARACTERIZATION OF PARTICLES IN IRON-RICH ATMOSPHERE OF URBAN AND INDUSTRIALIZED REGIONS

CARACTERIZAÇÃO QUÍMICA DO MATERIAL PARTICULADO EM REGIÕES URBANAS E INDUSTRIALIZADAS COM ATMOSFERA RICA EM FERRO

VITÓRIA

2018

ELSON SILVA GALVÃO

CHEMICAL CHARACTERIZATION OF PARTICLES IN IRON-RICH ATMOSPHERE OF URBAN AND INDUSTRIALIZED REGIONS

Thesis submitted to Programa de Pós-Graduação em Engenharia Ambiental of the Centro Tecnológico da Universidade Federal do Espírito Santo, for the degree of Doctor in Environmental Engineering.

Supervisors: Prof. Jane Meri Santos, PhD.

Co-supervisors: Prof. Ana Teresa Lima, PhD, and Prof. Richard M. Stuetz, PhD.

VITÓRIA

2018

Chemical Characterization of particles in iron-rich atmosphere of urban and industrialized regions

Elson Silva Galvão

Banca Examinadora:

_____
Prof.ª Dr.ª Jane Méri Santos
Orientadora - PPGEA/CT/UFES

_____
Prof.ª Drª Ana Teresa Lima
Coorientadora - DEA/CT/UFES

_____
Prof.ª Drª. Taciana de Almeida Albuquerque
Examinadora Interna – PPGEA/UFES

_____
Prof. Dr. Davidson Martins Moreira
Examinador Interno – PPGEA/CT/UFES

_____
Profª. Drª. Maria de Fátima Andrade
Examinadora Externa DCA/IAG/USP

_____
Prof. Dr. Jorge Alberto Martins
Examinador Externo – DF/UFTPR

Diogo Costa Buarque
Coordenador do Programa de Pós-Graduação em Engenharia Ambiental
UNIVERSIDADE FEDERAL DO ESPÍRITO SANTO

Vitória-ES, 30 de agosto de 2018.

AGRADECIMENTOS

Agradeço grandiosamente à Deus por todas as bênçãos concedidas.

Agradeço imensamente à minha mãe, Dona Rosalina, por todo o carinho, atenção, amor e educação que me destes. Uma criação que formou não somente um homem bom, mas um homem justo, moralmente e eticamente, na qual jamais se acovardou de suas obrigações e deveres, ou se escorou nos esforços de outros.

Agradeço aos meus irmãos Wilson, Débora e Samires pelo apoio, torcida e conselhos que auxiliaram no meu sucesso.

Agradeço a Rita por toda a paciência, carinho e dedicação em suportar minhas reclamações e me apoiar nessa jornada.

Aos bons professores que participaram dessa construção em minha vida acadêmica, um obrigado. Agradeço a minha orientadora Jane pela orientação e oportunidade. Agradeço ao professor Richard Stuetz pelas contribuições e co-orientação nos trabalhos. Em especial, agradeço à professora Ana Lima pelas discussões, ideias e principalmente pela amizade construída. Assim como ao professor Marcos Tadeu pelos ensinamentos, colaboração e apoio nos três dias e noites consecutivos de trabalho no Laboratório Nacional de Luz Síncrotron.

Agradeço ao Laboratório Nacional de Luz Síncrotron (LNLS, Campinas) pela oportunidade nos cedendo tempo de máquina e apoio técnico.

Agradecimento à organização não-governamental Juntos SOS ES Ambiental por disponibilizar a verba parlamentar PT RES 119857 (fonte 100), que financiou parte das análises de carbono elementar e orgânico desse estudo.

Agradecimento a CAPES e FAPES pelo apoio financeiro.

ABSTRACT

Epidemiological studies have shown the association of airborne particulate matter (PM) size and chemical composition with health problems affecting the cardiorespiratory and central nervous systems. Therefore, PM source identification is an important step in air quality management programs. Receptor models are frequently used for PM source apportionment studies to identify the contribution of local sources. Despite the benefits of using receptor models for air quality management, limitations such as collinearity effects in which sources have similar chemical profiles restrict their application or compromise the accurate separation of sources. For highly correlated sources, the identification of specific markers is still the best way for more accurate source apportionment. There are several works using different analytical techniques in PM chemical and physical characterization to supply information for source apportionment models. The choice among available techniques depends on: particles physical properties, sampling and measuring time, access to facilities and the costs associated to equipment acquisition, among other considerations. Despite the numerous analytical techniques described in the literature for PM characterization, laboratories are normally limited to in-house available techniques, which raises the question if a given technique is suitable for the purpose of a specific experimental work. In this work, the state of art on available technologies for PM characterization is stablished and a guide to choose the most appropriate technique(s) for a specific study is proposed. A new approach is also proposed to identify the most appropriated sources associated to the factors revealed by the Positive Matrix Factorization modelling by characterizing inorganic and organic chemical species and using pollutant roses. PM samples were collected in a coastal, urban/industrialized region in Brazil and analyzed by EDXRF, TD-GC-MS and TOC for the characterization of metals, PAHs, EC and OC. This region presents an atypical iron-rich atmosphere due to the presence of pelletizing and steelmaking industries. The proposed methodology revealed that consolidated markers for vehicular: elemental carbon (EC) and organic carbon (OC), sea salt: chloride (Cl) and sodium (Na), and industrial: iron (Fe) sources, were also associated to other sources. Cl, a typical marker of sea salt, was also attributed to industrial sintering activities. Some PMF factors showed high OC loadings, a typical marker for both vehicular exhaust and coal burning. The definition of the most appropriate source for those factors was only possible due to the assessment of the pollutant roses. Potassium (K), a usual marker of biomass burning, was predominantly associated to winds from an industrial park placed at Northeast of the sampling sites and, therefore, most likely associated to sintering emissions. Some PAHs such as naphtalene, chrysene, phenanthrene, fluorine and acenaphtylene were key markers allowing the apportionment of sources with similar inorganic chemical profiles, among them the industrial sintering, pelletizing and biomass burning.

Results showed that combining both organic and inorganic chemical markers with pollutant roses for identification of the directionality of predominant sources improved the interpretation of PMF factor numbers in source apportionment studies.

In addition, the Resonant Synchrotron X-ray Diffraction (RSr-XRD) technique was conducted at the *Laboratório Nacional de Luz Synchrotron* (LNLS) in Campinas, Brazil, to analyze settleable particles (SP), total suspended particulate matter (TSP), PM_{10}, and $PM_{2.5}$ samples showing high levels of iron-based crystalline phases. In comparison to the use of chemical elemental species, the identification of the crystalline phases provided an enhanced approach to classify specific iron-based source markers. α-Fe_2O_3, metallic Fe, FeS_2 and $K_2Fe_2O_4$ are associated, respectively, to iron ore, pelletizing, and sintering; blast furnaces and steelmaking; coal deposits; and sintering emissions. The attribution of crystal rather than elemental composition in the identification of sources improved the accuracy of source apportionment studies. Compounds such as $K_2Fe_2O_4$ and NH_4ClO_4 are specifically linked to the sintering process, mainly formed during raw materials furnace roasting. Uncommon sulfates crystals such as $FeAl_2(SO_4)_4.22H_2O$ and $(NH_4)_3Fe(SO_4)_3$ present in the $PM_{2.5}$ samples showed the high influence of α-Fe_2O_3 in the atmospheric photo-reduction of Fe into sulfates. Results also showed high influence of other sources than sea with a high Cl contribution, such as sintering and coke ovens. Therefore, we believe that the use of receptor models in tandem with source profiles defined by crystalline phases, elemental species, and organic compounds, such as the PAHs, can improve distinction of highly correlated sources.

RESUMO

Estudos epidemiológicos mostram a associação do tamanho do material particulado (MP) no ar e sua composição química com problemas de saúde, nas quais afetam o sistema nervoso central e cardiorrespiratório. Portanto, a identificação das fontes de MP é um passo importante nos programas de gerenciamento da qualidade do ar. Modelos receptores são frequentemente utilizados em estudos de distribuição de fontes de MP a fim de identificar a contribuição de fontes locais. Apesar dos benefícios do uso desses modelos no gerenciamento da qualidade do ar, algumas limitações como efeitos de colinearidade, principalmente para fontes que possuem perfis químicos similares, restringem sua aplicação ou comprometem uma separação precisa de fontes. Para fontes altamente correlacionadas, a identificação de marcadores específicos ainda é o melhor caminho para uma distribuição de fontes mais precisa. Existem vários trabalhos usando diferentes técnicas analíticas na caracterização química e física do MP a fim de fornecer informações de entrada para os modelos receptores. A escolha entre tais técnicas depende de: as propriedades físicas das partículas, do tipo de amostragem, do tempo de medição, do acesso às instalações e equipamentos, dos custos associados à aquisição e manutenção de equipamentos, entre outras considerações. Apesar das numerosas técnicas analíticas descritas na literatura para caracterização de MP, os laboratórios são normalmente limitados às técnicas disponíveis internamente, o que levanta a questão se uma determinada técnica é adequada para o propósito de um trabalho experimental específico. Neste trabalho, é apresentado o estado da arte sobre as tecnologias disponíveis para a caracterização de MP. Adicionalmente, é proposto um guia para a escolha da(s) técnica(s) mais apropriada(s) para um estudo específico. Uma nova abordagem também é proposta para identificar as fontes mais apropriadas associadas aos fatores revelados através do modelo Fatoração de Matriz Positiva (PMF), na qual são utilizados conjuntamente a caracterização de espécies químicas, inorgânicas e orgânicas, e a direcionalidade dessas espécies através das rosas dos poluentes. Amostras de MP foram coletadas em uma região costeira, urbana e industrializada no Brasil e analisadas por EDXRF, TD-GC-MS e TOC para a caracterização de metais, PAHs, EC e OC. Esta região possui uma particularidade, uma atmosfera rica em ferro devido à presença de indústrias de pelotização e siderurgia. A metodologia proposta revelou que marcadores consolidados pela literatura: veiculares como o carbono elementar (EC) e carbono orgânico (CO), marcador de sal marinho: cloreto (Cl) e sódio (Na) e marcador industrial: ferro (Fe), também estavam fortemente associados a outras fontes. Cl, um marcador típico de sal marinho, também foi atribuído às atividades industriais de sinterização. Alguns fatores de PMF mostraram altas cargas de CO, um marcador típico tanto para exaustão veicular quanto para queima de carvão. A definição da fonte mais adequada para esses fatores só foi possível devido à avaliação da direcionalidade dessas

espécies pelas rosas dos poluentes. O potássio (K), um marcador comum de queima de biomassa, foi predominantemente associado a ventos advindos de um parque industrial e, portanto, provavelmente associado a emissões do processo de sinterização. Alguns PAHs como naftaleno, criseno, fenantreno, fluoreno e acenaftileno foram essenciais como marcadores que permitiram a separação de fontes com perfis químicos inorgânicos similares, entre elas a sinterização, a pelotização e a queima de biomassa. Os resultados mostraram que a combinação de marcadores químicos orgânicos e inorgânicos, e a análise das rosas dos poluentes para a identificação da direcionalidade das fontes melhorou a interpretação dos resultados do PMF no estudo de distribuição de fontes.

Além disso, a técnica de Difração Ressonante de Raios-X por Luz Síncrotron (RSr-XRD) foi conduzida no Laboratório Nacional de Luz Síncrotron (LNLS) em Campinas, Brasil, para análise de partículas sedimentáveis (SP), partículas suspensas totais (TSP), PM_{10} e $PM_{2.5}$. Os resultados mostram altos níveis de fases cristalinas baseadas em ferro. Em comparação com o uso de espécies químicas elementares, a identificação das fases cristalinas proporcionou uma abordagem aprimorada para classificar marcadores específicos de fontes baseadas em ferro. Compostos como $\alpha\text{-}Fe_2O_3$, Fe metálico, FeS_2 e $K_2Fe_2O_4$ estão associados, respectivamente, ao minério de ferro, pelotização e sinterização; altos fornos e siderurgia; depósitos de carvão; e emissões de sinterização. A atribuição da composição cristalina, e não apenas elementar, na identificação de fontes melhorou a precisão dos estudos de distribuição de fontes. $K_2Fe_2O_4$ e NH_4ClO_4 são compostos especificamente ligados ao processo de sinterização, formado principalmente durante a queima de matérias-primas em fornos. Cristais de sulfatos incomuns como $FeAl_2(SO_4)_4.22H_2O$ e $(NH_4)_3Fe(SO_4)_3$ em amostras de $PM_{2.5}$ mostraram a forte influência de $\alpha\text{-}Fe_2O_3$ na foto-redução atmosférica de Fe em sulfatos. Os resultados também mostraram, além do mar, alta influência de outras fontes com alta contribuição de Cl, como sinterização e fornos de coque. Portanto, acreditamos que o uso de modelos de receptores em conjunto com os perfis químicos das fontes definidos por fases cristalinas, espécies elementares e compostos orgânicos, como os HPAs, podem melhorar os resultados de fontes altamente correlacionadas.

LIST OF ACRONYMS

AES	Atomic emission spectrometry
AES	Auger electron spectroscopy
CE	Capillary electrophoresis
CRM	Certified reference materials
CVAAS	Cold vapor-atomic absorption spectrophotometry
DL	Detection limit
EC	Elemental carbon
EDXRF	Energy dispersive X-ray fluorescence
EF	Enrichment factor
FAAS	Flame atomic absorption spectroscopy
FID	Flame ionization detector
GC	Gas chromatography
GFAAS	Graphite furnace atomic absorption spectroscopy
IC	Ion chromatography
ICP	Inductively coupled plasma
IMPROVE	Interagency monitoring of protected visual environ.
INAA	Instrumental neutron activation analysis
LA	Laser ablation
LC	Liquid chromatography
LNLS	Laboratório Nacional de Luz Síncrotron
MARGA	Monitor for aerosols and gases
MS	Mass spectrometry
NIOSH	National institute for occupational safety and health
OC	Organic carbon
OES	Optical emission spectrometry
PAH	Polycyclic aromatic hydrocarbon
PEEM	Photoemission electron microscopy
PESA	Particle elastic scattering analysis
PIGE	Particle-induced γ-ray emission
PILS	Particle into liquid sampler
PIXE	Proton-induced x-ray emission
PM	Particulate matter
PM$_{2.5}$	Particulate matter less than 2.5 µm
PM$_{10}$	Particulate matter less than 10 µm
PMF	Positive matrix factorization
RBS	Rutherford backscattering spectrometry
SEM	Standard reference materials
SEM	Scanning electron microscope
SIMS	Secondary ion mass spectrometry
SP	Setteable particles
SPEM	Scanning photoelectron microscopy
RSr	Resonant Synchrotron radiation
TD	Thermal desorption
ToF	Time-of-flight
TOR	Thermal/optical reflectance
TOT	Thermal/optical transmittance
TSP	Total suspended particulate
TXRF	Total reflection X-ray fluorescence
VOC	Volatile organic carbon

WDXRF   Wavelength dispersive X-ray fluorescence
XPS   X-ray photoelectron spectroscopy
XRD   X-ray diffraction
XRF   X-ray fluorescence

LIST OF FIGURES

LIST OF TABLES

SUMMARY

1. INTRODUCTION

Particulate matter (PM) has been the subject of intricate air quality studies, mainly due to its implications in human health related problems, both physiologically (Brunekreef and Holgate, 2002; Dockery and Pope, 1994; Dolk and Vrijheid, 2003; Kappos et al., 2004) and psychologically (Crilley et al., 2017; Wang et al., 2017). Rather than total mass deposition, PM-driven health problems are more strongly associated with its chemical composition (Ghio and Devlin, 2001; Lippmann and Chen, 2009; Liu et al., 2017) and can be applied as biological metric for the assessment of public health risk (Rohr and Wyzga, 2012).

PM can be constituted by solid or liquid particles and characterized by size, shape and chemical composition which is influenced by its emission source and the physical and chemical transformations that occur as it is transported in the atmosphere (Finlayson-Pitts and Pitts, 2000). Despite differences in chemical composition and morphology, PM is usually classified by its aerodynamic diameter, which indicates the potential and local of deposition in the respiratory system (Atkinson et al., 2001). PM is usually classified as Total Suspended Particulate (TSP) ranging from 0.005 to 100 µm, inhalable particulate (PM_{10}) with aerodynamic diameter of less than 10 µm, capable to penetrate the respiratory system and fine particulate ($PM_{2.5}$), which is considered to be the major contributor to health effects having the potential to penetrate the innermost region of the lungs (Holgate et al., 1999). Over the last ten years, great concern has been attributed to ultrafine particles ($PM_{0.1}$) due to lack of information about their effects on the human health (WHO, 2006). Despite the importance of the aerodynamic diameter in determining the local of deposition in the respiratory tract, according to (Ghio and Devlin, 2001) the health effects over the exposed population to PM can be strongly related to the components that constitute the material, its chemical composition.

PM originates from both natural and anthropogenic sources. Natural PM comes from sea salt, soil, pollen, volcanic activities and burning, while anthropogenic sources include vehicles, industrial chimneys, quarries, waste incineration, among others, all abundant in urban areas. PM composition relates to source characteristics and the formation of secondary particles by reactions in the atmosphere between primary particles and gases including hydroxyl (OH^-), sulfur compounds (SO_2, SO_3^{2-}, SO_4^{2-}, H_2S) nitrogen compounds (NO, NO_2, NO_3^-, NH_3, NH_4^+), tropospheric ozone (O_3), water vapor, and oxygen (Seinfeld and Pandis, 2006, Wilson et al., 2002, Chow and Watson, 1998). Atmospheric PM composition may contain metals (geological, industrial and vehicular), elemental carbon (industrial and vehicular), organic carbon (landfill, wastewater, vehicular, industrial, fuel storage tanks, domestic), ionic species (industrial, natural: sea, estuary) and water.

PM physical, chemistry and optical particles properties are strongly correlated to the particles size (Feng et al., 2009). Aerodynamic diameter, density, and meteorological conditions determine how far particles are transported from sources.

PM participate in a variety of redox chemical reactions in the atmosphere, in which the speciation of the iron valence and its solubility can drive physical and chemical process (Kopcewicz *et al.*, 2015; Zuo and Deng 1997). Iron (Fe) is the most abundant metal species in PM (d'Acapito et al., 2014), affecting atmospheric redox reactions in the formation of complexes, like SO_2 (S^{4+}) to H_2SO_4 (S^{6+}), and influencing the partitioning of PM in the atmosphere, especially $PM_{2.5}$ (Hoffmann et al., 1996). Fe complexes are sources of OH^- and H_2O_2 (Siefert et al., 1994), affecting O_3 formation rate (Carter, 1994) and promoting the oxidation of organic compounds with the formation of organic radicals (Atkinson, 2000, 1997; Atkinson and Arey, 2003; Galvão et al., 2016). PAHs are found in the atmosphere as both gas and solid phase, adsorbed, absorbed, and/or condensed onto PM (Allen *et al.*, 1996; Ravindra *et al.*, 2008). The identification of PM sources is the first step in air quality management (Chen *et al.*, 2007; Pant *et al.*, 2014; Taiwo *et al.*, 2014), and the attribution of reliable chemical profiles of local sources is the best way to achieve accurate PM source apportionment (Raman and Hopke, 2007; Guo *et al.*, 2017).

Many techniques used in sampling and characterizing atmospheric particles are presented in the literature. The choice of sampling and measuring techniques is largely dependent on the chemical compounds to be identified, the need to preserve the sample for future analysis and also if quantification is needed, on the concentration ranges. Different regions present different types of source and meteorological conditions, which will affect particles concentration, size and chemical composition, and, therefore, the type of sampling and analysis technique to be performed.

Receptor models are used for quantifying source contributions based on fingerprints (H. Guo et al., 2009; Lee et al., 2008; Norris et al., 2014; Song et al., 2006). Despite the benefits, limitations are that all sources are non-collinear or linearly independents (Hopke, 2003; Paatero, 1997; Thurston and Lioy, 1987), since collinearity implies on sensitivity loss due to higher error and bias, especially when the Pearson correlation coefficients are deteriored (Habre *et al.*, 2011; Tian *et al.*, 2013; Shi *et al.*, 2014). Several approaches have been adopted to minimize the collinearity problem (Wittig and Allen, 2008; Roy *et al.*, 2011; Blanchard *et al.*, 2012), including hybrid models coupling different receptor models (Shi et al., 2014a, 2011, 2009). Nevertheless, for highly correlated sources, elevated error and bias are still reported, therefore, the addition of specific markers can lead to improved source apportionment.

Positive Matrix Factorization (PMF) is a receptor model based on the decomposition of a matrix X_{ij} of speciated data into two matrices: factor contributions G_{ik}, and factor profiles F_{ik} (Norris et al., 2014). Factor profiles needs the interpretation by the user, usually made by the association of chemical markers into each PMF factor with a source. It is a subjective process that can lead to incorrect interpretations. For example, iron (Fe) is reported as a marker of industrial (Song et al., 2006; Tauler et al., 2009), vehicular sources (Viana *et al.*, 2008; Karnae and John, 2011) and crustal sources (Gildemeister *et al.*, 2007; J. Wang *et al.*, 2016; Niu *et al.*, 2016). Elemental carbon (EC) and organic carbon (OC) are reported as markers of vehicular sources (Cheng et al., 2015; Owoade et al., 2016). However, the same species are also used as markers of biomass combustion (Kotchenruther, 2016), and coal burning (Vossler et al., 2016).

In fact, elemental chemical species can be emitted from several different sources, however, in different crystal phases. For example, metallic Fe (Fe^0) can be emitted by steelmaking and blast furnaces (USEPA, 1986), and by vehicles due to the brakes wear (Thorpe and Harrison, 2008). Fe_2O_3 is emitted by iron ore, and agglomerates (sinter and pellets) stockpiles (de Souza et al., 1998; Rosière and Chemale Jr, 2000). Besides, sintering and pelletizing furnaces stacks also can emit α-Fe_2O_3 during the agglomeration of iron ore, as so γ-Fe_2O_3 during the transition of magnetite (Fe_3O_4) to α-Fe_2O_3 by the heating process (Jiang et al., 2008). Pyrite (FeS_2) is other Fe phase found as a constituent of coal deposits (Cohn et al., 2006; Deng et al., 2015). FeS_2 is fully decomposed during the coking process at temperatures higher than 1600 ℃, temperature above the typical coke ovens (Gornostayev et al., 2009), therefore, FeS_2 can also be released by coke ovens stacks. Lastly, goethite (FeOOH) and Fe-bound silicates are typically found as constituents of soils (Fabris et al., 1997; Moreno et al., 2004). Therefore, the study of crystalline phases of the chemical species can be used to correlate the compounds with the specific process as an additional information for the source apportionment studies using receptor models.

In order to improve the PMF outcomes reducing the uncertainty, a few authors have used both organic and inorganic markers to interpret the PMF factors resulting in improved analysis (Choi et al., 2015; Dutton et al., 2010; Qadir et al., 2014; Vossler et al., 2016; Wang et al., 2015). Some PAHs species such as Fluoranthene (Flt), Pyrene (Pyr), Benzo[a]anthracene (BaA), and Chrysene (Chr) are reported as diesel vehicular markers (Wu et al., 2014). Benzo[b,k]fluoranthene (BbkF), Benzo[a]pyrene (BaP), and Benzo[g,h,i]perylene (BghiP) are often used as markers for gasoline vehicular emissions (Devos et al., 2006). Industrial PAHs emissions come from several process (Niu et al., 2017). Some PAHs species such as Pyr and Flt are reported as biomass burning markers (Venkataraman and Friedlander, 1994), while fluorene (Flu), Naphtalene (Nap), Phenanthrene

(Phe), Flt, and Pyr is associated to coke oven source (Dat and Chang, 2017; Zhou et al., 2014). Iron and steel industries also show organic markers associated to specific process. Nap is reported as the major organic marker of steelmaking. Nap, Phe, and Acenaphthylene (Acy) as markers of iron pellet plants, while Chr, BghiP, Dibenzo[ah]anthracene (DahA), BaA, Flu, Pyr, Nap, Phe, and BbkF are markers of sinter plants (Y. Guo et al., 2017). Despite the benefits of using organic markers in the interpretation of PMF factors, some uncertainty still relies on the source apportionment due to similarity on the PAHs profiles. Therefore, in urban and industrialized regions with several sources, the designation of markers without the knowledge of the directional pattern of the chemical species and their associated sources before the interpretation of PMF factors can lead to data misinterpretation.

In the Region of Greater Vitória, state of Espírito Santo, Brazil, some works have treated the subject. For a period of 2 years, from April 2009 to March 2011, Santos *et al*., (2017) quantified settleable particle (SP) deposition rate, for further elemental characterization. The authors have used the chemical composition for studies with CMB model in order to state the main contributors in the region. The study concluded that the region is largely affected by SP deposition rates when associated with winds blowing from northeast (NE), the location of the main industrial park in RGV. The results revealed RGV as a complex mix of sources including industrial and anthropogenic sources as the main contributors. Due to the complexity of the region in which similar processes such as steel and iron industries are at the same location, CMB was unable to differentiate between those two industries and its complexes: the ore stockpiles, pellet stockpiles and the main furnaces at the iron ore pelletizing industry, which was the source group presenting the large contribution to SP. The authors suggest the need of additional studies about the characterization of particles in RGV and new source apportionment studies. In 2015, Nascimento (2015) conducted a study about the influence of PM_{10} and $PM_{2.5}$ mass and their chemical composition over the incidence of respiratory disease in children. The author have determined the epidemiological risk in the respiratory morbity, showing that PM_{10} and SO_2 impact over the acute respiratory events within the day of exposure showing great relative risk, while fine particles ($PM_{2.5}$) have shown more evident effects after a six-day period from the exposure. Among the PM chemical components, silicon (Si), sulfur (S), Titanium (Ti) and EC show greater relative risk of causing acute respiratory diseases.

2. OBJECTIVES

The main objective of this work consists of using specific analytical techniques such as X-ray Fluorescence, Synchrotron Resonant X-ray Diffraction and Gas Chromatography coupled to Mass Spectrometer to characterize the chemical composition of particles in an complex iron-rich atmosphere of an urban and industrialized regions, in order to provide improved imformation for source apportionment studies. In order to achieve this main objective, the following specific objectives were drawn:

- ✓ Investigate the main and new trends in analytical techniques;
- ✓ Establish the state-of-the-art of the available analytical techniques applied to the characterization of particulate matter;
- ✓ Analysis of elemental constituents present in SP, TSP, PM_{10} and $PM_{2.5}$ of the Great Vitoria Region (RGV) iron-rich atmosphere;
- ✓ Characterization of specific markers for iron-rich particles in the RGV using EDXRF;
- ✓ Characterization of specific markers for organic species in PM collected in the RGV using TD-GC-MS;
- ✓ Characterization of specific markers for the crystal phases in PM collected in the RGV using RSr-XRD;
- ✓ Use of Positive Matrix Factorization (PMF) model for the source apportionment of PM_{10} and $PM_{2.5}$ in the RGV.

3. REVIEW OF THE LITERATURE

In this chapter will be show a comprehensive review of the literature about the main and new trends in analytical techniques applied to the characterization of particulate matter. This review is part of the article published in the journal Chemosphere in February 2018 (Galvão et al., 2018).

3.1 Sampling and Preparation Methods

Sampling is a critical step that can define the success or failure of an experimental work. Contaminations can occur due to careless handling or non-compliance with preparation protocols, as well as erroneous results can be drawn due to inadequate use of filters and membranes containing similar chemical composition to the sample. There are two types of sampling methods: (i) on-line – methods based on automated sampling and direct measurements; and (ii) off-line – methods based on the collection of a sample in the site and transported to a laboratory for analysis.

On-line and hyphenated techniques like as MARGA and PILS-IC are usually used for the analysis of PM requiring no sample handling, and, therefore, minimizing the risk of contamination. This method can also provide a valuable information for studies about source apportionment and formation processes of PM with a short time resolution of 1 hour or less (Li et al., 2017). A cyclone or an impactor at the intake separate the size of the aerosol particles to be analyzed, e.g. PM_1, $PM_{2.5}$, PM_{10} (Wilson et al., 2002). Wilson et al. (2002) present a good review on separation methods of fine and coarse PM.

Off-line techniques have poor time resolution, 24 hours or more, although the relatively low cost of the sampling instruments, if compared to on-line monitors, allows the installation of several instruments at the same time at different sites, improving the spatial resolution. Off-line techniques require, besides the size selection, a filter medium to collect the PM. These filter medium consist of a tightly woven fibrous material or a plastic membrane that has been penetrated by microscopic pores (Chow and Watson, 1998). Unfortunately, no single filter medium can be used as there may exist some incompatibilities associated with the sample and filter compositions. Factors as, efficiency of sampling, mechanical, chemical and physical stability, blank concentrations and loading capacity (Chow and Watson, 1998) can lead to misleading results if the filter medium is incorrectly chosen.

Teflon and polycarbonate filters are typically used for elemental analysis, for instance, XRF, PIXE or ICP (see Table S1 – Appendix A) due to their low blank levels and inertness to gases adsorption. However, their chemical composition (carbon-based) is not feasible to carbon analysis. On the

other hand, pure quartz is highly used for carbon analysis (EC, OC, particle-bound PAH) and ion analysis due to low blank levels and chemical composition. However, these filters medium can passively adsorb gases like VOC's, HNO_3, SO_2 and NO_2 and the use of denuders should be considered for the removal of those artifacts. Glass fiber filters can also be applied for carbon analysis, but can present high blank levels. Both quartz and glass fiber can be used for elemental analysis, as long as one is aware of their chemical composition (Al and Si, with large and variable quantities of Na). Polyvinyl chloride filters are compatible with XRD analysis, while cellulose esters filters are employed to scanning and transmission electron microscope (SEM and TEM), as so for XRD. Chow and Watson (1998) prepared a document "Guideline on Speciated Particulate Monitoring" that offers a complete insight about references methods applied to PM sampling. A short discussion on sample preparation and handling methods is included to each technique described in section 3.

Table 1 shows a compilation of articles published over the last 20 years on PM characterization including the information about the analytical techniques and filter medium used.

The use of blank filters is imperative in the elemental characterization of PM, mainly if the analysis is performed by X-ray techniques, like XRF and PIXE. X-ray peaks consist on a background of radiation scattered from the sampling filters, or substrates, and this background spectrum has the same features (shape) of the sample if the mass of the substrate is relatively higher than the sampled mass (Chow and Watson, 1998, Russ, 1977).

Table 1 compiles information about PM characterization analytical techniques and filter medium used in over 40 studies carried out in the last 20 years. These studies can be grouped according to their main motivations:

- PM characterization to be used in source apportionment studies using receptor models (CMB, PMF, UNMIX, etc.), multivariate analysis (PCA, Enrichment Factors, Cluster Analysis, Fourier Analysis, etc.), or to understand PM formation processes in atmosphere and its meteorological implications (Almeida et al., 2017; Avino et al., 2008; Chithra and Shiva Nagendra, 2013; Diapouli et al., 2017; Elorduy et al., 2016; Ezeh et al., 2014; Gonçalves et al., 2016; H. Guo et al., 2009; Hang and Kim Oanh, 2014; Huang et al., 2014; Landis et al., 2017; López-García et al., 2017; Mijić et al., 2010; Nair et al., 2006; Omidvarborna et al., 2014; van Drooge et al., 2012; J. Wang et al., 2016);

- PM inference on human health: its impacts, risk and toxicity assessment (Dieme et al., 2012; Furuyama et al., 2011; Geldenhuys et al., 2015; Godelitsas et al., 2011; Godoi et al., 2008; Guanghua and Guangfu, 1998; J. Guo et al., 2017; Lomboy et al., 2015; Mercier et al., 2012; Saarnio et al., 2008; Wu et al., 2017; Z.-H. Zhang et al., 2017);

- Assessment and improvement of techniques/methods and its applications (Borgese et al., 2012; Bruno et al., 2007; Calzolai et al., 2015, 2008; Canepari et al., 2009; Chiari et al., 2015; Dabek-Zlotorzynska et al., 2003, 2002; Ezeh et al., 2015; Khuzestani et al., 2017; Kopcewicz et al., 2015; Mukhtar and Limbeck, 2009; Rizzio et al., 2000; Schmeling et al., 1997; Sharma et al., 2007; Tomiyasu et al., 2004; Vander Wal et al., 2016; Wonglee et al., 2011).

Table 1. List of articles on PM characterization including the information about the analytical techniques and filter medium used.

Author	Year	Technique			Sampling information	Location
		Principal	Variants	Application		
(Diapouli et al.)	2017	X-ray	EDXRF	Elemental	PM_{10} and $PM_{2.5}$ onto PTFE filters	Greece
(Khuzestani et al.)	2017	Carbon analysis Optical	TOT OCSSS	EC/OC	$PM_{2.5}$ onto quartz and Teflon filters	China
(Almeida et al.)	2017	Atomic Spectr.	ICP-MS ICP-OES	Elemental	TSP onto glass fiber filter	Brazil
(Wu et al.)	2017	Atomic Spectr. Chromatography	ICP-OES GC-MS	Elemental PAH	$PM_{2.5}$ onto PTFE filters	China
(Landis et al.)	2017	X-ray Atomic Spectr.	EDXRF ICP-MS	Elemental	PM_{10} and $PM_{2.5\text{-}10}$ onto PTFE filters	Canada
(Guo et al.)	2017	Atomic Spectr.	CVAAS	Elemental	TSP onto quartz filters	Nepal, South Asia
(López-García et al.)	2017	Atomic Spectr.	ETAAS	Elemental	TSP onto cellulose and glass fiber filters digested in acid	Canary Islands
(Vander Wal et al.)	2016	X-ray	XPS	Elemental Compounds	nvPM onto quartz filters	USA
(Wang et al.)	(2016b, 2016a)	Chromatography Carbon analysis	IC TOR	Ions EC/OC	PM onto quartz filters	China
(Gonçalves et al.)	2016	Atomic Spectr. Chromatography Carbon analysis	ICP-MS IC/GC TOC	Elemental Ions/PAH EC/OC	TSP onto quartz filters	Brazil
(Elorduy et al.)	2016	Chromatography	TD-GC-MS	PAH	PM_{10} onto quartz fiber filters desorbed by thermally	Bilbao, Spain
(Choung et al.)	2016	X-ray	XRD	Mineral composition	$PM_{2.5}$ onto quartz and glass fiber filters	Korea
(Zhang et al.)	2016	Surface Sensitive Analysis	TOF-SIMS	Molecular and ion groups	Aerosols sample collected by Cascade Impactor	Beijing, China
(Ezeh et al.)	2015	Ion beam analysis	PIXE PIGE	Elemental	$PM_{2.5\text{-}10}$ onto polycarbonate membranes	Nigeria
(Lomboy et al.)	2015	X-ray	EDXRF	Elemental	$PM_{2.5}$ onto PTFE filters	Philippines
(Calzolai et al.)	2015	Ion beam analysis	PIXE	Elemental	$PM_{2.5\text{-}10}$ onto polycarbonate filters	Italy
(Chiari et al.)	2015	Ion beam analysis	PESA	Elemental (Low-Z)	$PM_{2.5}$ onto PTFE and quartz filters	
(Geldenhuys et al.)	2015	Chromatography	TD-GC-MS	PAH	Diesel exhaust samples onto PDMS absorbent traps desorbed thermally	South Africa
(Kopcewicz et al.)	2015	Surface Sensitive Analysis	Mössbauer	Chemical speciation	$PM_{2.5}$ and coarse onto glass fiber filter	Poland
(Omidvarborna et al.)	2014	Atomic Spectr.	ICP-OES	Elemental / EC/OC	PM onto quartz filters	USA

Author	Year	Technique			Sampling information	Location
		Principal	Variants	Application		
(Hang and Kim Oanh)	2014	Carbon analysis Atomic Spectr. Chromatography	TOT/TOR ICP-OES IC	EC/OC Elemental Ions	$PM_{2.5}$ onto quartz and MCE filters	Vietnam
(Ezeh et al.)	2014	Ion beam analysis	PIXE PIGE	Elemental	$PM_{2.5}$ and $PM_{2.5-10}$ onto polycarbonate filters	Nigeria
(Huang et al.)	2014	Carbon analysis Atomic Spectr.	TOC ICP-MS	EC/OC Elemental	SPM into polyethylene barrels	China
(Jancsek-Turóczi et al.)	2013	Surface Sensitive Analysis	SEM/EDS	Elemental/morphology	PM_{1-10} in cyclone separator and PM_1 samples onto PTFE filters	Hungary
(Vargas Jentzsch et al.)	2013	Vibrational Spectroscopy	RAMAN	Structural	Reagents simulating salts in atmosphere	Germany
(Chithra and Shiva Nagendra)	2013	Atomic Spectr. Chromatography Carbon analysis	ICP-OES IC TOR	Elemental Ions EC/OC	SPM onto PTFE filters	India
(van Drooge et al.)	2012	Chromatography	GC-MS	PAH	PM_1 onto quartz filters	Spain
(Borgese et al.)	2012	X-ray	TXRF XSW	Elemental	PM_{10} onto PTFE filters	Italy
(Mercier et al.)	2012	Chromatography	TD-GC-MS	SVOC	PM_{10} onto quartz filters	France
(Dieme et al.)	2012	Chromatography Atomic Spectr.	GC-MS IC ICP-MS	VOC/PAH Ions Elemental	$PM_{2.5}$ onto aluminum foil	Senegal
(Wonglee et al.)	2011	Ion beam analysis	WD-PIXE	Elemental	$PM_{0.43-11}$ onto aluminum foils	Tokyo, Japan
(Furuyama et al.)	2011	Atomic Spectr. Ion beam analysis	RBS PIXE	Elemental	PM onto glass fiber filters and Al foils	Japan
(Godelitsas et al.)	2011	X-ray	SR µ-XRF	Elemental	$PM_{2.5}$ and $PM_{2.5-10}$ onto quartz filters	Greece
(Mijić et al.)	2010	Atomic Spectrometry	ETAAS	Elemental	PS digested in acid medium	Belgrade (Serbia)
(Ding et al.)	2009	Chromatography Carbon analysis	TD-GC-MS TOR	PAH EC/OC	$PM_{2.5}$ onto quartz filters	Canada
(Canepari et al.)	2009	X-ray Chromatography Atomic Spectr.	EDXRF IC ICP-OES	Elemental Ions Elemental	$PM_{2.5}$ and PM_{10} onto PTFE filters	Rome
(Mukhtar and Limbeck)	2009	Atomic Spectrometry	ETAAS	Elemental	PM_{10} onto MCE filters	Austria
(Saarnio et al.)	2008	Chromatography	GC-MS	PAH	$PM_{0.2-10}$ PU substrates and quartz filters	European cities
(Godoi et al.)	2008	X-ray	EDXRF EPMA	Elemental	$PM_{0.5-8}$ onto polycarbonate	Brazil
(Calzolai et al.)	2008	X-ray Ion beam analysis	EDXRF PIXE	Elemental	$PM_{2.5-10}$ onto PTFE, polycarbonate and MCE filters	Italy
(Avino et al.)	2008	Activation Analysis	INAA	Elemental	PM_{10} onto polycarbonate filters	Rome
(Sharma et al.)	2007	Fluorescence	SFS	PAH	PM onto quartz filters	India
(Bruno et al.)	2007	Chromatography	GC-MS	PAH	$PM_{2.5}$ onto quartz filters	Italy
(Nair et al.)	2006	Atomic Spectr.	FAAS	Elemental	PM_{10} onto quartz fiber filters acid extracted	India
(Tomiyasu et al.)	2004	X-ray MS	EPMA ToF-SIMS	Elemental / surface	PM diesel exhaust particles	Japan
(Dabek-Zlotorzynska et al.)	2002	Electrochemical	CE	Ions	NIST 1648 Urban Air Particulate Matter	Canada
Rizzio et al	2000	Activation Analysis	INAA	Elemental	TSP onto cellulose filters	Italy
(Guanghua and Guangfu)	1998	Ion beam analysis	PIXE	Elemental	$PM_{0.25-16}$ onto polycarbonate filters	China
(Schmeling et al.)	1997	X-ray	TXRF	Elemental	PM onto cellulose nitrate filters	Germany

The choice between on-line or off-line techniques must be considered based on previous knowledge of the particles composition, equipment and financial resources available, as well as on the information or answer one is requiring from the analysis. Figure 1 shows a decision tree in

order to help readers to find the group of analytical techniques mostly appropriated for an experimental work. In section 3.2, readers will find a useful technical discussion about each technique to follow the proposed decision tree.

3.2 Analytical Techniques

A complete PM chemical or physical characterization is not possible with the use of only one technique, neither by a unique equipment. Each technique, in essence, is complementary to the whole process for mass closure. Therefore, although the discussions are carried out considering the analytical information required, the techniques presented here are classified according to their physical principles or working group: Atomic Spectrometry-based techniques, capillary electrophoresis, X-ray and ion beam based techniques, activation analysis, organic and carbonaceous techniques and surface sensitive techniques. It aims to provide support to the readers for choosing the most appropriated analytical technique among the working group indicated by using the decision tree shown in Figure 1.
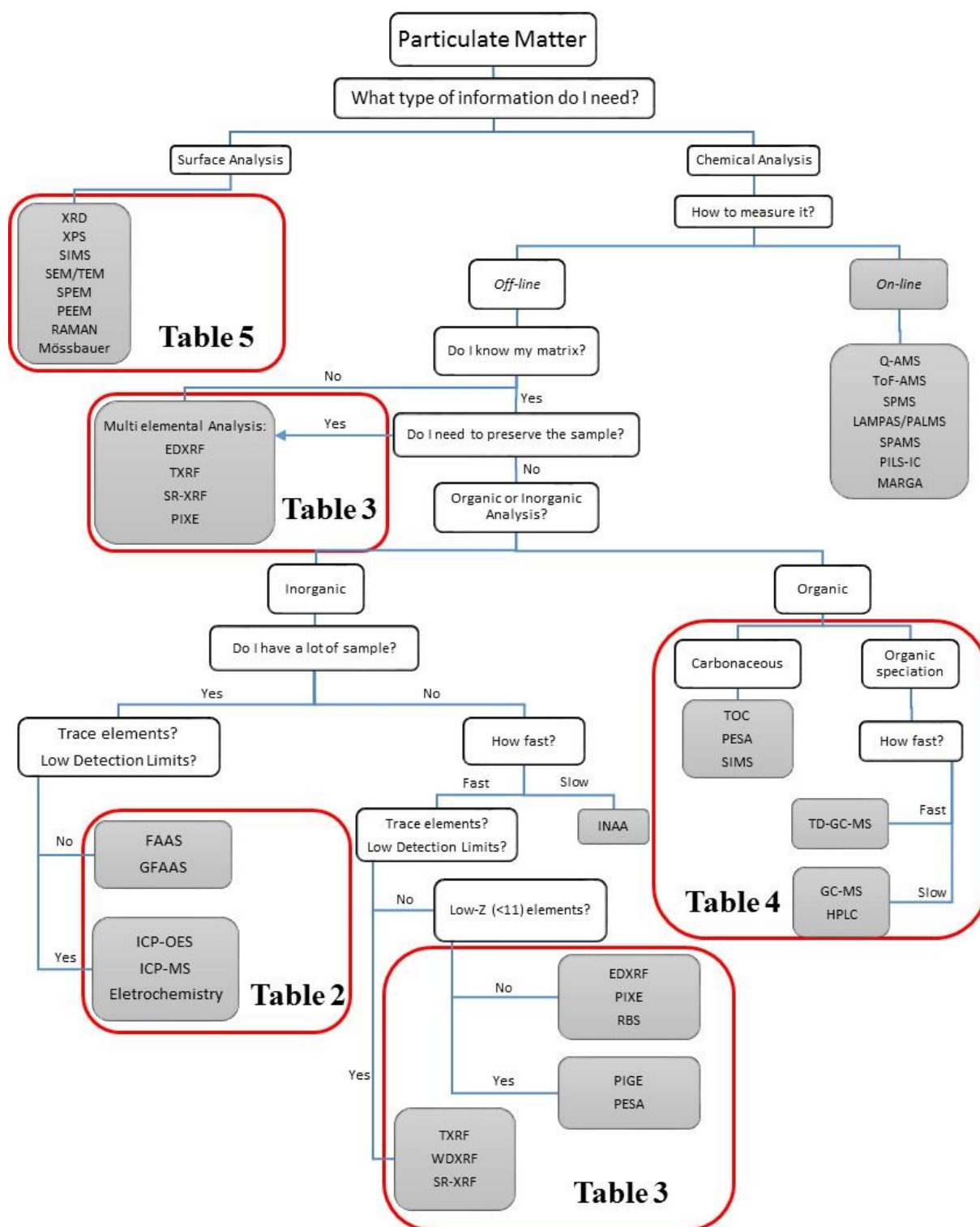
Figure 1. Decision tree for the choice between several analytical techniques and its applications considering the sample matrix.

3.2.1 Trends in Elemental Analysis

The mostly elemental analysis is performed by techniques based on atomic spectrometry, X-ray and activation analysis, however, some analytical techniques have shown be more prominent over

the last two decades. In order to understand current and past trends, a literature review was conducted on analytical techniques for PM qualitative and quantitative characterization. The most cited analytical techniques in the literature are ICP-MS, ICP-OES, EDXRF, PIXE, FAAS, INAA, GFAAS, TXRF, CVAAS, PESA, SR-XRF, in the order from the most to the least cited one. The selected articles are compiled in Appendix A - Supplemental Material (Table S1 and S2 and Figure S1 and S2).

Although atomic spectrometry represents the most used technique for elemental characterization of PM, ICP-MS accounts for almost two-thirds of all atomic spectrometry-based techniques used for characterization of PM, especially from 2010 onwards, when the number of works using ICP-MS practically doubled (Figure S1b). Activation analysis based techniques has shown a flat trend of use through the last 20 years (Figure S1a), not showing any evidence of increase or obsolescence. Following atomic spectrometry, the use of X-ray based techniques (Figure S1a) has shown a continuous increase since 2003, mainly led by EDXRF (Figure S1c). EDXRF has surpassed the total number of studies using PIXE by 2003. In fact, over the last two decades, PIXE has shown a slight declining trend (Figure S1c). This behavior is more evident in studies related to Atmos. Res. (as can be seen in Figure S2 and Table S2).

The preferential use of atomic spectrometry for elemental analysis in atmospheric related articles is observed, especially since 2002, with a similar difference between the number of publications using atomic spectrometry and X-ray based techniques to the general trend (Figure S2a). Atomic spectrometry-based techniques like as ICP-MS, ICP-OES, FAAS, GFAAS and CVAAS represent about 60% of all works published. X-ray based techniques contribute for about 35%, pushed mainly by EDXRF, and Activation Analysis (INAA) account for less than 5 %. X-ray techniques represent about 35% of the total number of published articles in the field of atmospheric sciences, depicted mainly by EDXRF, and lastly, Activation Analysis (INAA) accounts for less than 5 %.

As in the general trend, ICP-MS is the most used atomic spectrometry-based technique, accounting for about 60% (Figure S2b). As for X-ray techniques, EDXRF and PIXE are both equally used in the field of atmospheric sciences (Figure S2c), with other techniques such WDXRF and PESA being less widely used. EDXRF and PIXE are also widely used in the fields of geochemistry, fuel applications, spectrochemical fundaments and applied analytical chemistry. However, in the field of atmospheric sciences, the tendency lines (yellow and blue) in Figure S2c shows an evident increase in the use of EDXRF over the last 20 years and a decreasing trend for PIXE. EDXRF has gradually climbed, step-by-step, over three distinct periods in the last 20 years. In the following

sections, the main techniques available concerning their use in the field of atmospheric sciences are presented: elemental analysis, organic and carbonaceous and surface analysis.

3.2.2 Elemental Analysis Techniques

Elemental analysis is often conducted in PM samples with the aim of understanding the full spectrum of metallic species constituting the sample and retrieve some information about the existence of species that can be harmful to human health (Lippmann and Chen, 2009; Wilson et al., 2002). However, metallic elemental composition information can also be used to define tracers of PM sources (Chow and Watson, 1998; Slezakova et al., 2008) and to infer its origin (Bernabé et al., 2005; Feng et al., 2009; Srivastava et al., 2008).

3.2.2.1 - Atomic Spectrometry-based Techniques

Inductively Coupled Plasma (ICP) is the most used technique for atomic spectrometry-based techniques. ICP is based on the ionization of a sample under intense argon plasma atmosphere and the principle of analysis and detection defines the terms Mass Spectrometry (MS) and Optical Emission Spectrometry (OES), sometimes referred by Atomic Emission Spectrometry (AES). High temperatures induced by the plasma excite electrons above steady-state. In the IPC-OES, when these electrons return to steady-state, a photon of light is emitted and then analyzed by interaction with electromagnetic radiation (absorption and emission) (Brown and Milton, 2005; Chow and Watson, 1998; Wilson et al., 2002). In the ICP-MS, the ions produced in argon plasma are introduced in a quadrupole or magnetic sector analyzer. The analyzer act as a mass filter that allows a single mass to charge ratio pass through at a given time, being detected by an electron multiplier (Brown and Milton, 2005; Gross, 2011; Hoffmann and Stroobant, 2007; Wilson et al., 2002).

ICP(OES and MS) have some attractive features for elemental analysis. They are a fast and multi-elemental technique that present high sensitivity and low detection limits (DL), typically in the order of ppb, although ICP-MS can show DL in the order of ppt, an order of magnitude lower than other elemental techniques (Brown and Milton, 2005, Wilson et al., 2002). These features turn this analytical technique an excellent choice if trace elements are concerned. ICP analysis is essentially destructive, as it requires the complete extraction and digestion of the sample in an acid medium. Maybe, that is the greatest disadvantage of this technique. The acid digest PM is time-consuming and user-accuracy dependent. There a few artifacts to the methodology, if digestion is incomplete, the solution can form co-precipitates and sample mass needs to be large, a few milligrams (Balcaen et al., 2015; Borgese et al., 2012; Walkner et al., 2017; N. Zhang et al., 2017). Sample handling

also increases the risk of contamination, requiring a specialized operation and more experienced technicians. ICP (OES and MS) are the most used techniques in the atomic spectrometry group and have been widely used in the investigation of the impacts of PM in the environment.

The results by ICP is largely used as input data for source apportionment models like as enrichment factor (EF), principal component analysis (PCA), positive matrix factor (PMF) among others (Aldabe et al., 2011; Clements et al., 2014; Khan et al., 2010; Pan et al., 2015). The continuous increase and extensively use of ICP-MS in PM elemental analysis over the last 20 years can be associated with the advent of the mass spectrometry detectors and its achievements in low DL. ICP-MS analyses have been widely used in the identification of isotopic signature of metals like Pb and Fe to identify the sources of these metals (Félix et al., 2015; Flament et al., 2008).

A more traditional technique, Atomic absorption spectrophotometry (AAS) is a based on the atomization or ionization of a given element at high temperatures (lower than ICP) and its detection at a specific wavelength by a monochromator. AAS presents three variants, Flame AAS (FAAS), Graphite Furnace (GFAAS), also known as Electro Thermal Furnace (ETAAS) and Cold Vapor AAS (CVAAS). The latter is more dedicated to mercury analysis. The main difference between each technique is the ionization method. FAAS uses a flame that can reach 3000 K, depending on the fuels and oxidants used for flame combustion, while GFAAS uses atomization temperatures over 3000 K, and CVAAS uses no vaporization system (Brown and Milton, 2005, Wilson et al., 2002).

AAS instruments are lower in cost if compared to ICP technology, user-friendly and of easy operation, and can be applied as a complementary technique for X-ray fluorescent analysis in the quantification of low-Z elements, specifically Be, Na and Mg. GFAAS achieves lower detection limits compared to FAAS (10 to 100 times better). However, this analytical group presents considerable disadvantages in its use. As with ICP, there is need for prior digestion of PM and large sample mass, and all the disadvantages of increasing sample preparation (time-consuming, the risk of contamination and co-precipitate formation) applies. Beside, AAS is a single elemental analysis technique and need individual analysis for each element. This feature increases the time of analysis and the consuming of certified reference materials, as well as the dependence of an operator during the entire analysis (Borgese et al., 2012; Brown and Milton, 2005; Novaes et al., 2016; Rizzio et al., 2000). Finally, AAS techniques also show high backgrounds and are inadequate for refractory elements, mainly Mo, W and Re.

One of the most concerning features of atomic spectrometry techniques is sample handling and the possibility of sample contamination. A new trend in atomic spectrometry techniques that can minimize the risk of contamination is the coupling of laser ablation (LA) to ICP-MS. LA-ICP-MS eliminates the digestion step by enabling the direct solid micro sampling and analysis. However, the technique shows the following drawbacks: elemental fractionation can occur, changes of the laser interaction with the sample matrix, transport efficiency of the ablated material and parameters of the set can lead to erroneous results for quantitative analysis (Gonzalez et al., 2006; Horn and Günther, 2003; Niehaus et al., 2015; Pickhardt et al., 2005; Trejos and Almirall, 2004; Voss et al., 2017).

3.2.2.2 - Capillary Electrophoresis

Capillary Electrophoresis (CE) is reported in the literature as a promising method for PM characterization that can perform multi-ion analysis on a small extract volume (Dabek-Zlotorzynska et al., 2003). Analysis by CE requires sample handling: acid digestion - which can induce low separation efficiency - and ultrafiltration. CE can perform efficient and fast separation of metals, depending on experimental conditions, and it is a very attractive technique for the purpose of element speciation, as an alternative option to the atomic spectrometric analysis (Dabek-Zlotorzynska et al., 2002). CE promotes an inexpensive and fast analysis, with high separation efficiency, requiring low sample volume, which is an importantfeature when dealing with PM sampling. Authors also describe occurrence of problems associated with the long-term stability of the migration times (Dabek-Zlotorzynska et al., 2003, 2002; Lara et al., 2016; Pacáková and Štulík, 2005).

The main features of atomic spectrometry and capillary electrophoresis-based techniques are summarized in Table 2.

Table 2. Summary of the most used **atomic spectrometry** and **capillary electrophoresis** techniques for particulate matter characterization.

Technique		Analytical Information	Advantages	Disadvantages	Time*	Authors
Principal	Variant					
Atomic Spectrometry	ICP-OES	Elemental	• High sensitivity; • Low detection limits; • Fast multi-element analysis; • Low volume of sample.	• Sample handling: • Time-consuming and contamination risk; • Destructive analysis; • Relative large amounts of samples.	H	(Walkner et al., 2017) (Zhang et al., 2017) (Novaes et al., 2016) (Balcaen et al., 2015) (Borgese et al., 2012)
Atomic Spectrometry	ICP-MS	Elemental	• High sensitivity; • Low detection limits: one order of magnitude lower than other elemental techniques;	• Sample handling: • Time-consuming and contamination risk; • Destructive; • Relative large amounts of samples.	H	(Walkner et al., 2017) (Zhang et al., 2017) (Novaes et al., 2016) (Balcaen et al., 2015) (Borgese et al., 2012) (Chow and Watson, 1998)

			• Fast multi-element analysis.			
Atomic Spectrometry	FAAS	Elemental	• Low cost; • Easy operation; • Complementary technique for Na and Mg.	• Destructive; • Insufficient atomization of some analytes; • High background; • Individual analysis for each element; • Sampling handling: risk of contamination and co-precipitate; • Inadequate for refractory elements.	H	(Novaes et al., 2016) (Borgese et al., 2012) (Brown and Milton, 2005) (Wilson et al., 2002) (Rizzio et al., 2000)
Atomic Spectrometry	GFAAS	Elemental	• Higher atomization temperatures than FAAS; • LOD comparable to ICP and 10-100 times better than FAAS.	• Destructive; • High background; • Individual analysis for each element; • Sampling handling: risk of co-precipitate and contamination; • Inadequate for refractory elements.	H	(Novaes et al., 2016) (Borgese et al., 2012) (Brown and Milton, 2005) (Wilson et al., 2002) (Rizzio et al., 2000)
Capillary Electrophoresis	CE	Inorganic ions	• High separation efficiency; • Low sample volume; • Inexpensive and fast analysis.	• Sample handling: digestion and ultrafiltration; • Reduced sensitivity; • Acid digestion induces low separation efficiency; • Problems associated to long-term stability of the migration times.	L	(Lara et al., 2016) (Pacáková and Štulík, 2005) (Dabek-Zlotorzynska et al., 2003) (Dabek-Zlotorzynska et al., 2002)

3.2.2.3 - X-ray based Techniques

X-ray techniques use a focused beam of charged particles or photons which excite electrons in the samples with a wavelength that is characteristic of the element, allowing a qualitative and quantitative trace analysis of the material. X-ray methods have been largely applied in many different areas, like geological materials, industrial materials, archaeological samples, forensics sample, as well as environmental samples (Brown and Milton, 2005; Janssens, 2013). Among all X-ray based techniques for PM characterization, the most applied ones are EDXRF, PIXE, TXRF, WDXRF, PESA and SR-XRF. These techniques are grouped as X-ray and ion beam techniques in Table 3.

Energy Dispersive X-ray Fluorescence (EDXRF) is a well-established method for quantitative elemental analysis and the most used X-ray fluorescence technique, including WDXRF, TXRF and SRXRF. X-ray fluorescence analysis (XRF) is based on atoms ionization by an energetic beam of primary X-rays. The radiation that is emitted by the ionized atoms upon relaxation contains a selective, qualitative and quantitative information of the elemental constituents present in the sample (Janssens, 2013, Brown and Milton, 2005, Wilson et al., 2002). EDXRF is essentially a non-destructive technique, although some lighter elements and semi-volatile compounds can be

lost due to X-ray radiation and under vacuum analysis. None or minimal sample preparation is needed, which reduces contamination risks, but a homogeneous sample is mandatory (Janssens, 2013; Okuda et al., 2014). A multichannel memory provides a fast and a selective multi-elemental analysis, with a wide range of detectable elements from Na to U. Another good feature of EDXRF is the possibility of liquid sample analysis. In principle, all fluorescence techniques can present interferences influencing fluorescent intensity. This interference is caused by matrix-effect that is associated with an attenuation of both primary and fluorescent radiation within the sample. The sensitivity of XRF depends on the energy of the incident radiation, the geometry of the instrument and the efficiency of the detector. EDXRF presents low DL's in the order of a few μg cm^{-2} or μg g^{-1}, which is comparable to the DL's of ICP-OES (see Tables 1 and 2). Although, EDXRF possesses low sensitivity for low-Z elements (Z < 11), a complementary technique is required for mass closure (Çevik et al., 2003; Dogan and Kobya, 2006; Ekinci et al., 2002; Gredilla et al., 2016; Janssens, 2013; Reyes-Herrera et al., 2015; Sitko, 2009; Yatkin et al., 2012; Yatkin and Gerboles, 2017). EDXRF is preferred over WDXRF due to its fast and multi-elemental analysis (Wilson et al., 2002).

(Niu et al., 2010) compared EDXRF to ICP-MS regarding measurement uncertainty associated with metals quantification in particulate matter (PM_{10}) using co-located duplicate samples for both 24-h and 2-week sampling. The results yield very good correlations ($R^2 > 0.7$) for elements that were above detection limits for both instruments (e.g. Fe, Mn, Zn, Pb and Cu). A similar result is shown by (Yatkin et al., 2012) stating that EDXRF can be considered as an alternative method to Teflon filters PM measurements with ICP-MS. EDXRF has been widely used for characterization of trace elements in PM samples with different objectives, as studies of source apportionment, human health impacts and influence on visibility, as reported by (Cheng et al., 2015; Díaz et al., 2014; Ivošević et al., 2015; Okuda et al., 2014; Tecer et al., 2012; Vossler et al., 2016).

Wavelength-Dispersive X-ray Fluorescence (WDXRF) is based on the diffraction of incident X-rays by a single crystal to separate characteristic wavelengths emitted by the sample. This technique presents low DL's (down to ppm levels) and improved sensitivity, which results in high spectral resolution with minimal peak overlap. Multi-elemental analysis is possible with the coupling wavelength-dispersive system, but moderate to high costs must be considered (Janssens, 2013, Chow and Watson, 1998). In addition, the use of high power excitation can result in heating and degradation of samples.

Total X-ray Fluorescence (TXRF) is based on the incoming radiation that focuses on the sample at less than the critical angle by the implementation of X-ray optical geometries that uses the total

reflection of the primary radiation on flat surfaces. The instrument geometry modification minimizes the scattering on the substrate improving DLs and avoids the correction for matrix effects. This method requires thin samples involving a sample pre-treatment and increasing the risk of sample contamination. In quantitative analysis, saturation effects caused by deviation in linear relation is observed in high sample masses due to differences in primary radiation (Bilo et al., 2017; Borgese et al., 2012; Meirer et al., 2010; Schmeling, 2004; Wagner et al., 2008; Wagner and Mages, 2010; Wilson et al., 2002).

Synchrotron radiation X-ray Fluorescence (SRXRF) uses the same physical principle of EDXRF, but with a source of synchrotron radiation for exciting X-rays. This multi-elemental, non-destructive and fast analytical technique has high detection sensitivity due to the high flux of polarized X-rays. As the Synchrotron facilities offer polarization options (circle or plane), the total X-ray polarization improves DLs (pg level) providing minimum background and requiring small amounts of sample. Plural and multiple scattering can influence SRXRF results (Janssens, 2013; Lü et al., 2012; Saisho, 1989; Wilson et al., 2002; Zeng et al., 2013). Although, the most considerable disadvantage about the SRXRF is the limited number of available synchrotron sources around the world, being 49 sources, 19 sources in Europe, 15 in Asia, 4 in Middle East, 1 in Oceania and 9 in Americas (7 in USA and 1 in Canada). Brazil has the only synchrotron source in Latin America, the National Laboratory of Synchrotron Light (LNLS) (Lightsources.org, 2017).

Particle (or Proton) Induced X-ray Emission (PIXE) is an ion beam method based on the detection of characteristic X-rays induced by a particle beam (protons or lighter ions) from electrostatic accelerators (Janssens, 2013; Wilson et al., 2002). PIXE is a multi-elemental analysis technique that covers a wide range of elements with high sensitivity, favoring the quantification of lighter elements. PIXE is a non-destructive technique and needs minimal sample handling, similar to EDXRF. However, contrary to XRF techniques, PIXE has higher sensitivity for lighter elements such as Na (Carmona et al., 2010; Crilley et al., 2017; Klockenkämper, 1987; Maenhaut, 2015; Maenhaut et al., 2011; Reyes-Herrera et al., 2015). This feature relates to the low use of proton energy, in the order of a few MeV. Thus, the cross-section for the production of X-rays favors the quantification of lighter elements as Na (Janssens, 2013, Wilson et al., 2002). PIXE is based on the excitation characteristics of X-rays using protons or other light ions irradiation (Janssens, 2013). This principle is similar to XRF but differs in the usage of fluorescent energy source excitation .

Due to some similar characteristics between PIXE and XRF, a comparison between some features of both techniques is mandatory. The sensitivity of X-ray and ion beam methods for lighter

elements analysis relies on the absorption of soft X-rays. PIXE analysis is more sensitive to lighter elements than EDXRF, since EDXRF presents absorption edges far below the required excitation energy. In PIXE, the higher the atomic number (Z) the lower is the sensitivity, and a strong decrease in the X-ray production cross sections results in lower sensitivity for heavy elements. Thus, as a rule of thumb, fluorescence is more suitable for medium to heavy elements, and ion-beam analysis is preferred for lighter elements (Table 3). Both techniques present better results when the measurements are made in a vacuum, although the risk of loss of some semi-volatiles is present (Janssens, 2013, Reyes-Herrera et al., 2015). Despite the similarity of the advantages and disadvantages of both techniques, PIXE is less expressive in research output compared to EDXRF in the last 15 years (See Figure 2 and Table 2 of the Supplemental Material). This trend can be associated with the easy operation and relatively low cost of EDXRF since sensitivity is similar to both techniques.

Particle-induced γ-ray emission (PIGE) theory is based on a projectile penetrating deep into the target nucleus producing long-lived excited states that usually decays with an emission of a gamma photon with well-known energies, typical widths in the order of 10−3 eV, which can be used for the determination of elemental composition of the samples. PIGE is a multi-elemental and non-destructive technique (Li et al., 2012; Zucchiatti and Redondo-Cubero, 2014) that uses excitation of gamma-rays performed by protons of 3 MeV or higher to increase the analyzed sample depth to about 100 μm. PIGE is an excellent technique applied for the determination of light elements such as Li, Be, B, C, O, F, Na and Mg (Allegro et al., 2016; Janssens, 2013), although it can also be used to detect heavier elements with appropriate nuclear reactions (Allegro et al., 2016). PIGE has high DLs with typical values in the order of tens of ppm. The loss of semi-volatiles elements and compounds when in a vacuum and the possibility of resonance must be considered (Allegro et al., 2016; Carmona et al., 2010; Csedreki and Huszank, 2015; Nayak and Vijayan, 2006; Zucchiatti and Redondo-Cubero, 2014).

Particle Elastic Scattering Analysis (PESA) with MeV energy proton beams is based on the detection of protons elastically scattered by the target nuclei in the forward directions, allowing quantitative information of C and other low-Z atoms like H, N and O (Chiari et al., 2015, 2004). Therefore, PESA is a multi-elemental technique used mainly for the determination of light elements. However, the estimation of organic matter by carbon combustion from quartz filters and estimation of organic matter by hydrogen in PM on Teflon filters is feasible, assuming the chemical states of sulfates and nitrates (Cahill et al., 1996; Malm et al., 1994; Wilson et al., 2002). Besides estimation of organic matter, other negative features associated to PESA are its application to only low-Z ($Z < 8$) elements, detectors limited lifetime and the usage of Teflon filters for H

detection (Chiari et al., 2015, 2004; Trompetter et al., 2013; Zucchiatti and Redondo-Cubero, 2014).

Rutherford Backscattering Spectrometry (RBS) is an ion beam based technique applied for a solid matrix that can be used for the determination of light elements (Janssens, 2013), although RBS is reported as a good technique applied for heavy elements in the light matrix (Jeynes et al., 2012). Poor mass resolution and spectrum influenced by multiple scattering are others features of this technique (Bauer et al., 1992; Jeynes et al., 2012)

Instrumental Neutron Activation Analysis (INAA) is based on the bombardment of a sample by neutrons that irradiates and activates the sample. A nuclear reaction occurs between neutrons and sample isotopes producing radionuclides that emit characteristic gamma rays energy specific to each element (Brown and Milton, 2005, Wilson et al., 2002). INAA is a high sensitivity technique with negligible matrix effects, providing results down to ultra-low (sub-ppm) concentrations. Technically, INAA is a non-destructive technique, but in essence, some elements in the sample are transformed in radioactive isotopes, which turns unfeasible the use of the samples for any other analysis (Wilson et al., 2002). The use of nuclear reactors makes INAA an expensive technique, and measurement time can take several hours (Brown and Milton, 2005; Chow and Watson, 1998; Dogan and Kobya, 2006; Sánchez-Rodas et al., 2015; Wilson et al., 2002).

The main features of X-ray and ion beam-based techniques are summarized in Table 3.

Table 3. Summary of the most used **X-ray** and **ion beam** techniques for particulate matter characterization.

Technique		Analytical Information	Advantages	Disadvantages	Time*	Authors
Principal	Variant					
X-ray	EDXRF	Elemental	• Non-destructive; • Fast and multi-elemental analysis; • Wide range of Z; • No sample handling; • Applied for liquid matrices; • Equivalent DL to ICP-AES in vacuum medium; inexpensive.	• Matrix-effect interference; • Low sensitivity for low-Z elements: applied for Z >11; • Loss of mass and semi-volatile compounds in vacuum medium; • Homogeneous sample is mandatory.	L	(Yatkin and Gerboles, 2017) (Gredilla et al., 2016) (Reyes-Herrera et al., 2015) (Naseerutheen et al., 2014) (Okuda et al., 2014) (Janssens, 2013) (Yatkin et al., 2012) (Sitko, 2009) (Dogan and Kobya, 2006) (Brown and Milton, 2005) (Çevik et al., 2003) (Wilson et al., 2002) (Ekinci et al., 2002)
X-ray	WDXRF	Elemental	• Simultaneous detection mode; • High spectral resolution: Minimum peak overlaps • Low DL's: below ppm • Single analysis	• High power excitation to improve the sensitivity (sample heating and degradation); • Loss of mass and semi-volatile compounds in vacuum medium;	L	(Janssens, 2013) (Wilson et al., 2002) (Chow and Watson, 1998)

X-ray	TXRF	Elemental	• Multi-elemental; • High flux of X-rays: high sensitivity; • Improved DL's; • Negligible matrix effect; • Reduced background; small sample amount.	• Sample handling: risk of contamination; • Risk of saturation effects.	M	(Bilo et al., 2017) (Borgese et al., 2012) (Borgese et al., 2011) (Wagner and Mages, 2010) (Meirer et al., 2010) (Wagner et al., 2008) (Schmeling, 2004) (Wilson et al., 2002)
X-ray	SR-XRF	Elemental	• Multi-elemental; • Non-destructive, and fast analysis; • High sensitivity: DL's in the order of pg; • Minimum background; • Small amounts of sample required.	• Influenced by plural and multiple scattering.	L	(Zeng et al., 2013) (Lü et al., 2012) (Wilson et al., 2002) (Saisho, 1989)
Ion beam analysis	PIXE	Elemental	• Multi-element analysis; • Favors lighter elements quantification; • Wide range of Z; • No sample handling, • Non-destructive; • High sensitivity.	• Strong decrease in X-ray production cross sections for higher-Z: applied for Z>11; • Risk of loss of semi-volatile; Not for H, C, N, O; • Only for solid samples.	L	(Maenhaut, 2015) (Reyes-Herrera et al., 2015) (Maenhaut et al., 2011) (Carmona et al., 2010) (Calzolai et al., 2008) (Wilson et al., 2002) (Klockenkämper, 1987)
Ion beam analysis	PIGE	Elemental	• High sensitivity for light elements; • Multi-elemental analysis; • No sample handling; • Non-destructive; • Easy operation.	• Loss of semi volatile compounds under vacuum medium; • Resonance feature; • Mostly used as complementary technique for PIXE: applied for Z<17; • Only for solid samples; • High DL's: Tens of ppm	L	(Allegro et al., 2016) (Csedreki and Huszank, 2015) (Zucchiatti and Redondo-Cubero, 2014) (Li et al., 2012) (Carmona et al., 2010) (Nayak and Vijayan, 2006)
Ion beam analysis	PESA	Elemental	• Determination of light elements (e.g.: H, C, N, O); • Estimative of organic matter by hydrogen.	• Applied only to low-Z (<8) elements; • Limited lifetime of detectors; • Limited to Teflon filters for H detection.	L	(Chiari et al., 2015) (Zucchiatti and Redondo-Cubero, 2014) (Trompetter et al., 2013) (Wilson et al., 2002)
Ion beam analysis	RBS	Elemental	• High sensitivity for heavy elements in light matrices.	• Poor mass resolution; • Spectrum influenced by multiple scattering; • Applied only for solids.	L	(Jeynes et al., 2012) (Bauer et al., 1992)
Activation Analysis	INAA	Elemental	• High sensitivity; • Matrix independent.	• High analytical time and cost; • Sample handling; • Require nuclear reactor; • Destructive technique: Transform some elements in radioactive isotopes.	L	(Sánchez-Rodas et al., 2015) (Dogan and Kobya, 2006) (Chow and Watson, 1998)

*Time consuming: L (Low); M (Medium); H (High).

3.2.2.4 - Sample Preparation and Handling

Both ICP and AAS are destructive techniques that require complete sample digestion. Common procedure involves acid-digestion using HNO_3, HCl, HF, and H_2O_2 in combination with heat, either via hotplates or microwave digestion (Félix et al., 2015; Flament et al., 2008; Pan et al.,

2015; Rizzio et al., 2000). To remove organic coatings, when the sample is highly organic, it is advised to pre-treat the sample via heat (furnace at 400 ºC for 3h) prior to digestion step (Rastogi and Sarin, 2009). High temperatures (above 90ºC) must be avoided for Hg analysis by CVAAS due to the high volatility of Hg (Iqbal and Kim, 2016; Xiu et al., 2005). The sample preparation procedure for analysis by CE is the similar to the applied for ICP and AAS analysis, an acid digestion in HNO3/HF heated at 100ºC, followed by ultrafiltration or centrifugation of the resultant solution (Dabek-Zlotorzynska et al., 2003, 2002; Lara et al., 2016; Pacáková and Štulík, 2005).

X-Ray based techniques are non-destructive and require minimal sample handling. EDXRF, WDXRF, PIXE, PESA, and PIGE require no sample digestion and can analyze PM directly in filters. Improvements in the detection of lighter elements like Na and K can be achieved in vacuum medium, therefore, depending on the sampling strategy (powder or filters) is necessary some handling. Samples deposited on filters can be directly analyzed in vacuum, however, powder samples must be pressed into pellets. Although x-ray-based, TXRF requires sample digestion prior to analysis. The choice of filter medium must be careful because different digestion methods are necessary depending on the nature of the filter. Teflon, cellulose and polycarbonate membranes can be easily digested by conventional methods, filters made in quartz and glass fiber need aggressive acids (HF, *aqua regia, etc.*) followed by microwave or hotplate digestion (Schmeling et al., 1997; Szigeti et al., 2015).

INAA turns the sample useless for complementation by any other analytical technique since samples have to be pressed into polyethylene or quartz containers prior to analysis (Alves et al., 1998; Merešová et al., 2008; Voutsa et al., 2002).

3.2.3 Organic and Carbonaceous Techniques

This group comprehends several analytical methods for the identification of organic and elemental carbon in PM samples. There is a large list of techniques in this group, but here we will focus on the most commonly cited in the literature (GC-MS, TD/GC-MS, LC, IC, CE, and TOC). Organic chemical characterization techniques consist on the analysis of organic species (volatiles), elemental or black carbon (non-volatile) such as soot; and carbonaceous chemical characterization consisting mainly on the identification of carbonate species such as Na_2CO_3, $CaCO_3$, etc. Organic and elemental carbon is the major fraction of the total aerosol mass in the atmosphere at both rural and urban environment (Chow and Watson, 1998; Wilson et al., 2002; Yadav et al., 2013).

Gas Chromatography Mass Spectrometry (GC-MS) is an analytical technique using gas chromatography separation together with the concepts of the mass spectrometry for the identification of volatile organic species (Chauhan et al., 2014). GC-MS is widely used in the characterization of PM-bond hydrocarbons in health risk assessment as well as source apportionment studies, usually focusing on polycyclic aromatic hydrocarbons (PAH) and volatile organic compounds (VOC). PAH's are resistant to degradation in the environment, hence classified as persistent organic pollutants (POP), and can present toxic and carcinogenic hazard (Atkins et al., 2010; Chen et al., 2012; Gao et al., 2015; Gupta et al., 2011; Wnorowski, 2017; Wu et al., 2017, 2014). Volatilization and oxidative degradation of PAH's are some sampling artifacts that can occur when collected onto filters leading to masses loss. While volatilization is strongly influenced by sampling flow and meteorological conditions, PAH oxidative degradation is driven by homogeneous gas-phase reactions or heterogeneous reactions on aerosol particles in atmosphere, although this degradation can also occur after the filter deposition, initiating reactions among PAH's onto sampling substrates and oxidant gases in the atmosphere, like OH, NO_2, and mainly O_3 due to its proportion in the ambient (Balducci et al., 2017; Schauer et al., 2003). The use of O_3 denuders may minimize PAH oxidative degradation and volatilization without causing significant mass loss. However, PAHs in the gas phase were not able to be detected with denuder sampling system (Liu et al., 2014). Lastly, Ladji et al. (2014) showed that about 95% of PAH's are present in particles less than 3 µm. Therefore, in $PM_{2.5}$-bound PAH's characterization, special attention should be given to the sampling (pre-treatment of filters), handling (storage, weighing) and analysis (extraction/desorption).

The high selectivity, resolution, and sensitivity of this technique have made the GC-MS a favorite in PM's PAH analysis, preferred over techniques as Liquid Chromatography (LC) (Pandey et al., 2011; Poster et al., 2006). GC-MS is a highly sensitive and accurate technique that provides low DLs and has a wide organic species library, in which species can be identified with no need of certified reference materials (CRM's). However, quantification using internal standards or CRM's is mandatory. Co-elution is a common problem in GC analysis but can be corrected by adjusting a temperature ramp. GC-MS is a costly technique that involves complex analytical procedures, demanding therefore highly specialized manpower (Chauhan et al., 2014; Chen et al., 2013; Helmig, 1999; Liu et al., 2007; Pandey et al., 2011; Poster et al., 2006). Some GC-MS features can limit the application of this technique though:

- Samples must be humidity free and analytes must vaporize between 30ºC and 300ºC.

- Matrix effects are a concern and often separation and pre-concentration methods are required.

- An extraction step needs to occur prior to GC-MS analysis. For instance, there are several methods for the extraction of PAHs, including Soxhlet extraction, ultrasonic extraction, supercritical fluid extraction, microwave-assisted extraction and accelerated solvent extraction, all characterized using toxic organic solvents. Specifically, PAH extraction from the particles is time-consuming, labor intensive, expensive and may cause contamination resulting in erroneous results (Bates et al., 2008; Gil-Moltó et al., 2009).

Thermal Desorption GC–MS (TD-GC-MS) couples the GC-MS to a thermal desorption unit in which no sample preparation is required, providing an automated and more sensitive alternative to solvent extraction. TD-GC-MS can be employed for the extraction of volatile and semi-volatile species from adsorbing matrices, including PM onto quartz filters (Gil-Moltó et al., 2009, Bates et al., 2008). This technique requires no sample preparation and reduced sample mass, it is a technique that is solvent-free, fast, highly sensitive, and accurate technique, which allows for high-resolution at low detection limits (Hays et al., 2003; Mercier et al., 2012). The use of a thermal desorption unit decreases the time/cost of analysis and reduces the risk of analyte loss or sample contamination (Bates et al., 2008). TD-GC-MS validation is performed for PAHs using standard reference materials (SRM1649 – urban dust, SRM1650 – diesel PM, SRM2787 – PM_{10}, among others). The results are highly reproducible and accurate and were found to be equivalent to results obtained using thermal desorption with classical solvent extraction methods (Bates et al., 2008; Grandesso et al., 2013; Hays et al., 2003; Ho et al., 2008; Mercier et al., 2012; van Drooge et al., 2009).

Ion Chromatography (IC) is, in essence, a liquid chromatography technique applied to identify inorganic cations, anions and low molecular weight water-soluble organic acids and bases. IC analyses eluents carrying the sample through a solid stationary phase (a packed column), which according to the ionic affinity and ionic strength of the species in the eluent, creates a differential rate through the column according to each species (Shaw and Haddad, 2004). This technique promotes low DLs, no loss of hydrophilic or volatile compounds is expected, and no derivatization is required. Although the risk of contamination exists, since pre-treatment of the samples is mandatory, interference in analytical results is considered minimal. In fact, only very weakly dissociated acids have been reported to interfere with IC results (Fischer, 2002; López-Ruiz, 2000; Sarzanini, 2002; Shaw and Haddad, 2004).

Thermal–optical carbon (TOC) analysis is widely used for determination of PM organic carbon (OC) and elemental carbon (EC). Particularly, thermal/optical reflectance (TOR) and thermal/optical transmission (TOT) are used in the analysis of OC and EC respectively (Wilson et al., 2002). Thermal-optical methods have been developed for the analysis of EC and OC on glass or quartz fiber filters, as described by the protocols IMPROVE, NIOSH and CalTech (Watson et al., 2005). In the thermal-optical analysis, OC is volatilized in two steps: at 350°C in an O_2-He mixture and at 600°C in pure He. The volatilized OC is oxidized to CO_2, and then reduced to CH_4, measuring the concentration of the latter via flame ionization detector (FID). EC is converted to CO_2 in O_2-He atmosphere at 400, 500, and 600°C, and the CO_2 is measured by FID (Huntzicker et al., 1982). Overall, thermal-optical techniques provide good information about the carbonaceous fraction of the PM. This technique:

- Promotes the discretization of OC and EC, serving as a complementary technique for mass closure balance.
- It is destructive and some care must be taken cause the risk of pyrolyzed carbon formation during analysis. The authors also report that 10% to 70% of all PM mass is composed of EC and OC, however, this partitioning is highly influenced by the chemical composition and sources (Cheng et al., 2011, Watson et al., 2005, Wilson et al., 2002, Huntzicker et al., 1982).

Proton Transfer Reaction Mass Spectrometry (PTR-MS) is a technique developed by Lindinger and Jordan (1998) for detecting VOC's in ambient air. This technique connects the idea of chemical ionization (CI) and the flow-drift tube type (FDT) technique. The principle of the PTR-MS is based on the chemical ionization of a gas inside a drift tube, usually by proton transfer from H_3O^+. A proton transfer reaction between H_3O^+ and an organic specie (R) produces H_2O and a protonated organic RH^+ inside the drift tube assembly. A mass analyzer detects the organic RH^+ as a m/z value equal to the original mass of the organic (R) plus 1 (M+1). Quadrupole analyzers (PTR-MS) does not properly distinguish between species that occur at the same nominal m/z (Wallace et al., 2018). To contour this limitation Time-of-Flight (ToF) analyzers were coupled to PTR-MS system rising the PTR-ToF-MS instruments with improved mass resolution with typical values ranging from 4000 to 5000 m/Δm, been able to separate compounds differing by 0.01 Da. PTR-MS is highly sensitive, presenting DL's in ppbv and pptv (Lindinger and Jordan, 1998; Pallozzi et al., 2016). Nevertheless, adding a TD unit to the PTR-MS enables the analysis of PM-bound PAHs. Many aerosols compounds do not fragment, allowing the detection at their protonated mass. This combination has been used widely used in recent works have dealt with the

investigation of organic aerosols, particularly PAHs (Masalaite et al., 2017; Salvador et al., 2016; Timkovsky et al., 2015).

3.2.3.1 - Sample Preparation and Handling

From 2000 to the begin of 2010 decade the most used extraction method for GC analysis was Soxhlet. This extraction method is based on the solubilization and concentration of organic compounds sorbed onto PM samples using a Soxhlet extractor. High purity solvents (acetone, dichloromethane, petroleum ether, etc) extract organic compounds from the filter medium, the extracts are concentrated with a rotary evaporator and cleaned by filtration with silica gel (Callén et al., 2013; Esen et al., 2008; Gaga and Ari, 2011; Ho et al., 2009; Liu et al., 2007). In the last eight years, ultrasonic extraction is the most used extraction method for PM. In this method, an appropriated solvent (methanol, dichloromethane) into an ultrasonic bath that extracts the PAHs from the sample for a period of 10 to 30 min. After the ultrasonic treatment, extracts are concentrated using a rotary evaporator, followed by evaporation under N_2 stream (Atkins et al., 2010; Gao et al., 2015; Wu et al., 2014). TD-GC-MS requires no sample preparation prior to analysis.

Analysis by IC requires extraction and manipulation since ions must be extracted from the PM into solution prior to analysis. This processes is relatively simple and consists in extracting ions from PM by an ultrasonic bath in deionized distilled water (or IC eluent), followed by a filtration (0,45 µm) to remove insoluble residues (Brown and Edwards, 2009; Haddad, 1989; USEPA, 1999).

TOC analysis requires minimal sample preparation. For PM that has been sampled in filters, a fraction of the filters is inserted directly into the instrument. Otherwise, PM needs to be placed on a filter prior to analysis.

PTR-MS analysis requires no sample preparation since it works on-line or coupled to a TD unit.

The main features of organic and carbonaceous-based techniques are summarized in Table 4.

Table 4. Summary of the most used **organic and carbonaceous** techniques for particulate matter characterization.

Technique		Analytical Information	Advantages	Disadvantages	Time[a]	DL's[b]	Authors
Principal	Variant						
Chromatography	GC-MS	Organics	• High sensitivity and accuracy; • Low DL; • Wide library for organics.	• Analytical complexity and high cost ; • Sample handling; requires analytes with vapor pressure between 30 - 300ºC; • Need of sample free of H_2O and salts; • Specialized operation; • Co-elution possibility.	M/H	sub-ppb (ng g^{-1})	(Chauhan et al., 2014) (Chen et al., 2013) (Bates et al., 2008) (Liu et al., 2007) (Poster et al., 2006) (Helmig, 1999)
Chromatography	TD/GC-MS	Organics	• High sensitivity and accuracy; • Low DL; • Wide library for organics; • No sample extraction.	• Analytical complexity and high cost ; • Requires analytes with vapor pressure between 30 - 300ºC; sample free of H_2O and salts; • Specialized operation; • Co-elution possibility.	L	sub-ppb (ng g^{-1})	(Geldenhuys et al., 2015) (Chauhan et al., 2014) (Grandesso et al., 2013) (Chen et al., 2013) (Mercier et al., 2012a) (Gil-Moltó et al., 2009) (Bates et al., 2008) (Helmig, 1999)
Chromatography	IC	Organic (acids/bases) and Inorganic (ions)	• Low detection limits; • No derivatization is required; • No loss of very hydrophilic or volatile compounds.	• Sample pretreatment: risk of contamination; • Interferences from very weakly dissociated acids.	M	sub-ppb (ng g^{-1})	(Shaw and Haddad, 2004) (Sarzanini, 2002) (Fischer, 2002) (López-Ruiz, 2000)
Thermal–optical	TOT TOR	EC/OC	• Separation of organic and elemental carbon; • Complementary technique for full mass balance for aerosols.	• Destructive technique; risk of pyrolyzed carbon formation; • High influence of chemical composition and source of carbonaceous aerosol in OC/EC split.	M	0.2 µgC cm^{-2}	(Cheng et al., 2011) (Watson et al., 2005) (Wilson et al., 2002) (Birch and Cary, 1996) (Chow et al., 1993) (Huntzicker et al., 1982)
Proton Transfer	PTR-MS PTR-ToF-MS	Organics	• High sensitivity and accuracy; • Fast spectra acquisition; • Low DL's; • No sample handling	• Analytical complexity; • Need a complete raw database of reference spectra;	L	ppb [~4000][c]	(Guo et al. 2018) (Wallace et al., 2018) (Masalaite et al., 2017) (Palozzi et al., 2016) (Salvador et al., 2016) (Timkovsky et al., 2015) (Holzinger et al., 2010)

[a]Time consuming: L (Low); M (Medium); H (High).
[b]Typical values.
[c]Resolution in $m/\Delta m$.

3.2.4 Surface Analysis Techniques

Surface Analysis comprehends a group of techniques applied for the investigation of the chemical structure of a shallow layer of solid surfaces, in the order of a few nanometers. In this section, we

discuss the most cited techniques in the literature for characterization of atmospheric particulate matter such as XPS, XRD, SIMS, SEM, SPEEM, PEEM, Raman, Mössbauer and AES.

X-ray Photoelectron Spectroscopy (XPS) bombards the sample with X-rays, detecting the ejected inner-shell or core electrons (Bowsher and Nichols, 1990). XPS gives information about particulates' outer surface and enables significant information concerning PM source (Gilham et al., 2008) as it allows the identification and relative concentration of elements and compounds including their chemical and electronic states of the core-ionized atoms (Corcoran et al., 2010; Papp and Steinrück, 2013; Qian et al., 2015). XPS is a non-destructive technique that requires no sample handling and has been used to identify (or quantify) light elements. Counterpointing other surface techniques like SIMS and SEM, XPS does not require a conductive surface, preserving the sample for later use. The classification of different functional carbon groups is another expressive feature. Some limiting features about XPS consist of the risk of thermal effects damage on the sample and the altering of atomic/molecular structures. In addition, it gives only information about the surface in order of 10 nm of depth. XPS presents slow acquisition and needs a complete database of reference spectra. Some difficulties in analysis of trace elements and chemical mapping of PM_{10} have been reported in the literature (Corcoran et al., 2010; Elmes and Gasparon, 2017; Gilham et al., 2008; González et al., 2016; Guascito et al., 2015; Huang et al., 2017; Papp and Steinrück, 2013; Qian et al., 2015).

X-ray Diffraction (XRD) is based on the principle that different crystalline structures in state solid materials diffract X-rays in different directions and intensities, allowing the identification of their crystal structure (Cienfuegos and Vaitsman, 2000). XRD is a non-destructive technique with high penetration power (in general up to 15µm) and negligible multiple scattering effects, which provides information about structural parameters. If the elemental composition is known, XRD can determine the fingerprint of the mineral (Chen, 1996; Choung et al., 2016; González et al., 2016). XRD requires relative large amounts of sample (≥100mg), although the use of Synchrotron Radiation X-ray Diffraction (SR-XRD) can work around this limitation. If the chemical elements of some compounds are known, the advantage to use XRD as a structural characterization technique is that it is possible to identify, allotropic, amorphous and nanostructured compounds, as consequence, it is possible to correlate with the synthesis processes, natural or industrial. Several works have been reported the application of XRD in PM characterization aiming source apportionment (Ahmady-Birgani et al., 2015; Bernabé et al., 2005; González et al., 2016; Jancsek-Turóczi et al., 2013; Satsangi and Yadav, 2014; Song et al., 2014).

Secondary Ion Mass Spectrometry (SIMS) is a surface technique in which secondary electrons, Auger electrons, photons, neutrons, and excited neutrals as well as positively and negatively charged secondary ions are formed if a surface is bombarded with a beam of positively charged primary ions (although only the secondary ions are detected by a mass spectrometer) (Janssens, 2013). Two types of SIMS are used to characterize PM: the time-of-flight secondary ion mass spectrometer (ToF-SIMS) and the nanoscale secondary ion mass spectrometer (NanoSIMS), both with distinct characteristics related to the primary ion beam and mass detector (Huang et al., 2017). SIMS can provide qualitative images of the ions with high sensitivity and lateral resolution. Low DLs for all elements are acquired at ppb level, including measurements of isotopic ratios. The fragmentation mechanism of SIMS turns data interpretation difficult, requiring complex data analysis by multivariate methods. Matrix effects can also make it difficult for quantification (Amstalden van Hove et al., 2010; Huang et al., 2017; Qian et al., 2015; Seebauer and Barlaz, 2016; Zhang et al., 2016).

Scanning Electron Microscope Equipped with an Energy-Dispersive X-Ray (SEM-EDX) is an analytical technique widely used to provide combined information about the physical, morphological and chemical properties of solid-phase particles (Janssens, 2013; Sobanska et al., 2003). SEM-EDX can provide information about mineralogical phases of individual particles, using small sample amounts. This is a common technique to use to infer PM sources (Cong et al., 2008; Conner and Williams, 2004). Automated systems for individual particle analysis can reduce the operational costs. SEM-EDX can only provide semi-quantitative results, with loss of sensitivity for low-Z elements (Z < 11). Electrons lose intensity while traveling through air, so SEM-EDX systems usually are vacuum-based instruments. This is a problem for sample reuse, since vacuum may cause loss of semi-volatile species during analysis (Bowsher and Nichols, 1990; Elmes and Gasparon, 2017; Pachauri et al., 2013; Qian et al., 2015).

Scanning Photoelectron Microscopy (SPEM) and Photoemission Electron Microscopy (PEEM) are based on the interactions between specimen surfaces and photons from a light source. The result of that interaction is the emission of photoelectrons and subsequent analysis by a detector. Both techniques provide information about the chemical bonding and surface images using different analytical modes, including high spatial and energy resolutions that improve the quality of the information from the top few nm of the sample surface. The techniques can separate the imaging and chemical information and have an independent optimization of energy resolution. Only information from the top few nanometers of the sample is given and some analytical parameters are required like a high vacuum, sample flatness, and semi-conducting characteristics (Qian et al., 2015).

RAMAN is based on the inelastic scattering characteristic when a monochromatic beam of light passes through a medium or sample (Qian et al., 2015). RAMAN can give PM analytical information concerning the molecular, structural and electronic state of organic and inorganic species. The main features of RAMAN concern: (i) sample preservation (non-destructive technique) requiring no sample handling; (ii) easy operation and high spatial resolution. Although the low sensitivity demand for samples with high concentration; and (iii) complex data interpretation (Bumbrah and Sharma, 2016; Cardell and Guerra, 2016; Chou and Wang, 2017; Gredilla et al., 2016; Kudelski, 2008; Qian et al., 2015).

Mössbauer spectrometry is element sensitive technique, however, is limited taken into account that the sample must present elements as Fe, Sn or In. This technique is based on the quantum mechanical "Mössbauer effect", that establishes a non-intuitive link between nuclear and solid-state physics, measuring the spectrum of energies at which specific nuclei absorb γ rays (Fe, Sn or In). This technique provides unique measurements of electronic, magnetic, and structural properties within materials, giving quantitative information on "hyperfine interactions," which are small energies from the interaction between the nucleus and its neighboring electron. If more than one crystallographic phase is present in a material containing ^{57}Fe or ^{119}Sn, it is often possible to determine the phase fractions at least semi-quantitatively (Fultz, 2011). Mössbauer spectrometry is a widely used technique for the identifying iron compounds speciation in PM (Dedik et al., 1992; Elzinga et al., 2011; Harchand and Raj, 1993), including its quantification (Kopcewicz et al., 2015). Mössbauer also gives information about the size distribution of iron-containing particles. Some features can limit the use of this technique, as it requires significant sample mass and long-time measurements to obtain good spectra and it is usually used only for Fe content analysis (Kopcewicz et al., 2015).

Auger Electron Spectroscopy (AES) is based on the bombardment of electron beams impinging on atomic, molecular or solid-state targets to investigate the electronic structure or to provide chemical maps of the surface of materials. AES is highly sensitive for Low-Z elements, although presents poor sensitivity for elements with $Z > 35$. AES is a valuable tool for the study of complex surfaces providing chemical maps. However, data is difficult to interpret because of the broad form of the Auger electron emissions (Bowsher and Nichols, 1990; Grekula et al., 1986; Taioli et al., 2010).

3.2.4.1 Sample Preparation and Handling

XPS, AES and Mössbauer techniques requires minimal sample preparation. In XPS and Mössbauer analysis, samples in powder or deposited on filters can be analysed directly in the instrument (Cheng et al., 2013; Gilham et al., 2008). AES requires that PM be pressed into a pellet (Theriault et al., 1975; Wieser et al., 1980).

XRD requires minimal sample preparation. For powdered samples, particles need to be grinded to a size below $100 \, \mu m$. As for samples placed in filters, no sample preparation is need. Nevertheless, filter/membrane composition is key to achieve optimal spectra. Silver membranes, cellulose esters membranes, and polyvinyl chloride membranes are the most suitable filters medium for analysis by XRD (Chow and Watson, 1998).

Analysis by SIMS requires some preparation and handling. Filter composition can interfere with the analysis and a reasonable comprehension about the matrix effects must be considered when choosing filter medium. Insulating filters, as conductive filters, can be applied for ToF-SIMS equipped with an electronic flood gun without coating. This can preserve the sample for future analysis by other techniques. However, for analysis performed by NanoSIMS a thin layer layer of carbon, gold or platinum as pre-coating is required for insulating samples (Huang et al., 2017; Qian et al., 2015; Zhang et al., 2016).

Typical sample preparation requirements for soils and powders consist of polished thin sections to be used in SEM analysis. Since the majority of PM is already collected in filters, polycarbonate and cellulose esthers membranes are the most recommended. In both cases, bulk or filter, a coating with a thin layer of gold or carbon is mandatory to avoid charging effects (Chow and Watson, 1998; Pachauri et al., 2013; Qian et al., 2015).

The main features of surface sensitive-based techniques are summarized in Table 5.

Table 5. Summary of the most used **surface sensitive** techniques for particulate matter characterization.

Technique		Analytical Information	Advantages	Disadvantages	Time [a]	DL's [Resol.][b]	Authors
Principal	**Variants**						
Surface Sensitive Analysis	XPS	Elemental Compounds (organic and inorganic); Electronic structure; Photoelectron images	• Non-destructive; • No sample handling; • Chemical structure and bonding information; • Applied to light elements; • Classification of different functional carbon groups; • Does not require conductive surface.	• Thermal effects can damage the sample and alter atomic/molecular structures; • Slow acquisition; • Only information about surface in order of 2 nm of depth; • Need a complete database of reference spectra; • Difficult in the analysis of trace elements and chemical mapping of PM<10μm.	M	0.1 atm%. [20-100 eV]	(Elmes and Gasparon, 2017) (Huang et al., 2017) (González et al., 2016) (Guascito et al., 2015) (Qian et al., 2015) (Cheng et al., 2013) (Papp and Steinrück, 2013) (Corcoran et al., 2010) (Gilham et al., 2008) (Bowsher and Nichols, 1990)
X-ray	XRD	Crystalline phase	• Non-destructive; • Provide information about mineral composition; • High penetration power; • Negligible multiple scattering effects.	• Relative large amount of sample; • Difficulty interpretation of data.	M	~1% [0.1-1 eV per step]	(Choung et al., 2016) (González et al., 2016) (Chen, 1996)
Surface Sensitive Analysis	SIMS	Image and spectral analysis of surfaces (organic and inorganic); Surface chemical reactions;	• Qualitative imaging; • Detection of all elements in ppb level; • Measurements of isotopic ratios; • High sensitivity and lateral resolution.	• Matrix effects make it difficult to quantify; • Require surface coating; • Complex data analysis by multivariate methods; • Intrinsically a destructive technique.	M	Sub-ppm [< 100 nm]	(Huang et al., 2017) (Seebauer and Barlaz, 2016) (Zhang et al., 2016) (Qian et al., 2015) (Amstalden van Hove et al., 2010)
Surface Sensitive Analysis	SEM/EDX	Elemental Morphology	• Characterization of mineralogical phases for individual particles; • Small sample amounts; • Automated system for individual particle analysis.	• Limited surface information due to electrons penetration in order of μm; • Semi-quantitative analysis; • Loss of semi-volatile species under vacuum; • Loss of sensitivity to low-Z elements (Z<11).	M	0.1 % [20 nm] [~150 eV]	(Elmes and Gasparon, 2017) (Huang et al., 2017) (Qian et al., 2015) (Pachauri et al., 2013) (Bowsher and Nichols, 1990)
Surface Sensitive Analysis	SPEM	Chemical bonding, surface images	• High spatial resolution; • Separated imaging and chemical information; • Independent optimization of energy resolution.	• Information only from the top few nm of the sample; • Need of high vacuum, sample flatness, semi-conducting characteristics.	L	[0.2 e V]	(Qian et al., 2015) (Abyaneh et al., 2011)
Surface Sensitive Analysis	PEEM	Chemical bonding, surface images	• Non-destructive, • High lateral resolution.	• Information only from the top few nm pf the sample.	L	[40–100 nm]	(Qian et al., 2015) (Peles and Simon, 2009)

Surface Sensitive Analysis	RAMAN	Molecular, structural and electronic (organic/inorganic)	• Non-destructive; • No sample handling; • Easy operation; • High spatial resolution.	• Low sensitivity; • Need of high concentration; • Difficulty interpretation of data for quantitative analysis.	L	Sub-ppm [2-10 cm^{-1}]	(Chou and Wang, 2017) (Gredilla et al., 2016) (Cardell and Guerra, 2016) (Bumbrah and Sharma, 2016) (Kudelski, 2008)
Surface Sensitive Analysis	Mössbauer	Chemical, structural, size, magnetic and time-dependent properties	• Provide information about the size distribution of iron-containing particles.	• Significant sample mass is need; • Require long-time measurements for good spectra; • Must be used only for Fe, Sn and In content analysis.	M	---	(Kopcewicz et al., 2015)
Surface Sensitive Analysis	AES	Elemental, electronic structure, chemical maps	• Sensitive for Low-Z elements; • Study of complex surface.	• Data are difficult to interpret because of the broad form of the Auger electron emissions; • Poor sensitivity.	M/H	0.01-0.1 atm%	(Taioli et al., 2010) (Bowsher and Nichols, 1990) (Grekula et al., 1986)

[a] Time consuming: L (Low); M (Medium); H (High).
[b] Typical values for DL's and [resolution].

3.2.5 On-line Particle Analysis Techniques

This analytical group comprehends techniques able to collect and measure PM and gases with a temporal resolution of less than 1 hour, providing a real-time chemical characterization of the atmosphere. On-line techniques provide high temporal resolution, although measurements at different locations can be a challenge due to logistics. The high costs of the instruments is also a limiting factor.

Aerodyne Aerosol Mass Spectrometer (AMS) can quantify the mass distribution and chemical composition of volatile and semi-volatile fine PM with high time resolution and detection limits in the order of µg m^{-3} (Allan et al., 2003). Refractory PM components like soot, fly ash and metals are not detected in AMS systems, limiting its application to non-refractory compounds like sulfate, nitrate, ammonium, chloride, and organics. The principle of AMS is based on the thermal ultra-high vacuum vaporization of PM and gases inside a tungsten vaporizer (400-600 ℃), followed by vapor molecules ionization by a 70 eV electron impact (EI) ionization source. Lastly, ions are quantified via mass spectrometry(Allan et al., 2004, 2003; DeCarlo et al., 2006; Elmes and Gasparon, 2017; Li et al., 2017). AMS is equipped with two detectors, a quadrupole (Q-AMS) and a Time-of-Flight (ToF-AMS), working alternately. In the MS mode, the average mass concentration of non-refractory species is determined, while in ToF mode the mass distribution associated with a specific chemical compound is monitored. The development of HR-ToF-AMS has improved the resolution allowing the separation of several ions from inorganic and organic species with the same nominal m/z (Allan et al., 2004, 2003; DeCarlo et al., 2006).

Single Particle Mass Spectrometers (SPMS) is based on particles' desorption and ionization by laser vaporization (Elmes and Gasparon, 2017; Li et al., 2017), branching into several other techniques such as ATOFMS, PALMS, LAMPAS, RSMS, LIBS, NAMS, SPAMS, SPLAT. Due to the limited information available on these techniques, we will expand ATOFMS and PALMS in this review.

Aerosol Time of Flight Mass Spectrometer (ATOFMS) is an SPMS variant technique employed to characterize the size and chemical composition of individual particles. ATOFMS is based on the desorption and ionization of fine PM (0.1 to 3 µm) through a narrow particle beam into a pulsed light scattering region. Particles velocity is determined by measuring the distance between two scattering lasers (Ar and He lasers) since velocity and size of the particles are directly related. A ToF analyzer separates the ions according to different m/z, generating a mass spectrum. ATOFMS provides qualitative information since laser ablation/ionization cause peaks intensity to vary greatly from shot to shot, not corresponding to the compound mass. Nevertheless, the particle number is a quantitative information (Elmes and Gasparon, 2017; Li et al., 2016; Monkhouse, 2011; Prather et al., 1994; Rodríguez et al., 2012).

Particle Analysis by Laser Mass Spectrometry (PALMS) provides a positive or negative mass spectrum for individual particles larger than about 200 nm in diameter. Particles are introduced to PALMS via a nozzle under high vacuum, where they cross a He-Ne laser beam. When particles reach the He-Ne laser beam, scattered lights triggers an excimer laser that shoots on the particles and start molecules' desorption and ionization. A ToF detector analyzes and generates the ion spectrum (Murphy and Thomson, 1995). PALMS has been used to characterize mercury in the PM and mineral composition of dust (Gallavardin et al., 2008; Murphy et al., 2006).

Several variant techniques derived from SPMS are described in the literature like LAMPAS, RSMS, LIBS, NAMS, SPAMS, SPLAT, and others. Few sources of information about these techniques are found in the literature. However some discussion can be found in the works presented by Li et al., (2017), Elmes and Gasparon (2017), Rodríguez e al., (2012), Monkhouse (2011), and Nash (2006).

The main features of surface sensitive-based techniques are summarized in Table 6.

Table 6. Summary of the most used **on-line particle analysis** techniques for particulate matter characterization.

Technique		Analytical Information	Advantages	Disadvantages	Time [a]	DL's [Resol.][b]	Authors
Principal	Variants						
AMS	Q-AMS	Nº particles Mass Organics Ions	• High mass resolution; • Low DL's.	• Destructive; • Limited to non-refractory compounds; • High cost; • Complexity in operation and maintenance. • Incomplete mass spectra;	L	---	(Li et al., 2017) (Elmes and Gasparon, 2017) (DeCarlo et al., 2006) (Allan et al., 2004, 2003)
3.AMS	ToF-AMS	Nº particles Mass Organics Ions	• High mass resolution; • Low DL's.	• Destructive; • Limited to non-refractory compounds; • High cost; • Complexity in operation and maintenance. • Incomplete mass spectra;	L	---	(Li et al., 2017) (Elmes and Gasparon, 2017) (DeCarlo et al., 2006) (Allan et al., 2004, 2003)
SPMS	ATOFMS	Nº particles Mass Organics Ions Metals	• Real-time size and chemical composition; • Capabilities from 100 nm to 3 µm; • Applied for refractory and non-refractory compounds.	• Destructive; • Expensive; • Complicated data processing;	L	Not Applied	(Elmes and Gasparon, 2017) (Li et al., 2016) (Rodríguez et al., 2012) (Monkhouse, 2011) (Prather et al., 1994)
SPMS	PAMLS	Metal Ions Biomass burning particles	• Capabilities from 150 nm to 3 µm; • Applied for refractory and non-refractory compounds.	• Destructive; • Expensive; • Qualitative information	L	[40 m/Δm]	(Elmes and Gasparon, 2017) (Gallavardin et al., 2008) (Murphy et al., 2006) (Murphy and Thomson, 1995)

3.3 Outlook

There are myriad techniques available to analyze solid-particulate matter. A thorough search of the literature can provide information on the latest instruments and techniques used in disciplines as varied as atmospheric sciences, soil sciences, geosciences, medicine, among others. Cutting-edge research continues pushing the techniques further with the development of new detectors, sampling methods and hyphenated techniques. Laboratories are normally limited to the in-house available techniques, but there is always a question about which is the best analytical technique to properly characterize a specific sample for a specific experimental work. Experienced lab users know that there is not an easy and definitive answer.

This review shows ICP-MS as the most used technique for metallic characterization of atmospheric PM, although the application of EDXRF has increased along last two decades, driven

mainly by easy operation and low cost, surpassing, since 2003, the number of studies using PIXE. Among all techniques applied for the characterization of metallic composition of atmospheric PM, X-ray based techniques show themselves as a useful tool, preserving samples for future replicates and reducing the risk of contamination due to minimal manipulation. At last decades, the organic characterization of PM-bond hydrocarbons is still dominated by chromatographic techniques, mainly GC-MS, preferred over liquid chromatography. No great changes in methodologies and techniques were realized in this field, expected by the advent of mass spectrometers. However, the development of thermal desorber units coupled to GC-MS has improved the sample preparation step, requiring no extraction processes, minimizing the risk of contaminations and loss of compounds, with similar statistical assurance to classical extraction methods such as Soxhlet or microwave digestion. PTR-MS has shown a new trend and efficient alternative for PM organic speciation, with both low DL's and high resolution. Information about the chemical structure of a shallow layer of solid surfaces can be achieved by surface analysis techniques such as XPS, XRD, SIMS, SEM, SPEEM, PEEM, Raman, Mössbauer and AES. For a thorough information about PM composition, XRD shows better features when compared with the others techniques. XRD, especially SR-XRD, can give a structural characterization enabling to identify, allotropic, amorphous and nanostructured compounds, as consequence, it is possible to correlate that information with the synthesis processes, being natural or industrial.

Since the 1990s, real-time measurements techniques have developed and presents new trends in PM characterization. AMS and SPMS based techniques have shown promising developments when applied to PM characterization. Currently, instrumental high costs are the main barrier to the application and expansion of this analytical group.

Off-line and On-line techniques are not mutually excluding but rather complementary in nature. On-line techniques show an improvement in PM characterization providing a quick (1 hour or less) and valuable information about the overall chemical composition of the atmosphere, important for local and regular air quality monitoring. However, when more information is necessary, like electronic state or crystal phase of the particles, off-line sampling instruments are able to collect several milligrams of particles for analysis. In addition, many off-line techniques are non-destructive, allowing the use of the same sample to analysis by other techniques. Therefore, as it happened with off-line techniques, the dissemination and development of on-line techniques can decrease the cost of the instruments, making the combined use of both, on-line and off-line, techniques feasible for a better understanding of local air pollution.

The specific choice among all techniques depends on the access to the available facilities, the costs associated with the acquisition of equipment, sampling and measuring time, among others considerations. Possibly, one of the most important parameters is the support of experienced and well trained technical support. We propose an analytical guide map in order to provide a guideline in the choice of the most appropriated technique for a given analytical information.

For this work, the investigation of the state-of-the-art allowed the construction of a decision tree (pg. 25) in which three analytical techniques were considered as the best-fit techniques for the purpose of this work, the Energy Dispersive X-ray Fluorescence (EDXRF), Synchrotron Resonant X-ray Diffraction (RSr-XRD) and the Gas Chromatography coupled to Mass Spectrometer (GC-MS). A detailed description of the fundaments of these techniques are shown below.

3.4 Fundaments of Analytical Techniques Applied in this Work

3.4.1 Energy Dispersive X-ray Fluorescence (EDXRF)

The X-ray are constituted of short wave electromagnetic radiation, between the ultraviolet and the gamma rays. The X-ray generation is achieved by the deceleration of high-energy electrons or the transition of electrons from the inner atoms orbitals and have a characteristic wavelength in the order of 10^{-5} Å to 100 Å. However, in conventional X-ray spectroscopy they do not vary from 0.1 Å to 25 Å (Cienfuegos and Vaitsman, 2000).
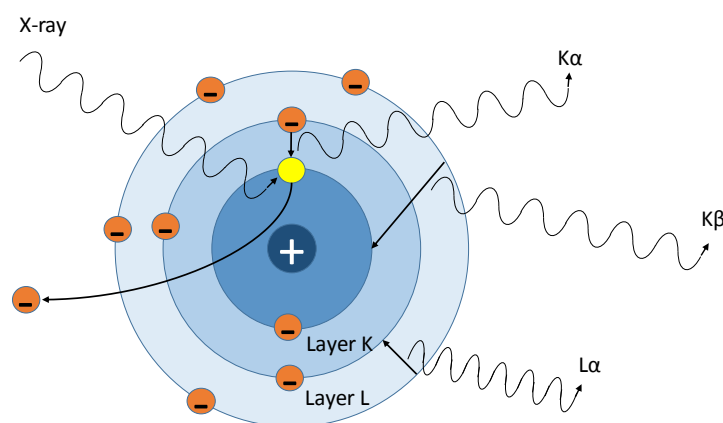
Figure 2. Energy transfer in the atom inner shell. Fluorescence principle.

In X-ray fluorescence, when atoms of a sample are excited by bombardment of high-energy electrons, or by primary X-ray, electrons are ejected from the innermost layers, creating in these atoms gaps in one or more orbitals, converting the atom into ions. The absorption of X-rays produces electronically excited ions that tend to return to their fundamental states, involving the transition of electrons from higher energy levels. This transition of electrons from outermost

orbitals as a way to return the ion to its ground state is characterized by the emission of secondary X-ray with characteristic wavelength for each element, in a process denominated fluorescence as shown in Figure 2 (Cienfuegos and Vaitsman, 2000; Holler *et al.*, 2009).

Each of the orbits corresponds to different energy levels, and the energy difference between the initial and final orbitals during the transition of the electrons is defined as the energy of the fluorescent photon (E). The energy (E) can be calculated by Equation 1,

$$E = \frac{hc}{\lambda} \tag{1}$$

Where, h is the Planck constant; c is the speed of light; and λ is the characteristic wavelength of each element.

The spectra of the X-ray line are products of the electronic transitions that occur in the innermost atoms orbitals. The higher energy K series is produced when high energy electrons collide on the electrons of the orbitals near the nucleus, removing them and resulting in the formation of excited ions, in which they emit X radiation at the moment the outer electrons of the orbital jump to the empty orbital (Holler *et al.*, 2009). The energy needed to eject an electron must be slightly larger than the emitted X-ray line itself, since the emission involves transitions of an electron of a higher energy level of the ion. The redistribution of the orbital electrons produces characteristic radiations, dependent on the original and final orbit, as shown in Figure 3.
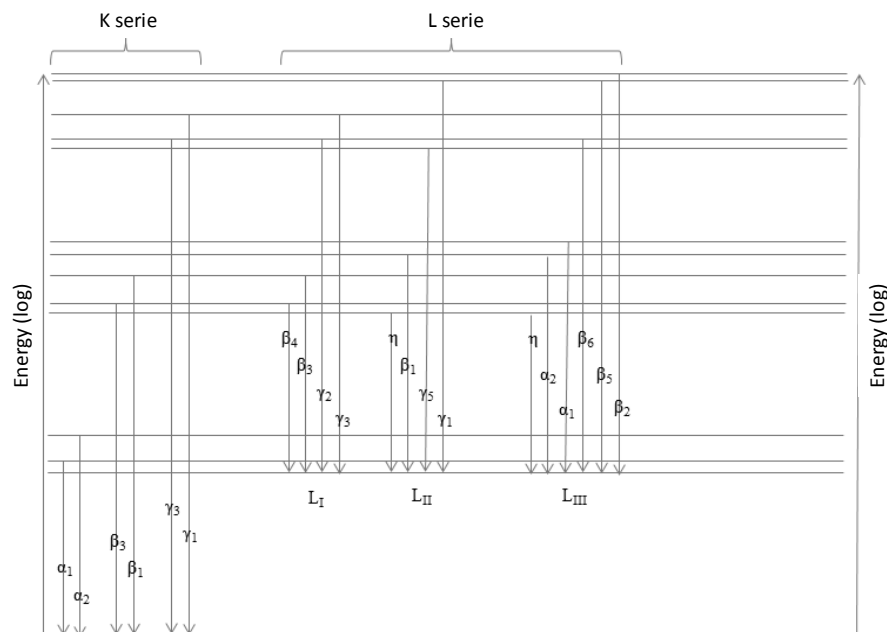
Figure 3. Energy levels diagram in the transition of electrons during X-ray production. Source. Adapted from Holler et al, 2009.

When fluorescence is generated by an X-ray tube, the operating voltage must be sufficient for the wavelength of the radiation is less than the absorption edge of the element whose spectrum must to be excited, as described by Equation 2.

$$E(keV) = \frac{12,4}{\lambda}$$

(2)

Where, the value 12.4 is a numerical constant.

X-Ray Fluorescence (XRF) is one of the techniques of X-ray spectrometry, while the EDXRF technique is one of the variant techniques of X-ray fluorescence.

3.4.2   X-ray Diffractrometry (XRD)

Crystalline materials diffract the X-rays in different directions and intensities, allowing the identification of their crystalline structure (Cienfuegos and Vaitsman, 2000). When X-rays colide on a material, the electrical vector of the incident radiation interacts with the electrons of the material producing a scattering, and a constructive or destructive interference may occur between the scattered rays. The interference is dependent on the distance between the spread centers and the wavelength number. When the difference between the scattering centers corresponds to an integer number of the wavelengths, there is a wave-in-phase scattering in which both mutually reinforce in a constructive interference called diffraction, as shown in Figure 4 (Cienfuegos e Vaitsman, 2000; Holler et al., 2009; Callister, 2009).
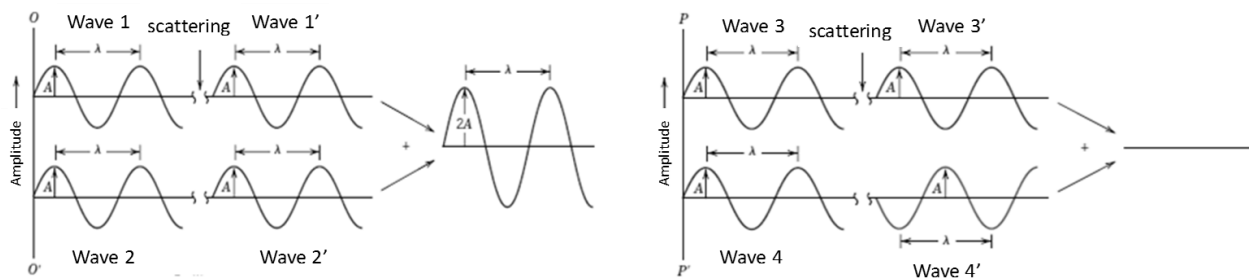
Figure 4. Diagram of (a) constructive and (b) destructive interference between waves. Source: Adapted from Callister (2009).

Focusing an X-ray beam on the surface of a crystal at an angle θ, a share of the beam is spread by the layer of atoms on the surface, the other non-scattered share goes to the next layer (or plane) of atoms, where part of the beam is spread, and so on. The Bragg's Law can be derived from a simple crystal with an atom at each point of a crystalline lattice, as shown in Figure 5.
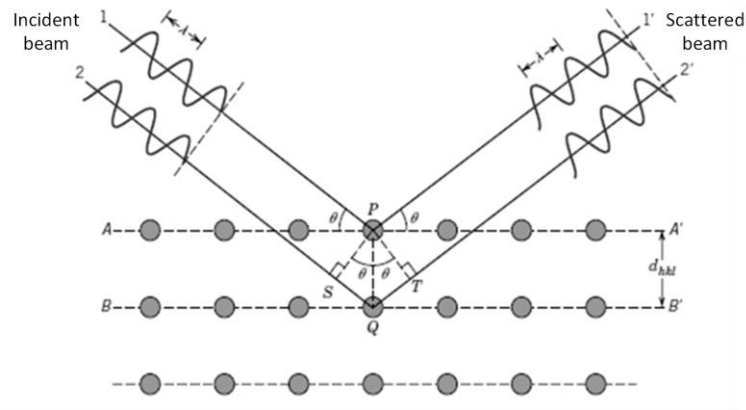
Figure 5. X-rays Diffraction on a plane of atoms. Source: Adapted from Callister (2009).

According to Hammond (2010), the distance between the waves scattered by the atoms of an adjacent crystalline plane (*hkl*) of interplanar spacing, d_{hkl}, is given by Equation 3.

$$SQ + QT = (d_{hkl}sen\theta + d_{hkl}sen\theta) = 2d_{hkl}sen\theta \tag{3}$$

Therefore, for constructive interference, (SQ + QT) is equal to $n\lambda$, so (3) can be expressed by the Bragg equation (4),

$$n\lambda = 2d_{hkl}sen\theta \tag{4}$$

Where, *n* is the order of diffraction, which must be an integer number.

X-rays will only be in phase if the angle of incidence satisfies the condition. For all other angles, there will be destructive interference (Holler et al., 2009).

The interplanar distance, d_{hkl}, is a function of the Miller indices (k, k and l) and lattice parameters (Equation 5),

$$d_{hkl} = \frac{a}{\sqrt{h^2 + k^2 + l^2}} \tag{5}$$

Where, *a* is the lattice parameter (edge length) of the unit cell.

3.4.3 Gas Cromatography coupled to Mass Spectrometer

Gas chromatography technique is based on the elution of the compounds present in a sample. After vaporization, the sample is introduced into a stream of gas (mobile phase) and the compounds are

forced by the gas through a column (stationary phase) by continuous action of the mobile phase, which results in a differential migration of these components, as shown in Figure 6 (Collins, 2011).
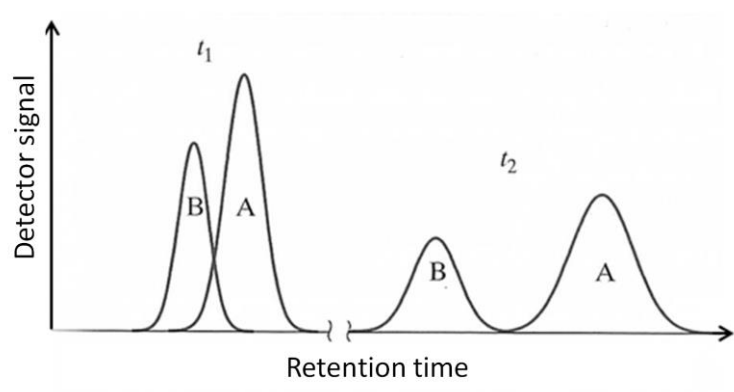
Figure 6. Scheme of different solutes migration through a column at different times, t_1 and t_2. Source: Adapted from Holler et al., (2009).

The compounds elution efficiency in a chromatographic column depends on the average velocity at which the solute migrates along the column, which in turn depends on the fraction of time the solute remains in the mobile phase, being lower for strongly retained solutes in the stationary phase, and higher when the solute has greater retention in the mobile phase. The velocity is a function of the distribution constants, K_c, for the reactions between the solutes and the mobile and stationary phases (Holler et al., 2009).

For low concentrations, the distribution constant K_c is given by Equation 6.

$$K_c = \frac{n_S / V_S}{n_M / V_M} \tag{6}$$

Where: n_S and n_M are the number of moles of the analyte in the stationary and mobile phases, respectively; and V_S and V_M are the volumes of the two phases.

However, K_c is not easily measured, and the concept of retention time, t_R, which is a function of K_c, is usually employed. Equations 7 and 8, respectively, give the linear mean velocity of solute migration across the column in cm.s^{-1} and the linear velocity of the mobile phase.

$$\overline{v} = \frac{L}{t_R} \tag{7}$$

$$u = \frac{L}{t_M} \tag{8}$$

Where: L is the length of the column filling; t_R is the retention time; and t_M is the empty time, which represents the time for a non-retained compound in the stationary phase to reach the detector.

Relating the rate of migration of the solute $\bar{v}$ with its distribution constant as a function of the linear velocity in the mobile phase, the retention factor, K_A, can be found by Equation 9.

$$K_A = \frac{t_R - t_M}{t_M} \tag{9}$$

According to Hoffmann and Stroobant (2007), the mass spectrometry principle consists in the ionization of compounds in the gas phase, with the production of a molecular ion (Equation 10).

$$M + e^- \longrightarrow M^{\bullet+} + 2e^- \tag{10}$$

Where: M represents a generic molecule.

The molecular ion is a radical that has the same molecular mass as the original molecule. Each ion formed from the molecular ion fragmentation can undergo successive fragmentations, being separated in the mass spectrometer according to its mass-charge ratio and detected as a function of its abundance. The production of molecular ions begins with the collision between molecules of the analyte and energetic electrons. The collision generates an excited state of the molecule, and its relaxation occurs by the fragmentation of the molecular ion into lower mass ions, as exemplified in the Figure 7 (Hoffmann e Stroobant, 2007; Holler *et al.*, 2009).
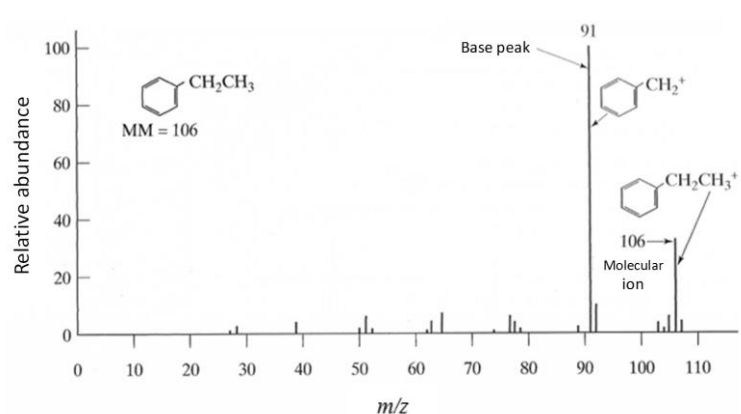
Figure 7. Mass spectrum of ethylbenzene. Source: Adapted from Holler *et al.*, (2009).

Mass analyzers have the function of separating the generated ions in the sources in function of their mass-charge (m/z) for further determination. There are several types of mass analyzers on the market, each with a technique or principle used in the generation of fields for the ions separation. Among the market-available mass analyzers, quadrupole analyzer is a device that uses

the stability of trajectory in oscillating electric fields to separate ions according to their mass/charge. Quadrupoles are composed of four rods of hyperbolic section, perfectly parallel. A positive ion entering the space between the rods will be drive to the negative rod. If the potential difference stabilizes before the ion discharges into the rod, it will change its direction and proceed to the detector, as shown in Figure 8.
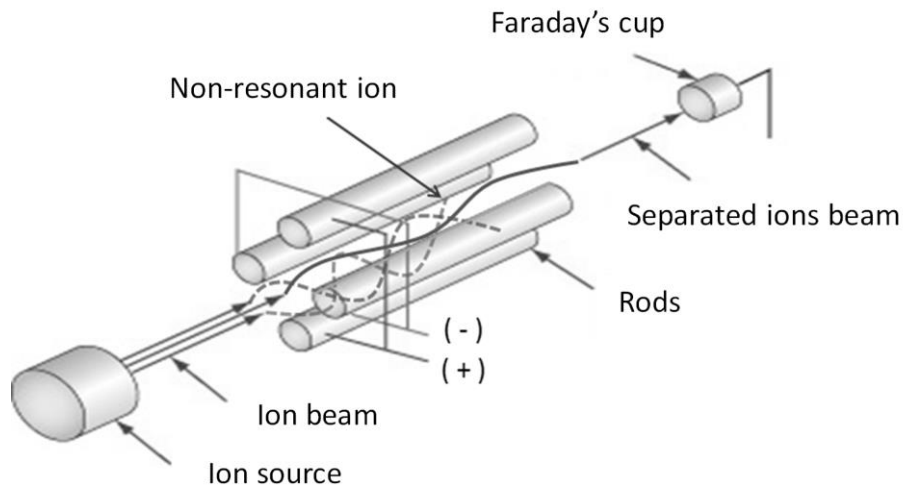
Figure 8. Scheme of a quadrupole analyzer. Source: Adapted from Kurt J. Lesker Company, 2016. Aviable at: http://www.lesker.com/newweb/technical_info/vacuumtech/rga_01_howrgaworks.cfm.

4. METHODOLOGY

4.1 Site Description

The Region of Greater Vitoria (RGV), state of Espírito Santo, southeast of Brazil (Figure 9), has a population of approximately 1.6 million inhabitants (IBGE, 2010). The RGV is a metropolitan urban-industrialized region with 717,000 vehicles and 88 industries registered as potential sources of air pollution (DENATRAN, 2018; IEMA/Ecosoft, 2011).

Figure 9. Region of Greater Vitória (RGV) (IJSN, 2017).

Among the industrial emissions, the mining and steel industries present the largest emissions of particulate matter and they are positioned very close together (E1 to E8 in Figure 12a). Steel production (7.5 million ton/year) causes emissions of approximately 150 kg h^{-1} de PM$_{10}$ and 90 kg h^{-1} de PM$_{2.5}$ from blast furnaces and steelmaking, coke ovens, sintering (stacks) and stockpiles. Mining production has an annual capacity of 332.4 million tons of iron ore and 36.7 million tons

of iron pellets, emitting approximately 330 kg h^{-1} of PM$_{10}$ and 150 kg h^{-1} of PM$_{2.5}$ from pelletizing furnaces (stacks) and stockpiles (IEMA/Ecosoft, 2011). The RGV has a port complex constituted by 8 terminals daily handling, charging and discharging iron ore, iron pellets, coal and others.

4.2 Climatology and Meteorology of the Region

The RGV climatological normal between 1961 and 1990 shows a short variability in the temperature of the region, ranging from 18.8 ℃ in July to 31.6 ℃ in February, with average value of 24.2 ℃. The RGV has climatological annual precipitation of 1252.3 mm. RGV shows two distinct periods, the dry period that occurs on winter (June to September), in which September is the drier month with precipitation of 40.3 mm, and the rainy period on summer (December to March) in which December has the largest precipitation with value of 175.8 mm (INMET, 2017).

During the sampling period, the total precipitation was 635 mm in which November was the rainiest period (280 mm) and January the drier period (57 mm). The sampling period had an irregular behavior compared to the climatological normal. Relative humidity show an average of 76% with maximum of 91% and minimum of 62% (Figure 10). Meteorological data was measured (average of 1h) by the surface meteorological station (SBVT) located in the airport of Vitória, ES, Brazil (WMS1 in Fig. 1a) and supplied by the *Centro de Previsão de Tempo e Estudos Climáticos* (CPTEC, 2017). The data was downloaded between October 18, 2016 and March 15, 2017.
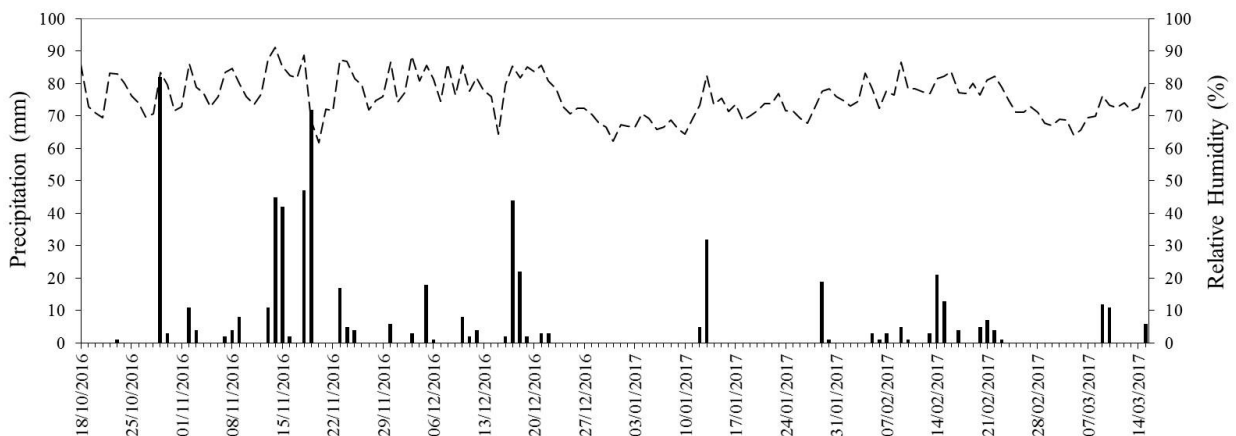
Figure 10. Times series during the sampling period (Octrober 2016 to March 2017) for precipitation (Solid columns) and relative humidity (dashed line). Source: Adapted from CPTEC (2018).

The wind pattern of RGV show prevailing winds from northeast (NE) quadrant with pronounced frequency of northwest (NW) winds in the months between January and March (Figure 11). The wind roses were generated by WRPLOT software (Lakes Environmental, Canada). The wind rose

for the first sampling period (October to December) used 1,536 observations and the wind rose for the second sampling period (January to March) used 1,416 observations.
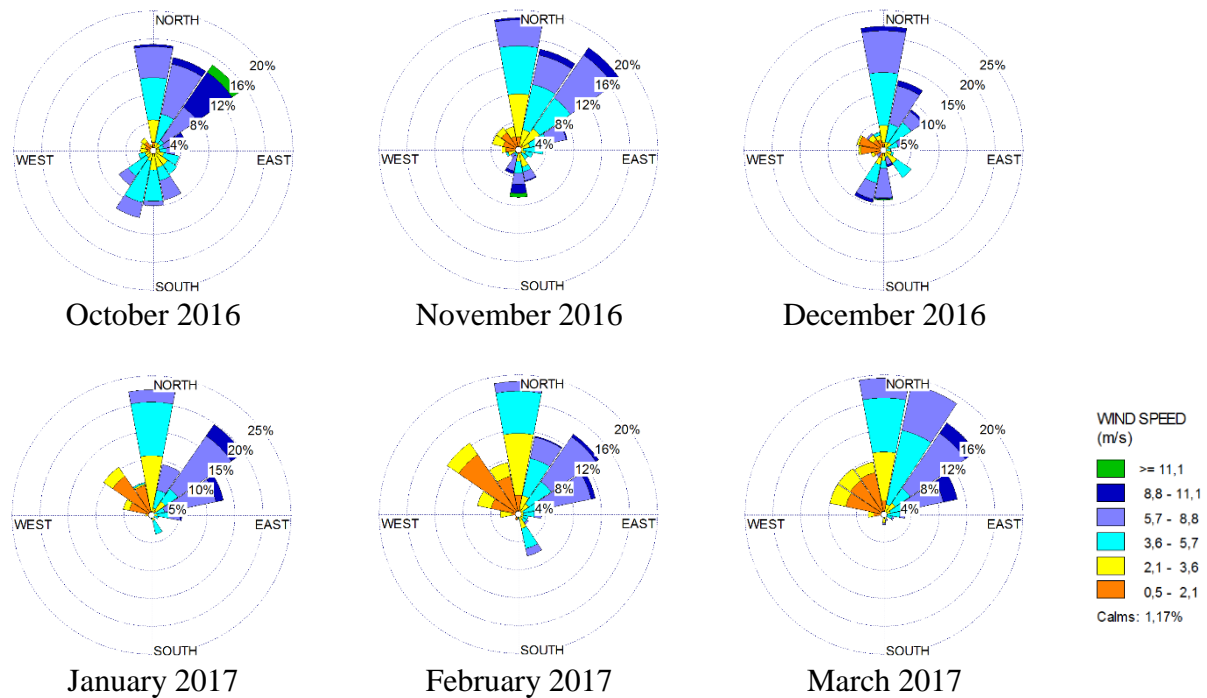
Figure 11. Wind roses (monthly) for the sampling period. Source: Adapted from CPTEC (2018) using WRPlot View. Available at: https://www.weblakes.com/products/wrplot/index.html.

4.3 Sampling Location

Settleable particulate (SP), total suspended particulate (TSP), PM less than 10 µm (PM_{10}) and PM less than 2.5 µm ($PM_{2.5}$) samples were collected at two sampling sites: M1 - Enseada do Suá (20°18′48.0″S; 40°17′26.7″W), and M2 - Ilha do Boi (20°18'39.39"S; 40°16'38.51"W) (Fig. 12a). Both sampling sites are directly influenced by emissions from E1-E7 due to the prevailing winds in RGV are from the Northeast (NE) quadrant, as shown in Figures 12c, and 12d.

230 samples were collected between October 2016 and March 2017. In 2016, from October 18 to December 21, 3 samples of SP, 33 samples of TSP, 33 samples of PM_{10}, and 33 samples of $PM_{2.5}$ were collected at M1. In 2017, from January 16 to March 15, 3 samples of SP, 30 samples of TSP, 30 samples of PM_{10} and 30 samples of $PM_{2.5}$ were collected at M2. 48 hour samples were collected by 6 Mini-Vol TAS samplers (Airmetrics, USA) operating at 5 L min^{-1}. All samples were collected on 47 mm PTFE filters (Whatman Inc, USA) previously equilibrated at a relative humidity between 30% and 40% (± 5%) and at a temperature between 20ºC and 23ºC (± 2ºC) for at least 24 hours (Chow and Watson, 1998) (Figure 13b).
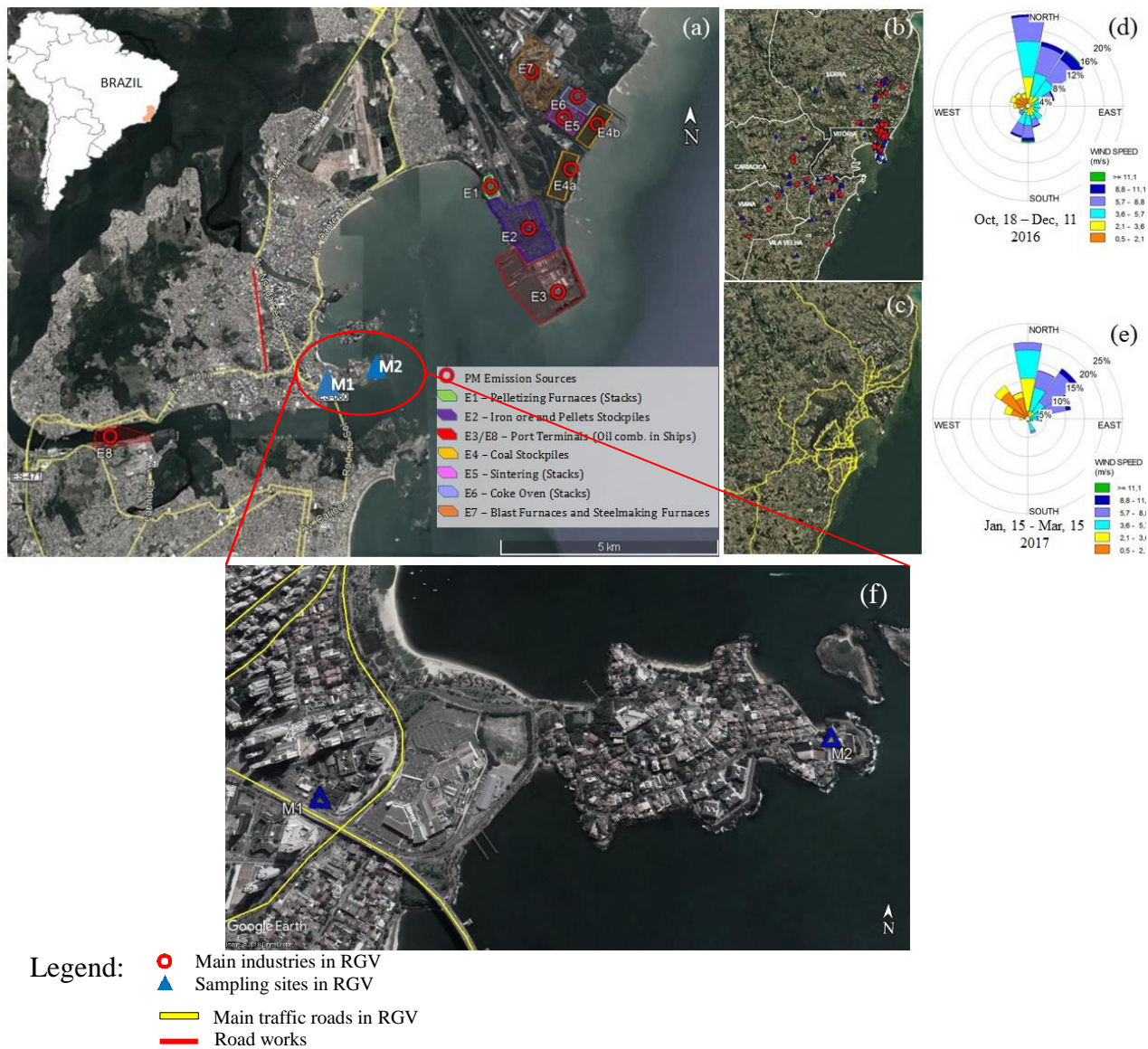
Figure 12. (a) Sampling sites locations and the main industrial sources, (b) main point and diffuse sources and (c) main traffic roads in RGV, (d) wind rose for the 1st campaign, (e) wind rose for the 2nd campaign, and (f) sampling sites. Adapted from Google earth, IEMA/Ecosoft (2011) and CPTEC (2017).

4.4 Instrumental Analysis

PM mass was determined gravimetrically. All filters were weighed in a microbalance model MSE6.6S (Sartorius, Germany), with a resolution of 0.001 mg, equipped with an ionizing blower model Stat-Fan YIB01-0UR (Sartorius, Germany) (Figure 13a).
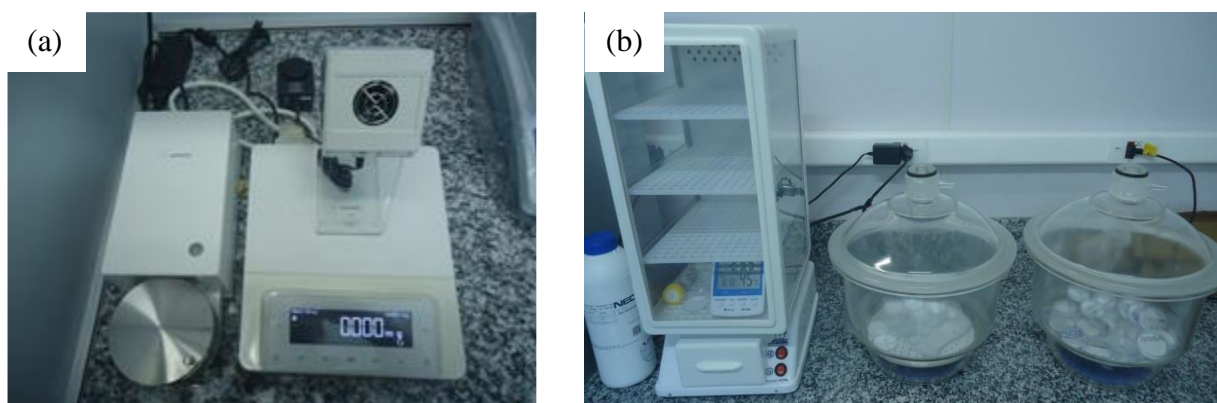
Figure 13. (a) Microbalance Sartorius MSE6.6S; (b) desiccator.

PM elemental analysis was determined by an Energy Dispersive X-ray Fluorescence Spectrometer (EDXRF) model EDX-720 (Shimadzu, Japan) (Figure 14). All samples were measured without any sample handling under vacuum (Galvão et al., 2018). EDXRF measurements were performed using a rhodium X-ray tube, 15-50 kV, resolution of 150 eV, 1000 (auto) µA, 1000 seconds of integration by channel and a Si(Li) detector. Blanks were also analyzed to evaluate analytical bias. The quantification was performed by calibration curves made by analysis of 47 certified reference materials (CRM) ranging from low-Z to high-Z elements (Na to Rg) deposited on thin mylar membranes with concentrations ranging from 40.3 to 58.8 µg cm^{-2} (Micromatter, USA).

Figure 14. EDX-720 (Shimadzu Corp. Japan). Laboratório de Poluição do Ar – UFES.

PAHs analysis was conducted by gas chromatography model Clarus 680 coupled to mass spectrometer model Clarus 600T (PerkinElmer, USA) (Figure 15a, b). The GC-MS is equipped with a thermal desorber unit (TD) model TurboMatrix 300 (PerkinElmer, USA) (Figure 15b) allowing the direct introduction of the quartz filters into the system for thermal desorption without any solvent extraction (Falkovich and Rudich, 2001; Ho *et al.*, 2008; van Drooge *et al.*, 2009; Grandesso *et al.*, 2013).
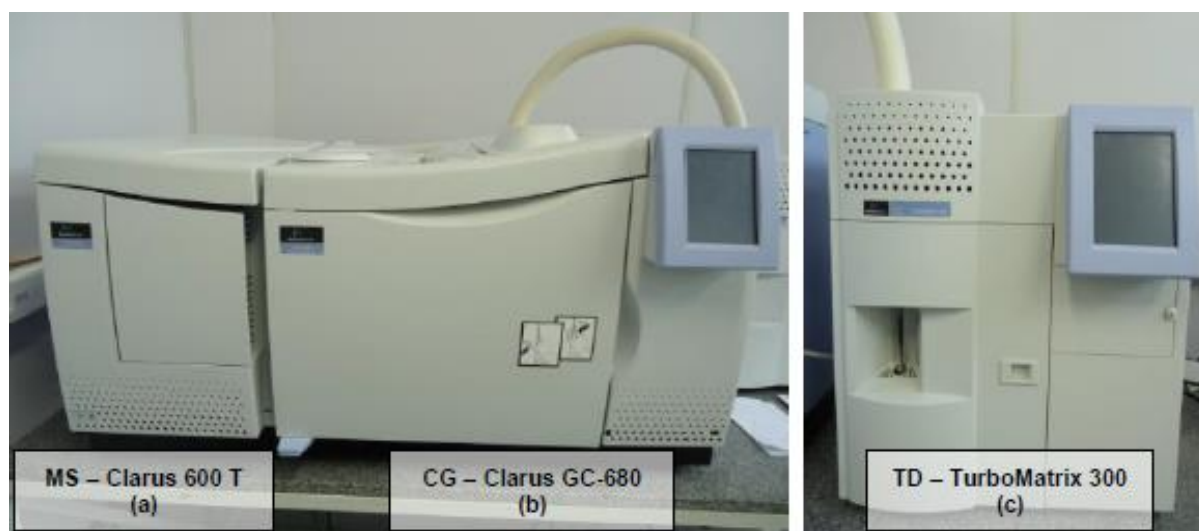
Figure 15. (a) Mass Spectrometer; (b) Gas Chromatograph; (c) Thermal Desorber. Laboratório de Poluição do Ar – UFES.

The GC-MS-TD system is equipped with a Elite-5MS column, 30 m x 0,25 mm id x 0,25 µm df (PerkinElmer, USA), and helium 6.0 as carrier gas at a flow of 1 mL min^{-1}. Prior to analysis, a half of quartz filters were cut and introduced into glass liners (90 mm x 4 mm id) previous cleaned at 350 ℃ for 3 hours under He stream of 20 mL min^{-1}. 16 priority PAHs were thermal desorbed at a temperature of 350 ℃ for 7 min under a He stream of 60 mL min-1, pre-concentrated at -20 ℃ in a trap glass tube filled with Tenax and heated at a rate of 100 ℃ s^{-1} injecting splitless into the capillary column for analysis. The oven ramp was initially set at 40 ℃ for 1 min, followed by a first ramp of 15 ℃ min^{-1} to 210 ℃ and a second ramp of 8℃ min^{-1} to 320 ℃ and held for 10 min. The detection was set in MS Scan mode (40 to 400 m/z).

Resonant X-ray diffraction (RSr-XRD) analysis was performed at the *Laboratório Nacional de Luz Synchrotron* (LNLS – Campinas, Brasil) (Figure 16). UVX-LNLS is a second-generation synchrotron source with 93.2 m of diameter that operates with the energy of 1.37 GeV, delivering approximately 4×10^{10} photons s^{-1} at 8 keV at the sample position. The injection system includes a 120 MeV linear accelerator and a Booster of 500 MeV, which operates with a current beam of 250 mA in *decay-mode* (Figure 17a). RSr-XRD analysis was performed at XRD1 Beam Line, an exclusive line dedicated to diffraction analysis in hard X-ray band of 5.5 to 14 KeV (Carvalho *et al*., 2017). XRD1 is equipped with a 3-circle powder diffractometer (Newport®, USA) and an MYTHEN 24K detector (Dectris®, USA) (Figure 17b).

Figure 16. UVX-LNLS - Second-generation synchrotron source at the *Laboratório Nacional de Luz Synchrotron* (LNLS – Campinas, Brasil).
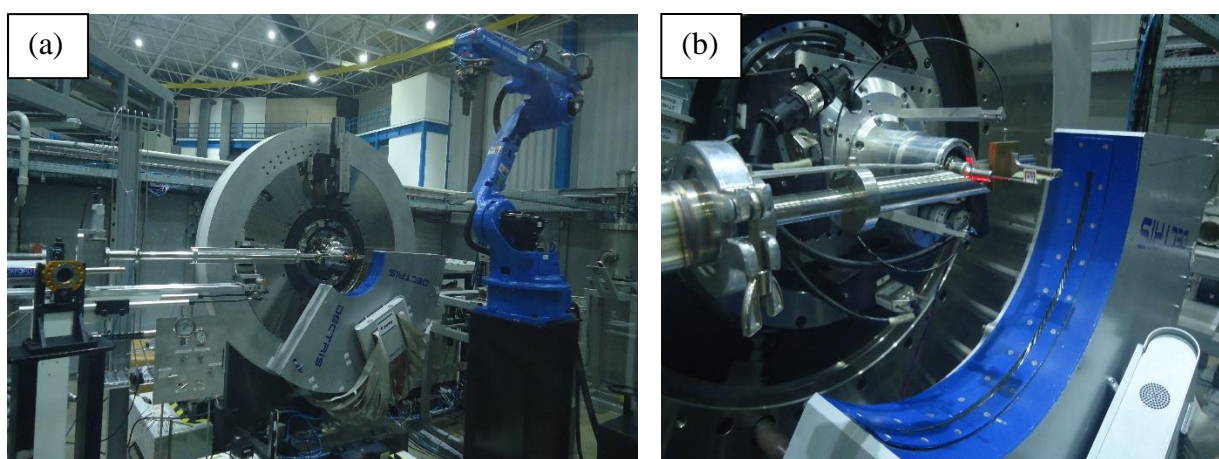
Figure 17. LNLS - XRD1 Beam Line dedicated to diffraction analysis in hard X-ray band of 5.5 to 14 KeV.

Prior to RSr-XRD analysis, all samples were transferred to a capillary tube with dimensions of 1.2 mm x 75 mm (Perfecta Lab, Brazil) demanded by Synchrotron machine specification (Figure 18). RSr-XRD technique was applied setting the XRD1 beam line energy in two distinct sets, 7.0 keV (1.77108 Å), energy close to the X-ray absorption edge of Fe (7.112 keV, 1.7433 Å), and 6.5 keV (1.90741 Å) far from the X-ray absorption edge of Fe. This technique aimed the improve the scattering of the crystal phases, avoiding the absorption of X-rays, and increasing the intensity and resolution of the peaks (Ferreira et al., 2008) (See discussion in Section S2 – Appendix B). Initially was used the energy of $E_1 = 6.5$ keV (1.90741 Å), which is far from the absorption edge of the iron, E = 7.112 keV (1.7433 Å), maximizing scattering of iron phases. A second energy $E_2 = 7.0$ keV (1.77108 Å), close to the energy's edge of the iron, for improvements in scattering signal of compounds like Mn, Ti, Cr, and Ca. This adjustment allowed the evaluation of difference of X-

ray patterns associated with compounds containing iron, in which improved signals were obtained using the energy of 6.5 keV (Fig. S3 in Appendix B). All samples were measured 5 times for 400 s to obtain average spectra.

Figure 18. PM samples into capillary tubes for RSr-XRD analysis.

RSr-XRD spectra were assessed by the Savitzky-Golay method, using 5 points and a polynomial order of 2, to improve the signal-to-noise ratio, especially for PM$_{2.5}$ samples. Peak parameters: 2θ angle, peak height, FWHM, and peak area for all spectra were then determined using the Fityk software, version 0.9.8 (Wojdyr, 2010). All 2θ angles were recalculated as the interplanar distance in angstrom (Å). Finally, PDF-2 software (JCPDS-ICDD) was used to determine the crystalline phases.

4.5 PM Source Apportionment

Source apportionment analysis was performed using USEPA PMF v5 software. From the 34 inorganic chemical species analyzed by EDXRF and TOC, 25 species were used in the PMF modeling. 9 species (Cd, Hg, Mo, Nb, Pb, Rb, Se, Y, and Zr) were weighted as "bad" due to low frequency in samples. All chemical species with S/N of less than 0.5 were also weighted as "bad". All uncertainties were calculated as recommended by USEPA PMF user guide (Norris et al., 2014). Initially, 5 to 10 factors were tested. An evaluation of the Q values and scaled residuals parameters show an optimum value of 7 factors for PM$_{10}$ at M1 and 5 factors for all other runs. Local source profiles reported by Santos *et al*. (2017) were used as input data to run the constrain mode.

5. Results and Discussion

In this section will be show the results about the PM chemical and physical characterization, and the apportionment of the sources. The PM mass concentration is shown in the section 5.1. In the section 5.2, the results about the elemental analysis are discussed. This section is an important content for the following sections. Section 5.3 shows the source apportionment results by PMF model using both organic and inorganic markers associated to their directionalities. The content of this section was written as an article and submitted to the Science of the Total Environment Journal on July 13, 2018. The section 5.4 shows the results about crystalline markers of sources found by RSr-XRD technique. The content of this section was submitted to the Chemosphere Journal on June 15, 2018. In the section 5.5, the quantification of the crystalline phases analyzed by RSr-XRD are associated with the corresponding sources as an additional information for the interpretation of the results by PMF model.

5.1 PM10 and PM2.5 Mass Concentration – Gravimetrical Analysis

Figure 19 shows the mass pollutant roses of PM_{10} and $PM_{2.5}$ at M1 and M2 stations. At M1, PM_{10} presents higher mass concentration associated to North-northwest (NNW) wind direction with a value of 31.6 µg m^{-3}, followed by Northeast winds (NE) with a value of 28.6 µg m^{-3} (Figure 10a), whereas at M2, higher PM_{10} mass concentration (40.0 µg m^{-3}) is found to be associated to North-northeast (NNE) winds (Figure 19b). The findings suggest that M1 is mostly influenced by PM_{10} emissions from Northwest (NW) and NE quadrants of RGV, whereas M2 is predominantly influenced by emission from sources located in the NE quadrant. This suggest that M1 is major affected by PM_{10} emitted from industrial and vehicular/resuspension sources, while M2 is predominantly affected by PM_{10} emissions from the industrial park. The WHO air quality guidelines states a limit of 50 µg m^{-3} for PM_{10} - 24-hour mean (WHO, 2005).

Higher $PM_{2.5}$ mass concentrations were found at M1 associated to NNW winds (14.9 µg m^{-3}), and East (E) winds (11 µg m^{-3}) (Figure 19c). NW of M1 is the main traffic roads in RGV, and E of M1 is the sea (Atlantic Ocean). At M2, $PM_{2.5}$ and PM_{10} show similar behavior, with higher mass concentration associated to NNE winds. Results show that $PM_{2.5}$ mass concentration at M1 is highly influenced by sources from NW quadrant (vehicular/resuspension), and from the east (Sea), while $PM_{2.5}$ at M2 is more influenced by emission from NE quadrant. The WHO air quality guidelines state a limit of 25 µg m^{-3} for $PM_{2.5}$ - 24-hour mean (WHO, 2005).

<table>
<tr><td>(a) PM₁₀ at M1 (Oct to Dec 2016)</td><td>(b) PM₁₀ at M2 (Jan to Mar 2017)</td></tr>
</table>

(a) PM_{10} at M1 (Oct to Dec 2016)   (b) PM_{10} at M2 (Jan to Mar 2017)

(c) $PM_{2.5}$ at M1 (Oct to Dec 2016)   (d) $PM_{2.5}$ at M2 (Jan to Mar 2017)
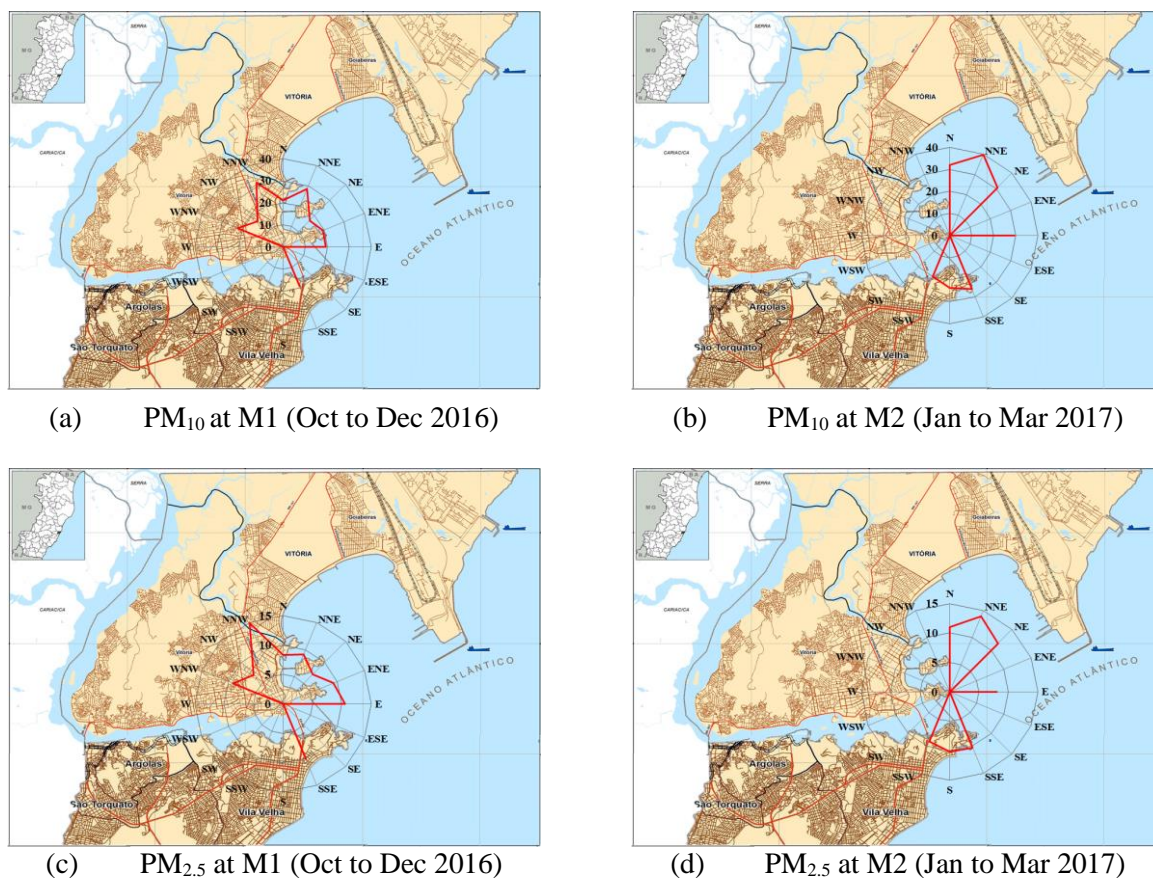
Figure 19. Pollutant roses of: (a) PM_{10} at M1; (b) PM_{10} at M2; (c) $PM_{2.5}$ at M1; and (d) $PM_{2.5}$ at M2.

5.2 Elemental Analysis

Table 7 shows the quantitative analysis of TSP, $PM_{10,}$ and $PM_{2.5}$ at M2 and M1. Cl, Na, Fe, S, EC, and OC are the most abundant at both stations. At M2, Cl and Na concentrations are higher than at M1, probably due to the closest proximity to the sea. However, the Cl/Na ratio ranges from 3.5 to 5.6 at both M1 and M2 suggesting contributions from other sources, in addition to sea salt. Iron concentration is higher at M1 than at M2, although the contribution in mass is not disparate between the two stations (Figure 19). This can be associated with the highest influence of sea salt at M2 which is approximately 2 times greater than at M1, lowering the contribution of Fe at M2. At M2, Fe concentration in TSP and PM_{10} is about 2 and 1.5 times lower than at M1. The exception is for $PM_{2.5}$, in which Fe and S are almost double (factor of 1.7) at M2 compared to M1, this is likely due to the secondary $PM_{2.5}$ formation. The correlation of these two elements suggest Fe-bound SO_4^{-2} species, justifying the higher Fe content in the $PM_{2.5}$ at M2. Previous studies suggest that mining, steel production, port and vehicular activities can be associated with the iron in the atmosphere (Choi et al., 2013; Y. Guo et al., 2017; Karnae and John, 2011; Tauler et al., 2009).

Aluminum (Al), Silicon (Si), Potassium (K), Calcium (Ca), and Magnesium (Mg) was determined to be the second most abundant elemental grouping. M1 shows greater concentrations than M2 of those elements, that are often associated with crustal sources (Choi et al. 2013; Gildemeister et al., 2007). RGV is almost fully paved having a reduced number of gravel roads, a large working site (2 km of wastewater gallery and repaving) located at 1.2 km NW from M1/M2 that was operating during the sampling period.

Several trace elements were found in TSP, PM_{10}, and $PM_{2.5}$. Titanium (Ti) shows greater concentration at M1 than at M2. Ti is an element frequently associated as a crustal marker (Cheng et al., 2015; Tecer et al., 2012). Some markers of vehicular sources like Ba and Cu (Kotchenruther, 2016; Schauer et al., 2006), and P (Ivošević et al., 2015; Cohen et al. 2010) are more abundant at M1 than at M2. Industrial markers like Manganese (Mn), Molybdenum (Mo), Chromium (Cr), and Nickel (Ni) (Duan and Tan, 2013; Tauler et al., 2009) are present in greater concentrations at M2 compared to M1, while Cd is present only at M2.

Table 7. Average concentration ($\mu g\ m^{-3}$) of elemental analysis by X-ray fluorescence of PM_{10} and $PM_{2.5}$ at M1 and M2, including the standard deviation ($\mu g\ m^{-3}$) and the respective limits of detection.

Element	PM10 - M1		PM10 - M2		PM2.5 - M1		PM2.5 - M2		DL's
	Average	St. Dev.	Average	St. Dev.	Average	St. Dev.	Average	St. Dev.	
					$\mu g\ m^{-3}$				
Cl	4.448	2.310	7.784	2.940	1.252	0.935	1.852	0.989	0.074
EC	2.141	0.975	1.174	0.683	1.334	0.739	0.832	0.533	0.120
OC	1.734	1.244	1.311	0.826	1.157	1.097	1.150	1.189	0.095
Na	0.798	0.250	2.105	0.673	0.298	0.071	0.544	0.197	0.013
Fe	0.954	0.402	0.699	0.429	0.145	0.053	0.247	0.514	0.003
S	0.916	0.233	1.651	0.405	0.640	0.184	1.046	0.500	0.105
Al	0.137	0.062	0.103	0.060	0.026	0.011	0.037	0.055	0.010
Si	0.384	0.186	0.287	0.162	0.064	0.028	0.106	0.172	0.006
K	0.138	0.063	0.202	0.089	0.095	0.070	0.101	0.111	0.019
Ca	0.347	0.178	0.317	0.177	0.074	0.103	0.086	0.198	0.010
Mg	0.094	0.029	0.242	0.078	0.030	0.009	0.084	0.082	0.007
Mn	0.012	0.004	0.008	0.003	0.001	0.000	0.005	0.004	0.003
Ag	0.052	0.039	0.046	0.019	0.032	0.017	0.036	0.019	0.011
Ba	0.050	0.011	0.044	0.017	0.019	0.029	0.018	0.001	0.021
Br	0.006	0.002	0.013	0.007	0.005	0.003	0.008	0.008	0.037
Cu	0.016	0.007	0.007	0.005	0.013	0.008	0.006	0.004	0.003
Ce	0.000	0.000	0.005	0.008	0.006	0.014	0.003	0.001	0.003
Cr	0.014	0.004	0.018	0.008	0.001	0.003	0.011	0.012	0.003
Cs	0.045	0.023	0.021	0.005	0.042	0.005	0.063	0.020	0.037
I	0.005	0.000	0.013	0.004	0.005	0.002	0.006	0.002	0.019
Ir	0.000	0.000	0.004	0.002	0.003	0.009	0.008	0.010	
La	0.000	0.000	0.005	0.001	0.018	0.005	0.000	0.000	0.013
Ni	0.003	0.000	0.005	0.000	0.004	0.002	0.007	0.004	0.003
P	0.049	0.017	0.092	0.052	0.027	0.011	0.053	0.039	0.009
Pd	0.012	0.006	0.008	0.003	0.012	0.010	0.011	0.003	0.001
Sn	0.044	0.015	0.067	0.019	0.000	0.000	0.061	0.010	0.020
Sb	0.041	0.011	0.093	0.044	0.048	0.017	0.120	0.091	0.097
Sr	0.006	0.004	0.009	0.003	0.006	0.002	0.006	0.004	0.003
Ti	0.024	0.009	0.014	0.008	0.009	0.005	0.027	0.030	0.004
V	0.010	0.008	0.000	0.000	0.006	0.008	0.006	0.004	0.005
Zn	0.017	0.008	0.009	0.004	0.009	0.004	0.010	0.009	0.006

Results in Table 8 show EC concentrations ranging from 0.8 to 2.1 µg m^{-3}, and OC concentrations ranging from 1.15 to 1.7 µg m^{-3} in both PM$_{2.5}$ and PM$_{10}$. EC concentrations reported in this study for RGV are lower than those previously found in other Brazilian cities, such as São Paulo (10.6 µg m^{-3}), Rio de Janeiro (3.4 µg m^{-3}), Curitiba (4.4 µg m^{-3}), and Porto Alegre (3.9 µg m^{-3}) (de Miranda et al., 2012), which have larger area and population than RGV (IBGE, 2010). EC and OC are reported as markers of vehicular sources and typical values of EC/OC ratio range from 0.04 to 0.4 (Contini et al., 2016, 2014; Karnae and John, 2011; Zou et al., 2017), however, in RGV the EC/OC ratio is 1.1 (PM$_{10}$) and 0.9 (PM$_{2.5}$). These values are significantly higher than in other cities (Table 1), suggesting that an additional and significant source of EC is present in the region. EC is reported predominantly to be associated with fossil-fuels (Szidat et al., 2004; Viana et al., 2008a). In RGV two major sources that are associated with the use of fossil fuels are: vehicular (yellow lines in Figure 12a,c) and a coke plant (E4b and E6 in Figure 12a).

Table 8. Comparative instrumental analysis results (µg m^{-3}) between this and previous works.

City	PM	Fe	EC	OC	EC/OC	Reference
		Concentration in µg m^{-3}				
GVR (Brazil)	PM$_{10}$	0.7 - 0.95	1.2 - 2.1	1.3 - 1.7	1.10	This study
	PM$_{2.5}$	0.15 - 0.25	0.8 - 1.3	1.15 – 1.16	0.91	
São Paulo (Brazil)	PM$_{10}$	NA	NA	NA		de Miranda et al., 2012
	PM$_{2.5}$	0.13	7.1	NA		
Rio de Janeiro (Brazil)	PM$_{10}$	0.28 - 0.68	NA	NA		Godoy et al., 2009; de Miranda et al., 2012
	PM$_{2.5}$	0.06 - 0.15	2.3	NA		
Belo Horizonte (Brazil)	PM$_{10}$	NA	NA	NA		de Miranda et al., 2012
	PM$_{2.5}$	0.11	3.4	NA		
Porto Alegre (Brazil)	PM$_{10}$	0.06 - 0.63	NA	NA		Braga et al., 2005; de Miranda et al., 2012
	PM$_{2.5}$	0.06	2.6	NA		
Donguan PRD (China)	PM$_{10}$	NA	NA	NA		Zou et al., 2017
	PM$_{2.5}$	NA	4.1	11.1		
Civitavecchia (Italy)	PM$_{10}$	0.2 - 0.38	0.4 - 1.0	2.7 - 3.6	0.22	Contini et al., 2016
	PM$_{2.5}$	NA	NA	NA		
Incheon (Korea)	PM$_{10}$	NA	NA	NA		Choi et al., 2013
	PM$_{2.5}$	0.71	1.79	8.04	0.22	
Texas (USA)	PM$_{10}$	NA	NA	NA		Karnae & John 2011
	PM$_{2.5}$	0.22	0.24	2.02	0.12	

NA – Not Available

Fe shows concentrations ranging from 0.7 µg m^{-3} to 0.95 µg m^{-3} in PM$_{10}$, and concentrations ranging from 0.15 µg m^{-3} to 0.25 µg m^{-3} in PM$_{2.5}$ (Table 7). The average Fe concentration observed in RGV is larger compared to other urbanized Brazilian cities such as São Paulo (de Miranda et al., 2012), Belo Horizonte (de Miranda et al., 2012), Rio de Janeiro (de Miranda et al., 2012; Godoy et al., 2009) and Porto Alegre (Braga et al., 2005) (Table 8). Further discussion on the influence of the directionality of the EC, OC and Fe pollutant roses, and their association with the most likely sources in RGV is found in Appendix C.

5.3 Inorganic and Organic Markers for the Apportionment of Highly Correlated Sources of Particulate Matter

Positive Matrix Factorization (PMF) is a receptor model based on the decomposition of a matrix X_{ij} of speciated data into two matrices: factor contributions G_{ik}, and factor profiles F_{ik} (Norris et al., 2014). Factor profiles needs the interpretation by the user, usually made by the association of chemical markers into each PMF factor with a source. It is a subjective process that can lead to incorrect interpretations. For example, iron (Fe) is reported as a marker of industrial (Song et al., 2006; Tauler et al., 2009), vehicular sources (Viana *et al.*, 2008; Karnae and John, 2011) and crustal sources (Gildemeister *et al.*, 2007; J. Wang *et al.*, 2016; Niu *et al.*, 2016). Elemental carbon (EC) and organic carbon (OC) are reported as markers of vehicular sources (Cheng et al., 2015; Owoade et al., 2016). However, the same species are also used as markers of biomass combustion (Kotchenruther, 2016), and coal burning (Vossler et al., 2016).

In order to improve the PMF outcomes reducing the uncertainty, a few authors have used both organic and inorganic markers to interpret the PMF factors resulting in improved analysis (Choi et al., 2015; Dutton et al., 2010; Qadir et al., 2014; Vossler et al., 2016; Wang et al., 2015). Some PAHs species such as Fluoranthene (Flt), Pyrene (Pyr), Benzo[a]anthracene (BaA), and Chrysene (Chr) are reported as diesel vehicular markers (Wu et al., 2014). Benzo[b,k]fluoranthene (BbkF), Benzo[a]pyrene (BaP), and Benzo[g,h,i]perylene (BghiP) are often used as markers for gasoline vehicular emissions (Devos et al., 2006). Industrial PAHs emissions come from several process (Niu et al., 2017). Some PAHs species such as Pyr and Flt are reported as biomass burning markers (Venkataraman and Friedlander, 1994), while fluorene (Flu), Naphtalene (Nap), Phenanthrene (Phe), Flt, and Pyr is associated to coke oven source (Dat and Chang, 2017; Zhou et al., 2014). Iron and steel industries also show organic markers associated to specific process. Nap is reported as the major organic marker of steelmaking. Nap, Phe, and Acenaphthylene (Acy) as markers of iron pellet plants, while Chr, BghiP, Dibenzo[ah]anthracene (DahA), BaA, Flu, Pyr, Nap, Phe, and BbkF are markers of sinter plants (Y. Guo et al., 2017). Despite the benefits of using organic markers in the interpretation of PMF factors, some uncertainty still relies on the source apportionment due to similarity on the PAHs profiles. Therefore, in urban and industrialized regions with several sources, the designation of markers without the knowledge of the directional pattern of the chemical species and their associated sources before the interpretation of PMF factors can lead to data misinterpretation.

This section proposes to combine the use of chemical markers with pollutant roses in order to state the directionality of chemical species, thereby linking them to specific sources and associating the

PMF factors numbers with the sources. This combined approach aims to minimize the risk of misinterpretation of the data and unexplained factors.

5.3.1 Source Apportionment (Factors Interpretation)

All PMF factors were associated to existing sources using organic and inorganic markers suggested in the literature and the pollutant roses produced from EDXRF results and meteorological data. If the use of organic and inorganic markers was not enough to eliminate the ambiguity in interpreting some of the factors, then the directionality of the chemical makers was used as a tool to improve their association to specific sources. A review of the literature including the main chemical species used in the interpretation of PMF factors can be found in the Supplementary Material (Table S3 – Appendix C).

5.1.1.1 - PM$_{2.5}$ at M1

Factor 1 – Sintering (stacks): This factor shows high loadings of Cl, Nap, and BbF, and moderates loadings of Pyr, and Chr (Figure 20a), all constituents in the sintering chemical profile as reported by Tsai *et al.* (2007) and Hleis *et al.* (2013). Cl is also reported as sea salt marker (Viana *et al.*, 2008), nevertheless, this factor shows a Cl/Na ratio greater than 1.54, which is the value reported for fresh sea salt (Cohen et al., 2011). It suggest an additional source of Cl in the region. The pollutant rose shows large Cl concentration associated with NNE winds (Figure 21a). In addition, the absence of Fe is a characteristic of sintering profiles (Y. Guo et al., 2017; Santos et al., 2017).

Factor 2 – Pelletizing Furnaces (stacks): Figure 20b shows high loadings of Acy, Phe and Flu, and moderate loading of Fe. These organic markers are reported as constituents of pelletizing furnaces profiles (Y. Guo et al., 2017). Despite the fact that Phe and Flu are also reported as coke ovens and sintering markers (Dat and Chang, 2017; Zhou et al., 2014), the absence of EC and OC (coke oven markers), and the moderate loading of Fe (not found in sintering) exclude this possibility. Fe is also reported as marker of crustal (Gildemeister *et al.*, 2007) and vehicular sources (Viana *et al.*, 2008), nevertheless, pollutant rose shows large concentrations associated with winds blowing from the direction of the pelletizing and steel industries (Figure 21b).

Factor 3 – Coke Ovens (stacks): High loadings of EC, S, and Flt associate this factor with coke ovens (Figure 20c). The pollutant rose shows large concentrations of EC associated with both NorthWest (NW) and South-Southeast (SSE) winds, which would point to vehicular sources (Figure 21c). However, the absence of OC in this factor, and the high concentration of Flt associate

specifically with East-Northeast winds (ENE) (Figure 21c) suggest this factor as coke oven emissions.
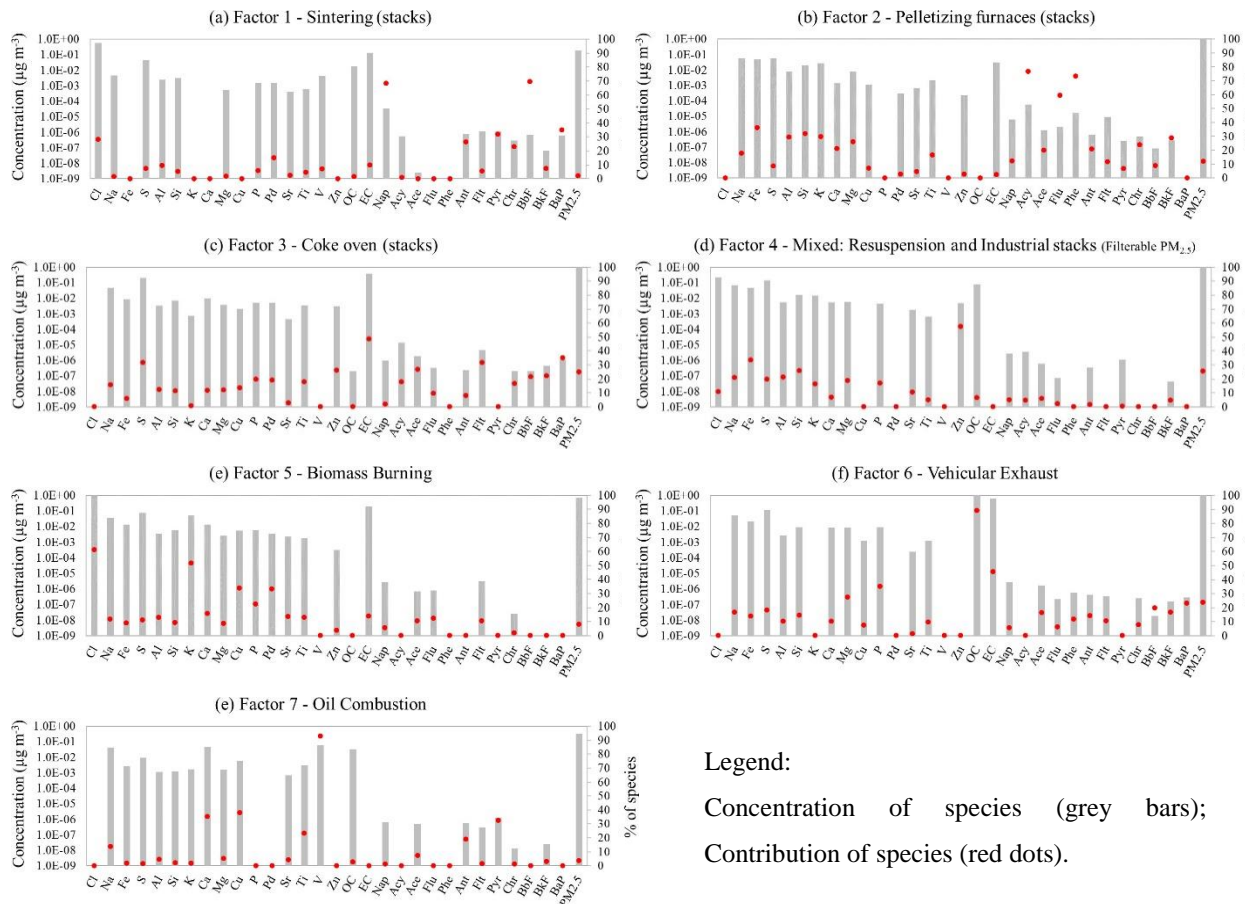
Figure 20. Source apportionment of PM$_{2.5}$ at M1 by PMF.

Factor 4 – Mixed: Resuspension and Industrial stacks (Filterable PM$_{2.5}$): Zn, Fe, Al and Si have the major loadings in this factor (Figure 20d). Fe, Al, Si and Zn are reported as markers of crustal/road traffic, vehicular and industrial sources (Viana *et al.*, 2008; Kotchenruther, 2016; Owoade *et al.*, 2016). In addition, Zn is present in chemical profiles from steelmaking, blast furnaces, coke oven and pelletizing furnaces (Yang *et al.*, 2015; Guo *et al.*, 2017). The pollutant rose (Figure 21d) shows large Al and Si and moderate Fe and Zn concentrations associated with winds blowing from NW and SE quadrants, suggesting a diffusive source due to the non-directionality of the markers. This pattern associated with the chemical characteristics the likely source is the resuspension of silt deposited on roads by the vehicles. Besides, high loading of Zn and Fe (Figure 20d) and their large concentrations associated with NE winds (Figure 21d), suggest an additional contribution from the stacks in the industrial plants, which seems to be a generalization of the factors 2 and 3. However, the absence of organic loadings suggests that this factor may be constituted by the filterable portion of stack emissions (solid/liquid phase), whereas the factors 2 and 3 are major constituted by both filterable and condensable portions, respectively,

solid/liquid and gas phases (Corio and Sherwell, 2000; Yang et al., 2015). Indeed, this factor can also be mostly associated with emissions by the stacks in blast furnaces and steelmaking processes as discussed in section 5.1.1.3 comparing $PM_{2.5}$ source apportionment at both M1 and M2 sampling sites. However, it is not possible separate the contributions of resuspension from industrial, and only the study of the iron crystalline phases (reduced or oxidized) could properly answer it.

Factor 5 – Biomass Burning: Figure 20e shows high loading of Cl and K, both reported as markers of sintering and biomass burning (Choi et al., 2013; Y. Guo et al., 2017). Despite the fact that the pollutant roses show large concentrations of both species associated with winds from the sinter plant direction (Figure 21e), the absence of major organic sintering markers such as Nap, Pyr, Chr, BbF and BaP disqualify this factor as a sintering representative.
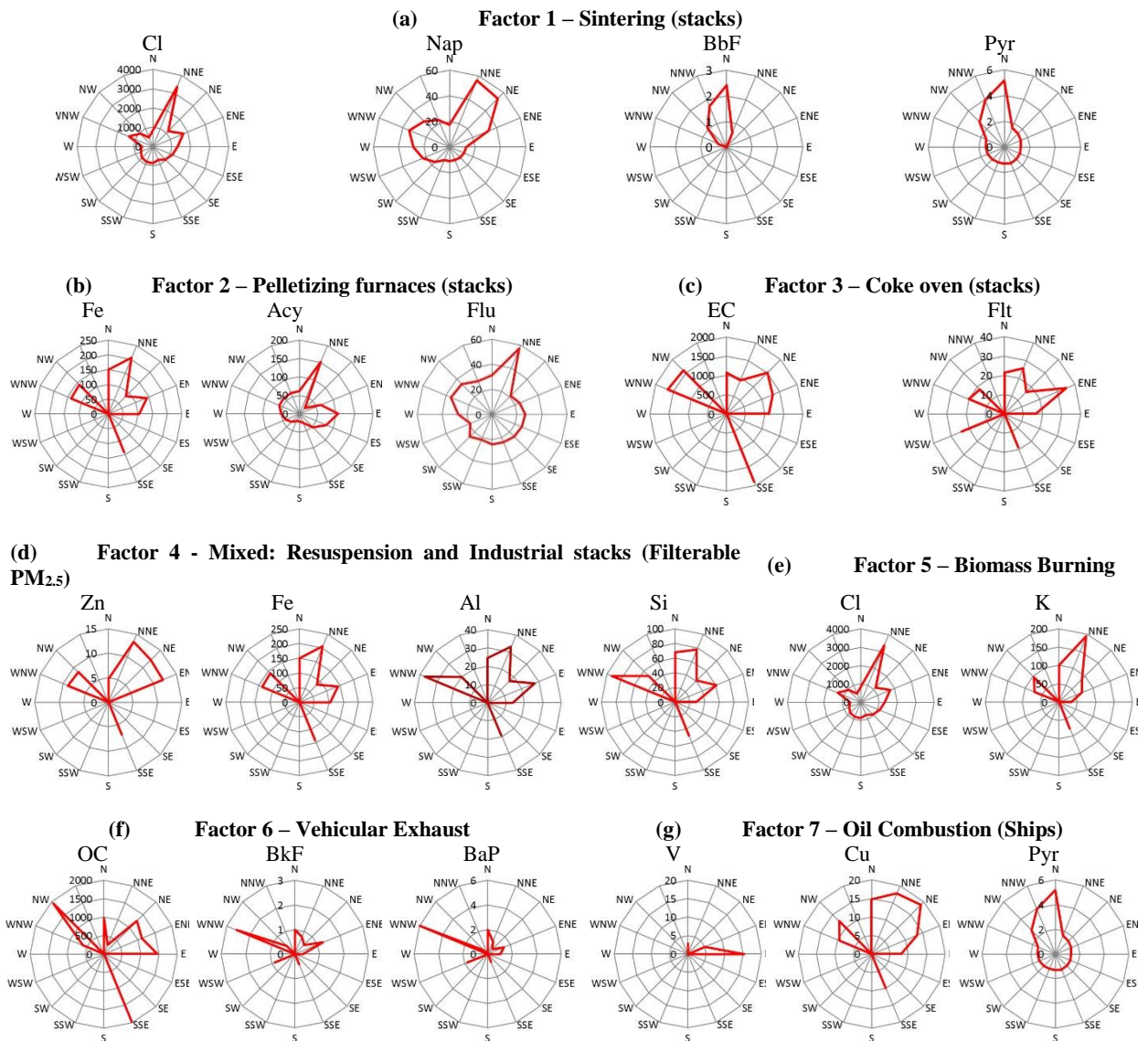
Figure 21. Pollutant roses of $PM_{2.5}$ at M1 (Elemental, EC and OC in $\mu g\ m^{-3}$; PAHs in $pg\ m^{-3}$).

Factor 6 – Vehicular Exhaust: In this factor high loadings of OC and EC, and moderate loadings of P, BkF and BaP suggest vehicular exhaust as the likely source (Figure 20f). P is not reported as a marker of vehicular exhaust, although, its presence is reported as a content of lubricating oil and diesel exhaust (Cheng *et al.*, 2015; Ivošević *et al*., 2015). OC, EC, BkF and BaP are reported as markers of gasoline vehicular sources (Devos et al., 2006), and the directionality of these species show large concentrations associated with WNW winds (Figure 21f), location of the most intense traffic roads in RGV (Figure 12a,c).

Factor 7 – Oil Combustion (ships): In this factor high loading of V, Cu and Pyr dominates, followed by Ant and Ace (Figure 20g). V and Cu are well-known markers of oil combustion and lubricating additive (Ivošević et al., 2015; F. Wang et al., 2016). Cu is also reported to be associated with crustal, vehicular and industrial sources (Duan and Tan, 2013; Owoade et al., 2015). However, the pollutant roses show large concentration of both, V and Cu, associated with NE and E winds (Figure 21g), suggesting oil combustion from port terminals as the likely source.

5.1.1.2 - PM$_{2.5}$ at M2

Factor 1 – Sintering (stacks): This factor shows high loadings of BghiP, Chr, Nap and BaA, and moderate loading of Cl (Figure 22a), all species found in the sintering chemical profile (Y. Guo et al., 2017). BghiP, Chr and BaA are also reported as vehicular markers (Devos et al., 2006; Wu et al., 2014), nevertheless, the pollutant roses (Figure 23a) shows large concentrations of these species associated with N winds. In addition, low OC loading excludes vehicular contributions.

Factor 2 – Pelletizing furnaces (stacks): Figure 22b shows high content of Fe, Flu and Phe, markers associated with pelletizing furnace emissions (Y. Guo et al., 2017). These species are also reported as sintering (Y. Guo et al., 2017) and coke oven markers (Zhou et al., 2014), however, large content of Fe and low contents of both Cl and EC strongly suggest pelletizing furnaces as a factor from PMF results.

Factor 3 – Coke oven (stacks): This factor shows high loadings of EC and S, and moderate loadings of Nap, Flu and Pyr (Figure 22c) species reported as coal burning markers (Dat and Chang, 2017; Zou et al., 2017). EC and Pyr are also reported as vehicular markers (Martuzevicius et al., 2011; Viana et al., 2008a), nevertheless, the pollutant roses show large concentration of EC and Pyr associated with winds blowing from the coke plant direction (Figure 23c).
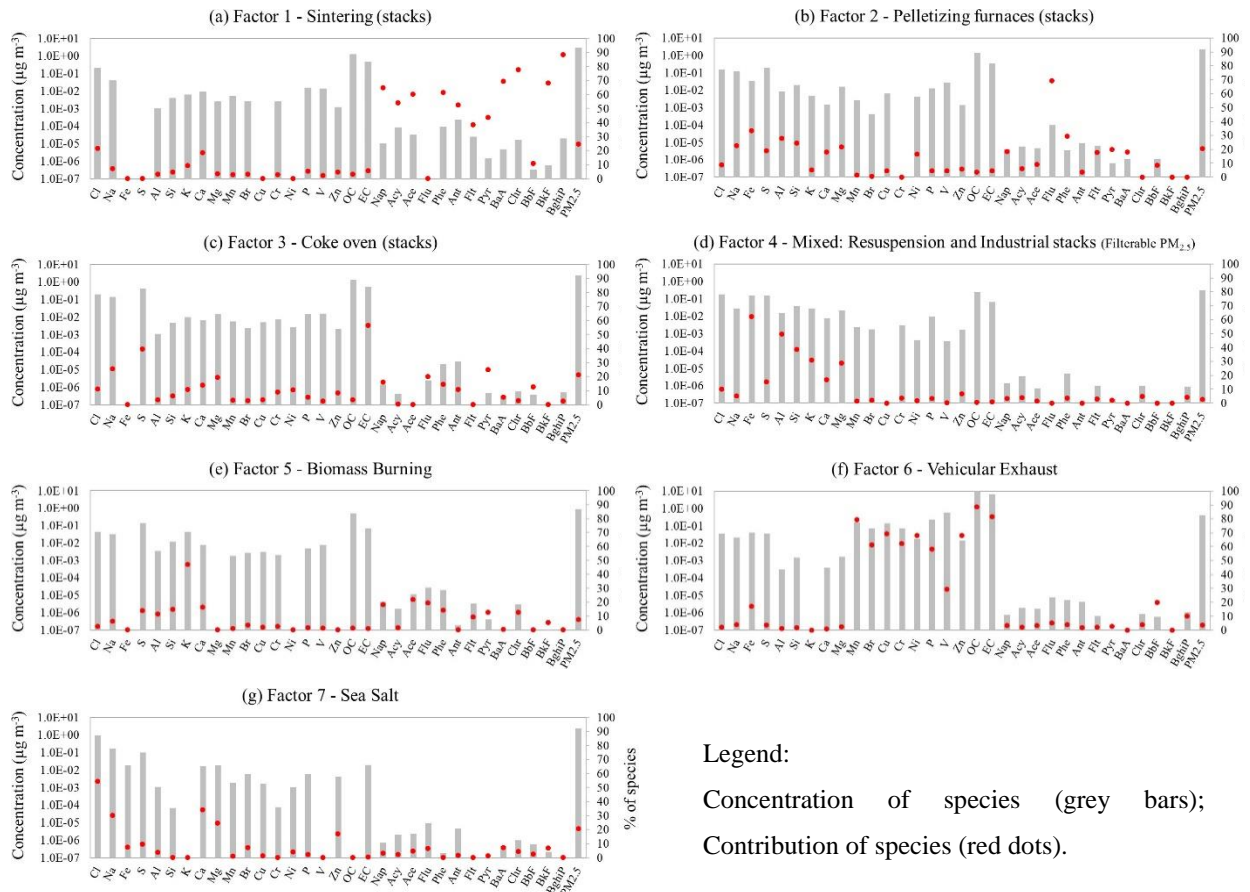
Figure 22. Source apportionment of PM$_{2.5}$ at M2 by PMF.

Factor 4 – Mixed: Resuspension and Industrial stacks (Filterable PM$_{2.5}$): High loadings of Fe, Al and Si, and the virtual absence of PAHs (Figure 22d) indicates this factor as a mixed of resuspension and filterable particles emitted from industrial processes such as steelmaking and blast furnaces (Detailed discussion in section 5.1.1.1 – Factor 4). Fe, Al and Si are reported as crustal/road traffic markers (Harrison and Smith, 1992; Viana *et al.*, 2008). Despite the pollutant roses shows Fe and Al mainly associated with N winds, location of the industrial plants, lower concentrations associated with winds rom S to NW are present suggesting a diffusive contribution likely by resuspension (Figure 23d). As discussed in section 5.1.1.1, in fact this factor can also be associated with other potential sources of (Fe,Zn)-rich filterable particles such as blast furnaces and steelmaking.

Factor 5 – Biomass Burning: This factor shows high loading of K, and moderate to low contents of organic species (Figure 22e). Among the organic species, Acenaphthene (Ace) shows large loading followed by Nap. Despite the presence of these species in sintering profiles, a significant contribution comes from locations not associated with sintering (Figure 23d). In addition, Cl, the major marker of sintering profiles is absent, confirming biomass burning as the likely source.
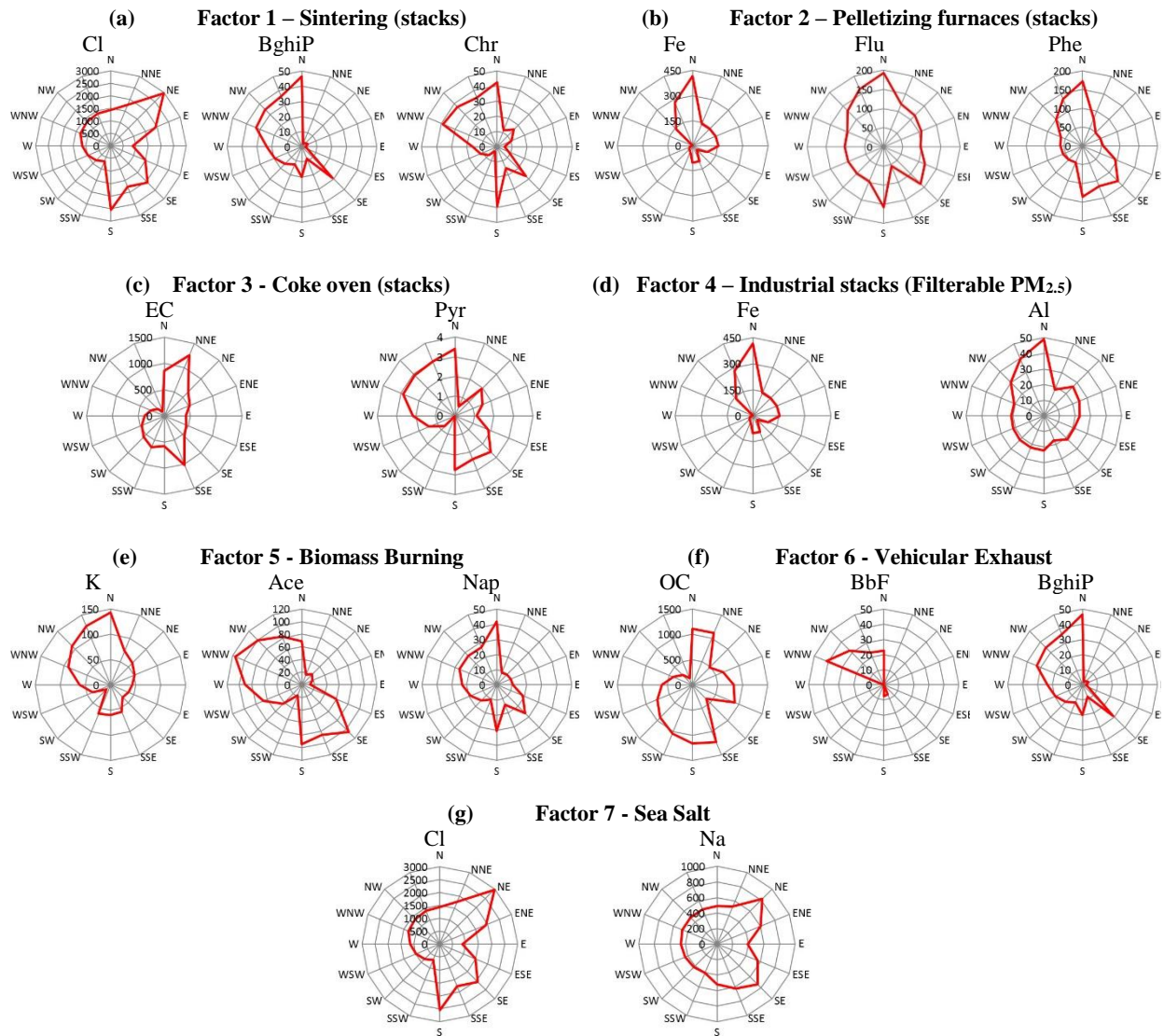
Figure 23. Pollutant roses of PM$_{2.5}$ at M2 (Elemental, EC and OC in µg m^{-3}; PAHs in pg m^{-3}).

Factor 6 – Vehicular Exhaust: High loading of OC and EC, and moderate loadings of BbF and BghiP characterize this factor (Figure 22f). The pollutant roses (Figure 23e) shows large OC concentrations associated with S winds (opposite location of the pelletizing and steel industries) and large BbF concentration associated with WNW winds. Despite the large concentration of BghiP associated with N winds, approximately a half is associated with WNW winds (location of the main traffic roads).

Factor 7 – Sea Salt: Figure 22g shows high loading of Cl and Na. The pollutant roses (Figure 23g) show large concentration of both species associated with sea breezes (S to E quadrant).

5.1.1.3 - PM$_{2.5}$ Source Apportionment

Figure 24 shows the source apportionment of PM$_{2.5}$ at M1 and M2. Despite the proximity between M1 and M2 (less than 1.5 km, Fig. 12a), significant differences in the source apportionment were

found. Sintering contributions prevail at M2 compared to M1 (25% to 2%), and the large difference can be explained by the large concentrations of sintering markers such as Cl, Nap, Pyr, Flu, Chr, BbF, BaA, BghiP at M2. Cl and PAHs concentrations at M2 are approximately 1.5 and 4.5 times larger than at M1, respectively (Tables S1 and S2 – Appendix C). Pelletizing furnaces contributions is doubled at M2 compared with M1 (20% to 12%). At M2, Fe, Phe and Flu, the major pelletizing markers are respectively 1.7, 6.9, and 7.3 times greater than at M1. Significant difference between the contributions of mixed resuspension and industrial (Filterable PM$_{2.5}$) at M1 and M2 is shown in Fig. 24a (26%), and 24b (3%). The likely explanation is the greater influence of intense traffic surrounding M1, whereas at M2 there is only local traffic by residents. In addition, at M2 greater concentration of PAHs in gas phase are increasing the portion of condensable PM$_{2.5}$ in the factors Sintering, Pelletizing furnaces and Coke oven. Lower concentration of PAHs in PM$_{2.5}$ at M1 is an indicative that filterable particles in solid/liquid phase prevails, which increase the filterable PM$_{2.5}$ portion (solid phase), lowering the contributions of condensable phases of PM$_{2.5}$ from Sintering, Pelletizing furnaces and Coke oven stacks. Figures 24a, and 24b show no significant difference in the contributions of Coke ovens and Biomass Burning. Vehicular Exhaust contributes with 24% of PM$_{2.5}$ mass at M1, while at M2, only 3% of PM$_{2.5}$ mass is associated to vehicular source. Intense vehicular traffic roads surround M1, whereas M2 has only local traffic. Sea Salt shows great contribution in PM$_{2.5}$ mass at M2, which is located on the seashore. Although M1 is also close to the sea, PMF was not able to separate any factor associated with sea salt, even by setting PMF runs with more factors.
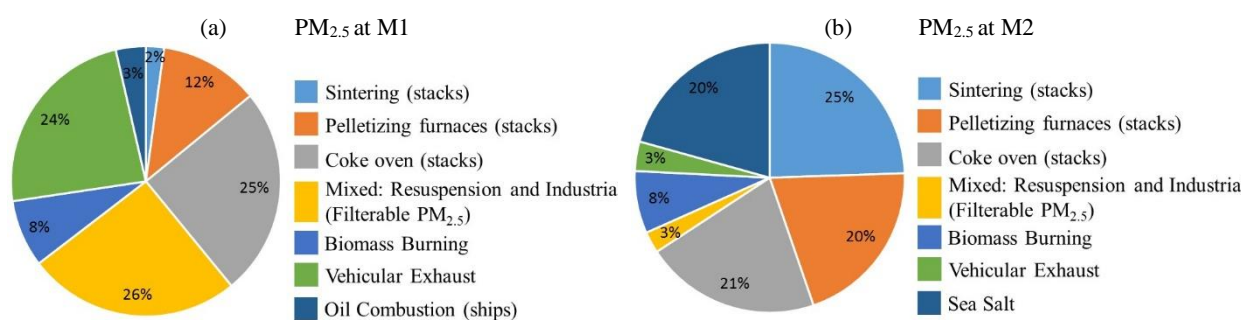
Figure 24. Source apportionment of PM$_{2.5}$ by PMF at M1 and M2 sampling sites.

Pelletizing and steel industry (E1 to E7 in Fig. 12a) explain 69% and 66% of the total mass, respectively at M2 and M1. At M1 (Fig. 24a), sintering and coke oven (steel industry) explain 27% and pelletizing furnaces (mining company) explains 12% of the total mass. Pelletizing furnaces and coke oven (Filterable PM$_{2.5}$), which can also include all kinds of sources emitting Fe-rich filterable particles from both, pelletizing and steel industries explains 26% of the total mass. Vehicular exhaust explains 24% and 3% of the total mass, respectively at M1 and M2. At M2 (Fig. 24b), sintering and coke oven (steel industry) explain 46% of the total mass, while pelletizing

furnaces explains 20%. The findings suggest M2 is more affected by $PM_{2.5}$ emissions from sintering, coke ovens and pelletizing furnaces than M1, whereas M1 is more affected by emissions from factor 4 (Industrial stacks - Filterable $PM_{2.5}$), which suggest that in fact other sources such as blast furnaces and steelmaking are likely the major contributors of the factor 4.

Despite the proximity of M1 with the sea, the PMF was not able to identify and separate this factor, inputting large loadings of Cl in the sintering stacks and biomass burning factors. Even for greater number of factors the PMF was not able to separate a factor with large loading of Cl and Na associating it with sea salt.

5.1.1.4 - PM$_{10}$ Source Apportionment

Figure 25 shows the source apportionment of PM_{10} at M1 and M2, and the factors associated with the sources are shown in Figures S4 and S5 (Section S3 in Appendix C). Figures 25a, and 25b show no significant difference in the contributions of sintering at M1 and M2, respectively 8% and 5%. However, Figures 24b and 25b show discrepant difference at M2 in the $PM_{2.5}$ and PM_{10} contributions of sintering, respectively 25% and 5%. This behavior is likely associated to the major portion of PAHs (>95%) adsorbed onto $PM_{2.5}$ (Table S2 in Appendix C), increasing the contribution of the $PM_{2.5}$ condensable fraction emitted from sintering stacks. The same pattern is shown for pelletizing furnaces (Figures 24b and 25b). At M2 a significant contribution of Industrial Stockpiles is shown, a factor not identified at M1. This factor shows high loadings of Fe, S, Ca, Mg, Zn, and low loadings of PAHs, suggesting a mix of industrial process such as handling and storage of iron ore and granulated pellet and sinter, activities associated with both pelletizing and steel industries. The main sources of those products in the RGV are E2, E3 and E5 (Figure 12a). The finding suggest that M2 is more affected by PM_{10} emitted from granulated iron ore, sinter and pellets handling and stockpiles than M1, whereas M1 is more susceptible to the emissions from vehicles (25%) than M2 (6%).

At M1 (Figure 25a), vehicular exhaust explains 25% of the total mass. Industrial activities explain 47% of the total mass, in which 26% are explicated by sintering and coke oven (steel industry), and 21% by pelletizing (pelletizing industry). At M2 (Figure 25b), industrial processes explain 65% of the total mass. Sintering and coke oven, and pelletizing explain, respectively, 18% and 5% of the total mass. Handling and storage of granulated products such as iron ore, pellet and sinter explain 42% of the total mass at M2. Therefore, M2 is more susceptible to emissions from these two industries than M1, mainly by emissions from handling and storage of products, although M1 is major affected by emissions from stacks than M2. The contribution of handling and storage of

Fe-rich products was only identified in PM_{10} source apportionment. This finding is consistent with the Inventory of Atmospheric Emissions of RGV (IEMA/Ecosoft, 2011), which reported that the $PM_{2.5}$/TSP emission ratio from the mining and steel industries is approximately 13%, while PM_{10}/TSP emission ratio ranges from 26% to 46%. Due to the high similarity among those sources showing products with high content of Fe and Ca, PMF model was not able to properly identify their contributions individually. According to the Inventory of Atmospheric Emissions of RGV (IEMA/Ecosoft, 2011), approximately 83 kg h^{-1} of PM_{10} is emitted by processes of handling and stockpiles (iron ore and pellets) in the mining and pelletizing industry. In the steel industry, the handling and storage of iron ore and fluxes is responsible for the emission of approximately 1 kg h^{-1} of PM_{10}.
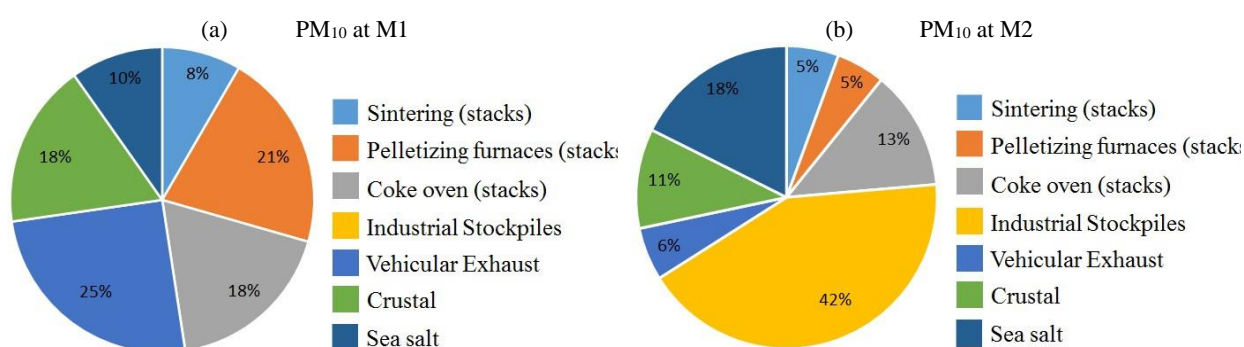
Figure 25. Source apportionment of PM_{10} by PMF at M1 and M2 sampling sites.

5.4 The Determination of Markers for Iron-Rich Particles by Resonant Synchrotron X-Ray Diffraction

Several approaches have been adopted to minimize the influence of collinearity over the results by receptor models (Blanchard *et al*., 2012; Roy et al. 2011; Wittig and Allen 2008b), including hybrid models coupling Principal Component Analysis (PCA) and Multi Linear Regression (MLR) into the iteration process of the CMB model (Shi et al., 2014b, 2009; Watson et al., 2002). Despite showing better results, hybrid model predictions still present high error and bias when sources are highly correlated and previous studies have shown that only the identification of source specific markers can improve the source apportionment modeling (Ivey et al., 2017; Y. Zhang et al., 2017).

Past studies have reported the inclusion of elemental species as markers for source apportionment studies. However, some of those chemical elements cannot be inferred as a specific marker of a single source. For example, iron is often documented as a tracer for different sources like industrial

(Flament et al., 2008; Y. Guo et al., 2017; Tecer et al., 2012), crustal (Niu et al., 2016; F. Wang et al., 2016), and vehicular (Achad et al., 2014; Thorpe and Harrison, 2008). Elemental Carbon (EC) and Organic Carbon (OC) are mainly used as vehicular tracers (Owoade et al., 2015; Yin et al., 2010), although can also be attributed to biomass burning (Karnae and John, 2011; Zou et al., 2017), and industrial emissions (J. Guo et al., 2017). Chlorine (Cl) and Sodium (Na) are related to contributions of sea salt (J. Wang et al. 2013; Louie et al. 2005), however Cl is also reported as constituting of biomass burning and sintering process (Cha and Spiegel, 2004; Y. Guo et al., 2017). EC, OC, and Sulfur (S) as Sulfate (SO_4^{-2}) are described as contributions from biomass burning, industrial coal and sinter plants (Amodio et al., 2013; H. Guo et al., 2009; Y. Guo et al., 2017; Zeng et al., 2013), and as secondary SO_4^{-2} aerosols (H Guo et al., 2009; Zou et al., 2017). In this context is often difficult to identify chemical elemental species as a marker of a single source.

This study hypothesis proposes that the identification of specific crystalline phases can act as markers of specific sources, particularly peaks without any overlapping, since different sources are associated to a specific pressure and temperature conditions, influencing in the crystalline phases. In this context, the work aims to present a new approach to define specific markers that contribute to PM accurate source apportionment. A comprehensive identification of crystalline phases of Total suspended particulate matter (TSP), particulate matter less than 10 µm (PM_{10}) and fine particulate matter less than 2.5 µm ($PM_{2.5}$) were assessed in the RGV using Resonant Synchrotron X-ray diffraction (RSr-XRD) to characterize the different crystalline phases and enables the differentiation of sources (i.e. industrial and vehicular).

5.4.1 Resonant Synchrotron X-Ray Diffraction (RSr-XRD) Analysis

RSr-XRD results only refer to TSP samples, since the diffraction peaks were easier to identify due to its intensity. However, Tables S1 and S2, and Fig. S4 (Section S5 in Appendix B) describe each marker and correspondent intensity in PM_{10} and $PM_{2.5}$.

5.4.1.1 - α-Fe$_2$O$_3$ Marker

Hematite (α-Fe$_2$O$_3$) was found at both M1 and M2 in all sample classes (Tables S2 and S3 in Appendix B). RSr-XRD spectra of the samples show two distinct peaks that appear with similar intensities at interplanar distances of 1.4861 Å, and 1.4535 Å, peaks that are associated with hematite (α-Fe$_2$O$_3$) (PDF#33-664 card in Figure 17e). Those peaks have no overlapping with any other compound in PM, therefore, can be used as a specific marker of α-Fe$_2$O$_3$ in PM. Figure 26 shows the RSr-XRD spectra of the TSP samples at M1 and M2.

At M1, the TSP RSr-XRD spectra showed α-Fe_2O_3 associated with prevailing winds from the north (N) (Fig. 26a), but also to prevailing winds from the south-southeast (SSE) (Figure 26b). However, there was a significant difference in the intensities of the peaks 1.4861 Å and 1.4535 Å, showing a dependence of the α-Fe_2O_3 transported according to wind direction. Figure 26a depicts the RSr-XRD spectra relative to PM originating from the northeast (NE), where an identical α-Fe_2O_3 X-ray powder diffraction pattern can be observed (PDF#33-664). The area and intensities of the NE samples' peaks are approximately 5 times great than in samples from the SSE (Figure 26b). Indeed, Figure 26b shows SSE PM diffraction patterns with noise prevalence, but with yet perceptible α-Fe_2O_3 peaks and, therefore, quantifiable.

Figure 26. RSr-XRD spectra: (a) TSP sample at M1 associated with N winds; (b) TSP sample at M1 associated with SSE winds; (c) TSP sample at M2 associated with NE winds; (d) TSP sample at M2 associated with S winds; (e) α-Fe_2O_3 X-ray powder diffraction pattern.

At M2, RSr-XRD spectra also show 3 times greater α-Fe_2O_3 peak intensities (1.4861 Å and 1.4535 Å) associated with prevailing winds from the N (Figure 26c) and lower intensity associated to prevailing winds from the south (S) (Figure 26d).

α-Fe_2O_3 shows distinct signatures in PM spectra with concentrations 2 times greater when associated with NE winds, suggesting the significant contribution of sources located NE of RGV (Figure 12). As discussed previously, Fe as a tracer was associated with industrial activities (Y. Guo et al., 2017; Moreno et al., 2006; Tecer et al., 2012), the sources located NE of the sampling points in the RGV (Figure 12). The mining and steel industries are the prevailing activity at the industrial complex in this location, in which iron ore is the main raw material for pellets and sinter production (de Souza et al., 2000, 1998; Fabris et al., 1997; Muwanguzi et al., 2012). Since α-Fe_2O_3 is the major component in iron ores, pellets, and sinter, therefore the peaks (1.4861 Å and 1.4535 Å) can be used as a specific marker of α-Fe_2O_3 in PM associated to iron ore storage piles, sintering, and pelletizing plants.

In the RGV, large amounts of iron ore are handled for the production of pellets (Sources E1-E3, Figure 12) and sinter (Source E5). Between the 4th trimester of 2016 and the 1st trimester of 2017 (overlapping this study sampling period), the mining company produced and transported by railroad about 101 million tons of iron ore from Minas Gerais state (Vale, 2017a, 2016) to the Tubarão complex at RGV. The same mining company operates a pelletizing with a nominal production capacity of 36.7 million tons per year (Vale, 2017b), and the steel company has a sinter plant with capacity of 6.5 million tons per year.

5.4.1.2 - Metallic Fe Marker

Metallic Fe was found at both M1 and M2 in TSP, PM_{10}, and $PM_{2.5}$ samples. RSr-XRD results show that metallic Fe is characterized by the presence of at least two major peaks at distances of 1.84 Å and 1.97 Å (PDF#34-529 in Figure 27f). Despite peak overlap at 1.84 Å by α-Fe_2O_3, the peak 1.97 Å shows no overlapping with any other compound and its presence, together with the peak at 1.84 Å, can be attributed to metallic Fe in PM – indicting a potentially good marker candidate.

As with α-Fe2O3 (Section 5.4.1.1), metallic Fe detection depends on wind direction especially at M1 (Fig. 27a, b, c). Although peaks in PM associated with East-Northeast (ENE) winds show distinct intensities (Figure 27a), PM associated to Northwest (NW) winds (Figure 27b) shows a peak at 1.84 Å, the peak 1.97 is too low with noise abundance. This suggests a negligible contribution of metallic Fe from sources North-West (NW) of RGV. In Figure 27c, no signal is observed at 1.84 Å nor at 1.97 Å, indicating the absence of metallic Fe sources located to SSE of RGV. The results suggest a predominant contribution of metallic Fe from sources located in the NE quadrant of RGV in PM and lower contribution from sources located at NW.

At M2, metallic Fe is not present neither in samples associated with NE winds (Figure 27d) nor S winds (Figure 27e). In fact, there are no peaks at 1.84 Å and at 1.97 Å at M2, and the absence of those peaks suggest that M2 is not affected by sources of metallic Fe (Figures 27d, and e). At M2, metallic Fe is not present neither in samples associated with NE winds (Figure 27d) nor S winds (Figure 27e).

Figure 27. RSr-XRD spectra: (a) TSP sample at M1 associated with ENE winds; (b) TSP sample at M1 associated with NW winds; (c) TSP sample at M1 associated with SSE winds; (d) TSP sample at M2 associated with NE winds; (e) TSP sample at M2 associated with S winds; (f) Metallic Fe X-ray powder diffraction pattern.

Figure 27 also suggests the predominant contributions of metallic Fe are from sources located to the ENE of M1, but the same PM sources do not affect M2, at least at concentrations that can be detected by RSr-XRD. Metallic Fe is a product of the reduction of sinter or pellets in blast furnaces (Strezov, 2006; Tugrul et al., 2009), and its presence is also found in steelmaking units. Located NE of RGV, a steel company (consisting of 3 blast furnaces and 3 steelmaking) with a nominal production capacity of 7.5 million tons of steel per year, which are the most likely sources of metallic Fe in PM associated with the NE winds over M1. The absence of metallic Fe at M2

indicate that, in terms of iron-rich particles, this area is more affected by emissions from the iron ore storage piles, pellets, and sinter plants (as discussed in section 5.4.1.1). This finding is consistent with the results by EDXRF (shown in Table 7), in which the total Fe content in PM is significantly greater at M1 than at M2 with Fe_{M1}/Fe_{M2} ratios of 2.1 and 1.4 for TSP and PM_{10}, respectively. In this context, the metallic Fe peaks at 1.84 Å and 1.97 Å can be used as markers of blast furnace and steelmaking activities (source E7 in Figure 12).

5.4.1.3 - FeS₂ Marker

Pyrite (FeS_2) was identified by RSr-XRD in all PM classes as a distinct and strong peak varying between 2.45 Å and 2.43 Å. FeS_2 X-ray powder diffraction pattern shows three major peaks with distances of 2.71 Å, 1.63 Å, and 2.42 Å (PDF#71-2219 in Figure 28e), clearly identified in the PM with no overlapping (Figure 28).
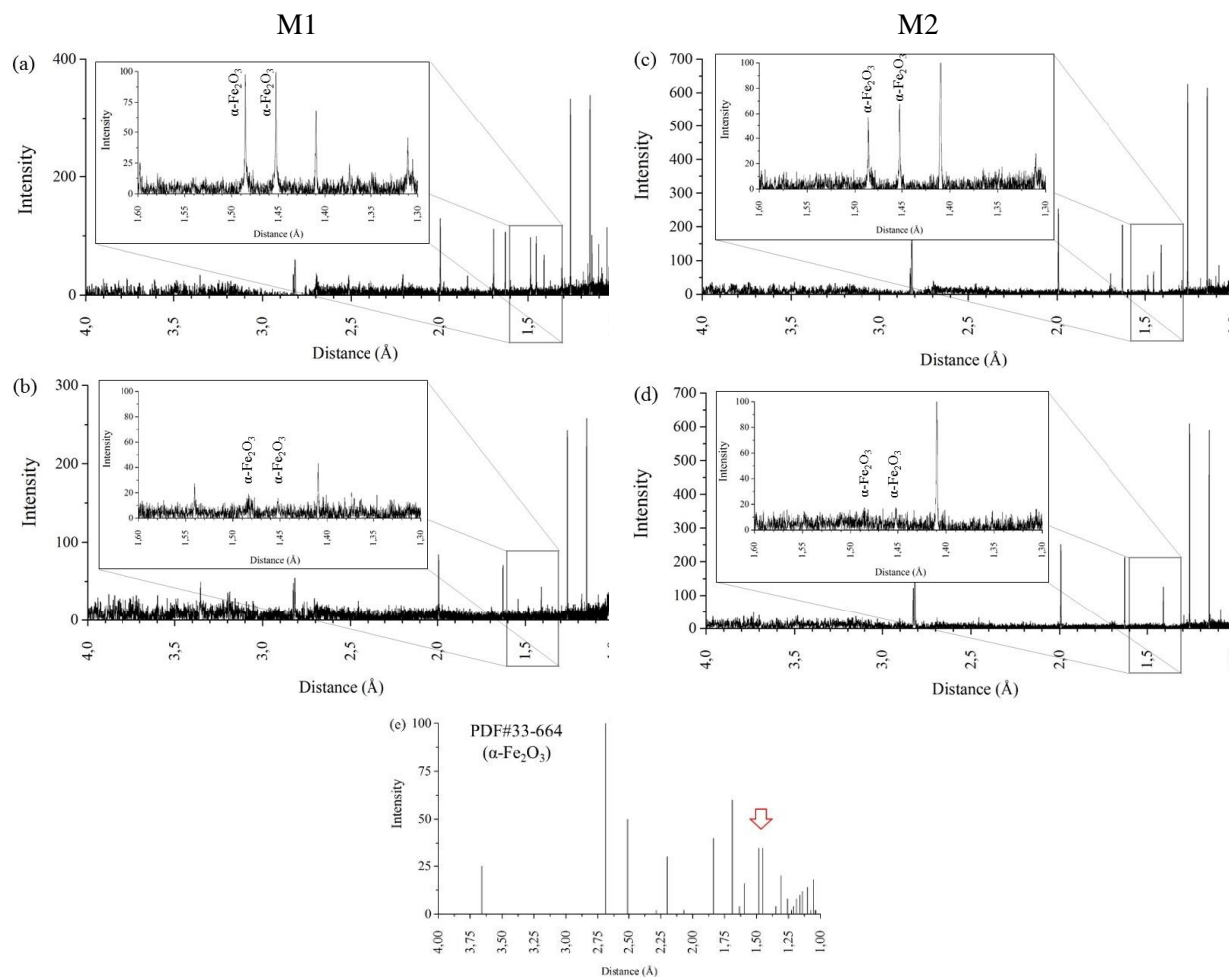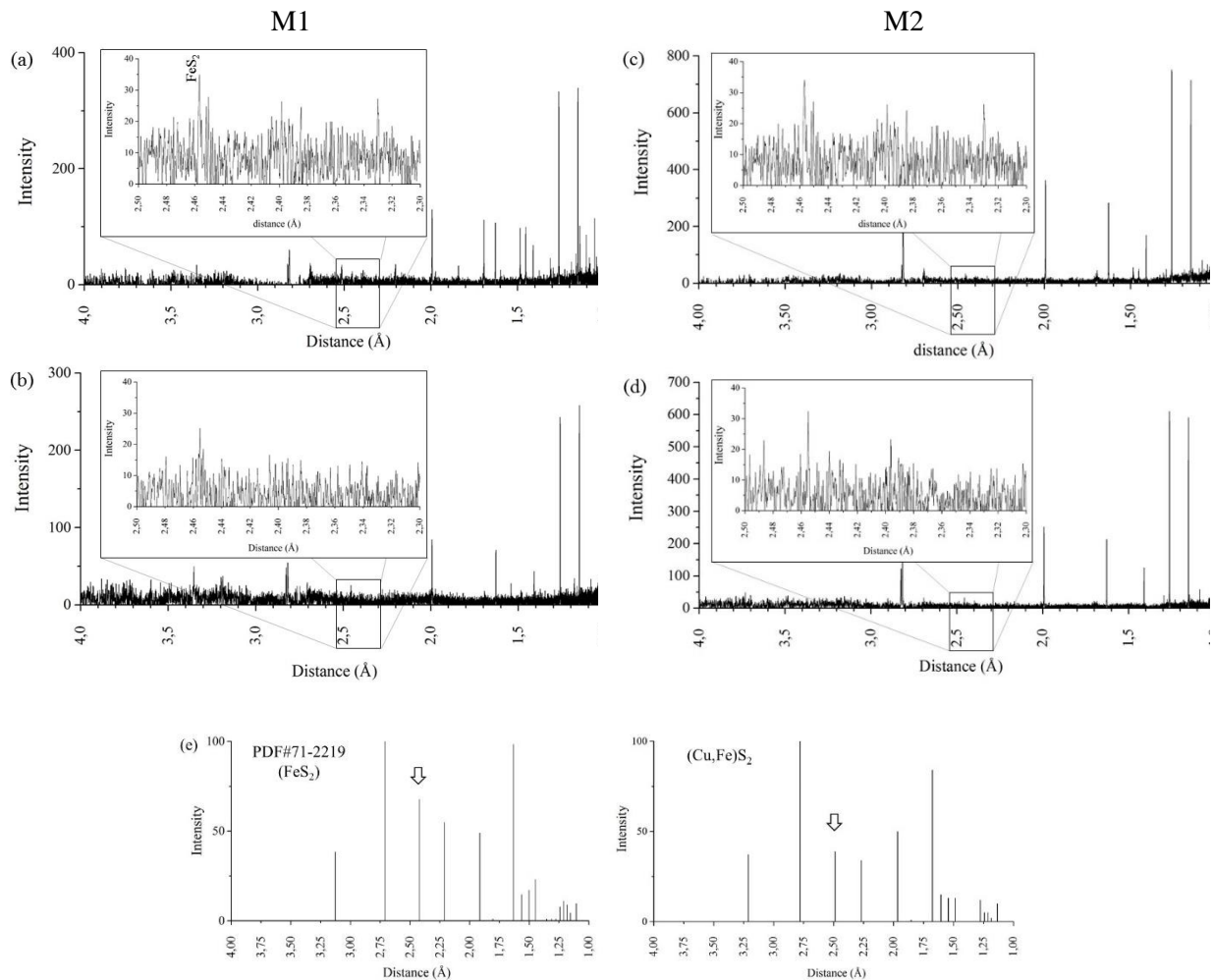

Figure 28. RSr-XRD spectra: (a) TSP sample at M1 associated with N winds; (b) TSP sample at M1 associated with SSE winds; (c) TSP sample at M2 associated with NE winds; (d) TSP sample at M2 associated with S winds; (e) FeS_2 X-ray powder diffraction pattern.

Figure 28 shows the TSP RSr-XRD spectra at both M1 (Figures 28a, b) and M2 (Figures 28c, d). At M1, we observe a distinct FeS_2 peak at 2.455 Å, about 40% more intense when associated with N winds (Figure 28a) than South-Southeast (SSE) winds (Figure 28b). At M2 (Figures 28c, d), we cannot observe any significant intensity difference of the peak 2.45 Å considering prevailing winds, although the difference in area is expressive, evidencing higher contributions from sources to the N of RGV, with area values of 8.62 and 2.69 for PM associated with N and S winds, respectively.

A peak displacement that identifies FeS_2 can be seen at 2.45 Å when compared to the third major peak (2.42 Å) of pure FeS_2 (PDF#71-2219). This displacement is explained by the presence of Cu in PM (Table 7), since CuS_2 and FeS_2 form a solid solution $(Cu, Fe)S_2$ containing Fe^{2+} that maintains, qualitatively, the same electronic state as pure FeS_2 (Schmid-Beurmann and Lottermoser, 1993). $(Cu, Fe)S_2$ diffraction patterns show a displacement of the peak at 2.43 Å to 2.48 Å (Schmid-Beurmann and Lottermoser, 1993). Therefore, fractions of Cu associated to FeS_2 in PM lead to the displacement of the peak 2.43 Å to 2.45 Å in the studied PM. In this context, the peak at 2.45 Å can be confirmed as a marker of FeS_2 in PM.

FeS_2 is reported to be associated with coal deposits (de Souza et al., 2000, 1998; Linak et al., 2007). In RGV, large amounts of coal is handled and processed at the port, pellet and coke plants. The Praia Mole Harbor (Source E3 in Figure 12), is a terminal dedicated to coal discharge and in 2016 handled approximately 11 million tons of coal and associated charges (Vale, 2017b). In this context, the presence of the 2.45 Å peak in PM is a clear indication of FeS_2 in PM that originated from coal activities.

5.4.1.4 - BaTiO₃ Marker

Barium titanium oxide ($BaTiO_3$) was identified by RSr-XRD analysis in TSP, PM_{10}, and $PM_{2.5}$ due to two major diffraction peaks at 2.82 Å and 2.83 Å (Figure 29). The presence of barium and titanium is confirmed by EDXRF results in which Ba appears in concentrations greater than most of the trace elements (Table 7). $BaTiO_3$ powder X-ray pattern (PDF#5-626 in Figure 29g) shows two major diffraction peaks at 2.838 Å and 2.825 Å with the same intensity and a minor peak at 1.997 Å. Despite the peak at 2.82 Å in PM being overlapped by NaCl presence, the 2.838 Å peak appears without any overlapping and, therefore, the presence of those two peaks together confirm the presence of $BaTiO_3$.

At M1 (Figures 29a, b, c), $BaTiO_3$ presents no tendency regarding wind direction, suggesting a diffuse, ubiquitous source. The 2.817 Å peak is greater than the 2.825 Å peak and does not show

similar intensities to the pure BaTiO$_3$ powder X-ray diffraction pattern (PDF#5-626 in Figure 29g). This pattern is due to overlapping of the most NaCl intense peak at 2.810 Å (PDF#2-818, ICDD 2007). Besides, EC (PDF#46-943, ICDD 2007) has the second most intense peak at 2.82 Å, also contributing to increasing the intensity of the peak at 2.817 Å (Figure 29). Figure 29c shows that both peaks at 2.825 Å and at 2.817 Å have the same intensity indicating no overlapping with any other compound.
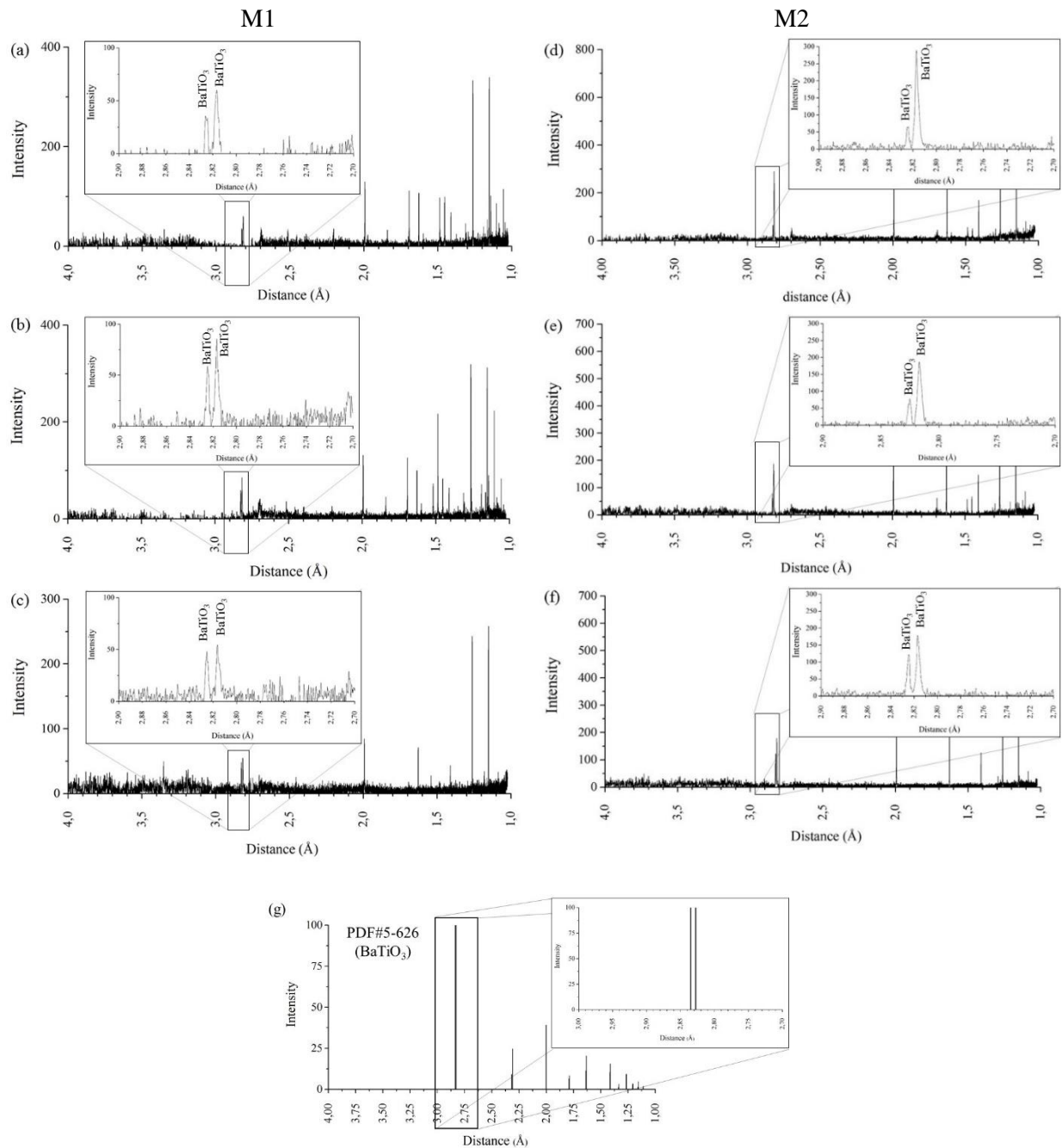
Figure 29. RSr-XRD spectra: (a) TSP sample at M1 associated with N winds; (b) TSP sample at M1 associated with NW winds; (c) TSP sample at M1 associated with SSE winds; (d) TSP sample at M2 associated with N winds; (e) TSP sample at M2 associated with NE winds; (f) TSP sample at M2 associated with S winds; (g) BaTiO$_3$ X-ray powder diffraction pattern.

At M2 (Figures 29d, e, f), the 2.82 Å peak is 2 to 3 times greater than the one found at M1. This suggests a strong contribution of a differentiated source at M2. As previously discussed, the peak at 2.82 Å has contributions from NaCl and EC. M2 is close to the sea (Figure 12a) and high contribution of NaCl is expected. However, the 2.82 Å peak is much larger (50% more intense) in samples associated with the N winds than to the NE winds (Figures 29d, and e). This finding suggests that the peak 2.82 Å is predominantly fed by EC industrial emissions from the N of M2, and the same conclusion can be extended to M1 since Figure 29c (S winds) shows no signal of NaCl and EC contributions. North of M2 is the Tubarão complex, which includes a coke, sinter, and pellet plants that can contribute to the increase of the 2.82 Å peak intensity with emissions of EC by chimneys.

Figure 29 shows that $BaTiO_3$ has no directional dependence with point sources in RGV. Barium is reported as vehicular tracer emitted by tire and break wear (Revuelta et al., 2014; Thorpe and Harrison, 2008). Ba and Ti are also reported as markers of soil resuspension, therefore, a sanitation and repaving construction site NW of M1 could be the main attributing source of $BaTiO_3$ in RGV, but $BaTiO_3$ intensities does not show a strong association with winds from this quadrant. Indeed, at M1, the intensities in the spectra for all wind directions are similar, showing a non-dependence with wind direction, suggesting predominant contributions of diffusive sources. M1 is surrounded by the main traffic roads in the RGV (Figure 12c), which has a fleet of 1.6 million vehicles (DENATRAN, 2018). In this context, the peaks at 2.82 Å and 2.83 Å can be used as a marker of $BaTiO_3$ associated with vehicular emissions.

5.4.1.5 - EC Marker

EC crystalline phases were identified by RSr-XRD in TSP, PM_{10}, and $PM_{2.5}$ samples with a strong dependence of sampling site (M1, M2) and wind direction (Figure 30). An EC crystalline phase was identified at both M1 and M2 with major diffraction peaks at 2.83 Å, 2.70 Å, and 1.99 Å (PDF#46-943, ICDD 2007), while a pseudo morph of graphite (rhombohedral system) was identified only at M1 with the most intense diffraction peak at 3.35 Å (PDF#26-1079 in Figure 30f). The EC crystalline phase overlapped $BaTiO_3$ or NaCl (as discussed in Section 5.4.1.4), and cannot be used as a sole marker. However, the pseudo morph of graphite (PDF#26-1079) shows a distinct peak at 3.35 Å, without any overlapping and, therefore, can be used as a carbon (graphite) marker.

Figures 30a, b, c show the TSP RSr-XRD spectra from M1, in which the peak at 3.35 Å is evident in all samples, although the intensity of the peak is 1.5 to 2.5 time lower in samples associated to ENE winds (Figure 30b) than in samples associate to NW and SSE winds (Figure 30a and 30c).
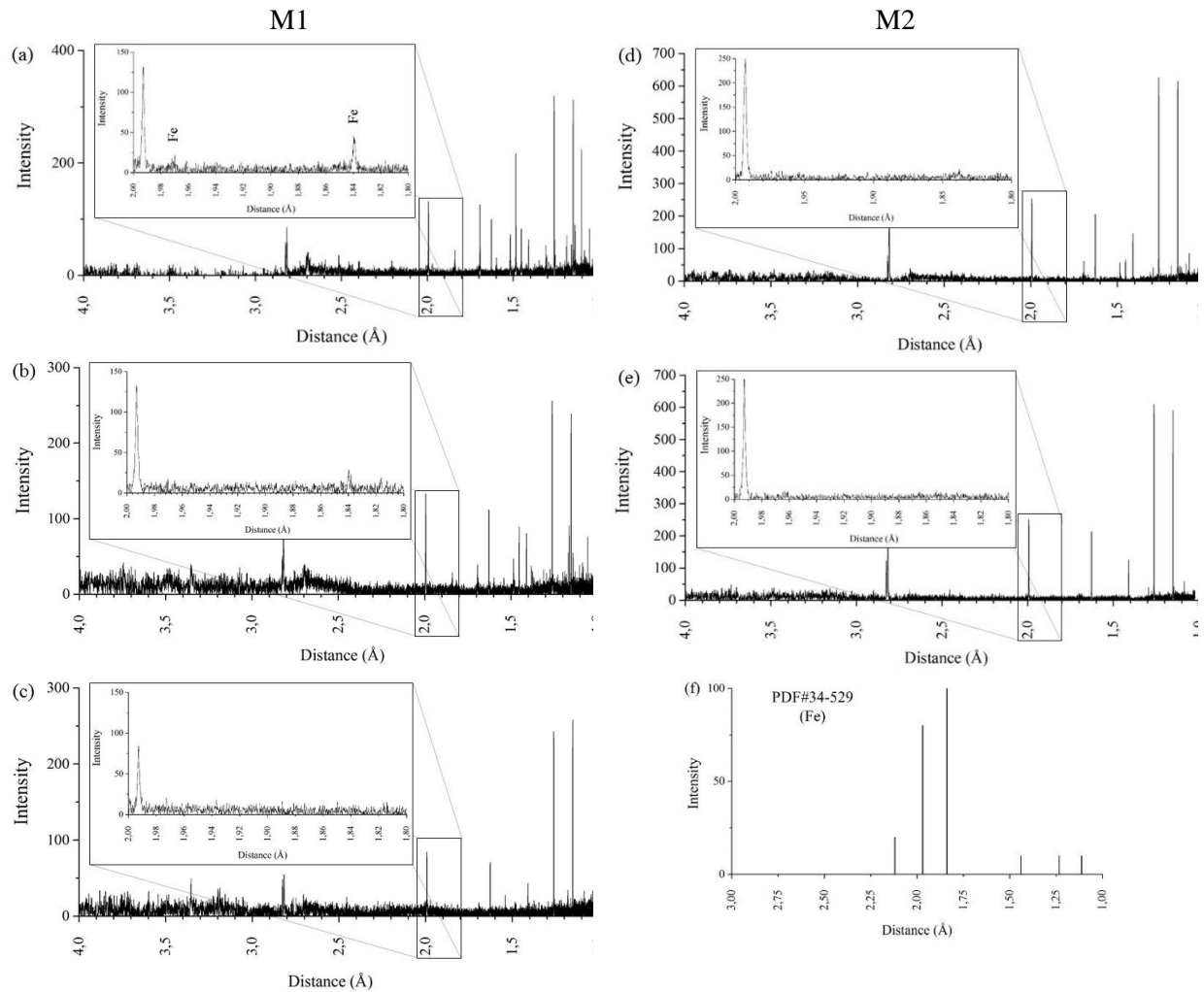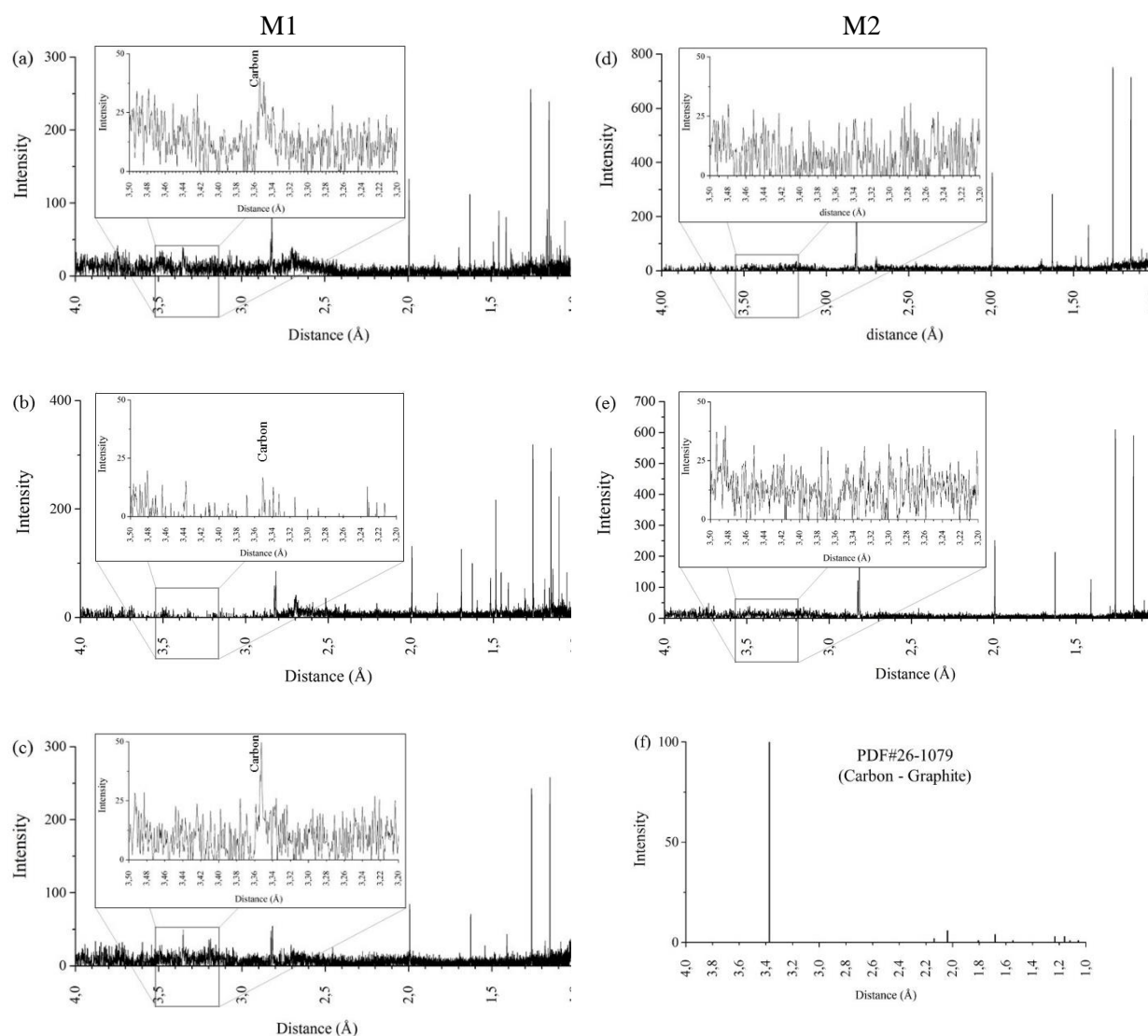

Figure 30. RSr-XRD spectra: (a) TSP sample at M1 associated with NW winds; (b) TSP sample at M1 associated with ENE winds; (c) TSP sample at M1 associated with SSE winds; (d) TSP sample at M2 associated with N winds; (e) TSP sample at M2 associated with S winds; (f) Elemental carbon (Graphite) X-ray powder diffraction pattern.

At M2 (Figure 30d, e, f), RSr-XRD spectra suggest only the presence of the crystalline phase of carbon with major peaks at 2.83 Å, 2.70 Å, and 1.99 Å (PDF#46-943), suggesting that M2 is not affected by the source of the carbon with major peak at 3.35 Å, or at least, the concentration of it is negligible.

The findings suggest that the EC with major peak at 3.35 Å (PDF#26-1079) is associated with emissions from locations highly influenced by vehicular emissions, while the EC with major peak

at 2.83 Å (PDF#46-943) is associated with emissions from locations with high influence of industrial activities.

5.5 Crystalline Phases in PM and Related Sources

The interpretation of factors provided by receptor models such as PMF and PCA is a subjective process that can lead to data misinterpretation due to the simplistic use of elemental species as source markers. Iron (Fe) is singularly reported as an industrial, vehicular, and crustal marker (Gildemeister et al., 2007; Song et al., 2006; Viana et al., 2008a). In fact, Fe can be emitted from all these sources, however, in different crystalline phases. For example, metallic Fe (Fe^0) can be emitted by steelmaking and blast furnaces (USEPA, 1986), and by vehicles due to the brakes wear (Thorpe and Harrison, 2008). Fe_2O_3, particularly, is emitted by iron ore, and agglomerates (sinter and pellets) stockpiles (de Souza et al., 1998; Rosière and Chemale Jr, 2000). In particular, sintering and pelletizing furnace stacks can also emit α-Fe_2O_3 during the agglomeration of iron ore, as γ-Fe_2O_3 during the transition of magnetite (Fe_3O_4) to α-Fe_2O_3 during the heating process (Jiang et al., 2008). Pyrite (FeS_2) is another Fe constituent of coal deposits (Cohn et al., 2006; Deng et al., 2015). FeS_2 is fully decomposed during the coking process at temperatures higher than 1600 ºC, a temperature which exceeds the typical coke ovens (Gornostayev et al., 2009), facilitating its release from coke ovens stacks. Lastly, goethite (FeOOH) and Fe-bound silicates are typically found as soil constituents (Fabris et al., 1997; Moreno et al., 2004). Therefore, the study of crystalline phases of chemical species can be used to correlate the compounds with specific process as additional information for the source apportionment studies using receptor models.

This section shows the qualitative and quantitative characterization by Resonant Synchrotron X-ray Diffraction (RSr-XRD) of the main crystalline phases in the PM (SP, TSP, PM_{10} and $PM_{2.5}$) associating them with the prevailing winds, in order to identify the directional contribution of these compounds and the likely sources. Additionally, the identification and quantification of the crystalline phases are used as a parameter to evaluate the sensibility of the PMF model in the PM_{10} and $PM_{2.5}$ source apportionment.

5.5.1 Crystal Phases in PM$_{2.5}$ and Associated Sources

The major crystalline phases found in $PM_{2.5}$ samples are shown in Table 9.

Fe-rich crystalline phases such as α-Fe_2O_3, FeS_2, $FeMnO_3$ and metallic Fe are always associated with NE quadrant winds (Figure 31) suggesting the industrial complex as the most likely source. α-Fe_2O_3 is the main crystal of Brazilian iron ores (Rosière and Chemale Jr, 2000), although magnetite (Fe_3O_4) is also reported by iron and steel industries (Muwanguzi et al., 2012). α-Fe_2O_3 is also linked with sintering and pelletizing furnaces emissions due to the conversion of iron ores phases (α-Fe_2O_3, Fe_3O_4) into α-Fe_2O_3 (Clout and Manuel, 2003; Jiang et al., 2008), as shown in Equation 11.

$$4Fe_3O_4 + O_2 \xrightarrow{>473K} 6\gamma Fe_2O_3 \xrightarrow{>673K} 6\alpha Fe_2O_3 \tag{11}$$
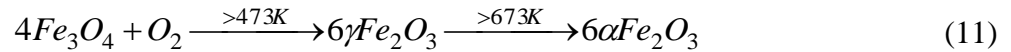
In fact, due to the aerodynamic diameter ($< 2.5\,\mu m$) is expected that this crystalline phase is greatly associated with sintering and pelletizing stacks emissions. At the Tubarão Complex (E1-E3 in Figure 12a), we find the two main industries of the RGV: a mining company and a steel company. In 2017, the mining company handled 335 thousand tons of iron ore daily and has a nominal capacity of 36.7 million tons/year of pellets (Vale, 2018), whereas the steel company has a nominal capacity of 6.5 million tons/year of sinter.
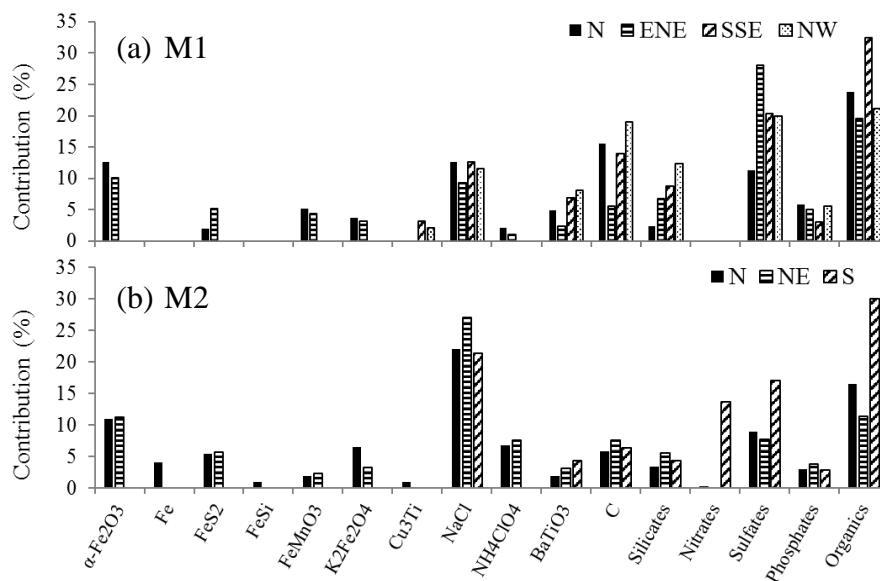
Figure 31. Crystalline phases in PM$_{2.5}$ at (a) M1 and (b) M2.

FeS_2 is a coal constituent (Gornostayev et al., 2009) and large contents at both M1 and M2 are associated with winds from N and NE quadrant (Figure 31), the location of industrial stockpiles (E4a, b). The absence of FeS_2 associated with winds originating from the industries opposite location suggests that the coal stockpiles are the likely source. As previously discussed, the complete FeS_2 dissociation needs a temperature above 1600 ºC (Gornostayev et al., 2009), thus a likely species emitted by the coke oven stacks. In addition, FeS_2 dissociates under an oxidant

atmosphere and therefore $FeSO_4$ and $Fe_2(SO_4)_3$ are formed (Gornostayev et al., 2009), explaining the presence of $FeAl_2(SO_4)_4.22H_2O$ in the samples. Besides, under inert atmosphere FeS_2 originates metallic Fe (Equation 12). All this process dependents of environment conditions such as temperature, oxygen concentration, flow conditions and particle size (Hu et al., 2006). Therefore, the emission of FeS_2 can also be associated to coke oven stacks and stockpiles.

$$FeS_2 \longrightarrow Fe_{1-x}S \longrightarrow FeS \longrightarrow Fe \qquad (12)$$
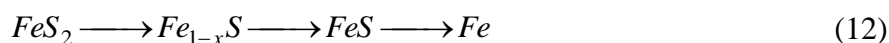
In the RGV large amounts of metallurgical coal are handled and processed. In 2017, the Praia Mole port terminal handled 13.2 million tons of coal (Vale, 2018). Part of this metallurgical coal was used by the steel company (E4b-E7 in Figure 12a) to produce coke. Two coke producing units are installed at the steel company site, one with a nominal capacity of 1.7 million tons/year and another one with a nominal capacity of 1.55 million tons/year of coke.

Figure 31 shows a greater EC concentration at M1 than M2 with mean values of 15% and 6%, respectively. EC is emitted by vehicle exhaust and industrial stacks such as coal burning, diesel combustion and biomass burning (Kotchenruther, 2016; Zou et al., 2017). At M1, greater EC contributions are associated with northwest (NW) and south-southeast (SSE) winds suggesting the large influence of vehicular sources (Figure 31a). At M2, EC contributions are mainly associated to diffusive sources such as vehicular, nevertheless a rather large contribution is associated to NE winds from the industrial location (Figure 31b). In the section 5.4.1.5, two different signatures of EC were identified, one mainly found at M2 with a major diffraction peak at 2.82 Å (linked to industrial stack emissions, see discussion in 5.4.1.4 - Figure 29), and the other one only identified at M1 with the most intense diffraction peak at 3.35 Å (Figure 30). The findings suggest that EC with a major peak at 3.35 Å (PDF#26-1079) was associated with diffusive emissions and present only when influenced by winds in the direction from locations with high vehicular emissions (yellow lines in Figure 12a, and c). EC main peak at 2.83 Å (PDF#46-943) can be associated with emissions from locations with high influence of industrial activities (E1 to E7 in Figure 12a).

$BaTiO_3$ is a compound not commonly reported in the literature, however, a consistent signature of this compound can be found in the samples (Figure 31). $BaTiO_3$ shows greater concentration associated with winds from NW and SSE at M1 and winds blowing from S at M2, suggesting a diffusive type of source such as vehicular emissions (Figure 31a and 31b). Ba is associated with organometallic fuel additives (Kittelson et al., 1978; Srimuruganandam and Shiva Nagendra, 2012), brake lining and brake wear dust (Viana et al., 2008a), whereas Ti as K_2TiO_3 is used in the production of brake pads to improve the wear and tear characteristics and heat resistance (Thorpe

and Harrison, 2008). The hypothesis is that $BaCO_3$ and K_2TiO_3 in the composition of brake lining and pads can react due to the high temperature during the brake action producing the $BaTiO_3$.

Figure 31b shows the presence of NH_4ClO_4 with values of 6% and 8% at M2, respectively associated with N and NE winds, whereas at M1 (Figure 31a) low contribution (approximately 3%) is associated with ENE winds. The results suggest that M2 is more impacted by NH_4ClO_4 than M1. The predominance of these species in samples when winds are from the NE quadrant suggests the industrial complex as the likely source. The sintering industrial process uses KCl as flux which decomposes liberating Cl^- as HCl, that then reacts with NH_3 to form NH_4Cl (Yang et al., 2015). The hypothesis is that the presence of oxidant species such as O_3, OH^- and H_2O_2 in the atmosphere or even into the industrial processes may be oxidizing the chloride (NH_4Cl) into a perchlorate compound (NH_4ClO_4). Therefore, the presence of the NH_4ClO_4 in the $PM_{2.5}$ (Figure 32) suggests that the likely source of these are the sintering stacks (E5 in Figure 12a).
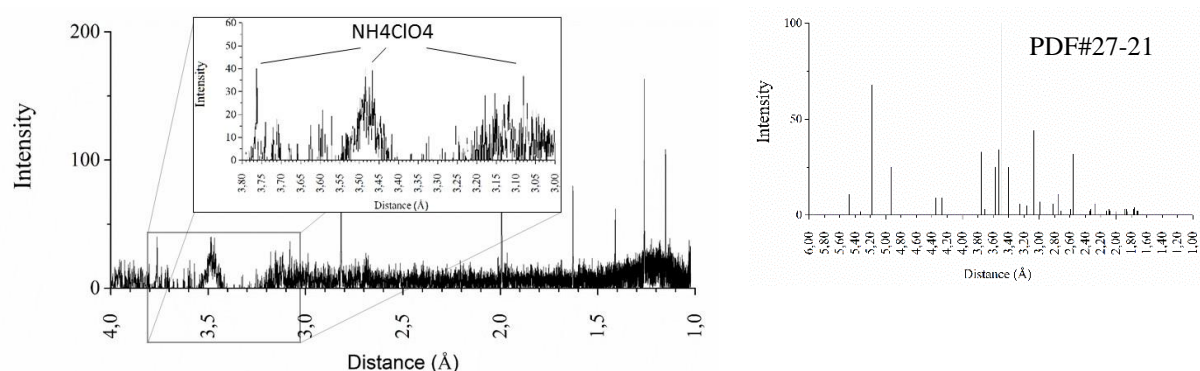
Figure 32. RSr-XRD spectra of $PM_{2.5}$ at M2 associated with N winds.

This conclusion is supported by the presence of higher $K_2Fe_2O_4$ concentrations associated with the same wind direction.

In fact, higher $K_2Fe_2O_4$ concentrations are often associated with N, NE and ENE winds (Figure 31), particularly with N at M2 (>10%, Figure 31b), but less than 5% at M1 when winds blow from ENE (Figure 31a). Biomass combustion studies e.g (Cha and Spiegel, 2004) have reported that the reaction between alkali chlorides (KCl) and hematite (α-Fe_2O_3) lead to the formation of $K_2Fe_2O_4$ and Cl_2 (Equation 13).

$$2KCl + Fe_2O_3 + 0.5O_2 \longrightarrow K_2Fe_2O_4 + Cl_2 \tag{13}$$

Since KCl and α-Fe_2O_3 are used as raw material in the sintering process (Yang et al., 2015), and the directionality of these compounds is always associated with the transport direction from the industrial complex, the formation and emission of $K_2Fe_2O_4$ in RGV is mainly attributed to

sintering stacks. $K_2Fe_2O_4$ contribution is higher at M2 (Figure 31b) than at M1 (Figure 31a), suggesting that M2 is more influenced by sintering stacks emissions.

Sulfates show higher average concentration at M1 than at M2, with a respective value of 18% and 11% (Figure 31a and 31b). $CaSO_4.2H_2O$ and $(NH_4)SO_4$ are commonly found in $PM_{2.5}$ (Chang et al., 2013; Yin et al., 2005), however, in the samples from the RGV, was found additional sulfates associated with Fe and Al, such as $FeAl_2(SO_4)_4.22H_2O$ and $(NH_4)_3Fe(SO_4)_3$. The presence of these crystalline phases can be explained by the reaction between (Al, Fe)-based oxides, such as α-Fe_2O_3 and Al_2O_3, with $(NH_4)_2SO_4$ under temperatures between 210 ºC and 550 ºC (Bayer et al., 1982), as shown in Equation 14 and 15.

$$\alpha Fe_2O_3 + 6(NH_4)_2SO_4 \xrightarrow{\text{210--280ºC}} 2(NH_4)_3Fe(SO_4)_3 + 6NH_3 + 3H_2O \qquad (14)$$

$$\alpha Fe_2O_3 + 3(NH_4)_2SO_4 \xrightarrow{\text{340--550ºC}} Fe_2(SO_4)_3 + 6NH_3 + 3H_2O \qquad (15)$$
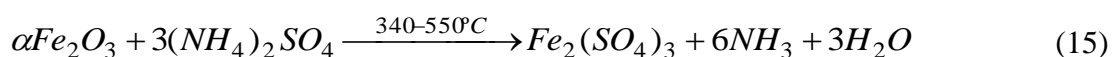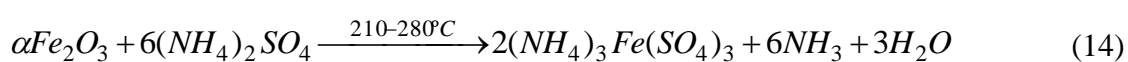
The abundance of iron oxides, such as α-Fe_2O_3, and SO_4^{2-} in the atmosphere may undergo a photo-reduction reaction (Ghio et al., 1999) and form complexes such as $(NH_4)_3Fe(SO_4)_3$ and $FeAl_2(SO_4)_4.22H_2O$. Therefore, these compounds can be emitted by industrial activities or form in the atmosphere via secondary reactions.

Figure 31 shows expressive contents of $NH_4Ca_2P_3O_{10}.2.5H_2O$, particularly 5% and 3% at M1 and M2 respectively, in which larger concentrations are associated with winds from the northeast (NE) quadrant (again industrial complex direction). $NH_4Ca_2P_3O_{10}.2.5H_2O$ is used as mineral fertilizer by the agriculture, where 7 million tons of fertilizers and grains in the RGV were discharged at the port terminal (E3 in Figure 12a) in 2017 alone (Vale, 2018).

5.5.2 Crystal Phases in PM_{10} and Associated Sources

The main difference between PM_{10} and $PM_{2.5}$ crystalline phases consists of the presence of maghemite (γ-Fe_2O_3), magnetite (Fe_3O_4) and goethite (FeOOH) in PM_{10} (Figure 24a), which was not identified in $PM_{2.5}$ (Figure 31).

Despite previous work by de Souza *et al.* (2000) reporting that FeOOH is associated with intense industrial contribution, no evidence suggests this in this study, including the absence of FeOOH at M2 (Figure 33b). In addition, FeOOH is not a constituent of Brazilian iron ores (Rosière and Chemale Jr, 2000), but instead it is reported as a constituent of tropical soils (Fabris et al., 1997). This suggests that FeOOH is associated with soil resuspension in our study. γ-Fe_2O_3 is present in

Itabirito amphibolite iron ore, produced in the state of Minas Gerais (Rosière and Chemale Jr, 2000), although this crystalline phase can also be present in PM originating from pelletizing and sintering processes, as shown in Equation 10. In fact, γ-Fe_2O_3 was predominantly found at M1 associated with N winds (Figure 33a). Fe_3O_4 shows higher contributions at both M1 and M2 when wind direction is predominantly N and NE (industrial complex, Figures 33a and 33b). de Souza et al. (1998) identified Fe_3O_4 in TSP and PM_{10} samples from the sources sintering dust, blast furnaces and steelmaking. α-Fe_2O_3 can be dissociated into Fe_3O_4 in the furnaces at 1350 ºC during the sintering and pelletizing processes (Clout and Manuel, 2003; Jiang et al., 2008), as shown in Equation 16.

$$6Fe_2O_3 \xrightarrow{\;>1350°C\;} 4Fe_3O_4 + O_2 \tag{16}$$

In fact, among the Fe-rich compounds, α-Fe_2O_3 is the most abundant at both M1 and M2. α-Fe_2O_3 is found in samples of iron ore deposits, pellet and sinter agglomerates (de Souza et al., 2000, 1998), although its presence is also reported in pelletizing and sintering stack emissions. In Figure 33a and 33b, higher contents of α-Fe_2O_3 are associated with N and NE winds, and lower contributions are associated with SSE, S and NW winds. Fe is listed as a main constituent of vehicular exhaust and crustal emissions (Thorpe and Harrison, 2008; Viana et al., 2008a), but the presence of other compounds are exclusively associated with industrial activities such as FeS_2 and phosphates mineral fertilizer also show contributions associated with SSE, S and NW winds. Therefore, the contribution of α-Fe_2O_3 associated with winds blowing from location is highly influenced by vehicular traffic, suggesting that PM may be undergoing resuspension.
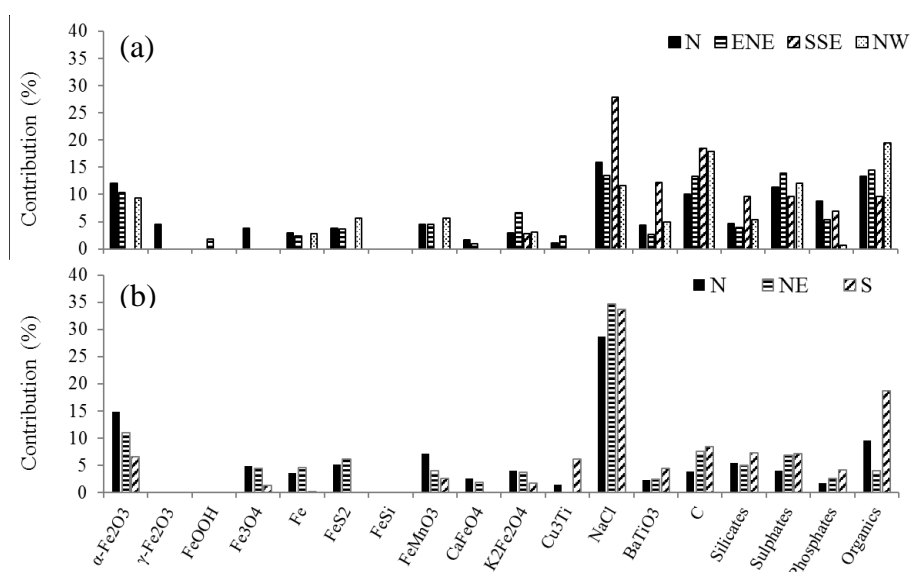
Figure 33. Crystalline phases in PM_{10} at (a) M1 and (b) M2.

NaCl is predominant at M2 due to the proximity of the sea (Figure 12a). Besides, the contribution of NaCl in PM_{10} is quite larger than other compounds (Figure 33b), a pattern not so evident in $PM_{2.5}$ (Figure 33b). This is likely due to the typical dimension of NaCl particles ranging from 2.5 to 10 µm (Moreno et al., 2004). α-Fe_2O_3 is the main industrial constituent, mainly when associated with winds from N and NE. When winds blow from S direction organic compounds gain a larger expression, suggesting higher influence of vehicular sources. Figure 33a shows that M1 is more populated with compounds such as $BaTiO_3$, EC, sulfates, phosphates and organics when compared to M2, and all these compounds are reported as vehicular markers (Cheng et al., 2015; Choi et al., 2013; Thorpe and Harrison, 2008). The findings suggest M1 is more influenced by vehicular emissions and resuspension, while industrial emissions are prevalent at M2.

5.5.3 Crystal Phases in TSP and Associated Sources

NaCl has a large contribution in TSP composition, in which is more evident the greater is the particle size (Figure 34). In TSP, α-Fe_2O_3 contributes with approximately 20% of all mass, mainly when winds blow from the industrial location (NE quadrant), whereas in PM_{10} and $PM_{2.5}$ this value is not greater than 15%. The finding suggests that larger the PM size, the greater the industrial contributions (Figure 34).

Figure 34b shows the greater contribution of $BaTiO_3$, EC, silicates and sulfates at M2. As previously discussed in section 5.5.1, these compounds are strongly associated with vehicular emissions (exhaust, wear, resuspension) suggesting that vehicular sources dominate the contribution of TSP at M1, whereas at M2 the industrial contribution predominates.
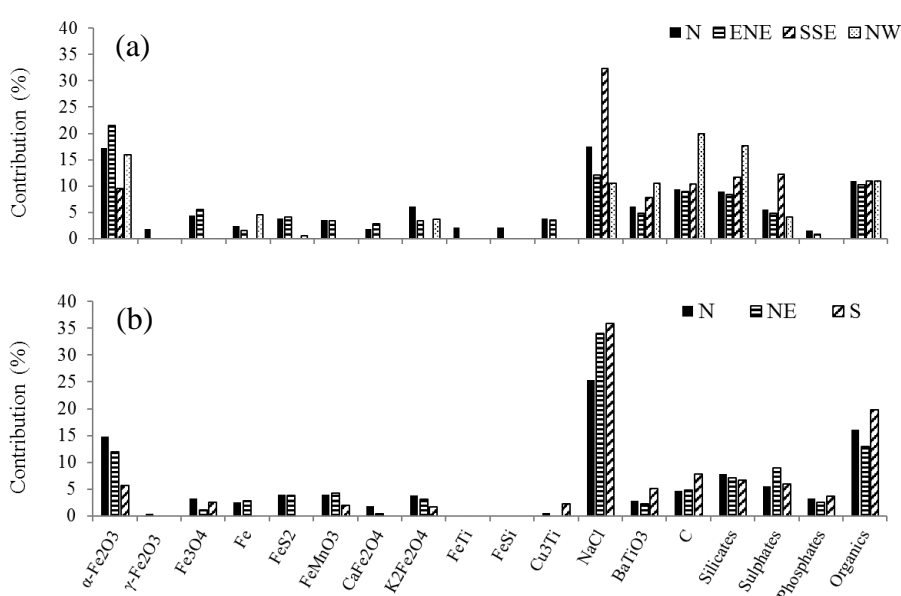
Figure 34. Crystalline phases in TSP at (a) M1 and (b) M2.

5.5.4   Crystal Phases in SP and Associated Sources

At M1 and M2, α-Fe_2O_3 contributions predominate over all compounds, including NaCl (Figure 35). Mechanical processes that "grind" PM to smaller sizes are activities such as iron ore, pellet and sinter handling and storage, besides carrying iron ore and pellets into the ships at the port. Industrial-related compounds such as γ-Fe_2O_3, Fe_3O_4, metallic Fe, $K_2Fe_2O_4$, and overall phosphates and limestone ($CaCO_3$) are higher at M2 than at M1. $CaCO_3$ is used as an additive in the production of sinter and iron pellet (Iljana et al., 2015). M1 is more affected by silicates and EC than M2, suggesting vehicular exhaust and resuspension as the likely sources. This corroborates that larger particles are indeed corresponding to industrial sources in the RGV, especially those emitted by raw materials handling and storage.
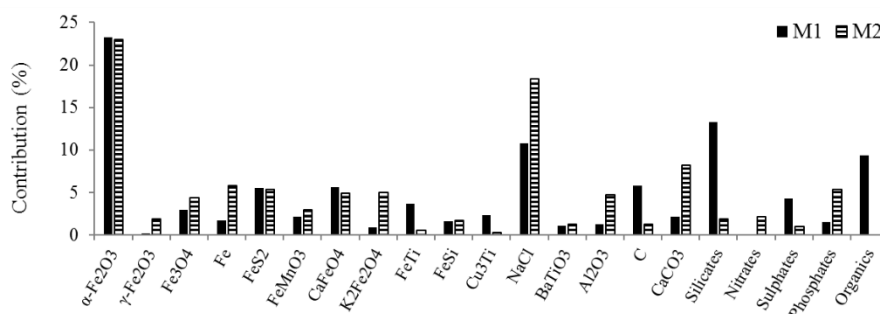
Figure 35. Crystalline phases in SP at (a) M1 and (b) M2.

5.5.5   Clustered Crystal Phases by Associated Sources

Table 9 shows the potential source tracers grouped according to the RGV sources.

The Industrial Fe-based cluster represents the contribution from handling and storage of iron products (pellet and sinter) and raw material (iron ore and alloys), and are associated with α-Fe_2O_3, γ-Fe_2O_3, Fe_3O_4, $CaFeO_4$, FeTi, FeSi and $FeMnO_3$. The Sinter-based cluster represents the contributions from sintering stacks, which is associated mainly with $K_2Fe_2O_4$, NH_3OHClO_4, and sulfates. The Coke and Coal-based cluster represent the contributions from coke oven stacks and coal stockpiles, mainly associated with FeS_2, metallic Fe, sulfates, organics and EC. Sea salt represents the marine spray associated with NaCl. Biomass burning cluster is associated mainly with $K_2Fe_2O_4$; Vehicular-based cluster represents the contributions from vehicular exhaust/wear, mainly associated with $BaTiO_3$, EC, organics and sulfates. The Steel-based cluster represents the contribution from sources of reduced iron, such as blast furnaces and steelmaking–BOF, mainly associated with metallic Fe. The Phosphate- and nitrate-based clusters represent the major contributions from terminal port activities during the discharging of mineral fertilizers. Lastly, the

organic-based cluster represents all other sources of organic carbon in addition to coke and vehicular sources.

Table 9. Potential source markers (crystals) grouped according to the RGV sources.

Crystalline phases	Iron Ore (handling and storage)	Pelletizing	Sintering	Blast furnaces and Steelmaking – BOF	Coke oven	Coke and Coal deposits	Biomass burning	Vehicular	Crustal and Resuspension	Marine spray	Port Terminals	Secondary
α-Fe_2O_3	X	X	X					X				
γ-Fe_2O_3	X	X	X									
Fe_3O_4	X	X	X									
$FeMnO_3$	X											
FeS_2					X	X						
Fe^0				X	X			X				
FeTi				X								
FeSi				X								
$CaFeO_4$		X										
$K_2Fe_2O_4$			X				X					
NH_4Cl			X									
NH_3OHClO_4			X									
$BaTiO_3$								X				
EC					X	X	X	X				
Organics		X	X	X			X	X				
$Na_2S_2O_3.2H_2O$												X
$FeAl_2(SO_4)_4.22H_2O$		X	X		X			X				X
$(NH_4)_3Fe(SO_4)_3$		X	X		X							X
$K_4Ca(SiO_3)_3$									X			
$CaMgSiO_4$									X			
SiO_2									X			
$MgSiO_3$									X			
NaCl										X		

5.5.5.1 – PM$_{2.5}$

Figure 36 shows the clustering for PM$_{2.5}$ at M1 (Figure 36a) and at M2 (Figure 36c). In addition, Figures 36b and 36d show the PM$_{2.5}$ source apportionment by PMF model was made using both organic (PAHs) and inorganic (metals and ions) markers, respectively at M1 and M2 (reported in section 5.1.1.3). It is important to state that the aim of this study is not the establishment of the clustering methodology as a source apportionment tool, but an additional information for the use in source apportionment studies using receptor models such as the PMF.

At M1, there is a significant contribution from the Industrial Fe-based cluster (iron ore, pellet and sinter) mainly associated with α-Fe_2O_3 and $FeMnO_3$ (Figure 27a), a contribution not identified by PMF. In Figure 36b, PMF separated other two factors, the Pelletizing Furnaces and

Resuspension/Industrial Filterable PM$_{2.5}$, highly influenced by elemental Fe contributions. Actually, PMF was only capable of separating the factor attributed to pelleting furnaces (stacks) when using both organic (PAHs) and inorganic (Fe) as markers. Since no crystalline phases could be exclusively attributed to pelletizing furnaces, it was not possible to define a specific cluster associated with pelletizing (Table 9). In addition, Pelletizing furnaces and Resuspension/Industrial Filterable PM$_{2.5}$ factors by PMF explain 38% of the total mass (Figure 36b), whereas Industrial Fe-based clustering (Figure 36a) explains 34% when associated with N winds, suggesting that in fact the composition of Resuspension/Industrial Filterable PM$_{2.5}$ can also have the influence of stockpiles emissions.
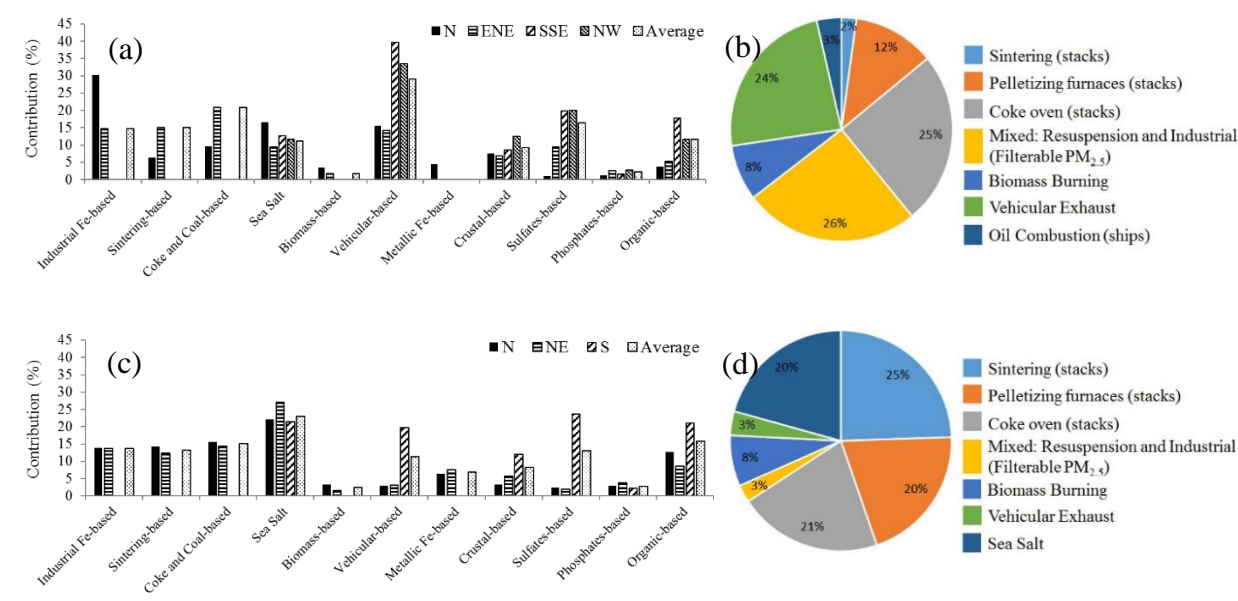
Figure 36. Clustered crystal phases of PM$_{2.5}$ at (a) M1 and (c) M2, and PMF source apportionment of PM$_{2.5}$ at (b) M1 and (d) M2.

The mixed factor Resuspension/Industrial Filterable PM$_{2.5}$ separated by the PMF model (Figure 36b) is mainly characterized by large loadings of Fe and Zn (industrial activities), and by Al, Si, Na, K and Mg (silt resuspension). However, PMF does not identify any exclusive factor associated with crustal. The RSr-XRD identified crystalline phases that clearly identify Crustal-based sources, such as K$_4$Ca(SiO$_3$)$_3$ and CaMgSiO$_4$ (Figure 36a).

In Figure 36b, PMF was not able to identify and separate a factor attributed to sea salt based on the Na and Cl profiles (as discussed in section 5.1.1.3), however, a 10% contribution is attributed to NaCl in M1. The likely explanations are the large Cl loading by other activities such as sintering, coke ovens, and biomass burning that highlight these sources, and lastly, the secondary reaction

decomposing the NaCl into sodium sulfates and nitrates (Zhang et al., 2000), as shown in Equation 17.

$$NaCl + HNO_3 \longrightarrow NaNO_3 + HCl \qquad (17)$$

At M2 (Figure 36c), NaCl predominates with an average value of 24%. Sea salt factor by PMF explains 20% of the total mass (Figure 36d). In addition, the contributions of sintering and Coke/Coal combined represent 24%s at M2 (Figure 36c), a value greater than M1 (10%, Figure 36a). The finding suggests that Cl additional sintering and coke ovens contributions increases PMF sensitivity and allows for marine spray separation from the remaining factors. It is only when Na and Cl concentrations are high that PMF can solve this factor, such in case of M2 (Figure 36d). At M1, the average Cl concentration is 1.2 μg m^{-3}, whereas, at M2, Cl concentration is 60% greater with an average value of 1.9 μg m^{-3}.

The discussion in section 5.5.1 shows that the contribution of $K_2Fe_2O_4$ and NH_3OHClO_4 (sintering markers) are larger at M2 than at M1, supporting the large difference found by PMF results (Figure 36b, and 36d). At M2, the clustering Industrial Fe-based, sintering-based, Coke/Coal-based and Metallic Fe-based contributes with 24% (Figure 36c), whereas at M1 the same clustering contributes with 18% (Figure 36a). Vehicular-based contribution at M1 shows an average value of 30%, whereas at M2 this value is 11%. Therefore, M1 is more affected by PM$_{2.5}$ emission from vehicles and M2 is more affected by emissions of PM$_{2.5}$ from industrial activities.

5.5.5.2 - PM$_{10}$

Industrial-based cluster (section 5.5.5 and Table 9) express 19% of the M1 contributions (Figure 37a). As previously discussed, these compounds can be found on both stack and stockpile PM profiles. At M1, the PMF separates a factor with less than 0.5% attributed to Industrial stockpiles (Figure 37b). Due to the high similarity among the sources pelletizing furnaces and iron ore, pellet and sinter (granulates), in which α-Fe_2O_3 is the main compound, PMF (using elemental Fe) isolates only one 21% factor attributed to Pelletizing furnaces (Figure 37b). This factor is associated with the pelletizing process due to the high loading of Fe and organic (PAHs) markers such as naphthalene, acenaphthylene and phenanthrene. However, α-Fe_2O_3 and $FeMnO_3$ are the main constituents of iron ore and manganese ore, and therefore, some fraction must be emitted by handling and storage activities, potentially generating mechanical formation of PM$_{10}$ (Seinfeld and Pandis, 2006). On the other hand, at M2 (Figure 37d), PMF separated a factor associated with Industrial Stockpiles that explains 42% of the mass with large loadings of Fe, Ca, Mg, Zn, S and P and low loadings of organic species. Indeed, when N and NE directions winds prevail (industrial

location), the contribution of Industrial Fe-based cluster assumes an expressive 30%, excluding coal deposits.

Figures 37a and 37c show that larger the PM size, the greater the influence of industrial Fe-based activities at M2, mainly when winds blow from N and NE. However, sintering- and Coke/Coal-based clusters show a greater contribution at M1 (Figure 37a). In addition, PMF results show that sintering and pelletizing contributions are greater at M1 than M2 (Figures 37b and 37d). In fact, the discussion in sections 5.5.1 and 5.5.2 shows that $K_2Fe_2O_4$ (sintering stacks marker) and γ-Fe_2O_3 (sintering and pelletizing stacks marker) are greater at M1. This pattern can also be associated with a large contribution of NaCl at M2, mounting to 32% (Figure 37c).
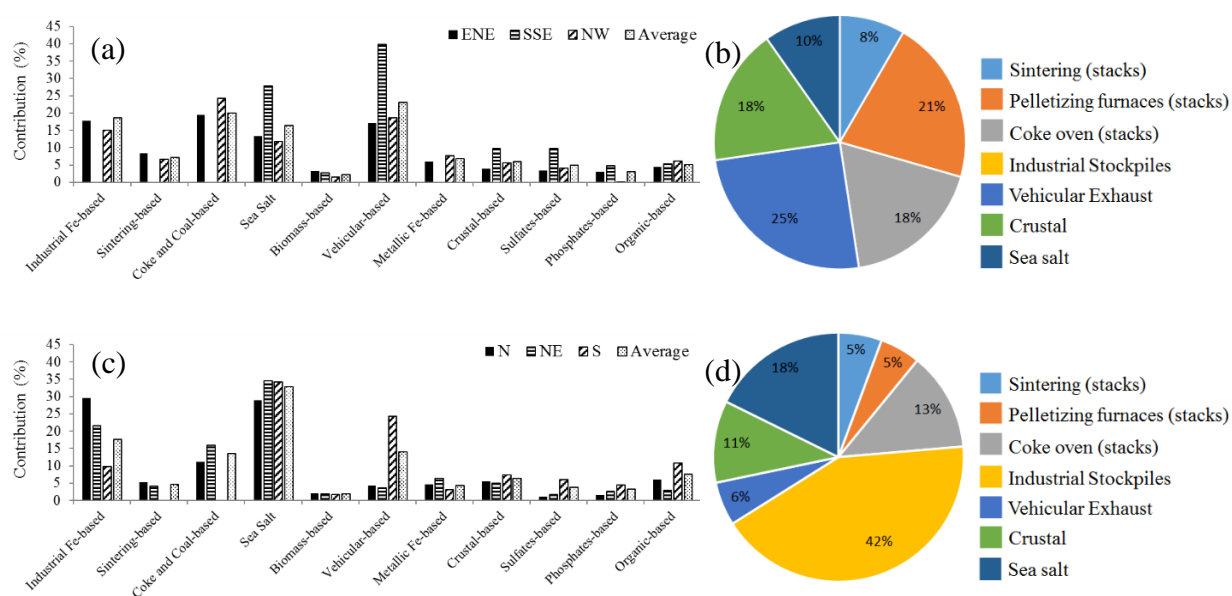
Figure 37. Clustered crystal phases of PM_{10} at (a) M1 and (c) M2, and PMF source apportionment of PM_{10} at (b) M1 and (d) M2.

The findings suggest that PMF show some difficulty in properly separate factors associated with highly correlated sources such as pelletizing furnaces and pellet/iron stockpiles. As previously discussed, the absence of some crystalline phase that can be used as a specific marker for pelletizing furnaces, pellets granulates and iron ore turns the separation of these sources a hard task.

6. Conclusions

A literature review revealed that there are no exclusive markers for any source, but a generalized association of the chemical species with several sources (Table S3 – Appendix C). Consolidated source markers such as OC and EC (vehicular), Cl and K (biomass burning), Fe (crustal and vehicular), in fact were highly correlated with industrial process, and the association of the likely

sources with PMF factors was possible only due to the combined use of both, organic and inorganic species characterization and pollutants roses. Sintering and pelletizing, process with high similarity in terms of chemical composition, were properly separate by PMF with the identification of some PAHs exclusives to each process. For example, sintering showed high loadings of Pyr, Chr, BbF and BghiP, whereas pelletizing showed Phe and Acy as the main markers. These signatures associated to the absence of Fe in the sintering profiles was crucial to separate those sources highly correlated. In other case, EC and Pyr, both markers of vehicular exhaust, in fact showed large concentrations associated with winds from the location of coke ovens. The high loading of S in this factor and the directionality of the EC and Pyr species helped to attribute this factor as coke oven emissions, avoiding the misinterpretation of this factor as vehicular emissions.

The results showed that there is a significant difference in the source apportionment for different particles aerodynamic diameter ranges. At monitoring station M1, the larger the diameter, the larger the contribution of industrial activities. Industrial activities explain for 42% of all mass in $PM_{2.5}$, and this value increases to 47% for PM_{10}. On the opposite way, vehicular related emissions (vehicle exhaust and resuspension) show that the smaller the diameter, the larger the contribution. At M1, vehicular related emissions explain 25% of all mass in PM_{10}, whereas this value increases to 50% in $PM_{2.5}$. At M2, the larger the diameter, the larger the contribution of mechanically generated industrial PM, in which explain 42% of all mass in PM_{10}. Sintering stacks, coke ovens and pelletizing furnaces are the major contributors of $PM_{2.5}$ at both M1 and M2. The handling and storage of industrial raw materials are the main contributor of larger particles at M2.

The joint use of organic and inorganic markers and the knowledge of the directional pattern of the chemical species minimized the misinterpretation of the PMF factors, making it easier and more reliable, furthermore, it minimized the possibility of occurrence of "unidentified" factors.

The use of receptor models in source apportionment studies is well-known to have some difficulties and uncertainties. Source definition based on chemical elements can lead to erroneous interpretation by non-experienced users. An appropriate source profile could bypass this artifact, but the acquisition of locally sourced profiles can be a challenge, especially if local industries resist in supplying samples or data. There is a clear need for more accurate and precise markers, which can be clearly linked to a specific source. Therefore, we proposed a new approach using RSr-XRD associated to EDXRF to determine if ambient PM would possess specific markers that could be linked to process specific crystalline phases. Crystalline phases determination using RSr-XRD technique, together with chemical elements analysis, proves to be an improved way to contour source collinearity problems.

The characterization of PM crystalline phases in combination with wind directionality allow the inference of PM likely sources. The results showed that α-Fe_2O_3 and FeS_2 are strongly associated with industrial activities such as iron ore, pellet and sinter granulates and coal deposits. In addition, the presence of some uncommon compounds in PM samples, such as γ-Fe_2O_3, metallic Fe, $K_2Fe_2O_4$, and $(NH_4)_3Fe(SO_4)_3$ and NH_3OHClO_4, are products of specific chemical reactions within the industrial processes. This finding proves to be an important information that complements the source apportionment studies using receptor models.

Results showed large contribution of NaCl in all particles aerodynamic ranges (from $PM_{2.5}$ to TSP). The influence of industrial activities is more evident in larger particles. For example, α-Fe_2O_3 is the main constituent of SP but its contribution decreases with particles diameter, being the fifth most abundant in $PM_{2.5}$.

Clustering crystalline phases to define source profiles help the differentiation of sources that were collinear identified in PMF results. Sea salt factor in $PM_{2.5}$ was affected by the large concentration of Cl emitted by the sintering and coke ovens, and therefore, it was not identified by PMF. Only for high NaCl contributions, such in the case of M2, the PMF could solve this factor. Nevertheless, NaCl crystals were present in PM2.5 samples at both M1 and M2 sampling sites.

These findings suggest that the use of receptor chemical profiles based on specific crystalline phases, together with organic compounds such as the PAHs, can improve receptor models sensitivity for highly correlated sources.

7. References

Achad, M., López, M.L., Ceppi, S., Palancar, G.G., Tirao, G., Toselli, B.M., 2014. Assessment of fine and sub-micrometer aerosols at an urban environment of Argentina. Atmos. Environ. 92, 522–532. https://doi.org/10.1016/J.ATMOSENV.2014.05.001

Ahmady-Birgani, H., Mirnejad, H., Feiznia, S., McQueen, K.G., 2015. Mineralogy and geochemistry of atmospheric particulates in western Iran. Atmos. Environ. 119, 262–272. https://doi.org/https://doi.org/10.1016/j.atmosenv.2015.08.021

Aldabe, J., Elustondo, D., Santamaría, C., Lasheras, E., Pandolfi, M., Alastuey, A., Querol, X., Santamaría, J.M., 2011. Chemical characterisation and source apportionment of PM2.5 and PM10 at rural, urban and traffic sites in Navarra (North of Spain). Atmos. Res. 102, 191–205. https://doi.org/https://doi.org/10.1016/j.atmosres.2011.07.003

Allan, J.D., Delia, A.E., Coe, H., Bower, K.N., Alfarra, M.R., Jimenez, J.L., Middlebrook, A.M., Drewnick, F., Onasch, T.B., Canagaratna, M.R., Jayne, J.T., Worsnop, D.R., 2004. A generalised method for the extraction of chemically resolved mass spectra from Aerodyne aerosol mass spectrometer data. J. Aerosol Sci. 35, 909–922. https://doi.org/10.1016/J.JAEROSCI.2004.02.007

Allan, J.D., Jimenez, J.L., Williams, P.I., Alfarra, M.R., Bower, K.N., Jayne, J.T., Coe, H., Worsnop, D.R., 2003. Quantitative sampling using an Aerodyne aerosol mass spectrometer 1. Techniques of data interpretation and error analysis. J. Geophys. Res. Atmos. 108. https://doi.org/10.1029/2002JD002358

Allegro, P.R.P., Rizzutto, M. de A., Medina, N.H., 2016. Improvements in the PIGE technique via gamma-ray angular distribution. Microchem. J. 126, 287–295. https://doi.org/http://dx.doi.org/10.1016/j.microc.2015.12.012

Allen, J.O., Dookeran, N.M., Smith, K.A., Sarofim, A.F., Taghizadeh, K., Lafleur, A.L., 1996. Measurement of Polycyclic Aromatic Hydrocarbons Associated with Size-Segregated Atmospheric Aerosols in Massachusetts. Environ. Sci. Technol. 30, 1023–1031. https://doi.org/10.1021/es950517o

Almeida, T.S., Sant´Ana, M.O., Cruz, J.M., Tormen, L., Frescura Bascuñan, V.L.A., Azevedo, P.A., Garcia, C.A.B., Alves, J. do P.H., Araujo, R.G.O., 2017. Characterisation and source identification of the total airborne particulate matter collected in an urban area of Aracaju,

Northeast, Brazil. Environ. Pollut. 226, 444–451. https://doi.org/http://dx.doi.org/10.1016/j.envpol.2017.04.018

Alves, L.C., Reis, M.A., Freitas, M.C., 1998. Air particulate matter characterisation of a rural area in Portugal. Nucl. Instruments Methods Phys. Res. Sect. B Beam Interact. with Mater. Atoms 136–138, 941–947. https://doi.org/10.1016/S0168-583X(97)00761-1

Amodio, M., Andriani, E., Dambruoso, P.R., de Gennaro, G., Di Gilio, A., Intini, M., Palmisani, J., Tutino, M., 2013. A monitoring strategy to assess the fugitive emission from a steel plant. Atmos. Environ. 79, 455–461. https://doi.org/10.1016/J.ATMOSENV.2013.07.001

Amstalden van Hove, E.R., Smith, D.F., Heeren, R.M.A., 2010. A concise review of mass spectrometry imaging. J. Chromatogr. A 1217, 3946–3954. https://doi.org/http://dx.doi.org/10.1016/j.chroma.2010.01.033

Atkins, A., Bignal, K.L., Zhou, J.L., Cazier, F., 2010. Profiles of polycyclic aromatic hydrocarbons and polychlorinated biphenyls from the combustion of biomass pellets. Chemosphere 78, 1385–1392. https://doi.org/10.1016/J.CHEMOSPHERE.2009.12.065

Atkinson, R., 2000. Atmospheric chemistry of VOCs and NOx. Atmos. Environ. 34, 2063–2101. https://doi.org/10.1016/S1352-2310(99)00460-4

Atkinson, R., 1997. Gas-Phase Tropospheric Chemistry of Volatile Organic Compounds: 1. Alkanes and Alkenes. J. Phys. Chem. Ref. Data 26, 215–290. https://doi.org/10.1063/1.556012

Atkinson, R., Arey, J., 2003. Atmospheric Degradation of Volatile Organic Compounds. Chem. Rev. 103, 4605–4638. https://doi.org/10.1021/cr0206420

Avino, P., Capannesi, G., Rosada, A., 2008. Heavy metal determination in atmospheric particulate matter by Instrumental Neutron Activation Analysis. Microchem. J. 88, 97–106. https://doi.org/http://dx.doi.org/10.1016/j.microc.2007.11.005

Balcaen, L., Bolea-Fernandez, E., Resano, M., Vanhaecke, F., 2015. Inductively coupled plasma – Tandem mass spectrometry (ICP-MS/MS): A powerful and universal tool for the interference-free determination of (ultra)trace elements – A tutorial review. Anal. Chim. Acta 894, 7–19. https://doi.org/http://dx.doi.org/10.1016/j.aca.2015.08.053

Balducci, C., Cecinato, A., Paolini, V., Guerriero, E., Perilli, M., Romagnoli, P., Tortorella, C.,

Nacci, R.M., Giove, A., Febo, A., 2017. Volatilization and oxidative artifacts of PM bound PAHs at low volume sampling (2): Evaluation and comparison of mitigation strategies effects. Chemosphere 189, 330–339. https://doi.org/10.1016/J.CHEMOSPHERE.2017.09.062

Bates, M., Bruno, P., Caputi, M., Caselli, M., de Gennaro, G., Tutino, M., 2008. Analysis of polycyclic aromatic hydrocarbons (PAHs) in airborne particles by direct sample introduction thermal desorption GC/MS. Atmos. Environ. 42, 6144–6151. https://doi.org/https://doi.org/10.1016/j.atmosenv.2008.03.050

Bauer, P., Steinbauer, E., Biersack, J.P., 1992. The width of an RBS spectrum: influence of plural and multiple scattering. Nucl. Instruments Methods Phys. Res. Sect. B Beam Interact. with Mater. Atoms 64, 711–715. https://doi.org/http://dx.doi.org/10.1016/0168-583X(92)95563-7

Bayer, G., Kahr, G., Muller-Vonmoos, M., 1982. Reactions of ammonium sulphates with kaolinite and other silicate and oxide minerals. Clay Miner. 17, 271–283.

Bernabé, J.M., Carretero, M.I., Galán, E., 2005. Mineralogy and origin of atmospheric particles in the industrial area of Huelva (SW Spain). Atmos. Environ. 39, 6777–6789. https://doi.org/http://dx.doi.org/10.1016/j.atmosenv.2005.07.073

Bilo, F., Borgese, L., Dalipi, R., Zacco, A., Federici, S., Masperi, M., Leonesio, P., Bontempi, E., Depero, L.E., 2017. Elemental analysis of tree leaves by total reflection X-ray fluorescence: New approaches for air quality monitoring. Chemosphere 178, 504–512. https://doi.org/http://dx.doi.org/10.1016/j.chemosphere.2017.03.090

Blanchard, C.L., Tanenbaum, S., Hidy, G.M., 2012. Source Contributions to Atmospheric Gases and Particulate Matter in the Southeastern United States. Environ. Sci. Technol. 46, 5479–5488. https://doi.org/10.1021/es203568t

Borgese, L., Salmistraro, M., Gianoncelli, A., Zacco, A., Lucchini, R., Zimmerman, N., Pisani, L., Siviero, G., Depero, L.E., Bontempi, E., 2012. Airborne particulate matter (PM) filter analysis and modeling by total reflection X-ray fluorescence (TXRF) and X-ray standing wave (XSW). Talanta 89, 99–104. https://doi.org/http://dx.doi.org/10.1016/j.talanta.2011.11.073

Bowsher, B.R., Nichols, A.L., 1990. Chemical characterisation of nuclear aerosols by surface analysis techniques. J. Aerosol Sci. 21, S591–S595.

https://doi.org/http://dx.doi.org/10.1016/0021-8502(90)90312-L

Braga, C.F., Teixeira, E.C., Meira, L., Wiegand, F., Yoneama, M.L., Dias, J.F., 2005. Elemental composition of PM10 and PM2.5 in urban environment in South Brazil. Atmos. Environ. 39, 1801–1815. https://doi.org/10.1016/J.ATMOSENV.2004.12.004

Brown, R.J.C., Edwards, P.R., 2009. Measurement of anions in ambient particulate matter by ion chromatography: A novel sample preparation technique and development of a generic uncertainty budget. Talanta 80, 1020–1024. https://doi.org/10.1016/J.TALANTA.2009.07.042

Brown, R.J.C., Milton, M.J.T., 2005. Analytical techniques for trace element analysis: an overview. TrAC Trends Anal. Chem. 24, 266–274. https://doi.org/http://dx.doi.org/10.1016/j.trac.2004.11.010

Brunekreef, B., Holgate, S.T., 2002. Air pollution and health. Lancet 360, 1233–1242. https://doi.org/10.1016/S0140-6736(02)11274-8

Bruno, P., Caselli, M., de Gennaro, G., Tutino, M., 2007. Determination of polycyclic aromatic hydrocarbons (PAHs) in particulate matter collected with low volume samplers. Talanta 72, 1357–1361. https://doi.org/http://dx.doi.org/10.1016/j.talanta.2007.01.043

Bumbrah, G.S., Sharma, R.M., 2016. Raman spectroscopy – Basic principle, instrumentation and selected applications for the characterization of drugs of abuse. Egypt. J. Forensic Sci. 6, 209–215. https://doi.org/http://dx.doi.org/10.1016/j.ejfs.2015.06.001

Cahill, T.A., Wakabayashi, P.H., James, T.A., 1996. Chemical states of sulfate at Shenandoah National Park during summer, 1991. Nucl. Instruments Methods Phys. Res. Sect. B Beam Interact. with Mater. Atoms 109, 542–547. https://doi.org/https://doi.org/10.1016/0168-583X(95)00965-5

Callén, M.S., López, J.M., Iturmendi, A., Mastral, A.M., 2013. Nature and sources of particle associated polycyclic aromatic hydrocarbons (PAH) in the atmospheric environment of an urban area. Environ. Pollut. 183, 166–174. https://doi.org/10.1016/J.ENVPOL.2012.11.009

Calzolai, G., Chiari, M., Lucarelli, F., Mazzei, F., Nava, S., Prati, P., Valli, G., Vecchi, R., 2008. PIXE and XRF analysis of particulate matter samples: an inter-laboratory comparison. Nucl. Instruments Methods Phys. Res. Sect. B Beam Interact. with Mater. Atoms 266, 2401–2404. https://doi.org/http://dx.doi.org/10.1016/j.nimb.2008.03.056

Calzolai, G., Lucarelli, F., Chiari, M., Nava, S., Giannoni, M., Carraresi, L., Prati, P., Vecchi, R., 2015. Improvements in PIXE analysis of hourly particulate matter samples. Nucl. Instruments Methods Phys. Res. Sect. B Beam Interact. with Mater. Atoms 363, 99–104. https://doi.org/http://dx.doi.org/10.1016/j.nimb.2015.08.022

Canepari, S., Perrino, C., Astolfi, M.L., Catrambone, M., Perret, D., 2009. Determination of soluble ions and elements in ambient air suspended particulate matter: Inter-technique comparison of XRF, IC and ICP for sample-by-sample quality control. Talanta 77, 1821–1829. https://doi.org/http://dx.doi.org/10.1016/j.talanta.2008.10.029

Cardell, C., Guerra, I., 2016. An overview of emerging hyphenated SEM-EDX and Raman spectroscopy systems: Applications in life, environmental and materials sciences. TrAC Trends Anal. Chem. 77, 156–166. https://doi.org/http://dx.doi.org/10.1016/j.trac.2015.12.001

Carmona, N., Ortega-Feliu, I., Gómez-Tubío, B., Villegas, M.A., 2010. Advantages and disadvantages of PIXE/PIGE, XRF and EDX spectrometries applied to archaeometric characterisation of glasses. Mater. Charact. 61, 257–267. https://doi.org/http://dx.doi.org/10.1016/j.matchar.2009.12.006

Carter, W.P.L., 1994. Development of Ozone Reactivity Scales for Volatile Organic Compounds. Air Waste 44, 881–899. https://doi.org/10.1080/1073161X.1994.10467290

Carvalho, A.M.G., Nunes, R.S., Coelho, A.A., 2017. X-ray powder diffraction of high-absorption materials at the XRD1 beamline off the best conditions: Application to (Gd, Nd)5Si4 compounds. Powder Diffr. 32, 10–14. https://doi.org/10.1017/S0885715616000646

Çevik, U., Ergen, E., Budak, G., Karabulut, A., Tiraşoğlu, E., Apaydin, G., Kopya, A.I., 2003. Elemental analysis of Akçaabat tobacco and its ash by EDXRF spectrometry. J. Quant. Spectrosc. Radiat. Transf. 78, 409–415. https://doi.org/http://dx.doi.org/10.1016/S0022-4073(02)00263-7

Cha, S.C., Spiegel, M., 2004. Fundamental Studies on Alkali Chloride Induced Corrosion during Combustion of Biomass, in: High Temperature Corrosion and Protection of Materials 6, Materials Science Forum. Trans Tech Publications, pp. 1055–1062. https://doi.org/10.4028/www.scientific.net/MSF.461-464.1055

Chang, S.-Y., Chou, C.C.., Liu, S., Zhang, Y., 2013. The Characteristics of PM2.5 and Its

Chemical Compositions between Different Prevailing Wind Patterns in Guangzhou. Aerosol Air Qual. Res. 13, 1373–1383. https://doi.org/10.4209/aaqr.2012.09.0253

Chauhan, A., Goyal, M.K., Chauhan, P., 2014. GC-MS Technique and its Analytical Applications in Science and Technology. J. Anal. Bioanal. Tech. 5, 1–5.

Chen, F., Hu, W., Zhong, Q., 2013. Emissions of particle-phase polycyclic aromatic hydrocarbons (PAHs) in the Fu Gui-shan Tunnel of Nanjing, China. Atmos. Res. 124, 53–60. https://doi.org/http://dx.doi.org/10.1016/j.atmosres.2012.12.008

Chen, H., 1996. Surface/interface X-ray diffraction. Mater. Chem. Phys. 43, 116–125. https://doi.org/http://dx.doi.org/10.1016/0254-0584(95)01618-5

Chen, H., Teng, Y., Wang, J., 2012. Source apportionment of polycyclic aromatic hydrocarbons (PAHs) in surface sediments of the Rizhao coastal area (China) using diagnostic ratios and factor analysis with nonnegative constraints. Sci. Total Environ. 414, 293–300. https://doi.org/https://doi.org/10.1016/j.scitotenv.2011.10.057

Chen, L.-W.A., Watson, J.G., Chow, J.C., Magliano, K.L., 2007. Quantifying PM2.5 Source Contributions for the San Joaquin Valley with Multivariate Receptor Models. Environ. Sci. Technol. 41, 2818–2826. https://doi.org/10.1021/es0525105

Cheng, W., Weng, L.-T., Li, Y., Lau, A., Chan, C.K., Chan, C.-M., 2013. Surface Chemical Composition of Size-Fractionated Urban Walkway Aerosols Determined by X-Ray Photoelectron Spectroscopy. Aerosol Sci. Technol. 47, 1118–1124. https://doi.org/10.1080/02786826.2013.824066

Cheng, Y., Lee, S., Gu, Z., Ho, K., Zhang, Y., Huang, Y., Chow, J.C., Watson, J.G., Cao, J., Zhang, R., 2015. PM2.5 and PM10-2.5 chemical composition and source apportionment near a Hong Kong roadway. Particuology 18, 96–104. https://doi.org/http://dx.doi.org/10.1016/j.partic.2013.10.003

Chiari, M., Calzolai, G., Giannoni, M., Lucarelli, F., Nava, S., Becagli, S., 2015. Use of proton elastic scattering techniques to determine carbonaceous fractions in atmospheric aerosols collected on Teflon filters. J. Aerosol Sci. 89, 85–95. https://doi.org/http://dx.doi.org/10.1016/j.jaerosci.2015.07.006

Chiari, M., Del Carmine, P., Lucarelli, F., Marcazzan, G., Nava, S., Paperetti, L., Prati, P., Valli, G., Vecchi, R., Zucchiatti, A., 2004. Atmospheric aerosol characterisation by Ion Beam

Analysis techniques: recent improvements at the Van de Graaff laboratory in Florence. Nucl. Instruments Methods Phys. Res. Sect. B Beam Interact. with Mater. Atoms 219, 166–170. https://doi.org/https://doi.org/10.1016/j.nimb.2004.01.047

Chithra, V.S., Shiva Nagendra, S.M., 2013. Chemical and morphological characteristics of indoor and outdoor particulate matter in an urban environment. Atmos. Environ. 77, 579–587. https://doi.org/http://dx.doi.org/10.1016/j.atmosenv.2013.05.044

Choi, J.-K., Ban, S.-J., Kim, Y.-P., Kim, Y.-H., Yi, S.-M., Zoh, K.-D., 2015. Molecular marker characterization and source appointment of particulate matter and its organic aerosols. Chemosphere 134, 482–491. https://doi.org/10.1016/J.CHEMOSPHERE.2015.04.093

Choi, J., Heo, J.-B., Ban, S.-J., Yi, S.-M., Zoh, K.-D., 2013. Source apportionment of PM2.5 at the coastal area in Korea. Sci. Total Environ. 447, 370–380. https://doi.org/10.1016/J.SCITOTENV.2012.12.047

Chou, I.-M., Wang, A., 2017. Application of laser Raman micro-analyses to Earth and planetary materials. J. Asian Earth Sci. https://doi.org/http://dx.doi.org/10.1016/j.jseaes.2017.06.032

Choung, S., Oh, J., Han, W.S., Chon, C.-M., Kwon, Y., Kim, D.Y., Shin, W., 2016. Comparison of physicochemical properties between fine (PM2.5) and coarse airborne particles at cold season in Korea. Sci. Total Environ. 541, 1132–1138. https://doi.org/http://dx.doi.org/10.1016/j.scitotenv.2015.10.021

Chow, J.C., Watson, J.G., 1998. Guideline on Speciated Particulate Monitoring; Prepared for U.S. Environmental Protection Agency, Research Triangle Park, NC, by Desert Research Institute. Reno, NV.

Cienfuegos, F., Vaitsman, D., 2000. Análise Instrumental, 1st ed. Editora Interciência, Rio de Janeiro.

Clements, N., Eav, J., Xie, M., Hannigan, M.P., Miller, S.L., Navidi, W., Peel, J.L., Schauer, J.J., Shafer, M.M., Milford, J.B., 2014. Concentrations and source insights for trace elements in fine and coarse particulate matter. Atmos. Environ. 89, 373–381. https://doi.org/https://doi.org/10.1016/j.atmosenv.2014.01.011

Clout, J.M.., Manuel, J.., 2003. Fundamental investigations of differences in bonding mechanisms in iron ore sinter formed from magnetite concentrates and hematite ores. Powder Technol. 130, 393–399. https://doi.org/10.1016/S0032-5910(02)00241-3

Cohen, D.D., Crawford, J., Stelcer, E., Bac, V.T., 2010. Characterisation and source apportionment of fine particulate sources at Hanoi from 2001 to 2008. Atmos. Environ. 44, 320–328. https://doi.org/10.1016/J.ATMOSENV.2009.10.037

Cohen, D.D., Stelcer, E., Garton, D., Crawford, J., 2011. Fine particle characterisation, source apportionment and long-range dust transport into the Sydney Basin: a long term study between 1998 and 2009. Atmos. Pollut. Res. 2, 182–189. https://doi.org/10.5094/APR.2011.023

Cohn, C.A., Laffers, R., Simon, S.R., O'Riordan, T., Schoonen, M.A.A., 2006. Role of pyrite in formation of hydroxyl radicals in coal: possible implications for human health. Part. Fibre Toxicol. 3, 16. https://doi.org/10.1186/1743-8977-3-16

Cong, Z., Kang, S., Dong, S., Liu, X., Qin, D., 2008. Elemental and individual particle analysis of atmospheric aerosols from high Himalayas. Environ. Monit. Assess. 160, 323. https://doi.org/10.1007/s10661-008-0698-3

Conner, T.L., Williams, R.W., 2004. Identification of possible sources of particulate matter in the personal cloud using SEM/EDX. Atmos. Environ. 38, 5305–5310. https://doi.org/https://doi.org/10.1016/j.atmosenv.2004.06.005

Contini, D., Cesari, D., Conte, M., Donateo, A., 2016. Application of PMF and CMB receptor models for the evaluation of the contribution of a large coal-fired power plant to PM10 concentrations. Sci. Total Environ. 560–561, 131–140. https://doi.org/10.1016/J.SCITOTENV.2016.04.031

Contini, D., Cesari, D., Genga, A., Siciliano, M., Ielpo, P., Guascito, M.R., Conte, M., 2014. Source apportionment of size-segregated atmospheric particles based on the major water-soluble components in Lecce (Italy). Sci. Total Environ. 472, 248–261. https://doi.org/http://dx.doi.org/10.1016/j.scitotenv.2013.10.127

Corcoran, C.J., Tavassol, H., Rigsby, M.A., Bagus, P.S., Wieckowski, A., 2010. Application of XPS to study electrocatalysts for fuel cells. J. Power Sources 195, 7856–7879. https://doi.org/http://dx.doi.org/10.1016/j.jpowsour.2010.06.018

Corio, L.A., Sherwell, J., 2000. In-Stack Condensible Particulate Matter Measurements and Issues. J. Air Waste Manage. Assoc. 50, 207–218. https://doi.org/10.1080/10473289.2000.10464002

Crilley, L.R., Lucarelli, F., Bloss, W.J., Harrison, R.M., Beddows, D.C., Calzolai, G., Nava, S.,

Valli, G., Bernardoni, V., Vecchi, R., 2017. Source apportionment of fine and coarse particles at a roadside and urban background site in London during the 2012 summer ClearfLo campaign. Environ. Pollut. 220, 766–778. https://doi.org/http://dx.doi.org/10.1016/j.envpol.2016.06.002

Csedreki, L., Huszank, R., 2015. Application of PIGE, BS and NRA techniques to oxygen profiling in steel joints using deuteron beam. Nucl. Instruments Methods Phys. Res. Sect. B Beam Interact. with Mater. Atoms 348, 165–169. https://doi.org/http://dx.doi.org/10.1016/j.nimb.2014.12.013

d'Acapito, F., Mazziotti Tagliani, S., Di Benedetto, F., Gianfagna, A., 2014. Local order and valence state of Fe in urban suspended particulate matter. Atmos. Environ. 99, 582–586. https://doi.org/https://doi.org/10.1016/j.atmosenv.2014.10.028

Dabek-Zlotorzynska, E., Aranda-Rodriguez, R., Buykx, S.E., 2002. Development and validation of capillary electrophoresis for the determination of selected metal ions in airborne particulate matter after sequential extraction. Anal. Bioanal. Chem. 372, 467–472. https://doi.org/10.1007/s00216-001-1114-9

Dabek-Zlotorzynska, E., Kelly, M., Chen, H., Chakrabarti, C.L., 2003. Evaluation of capillary electrophoresis combined with a BCR sequential extraction for determining distribution of Fe, Zn, Cu, Mn, and Cd in airborne particulate matter. Anal. Chim. Acta 498, 175–187. https://doi.org/http://dx.doi.org/10.1016/j.aca.2003.06.002

Dat, N.-D., Chang, M.B., 2017. Review on characteristics of PAHs in atmosphere, anthropogenic sources and control technologies. Sci. Total Environ. 609, 682–693. https://doi.org/10.1016/J.SCITOTENV.2017.07.204

de Miranda, R.M., de Fatima Andrade, M., Fornaro, A., Astolfo, R., de Andre, P.A., Saldiva, P., 2012. Urban air pollution: a representative survey of PM2.5 mass concentrations in six Brazilian cities. Air Qual. Atmos. Heal. 5, 63–77. https://doi.org/10.1007/s11869-010-0124-1

de Souza, P.A., de Queiroz, R.S., Morimoto, T., Guimarães, A.F., Garg, V.K., 2000. Air Pollution Investigation in Vitória Metropolitan Region, ES, Brazil. J. Radioanal. Nucl. Chem. 246, 85–90. https://doi.org/10.1023/A:1006729014335

de Souza, P.A., de Queiroz, R.S., Morimoto, T., Guimarães, A.F., Garg, V.K., Klingelhöfer, G.,

2002. Precise Indication of Air Pollution Sources. Hyperfine Interact. 139, 641–649. https://doi.org/10.1023/A:1021295416941

de Souza, P.A., Rodrigues, O.D., Morimoto, T., Garg, V.K., 1998. Industrial Responsibility in the Emission of Particulate Matter in the Atmosphere. Hyperfine Interact. 112, 133–138. https://doi.org/10.1023/A:1011057231700

DeCarlo, P.F., Kimmel, J.R., Trimborn, A., Northway, M.J., Jayne, J.T., Aiken, A.C., Gonin, M., Fuhrer, K., Horvath, T., Docherty, K.S., Worsnop, D.R., Jimenez, J.L., 2006. Field-Deployable, High-Resolution, Time-of-Flight Aerosol Mass Spectrometer. Anal. Chem. 78, 8281–8289. https://doi.org/10.1021/ac061249n

Dedik, A.N., Hoffmann, P., Ensling, J., 1992. Chemical characterization of iron in atmospheric aerosols. Atmos. Environ. Part A. Gen. Top. 26, 2545–2548. https://doi.org/https://doi.org/10.1016/0960-1686(92)90106-U

DENATRAN, 2018. National vehicular fleet.

Deng, J., Ma, X., Zhang, Y., Li, Y., Zhu, W., 2015. Effects of pyrite on the spontaneous combustion of coal. Int. J. Coal Sci. Technol. 2, 306–311. https://doi.org/10.1007/s40789-015-0085-y

Devos, O., Combet, E., Tassel, P., Paturel, L., 2006. EXHAUST EMISSIONS OF PAHs OF PASSENGER CARS. Polycycl. Aromat. Compd. 26, 69–78. https://doi.org/10.1080/10406630500519346

Diapouli, E., Manousakas, M., Vratolis, S., Vasilatou, V., Maggos, T., Saraga, D., Grigoratos, T., Argyropoulos, G., Voutsa, D., Samara, C., Eleftheriadis, K., 2017. Evolution of air pollution source contributions over one decade, derived by PM10 and PM2.5 source apportionment in two metropolitan urban areas in Greece. Atmos. Environ. 164, 416–430. https://doi.org/http://dx.doi.org/10.1016/j.atmosenv.2017.06.016

Díaz, R. V, López-Monroy, J., Miranda, J., Espinosa, A.A., 2014. PIXE and XRF analysis of atmospheric aerosols from a site in the West area of Mexico City. Nucl. Instruments Methods Phys. Res. Sect. B Beam Interact. with Mater. Atoms 318, 135–138. https://doi.org/https://doi.org/10.1016/j.nimb.2013.05.095

Dieme, D., Cabral-Ndior, M., Garçon, G., Verdin, A., Billet, S., Cazier, F., Courcot, D., Diouf, A., Shirali, P., 2012. Relationship between physicochemical characterization and toxicity of fine

particulate matter (PM2.5) collected in Dakar city (Senegal). Environ. Res. 113, 1–13. https://doi.org/http://dx.doi.org/10.1016/j.envres.2011.11.009

Dockery, D.W., Pope, C.A., 1994. Acute Respiratory Effects of Particulate Air Pollution. Annu. Rev. Public Health 15, 107–132. https://doi.org/10.1146/annurev.pu.15.050194.000543

Dogan, O., Kobya, M., 2006. Elemental analysis of trace elements in fly ash sample of Yatağan thermal power plants using EDXRF. J. Quant. Spectrosc. Radiat. Transf. 101, 146–150. https://doi.org/http://dx.doi.org/10.1016/j.jqsrt.2005.11.072

Dolk, H., Vrijheid, M., 2003. The impact of environmental pollution on congenital anomalies. Br. Med. Bull. 68, 25–45.

Duan, J., Tan, J., 2013. Atmospheric heavy metals and Arsenic in China: Situation, sources and control policies. Atmos. Environ. 74, 93–101. https://doi.org/http://dx.doi.org/10.1016/j.atmosenv.2013.03.031

Dutton, S.J., Vedal, S., Piedrahita, R., Milford, J.B., Miller, S.L., Hannigan, M.P., 2010. Source apportionment using positive matrix factorization on daily measurements of inorganic and organic speciated PM2.5. Atmos. Environ. 44, 2731–2741. https://doi.org/10.1016/J.ATMOSENV.2010.04.038

Ekinci, N., Astam, N., Sahin, Y., 2002. Qualitative and quantitative analysis of the cataract using EDXRF. J. Quant. Spectrosc. Radiat. Transf. 72, 783–787. https://doi.org/http://dx.doi.org/10.1016/S0022-4073(01)00157-1

Elmes, M., Gasparon, M., 2017. Sampling and single particle analysis for the chemical characterisation of fine atmospheric particulates: A review. J. Environ. Manage. 202, 137–150. https://doi.org/http://dx.doi.org/10.1016/j.jenvman.2017.06.067

Elorduy, I., Elcoroaristizabal, S., Durana, N., García, J.A., Alonso, L., 2016. Diurnal variation of particle-bound PAHs in an urban area of Spain using TD-GC/MS: Influence of meteorological parameters and emission sources. Atmos. Environ. 138, 87–98. https://doi.org/http://dx.doi.org/10.1016/j.atmosenv.2016.05.012

Elzinga, E.J., Gao, Y., Fitts, J.P., Tappero, R., 2011. Iron speciation in urban dust. Atmos. Environ. 45, 4528–4532. https://doi.org/https://doi.org/10.1016/j.atmosenv.2011.05.042

Esen, F., Tasdemir, Y., Vardar, N., 2008. Atmospheric concentrations of PAHs, their possible

sources and gas-to-particle partitioning at a residential site of Bursa, Turkey. Atmos. Res. 88, 243–255. https://doi.org/10.1016/J.ATMOSRES.2007.11.022

Ezeh, G.C., Obioh, I.B., Asubiojo, O.I., Chiari, M., Nava, S., Calzolai, G., Lucarelli, F., Nuviadenu, C., 2015. The complementarity of PIXE and PIGE techniques: A case study of size segregated airborne particulates collected from a Nigeria city. Appl. Radiat. Isot. 103, 82–92. https://doi.org/http://dx.doi.org/10.1016/j.apradiso.2015.05.015

Ezeh, G.C., Obioh, I.B., Asubiojo, O.I., Chiari, M., Nava, S., Calzolai, G., Lucarelli, F., Nuviadenu, C.K., 2014. Elemental compositions of PM10–2.5 and PM2.5 aerosols of a Nigerian urban city using ion beam analytical techniques. Nucl. Instruments Methods Phys. Res. Sect. B Beam Interact. with Mater. Atoms 334, 28–33. https://doi.org/http://dx.doi.org/10.1016/j.nimb.2014.04.022

Fabris, J.D., de Jesus Filho, M.F., Coey, J.M.D., Mussel, W. da N., Goulart, A.T., 1997. Iron-rich spinels from Brazilian soils. Hyperfine Interact. 110, 23–32. https://doi.org/10.1023/A:1012619331408

Falkovich, A.H., Rudich, Y., 2001. Analysis of Semivolatile Organic Compounds in Atmospheric Aerosols by Direct Sample Introduction Thermal Desorption GC/MS. Environ. Sci. Technol. 35, 2326–2333. https://doi.org/10.1021/es000280i

Félix, O.I., Csavina, J., Field, J., Rine, K.P., Sáez, A.E., Betterton, E.A., 2015. Use of lead isotopes to identify sources of metal and metalloid contaminants in atmospheric aerosol from mining operations. Chemosphere 122, 219–226. https://doi.org/https://doi.org/10.1016/j.chemosphere.2014.11.057

Feng, X., Dang, Z., Huang, W., Shao, L., Li, W., 2009. Microscopic morphology and size distribution of particles in PM2.5 of Guangzhou City. J. Atmos. Chem. 64, 37–51. https://doi.org/10.1007/s10874-010-9169-7

Ferreira, F.F., Bueno, P.R., Setti, G.O., Giménez-Romero, D., García-Jareño, J.J., Vicente, F., 2008. Resonant x-ray diffraction as a tool to calculate mixed valence ratios: Application to Prussian Blue materials. Appl. Phys. Lett. 92, 264103. https://doi.org/10.1063/1.2952457

Fischer, K., 2002. Environmental analysis of aliphatic carboxylic acids by ion-exclusion chromatography. Anal. Chim. Acta 465, 157–173. https://doi.org/http://dx.doi.org/10.1016/S0003-2670(02)00204-0

Flament, P., Mattielli, N., Aimoz, L., Choël, M., Deboudt, K., Jong, J. de, Rimetz-Planchon, J., Weis, D., 2008. Iron isotopic fractionation in industrial emissions and urban aerosols. Chemosphere 73, 1793–1798. https://doi.org/https://doi.org/10.1016/j.chemosphere.2008.08.042

Fultz, B., 2011. "Mössbauer Spectrometry", in Characterization of Materials. John Wiley, New York.

Furuyama, Y., Fujita, H., Taniike, A., Kitamura, A., 2011. Ion beam analyses of particulate matter in exhaust gas of a ship diesel engine. Nucl. Instruments Methods Phys. Res. Sect. B Beam Interact. with Mater. Atoms 269, 3063–3066. https://doi.org/http://dx.doi.org/10.1016/j.nimb.2011.04.071

Gaga, E.O., Ari, A., 2011. Gas–particle partitioning of polycyclic aromatic hydrocarbons (PAHs) in an urban traffic site in Eskisehir, Turkey. Atmos. Res. 99, 207–216. https://doi.org/10.1016/J.ATMOSRES.2010.10.013

Gallavardin, S., Lohmann, U., Cziczo, D., 2008. Analysis and differentiation of mineral dust by single particle laser mass spectrometry. Int. J. Mass Spectrom. 274, 56–63. https://doi.org/10.1016/J.IJMS.2008.04.031

Galvão, E.S., Santos, J.M., Lima, A.T., Reis, N.C., Orlando, M.T.D., Stuetz, R.M., 2018. Trends in analytical techniques applied to particulate matter characterization: A critical review of fundaments and applications. Chemosphere 199. https://doi.org/10.1016/j.chemosphere.2018.02.034

Galvão, E.S., Santos, J.M., Reis Junior, N.C., Stuetz, R.M., 2016. Volatile organic compounds speciation and their influence on ozone formation potential in an industrialized urban area in Brazil. Environ. Technol. (United Kingdom) 37. https://doi.org/10.1080/09593330.2016.1142001

Gao, B., Wang, X.-M., Zhao, X.-Y., Ding, X., Fu, X.-X., Zhang, Y.-L., He, Q.-F., Zhang, Z., Liu, T.-Y., Huang, Z.-Z., Chen, L.-G., Peng, Y., Guo, H., 2015. Source apportionment of atmospheric PAHs and their toxicity using PMF: Impact of gas/particle partitioning. Atmos. Environ. 103, 114–120. https://doi.org/https://doi.org/10.1016/j.atmosenv.2014.12.006

Geldenhuys, G., Rohwer, E.R., Naudé, Y., Forbes, P.B.C., 2015. Monitoring of atmospheric gaseous and particulate polycyclic aromatic hydrocarbons in South African platinum mines

utilising portable denuder sampling with analysis by thermal desorption–comprehensive gas chromatography–mass spectrometry. J. Chromatogr. A 1380, 17–28. https://doi.org/http://dx.doi.org/10.1016/j.chroma.2014.12.062

Ghio, A.J., Devlin, R.B., 2001. Inflammatory Lung Injury after Bronchial Instillation of Air Pollution Particles. Am. J. Respir. Crit. Care Med. 164, 704–708. https://doi.org/10.1164/ajrccm.164.4.2011089

Ghio, A.J., Stoneheurner, J., McGee, J.K., Kinsey, J.S., 1999. Sulfate content correlates with iron concentrations in ambient air pollution particles. Inhal. Toxicol. 11, 293–307. https://doi.org/10.1080/089583799197104

Gil-Moltó, J., Varea, M., Galindo, N., Crespo, J., 2009. Application of an automatic thermal desorption–gas chromatography–mass spectrometry system for the analysis of polycyclic aromatic hydrocarbons in airborne particulate matter. J. Chromatogr. A 1216, 1285–1289. https://doi.org/https://doi.org/10.1016/j.chroma.2008.12.080

Gildemeister, A.E., Hopke, P.K., Kim, E., 2007. Sources of fine urban particulate matter in Detroit, MI. Chemosphere 69, 1064–1074. https://doi.org/10.1016/J.CHEMOSPHERE.2007.04.027

Gilham, R.J.J., Spencer, S.J., Butterfield, D., Seah, M.P., Quincey, P.G., 2008. On the applicability of XPS for quantitative total organic and elemental carbon analysis of airborne particulate matter. Atmos. Environ. 42, 3888–3891. https://doi.org/http://dx.doi.org/10.1016/j.atmosenv.2008.01.007

Godelitsas, A., Nastos, P., Mertzimekis, T.J., Toli, K., Simon, R., Göttlicher, J., 2011. A microscopic and Synchrotron-based characterization of urban particulate matter (PM10–PM2.5 and PM2.5) from Athens atmosphere, Greece. Nucl. Instruments Methods Phys. Res. Sect. B Beam Interact. with Mater. Atoms 269, 3077–3081. https://doi.org/http://dx.doi.org/10.1016/j.nimb.2011.04.063

Godoi, R.H.M., Braga, D.M., Makarovska, Y., Alfoldy, B., Carvalho Filho, M.A.S., Van Grieken, R., Godoi, A.F.L., 2008. Inhable particulate matter from lime industries: Chemical composition and deposition in human respiratory tract. Atmos. Environ. 42, 7027–7033. https://doi.org/http://dx.doi.org/10.1016/j.atmosenv.2008.07.002

Godoy, M.L.D.P., Godoy, J.M., Roldão, L.A., Soluri, D.S., Donagemma, R.A., 2009. Coarse and fine aerosol source apportionment in Rio de Janeiro, Brazil. Atmos. Environ. 43, 2366–2374.

https://doi.org/10.1016/J.ATMOSENV.2008.12.046

Gonçalves, C., Figueiredo, B.R., Alves, C.A., Cardoso, A.A., da Silva, R., Kanzawa, S.H., Vicente, A.M., 2016. Chemical characterisation of total suspended particulate matter from a remote area in Amazonia. Atmos. Res. 182, 102–113. https://doi.org/http://dx.doi.org/10.1016/j.atmosres.2016.07.027

Gonzalez, J., Dundas, S.H., Yi Liu, C., Mao, X., Russo, R.E., 2006. UV-femtosecond and nanosecond laser ablation-ICP-MS: internal and external repeatability. J. Anal. At. Spectrom. 21, 778–784. https://doi.org/10.1039/B603492F

González, L.T., Rodríguez, F.E.L., Sánchez-Domínguez, M., Leyva-Porras, C., Silva-Vidaurri, L.G., Acuna-Askar, K., Kharisov, B.I., Villarreal Chiu, J.F., Alfaro Barbosa, J.M., 2016. Chemical and morphological characterization of TSP and PM2.5 by SEM-EDS, XPS and XRD collected in the metropolitan area of Monterrey, Mexico. Atmos. Environ. 143, 249–260. https://doi.org/http://dx.doi.org/10.1016/j.atmosenv.2016.08.053

Gornostayev, S., Härkki, J., Kerkkonen, O., 2009. Transformations of pyrite during formation of metallurgical coke. Fuel 88, 2032–2036. https://doi.org/10.1016/J.FUEL.2009.02.044

Grandesso, E., Pérez Ballesta, P., Kowalewski, K., 2013. Thermal desorption GC–MS as a tool to provide PAH certified standard reference material on particulate matter quartz filters. Talanta 105, 101–108. https://doi.org/10.1016/J.TALANTA.2012.11.047

Gredilla, A., Fdez-Ortiz de Vallejuelo, S., Elejoste, N., de Diego, A., Madariaga, J.M., 2016. Non-destructive Spectroscopy combined with chemometrics as a tool for Green Chemical Analysis of environmental samples: A review. TrAC Trends Anal. Chem. 76, 30–39. https://doi.org/http://dx.doi.org/10.1016/j.trac.2015.11.011

Grekula, A., Ristolainen, E., Tanninen, V.P., Hyvärinen, H.-K., Kalliomäki, P.-L., 1986. Surface and bulk chemical analysis on metal aerosols generated by manual metal arc welding of stainless steel. J. Aerosol Sci. 17, 1–9. https://doi.org/http://dx.doi.org/10.1016/0021-8502(86)90002-9

Gross, J., 2011. Mass Spectrometry, 2nd ed. Springer, Berlin.

Guanghua, Z., Guangfu, W., 1998. Investigation of the particulate derived from indigenous zinc smelting using PIXE analytical technique. Nucl. Instruments Methods Phys. Res. Sect. B Beam Interact. with Mater. Atoms 136, 966–969.

https://doi.org/http://dx.doi.org/10.1016/S0168-583X(97)00756-8

Guascito, M.R., Cesari, D., Chirizzi, D., Genga, A., Contini, D., 2015. XPS surface chemical characterization of atmospheric particles of different sizes. Atmos. Environ. 116, 146–154. https://doi.org/http://dx.doi.org/10.1016/j.atmosenv.2015.06.028

Guo, H., Ding, A.J., So, K.L., Ayoko, G., Li, Y.S., Hung, W.T., 2009. Receptor modeling of source apportionment of Hong Kong aerosols and the implication of urban and regional contribution. Atmos. Environ. 43, 1159–1169. https://doi.org/10.1016/J.ATMOSENV.2008.04.046

Guo, H., Ding, A.J., So, K.L., Ayoko, G., Li, Y.S., Hung, W.T., 2009. Receptor modeling of source apportionment of Hong Kong aerosols and the implication of urban and regional contribution. Atmos. Environ. 43, 1159–1169. https://doi.org/http://dx.doi.org/10.1016/j.atmosenv.2008.04.046

Guo, J., Kang, S., Huang, J., Zhang, Q., Rupakheti, M., Sun, S., Tripathee, L., Rupakheti, D., Panday, A.K., Sillanpää, M., Paudyal, R., 2017. Characterizations of atmospheric particulate-bound mercury in the Kathmandu Valley of Nepal, South Asia. Sci. Total Environ. 579, 1240–1248. https://doi.org/http://dx.doi.org/10.1016/j.scitotenv.2016.11.110

Guo, Y., Gao, X., Zhu, T., Luo, L., Zheng, Y., 2017. Chemical profiles of PM emitted from the iron and steel industry in northern China. Atmos. Environ. 150, 187–197. https://doi.org/10.1016/J.ATMOSENV.2016.11.055

Gupta, S., Kumar, K., Srivastava, A., Srivastava, A., Jain, V.K., 2011. Size distribution and source apportionment of polycyclic aromatic hydrocarbons (PAHs) in aerosol particle samples from the atmospheric environment of Delhi, India. Sci. Total Environ. 409, 4674–4680. https://doi.org/10.1016/J.SCITOTENV.2011.08.008

Habre, R., Coull, B., Koutrakis, P., 2011. Impact of source collinearity in simulated PM2.5 data on the PMF receptor model solution. Atmos. Environ. 45, 6938–6946. https://doi.org/http://dx.doi.org/10.1016/j.atmosenv.2011.09.034

Haddad, P.R., 1989. Chapter II Sample Handling in Ion Chromatography. J. Chromatogr. Libr. 39, 33–81. https://doi.org/10.1016/S0301-4770(08)61580-8

Hang, N.T., Kim Oanh, N.T., 2014. Chemical characterization and sources apportionment of fine particulate pollution in a mining town of Vietnam. Atmos. Res. 145, 214–225. https://doi.org/http://dx.doi.org/10.1016/j.atmosres.2014.04.009

Harchand, K.S., Raj, D., 1993. Mössbauer spectroscopic studies of iron particulate matter in coal soot. Nucl. Instruments Methods Phys. Res. Sect. B Beam Interact. with Mater. Atoms 76, 246–248. https://doi.org/https://doi.org/10.1016/0168-583X(93)95197-D

Harrison, R.M., Smith, D.J.T., 1992. THE CHEMICAL COMPOSITION OF ATMOSPHERIC AEROSOLS: WHAT CAN IT TELL US? J. Aerosol Sci. 23, 863–856.

Hays, M.D., Smith, N.D., Kinsey, J., Dong, Y., Kariher, P., 2003. Polycyclic aromatic hydrocarbon size distributions in aerosols from appliances of residential wood combustion as determined by direct thermal desorption—GC/MS. J. Aerosol Sci. 34, 1061–1084. https://doi.org/https://doi.org/10.1016/S0021-8502(03)00080-6

Helmig, D., 1999. Air analysis by gas chromatography. J. Chromatogr. A 843, 129–146. https://doi.org/http://dx.doi.org/10.1016/S0021-9673(99)00173-9

Hleis, D., Fernández-Olmo, I., Ledoux, F., Kfoury, A., Courcot, L., Desmonts, T., Courcot, D., 2013. Chemical profile identification of fugitive and confined particle emissions from an integrated iron and steelmaking plant. J. Hazard. Mater. 250–251, 246–255. https://doi.org/10.1016/J.JHAZMAT.2013.01.080

Ho, K.F., Ho, S.S.H., Lee, S.C., Cheng, Y., Chow, J.C., Watson, J.G., Louie, P.K.K., Tian, L., 2009. Emissions of gas- and particle-phase polycyclic aromatic hydrocarbons (PAHs) in the Shing Mun Tunnel, Hong Kong. Atmos. Environ. 43, 6343–6351. https://doi.org/10.1016/J.ATMOSENV.2009.09.025

Ho, S.S.H., Yu, J.Z., Chow, J.C., Zielinska, B., Watson, J.G., Sit, E.H.L., Schauer, J.J., 2008. Evaluation of an in-injection port thermal desorption-gas chromatography/mass spectrometry method for analysis of non-polar organic compounds in ambient aerosol samples. J. Chromatogr. A 1200, 217–227. https://doi.org/10.1016/J.CHROMA.2008.05.056

Hoffmann, E., Stroobant, V., 2007. Mass Spectrometry - Principles and Applications, 1st ed. Academic Press, London.

Hoffmann, P., Dedik, A.N., Ensling, J., Weinbruch, S., Weber, S., Sinner, T., Gütlich, P., Ortner, H.M., 1996. Speciation of iron in atmospheric aerosol samples. J. Aerosol Sci. 27, 325–337. https://doi.org/http://dx.doi.org/10.1016/0021-8502(95)00563-3

Hopke, P.K., 2003. Recent developments in receptor modeling. J. Chemom. 17, 255–265. https://doi.org/10.1002/cem.796

Horn, I., Günther, D., 2003. The influence of ablation carrier gasses Ar, He and Ne on the particle size distribution and transport efficiencies of laser ablation-induced aerosols: implications for LA–ICP–MS. Appl. Surf. Sci. 207, 144–157. https://doi.org/https://doi.org/10.1016/S0169-4332(02)01324-7

Hu, G., Dam-Johansen, K., Wedel, S., Hansen, J.P., 2006. Decomposition and oxidation of pyrite. Prog. Energy Combust. Sci. 32, 295–314. https://doi.org/10.1016/J.PECS.2005.11.004

Huang, D., Hua, X., Xiu, G.-L., Zheng, Y.-J., Yu, X.-Y., Long, Y.-T., 2017. Secondary ion mass spectrometry: The application in the analysis of atmospheric particulate matter. Anal. Chim. Acta. https://doi.org/http://dx.doi.org/10.1016/j.aca.2017.07.042

Huang, W., Duan, D., Zhang, Y., Cheng, H., Ran, Y., 2014. Heavy metals in particulate and colloidal matter from atmospheric deposition of urban Guangzhou, South China. Mar. Pollut. Bull. 85, 720–726. https://doi.org/http://dx.doi.org/10.1016/j.marpolbul.2013.12.041

Huntzicker, J.J., Johnson, R.L., Shah, J.J., Cary, R.A., 1982. Analysis of Organic and Elemental Carbon in Ambient Aerosols by a Thermal-Optical Method BT - Particulate Carbon: Atmospheric Life Cycle, in: Wolff, G.T., Klimisch, R.L. (Eds.), . Springer US, Boston, MA, pp. 79–88. https://doi.org/10.1007/978-1-4684-4154-3_6

IBGE, 2010. Censo demográfico [WWW Document]. URL https://cidades.ibge.gov.br/

ICDD, 2007. PDF-2, 2007 (Database), edited by Dr. Soorya Kabekkodu.

IEMA/Ecosoft, 2011. Inventory of atmospheric emissions of Great Vitória Region.

Iljana, M., Kemppainen, A., Paananen, T., Mattila, O., Pisilä, E., Kondrakov, M., Fabritius, T., 2015. Effect of adding limestone on the metallurgical properties of iron ore pellets. Int. J. Miner. Process. 141, 34–43. https://doi.org/10.1016/J.MINPRO.2015.06.004

Iqbal, M.A., Kim, K.-H., 2016. Sampling, pretreatment, and analysis of particulate matter and trace metals emitted through charcoal combustion in cooking activities. TrAC Trends Anal. Chem. 76, 52–59. https://doi.org/10.1016/J.TRAC.2015.11.005

Ivey, C., Holmes, H., Shi, G., Balachandran, S., Hu, Y., Russell, A.G., 2017. Development of PM2.5 Source Profiles Using a Hybrid Chemical Transport-Receptor Modeling Approach. Environ. Sci. Technol. 51, 13788–13796. https://doi.org/10.1021/acs.est.7b03781

Ivošević, T., Orlić, I., Radović, I.B., 2015. Long term fine aerosol analysis by XRF and PIXE techniques in the city of Rijeka, Croatia. Nucl. Instruments Methods Phys. Res. Sect. B Beam Interact. with Mater. Atoms 363, 119–123. https://doi.org/https://doi.org/10.1016/j.nimb.2015.08.030

Jancsek-Turóczi, B., Hoffer, A., Nyírő-Kósa, I., Gelencsér, A., 2013. Sampling and characterization of resuspended and respirable road dust. J. Aerosol Sci. 65, 69–76. https://doi.org/http://dx.doi.org/10.1016/j.jaerosci.2013.07.006

Janssens, K., 2013. X–Ray Based Methods of Analysis, in: Modern Methods for Analysing Archaeological and Historical Glass. John Wiley & Sons Ltd, pp. 79–128. https://doi.org/10.1002/9781118314234.ch5

Jeynes, C., Bailey, M.J., Bright, N.J., Christopher, M.E., Grime, G.W., Jones, B.N., Palitsin, V. V, Webb, R.P., 2012. "Total IBA" – Where are we? Nucl. Instruments Methods Phys. Res. Sect. B Beam Interact. with Mater. Atoms 271, 107–118. https://doi.org/http://dx.doi.org/10.1016/j.nimb.2011.09.020

Jiang, T., Zhang, Y.B., Huang, Z.C., Li, G.H., Fan, X.H., 2008. Preheating and roasting characteristics of hematite–magnetite (H–M) concentrate pellets. Ironmak. Steelmak. 35, 21–26. https://doi.org/10.1179/174328107X174771

Kappos, A.D., Bruckmann, P., Eikmann, T., Englert, N., Heinrich, U., Höppe, P., Koch, E., Krause, G.H.M., Kreyling, W.G., Rauchfuss, K., Rombout, P., Schulz-Klemp, V., Thiel, W.R., Wichmann, H.-E., 2004. Health effects of particles in ambient air. Int. J. Hyg. Environ. Health 207, 399–407. https://doi.org/http://dx.doi.org/10.1078/1438-4639-00306

Karnae, S., John, K., 2011. Source apportionment of fine particulate matter measured in an industrialized coastal urban area of South Texas. Atmos. Environ. 45, 3769–3776. https://doi.org/10.1016/J.ATMOSENV.2011.04.040

Khan, M.F., Hirano, K., Masunaga, S., 2010. Quantifying the sources of hazardous elements of suspended particulate matter aerosol collected in Yokohama, Japan. Atmos. Environ. 44, 2646–2657. https://doi.org/https://doi.org/10.1016/j.atmosenv.2010.03.040

Khuzestani, R.B., Schauer, J.J., Wei, Y., Zhang, Y., Zhang, Y., 2017. A non-destructive optical color space sensing system to quantify elemental and organic carbon in atmospheric particulate matter on Teflon and quartz filters. Atmos. Environ. 149, 84–94.

https://doi.org/http://dx.doi.org/10.1016/j.atmosenv.2016.11.002

Kim, E., Hopke, P.K., 2008. Source characterization of ambient fine particles at multiple sites in the Seattle area. Atmos. Environ. 42, 6047–6056. https://doi.org/10.1016/J.ATMOSENV.2008.03.032

Kittelson, D.B., Dolan, D.F., Diver, R.B., Aufderheide, E., 1978. Diesel Exhaust Particle Size Distributions - Fuel and Additive Effects. https://doi.org/10.4271/780787

Klockenkämper, R., 1987. X-ray spectral analysis—present status and trends. Spectrochim. Acta Part B At. Spectrosc. 42, 423–429. https://doi.org/http://dx.doi.org/10.1016/0584-8547(87)80020-4

Kopcewicz, B., Kopcewicz, M., Pietruczuk, A., 2015. The Mössbauer study of atmospheric iron-containing aerosol in the coarse and PM2.5 fractions measured in rural site. Chemosphere 131, 9–16. https://doi.org/http://dx.doi.org/10.1016/j.chemosphere.2015.02.038

Kotchenruther, R.A., 2016. Source apportionment of PM2.5 at multiple Northwest U.S. sites: Assessing regional winter wood smoke impacts from residential wood combustion. Atmos. Environ. 142, 210–219. https://doi.org/10.1016/J.ATMOSENV.2016.07.048

Kudelski, A., 2008. Analytical applications of Raman spectroscopy. Talanta 76, 1–8. https://doi.org/http://dx.doi.org/10.1016/j.talanta.2008.02.042

Ladji, R., Yassaa, N., Balducci, C., Cecinato, A., 2014. Particle size distribution of n-alkanes and polycyclic aromatic hydrocarbons (PAHS) in urban and industrial aerosol of Algiers, Algeria. Environ. Sci. Pollut. Res. 21, 1819–1832. https://doi.org/10.1007/s11356-013-2074-2

Landis, M.S., Patrick Pancras, J., Graney, J.R., White, E.M., Edgerton, E.S., Legge, A., Percy, K.E., 2017. Source apportionment of ambient fine and coarse particulate matter at the Fort McKay community site, in the Athabasca Oil Sands Region, Alberta, Canada. Sci. Total Environ. 584, 105–117. https://doi.org/http://dx.doi.org/10.1016/j.scitotenv.2017.01.110

Lara, F.J., Airado-Rodríguez, D., Moreno-González, D., Huertas-Pérez, J.F., García-Campaña, A.M., 2016. Applications of capillary electrophoresis with chemiluminescence detection in clinical, environmental and food analysis. A review. Anal. Chim. Acta 913, 22–40. https://doi.org/http://dx.doi.org/10.1016/j.aca.2016.01.046

Lee, S., Liu, W., Wang, Y., Russell, A.G., Edgerton, E.S., 2008. Source apportionment of PM2.5:

Comparing PMF and CMB results for four ambient monitoring sites in the southeastern United States. Atmos. Environ. 42, 4126–4137. https://doi.org/http://dx.doi.org/10.1016/j.atmosenv.2008.01.025

Li, W., Shao, L., Zhang, D., Ro, C.-U., Hu, M., Bi, X., Geng, H., Matsuki, A., Niu, H., 2016. A review of single aerosol particle studies in the atmosphere of East Asia: morphology, mixing state, source, and heterogeneous reactions. J. Clean. Prod. 112, 1330–1349. https://doi.org/10.1016/J.JCLEPRO.2015.04.050

Li, X.F., Wang, G.F., Chu, J.H., Yu, L.D., 2012. Charge integration in external PIXE–PIGE for the analysis of aerosol samples. Nucl. Instruments Methods Phys. Res. Sect. B Beam Interact. with Mater. Atoms 289, 1–4. https://doi.org/http://dx.doi.org/10.1016/j.nimb.2012.08.009

Li, Y.J., Sun, Y., Zhang, Q., Li, X., Li, M., Zhou, Z., Chan, C.K., 2017. Real-time chemical characterization of atmospheric particulate matter in China: A review. Atmos. Environ. 158, 270–304. https://doi.org/https://doi.org/10.1016/j.atmosenv.2017.02.027

Lightsources.org, 2017. Lightsources of the World [WWW Document]. URL http://www.lightsources.org/regions

Linak, W.P., Yoo, J.-I., Wasson, S.J., Zhu, W., Wendt, J.O.L., Huggins, F.E., Chen, Y., Shah, N., Huffman, G.P., Gilmour, M.I., 2007. Ultrafine ash aerosols from coal combustion: Characterization and health effects. Proc. Combust. Inst. 31, 1929–1937. https://doi.org/10.1016/J.PROCI.2006.08.086

Lindinger, W., Jordan, A., 1998. Proton-transfer-reaction mass spectrometry (PTR-MS): on-line monitoring of volatile organic compounds at pptv levels. Chem. Soc. Rev. 27, 347–375. https://doi.org/10.1039/A827347Z

Lippmann, M., Chen, L.-C., 2009. Health effects of concentrated ambient air particulate matter (CAPs) and its components. Crit. Rev. Toxicol. 39, 865–913. https://doi.org/10.3109/10408440903300080

Liu, C., Cai, J., Qiao, L., Wang, H., Xu, W., Li, H., Zhao, Z., Chen, R., Kan, H., 2017. The Acute Effects of Fine Particulate Matter Constituents on Blood Inflammation and Coagulation. Environ. Sci. Technol. 51, 8128–8137. https://doi.org/10.1021/acs.est.7b00312

Liu, K., Duan, F., He, K., Ma, Y., Cheng, Y., 2014. Investigation on sampling artifacts of particle associated PAHs using ozone denuder systems. Front. Environ. Sci. Eng. 8, 284–292.

https://doi.org/10.1007/s11783-013-0555-7

Liu, L., Liu, Y., Lin, J., Tang, N., Hayakawa, K., Maeda, T., 2007. Development of analytical methods for polycyclic aromatic hydrocarbons (PAHs) in airborne particulates: A review. J. Environ. Sci. 19, 1–11. https://doi.org/http://dx.doi.org/10.1016/S1001-0742(07)60001-1

Lomboy, M.F.T.C., Quirit, L.L., Molina, V.B., Dalmacion, G. V, Schwartz, J.D., Suh, H.H., Baja, E.S., 2015. Characterization of particulate matter 2.5 in an urban tertiary care hospital in the Philippines. Build. Environ. 92, 432–439. https://doi.org/http://dx.doi.org/10.1016/j.buildenv.2015.05.018

López-García, P., Gelado-Caballero, M.D., Collado-Sánchez, C., Hernández-Brito, J.J., 2017. Solubility of aerosol trace elements: Sources and deposition fluxes in the Canary Region. Atmos. Environ. 148, 167–174. https://doi.org/http://dx.doi.org/10.1016/j.atmosenv.2016.10.035

López-Ruiz, B., 2000. Advances in the determination of inorganic anions by ion chromatography. J. Chromatogr. A 881, 607–627. https://doi.org/http://dx.doi.org/10.1016/S0021-9673(00)00244-2

Louie, P.K.K., Watson, J.G., Chow, J.C., Chen, A., Sin, D.W.M., Lau, A.K.H., 2005. Seasonal characteristics and regional transport of PM2.5 in Hong Kong. Atmos. Environ. 39, 1695–1710. https://doi.org/10.1016/J.ATMOSENV.2004.11.017

Lü, S., Zhang, R., Yao, Z., Yi, F., Ren, J., Wu, M., Feng, M., Wang, Q., 2012. Size distribution of chemical elements and their source apportionment in ambient coarse, fine, and ultrafine particles in Shanghai urban summer atmosphere. J. Environ. Sci. 24, 882–890. https://doi.org/http://dx.doi.org/10.1016/S1001-0742(11)60870-X

Maenhaut, W., 2015. Present role of PIXE in atmospheric aerosol research. Nucl. Instruments Methods Phys. Res. Sect. B Beam Interact. with Mater. Atoms 363, 86–91. https://doi.org/http://dx.doi.org/10.1016/j.nimb.2015.07.043

Maenhaut, W., Raes, N., Wang, W., 2011. Analysis of atmospheric aerosols by particle-induced X-ray emission, instrumental neutron activation analysis, and ion chromatography. Nucl. Instruments Methods Phys. Res. Sect. B Beam Interact. with Mater. Atoms 269, 2693–2698. https://doi.org/http://dx.doi.org/10.1016/j.nimb.2011.08.012

Malm, W.C., James, F.S., Huffman, D., Robert, A.E., Thomas, A.C., 1994. Spatial and seasonal

trends in particle concentration and optical extinction in the United States. J. Geophys. Res. Atmos. 99, 1347–1370. https://doi.org/10.1029/93JD02916

Martuzevicius, D., Kliucininkas, L., Prasauskas, T., Krugly, E., Kauneliene, V., Strandberg, B., 2011. Resuspension of particulate matter and PAHs from street dust. Atmos. Environ. 45, 310–317. https://doi.org/10.1016/J.ATMOSENV.2010.10.026

Masalaite, A., Holzinger, R., Remeikis, V., Röckmann, T., Dusek, U., 2017. Characteristics, sources and evolution of fine aerosol (PM1) at urban, coastal and forest background sites in Lithuania. Atmos. Environ. 148, 62–76. https://doi.org/10.1016/J.ATMOSENV.2016.10.038

Meirer, F., Singh, A., Pianetta, P., Pepponi, G., Meirer, F., Streli, C., Homma, T., 2010. Synchrotron radiation-induced total reflection X-ray fluorescence analysis. TrAC Trends Anal. Chem. 29, 479–496. https://doi.org/http://dx.doi.org/10.1016/j.trac.2010.04.001

Mercier, F., Glorennec, P., Blanchard, O., Le Bot, B., 2012. Analysis of semi-volatile organic compounds in indoor suspended particulate matter by thermal desorption coupled with gas chromatography/mass spectrometry. J. Chromatogr. A 1254, 107–114. https://doi.org/http://dx.doi.org/10.1016/j.chroma.2012.07.025

Merešová, J., Florek, M., Holý, K., Ješkovský, M., Sýkora, I., Frontasyeva, M.V., Pavlov, S.S., Bujdoš, M., 2008. Evaluation of elemental content in air-borne particulate matter in low-level atmosphere of Bratislava. Atmos. Environ. 42, 8079–8085. https://doi.org/10.1016/J.ATMOSENV.2008.06.029

Mijić, Z., Stojić, A., Perišić, M., Rajšić, S., Tasić, M., Radenković, M., Joksić, J., 2010. Seasonal variability and source apportionment of metals in the atmospheric deposition in Belgrade. Atmos. Environ. 44, 3630–3637. https://doi.org/http://dx.doi.org/10.1016/j.atmosenv.2010.06.045

Monkhouse, P., 2011. On-line spectroscopic and spectrometric methods for the determination of metal species in industrial processes. Prog. Energy Combust. Sci. 37, 125–171. https://doi.org/10.1016/J.PECS.2010.05.002

Moreno, T., Jones, T.P., Richards, R.J., 2004. Characterisation of aerosol particulate matter from urban and industrial environments: examples from Cardiff and Port Talbot, South Wales, UK. Sci. Total Environ. 334–335, 337–346. https://doi.org/10.1016/J.SCITOTENV.2004.04.074

Moreno, T., Querol, X., Alastuey, A., Viana, M., Salvador, P., Sánchez de la Campa, A., Artiñano,

B., de la Rosa, J., Gibbons, W., 2006. Variations in atmospheric PM trace metal content in Spanish towns: Illustrating the chemical complexity of the inorganic urban aerosol cocktail. Atmos. Environ. 40, 6791–6803. https://doi.org/10.1016/J.ATMOSENV.2006.05.074

Mukhtar, A., Limbeck, A., 2009. A new approach for the determination of silicon in airborne particulate matter using electrothermal atomic absorption spectrometry. Anal. Chim. Acta 646, 17–22. https://doi.org/http://dx.doi.org/10.1016/j.aca.2009.05.009

Murphy, D.M., Hudson, P.K., Thomson, D.S., Sheridan, P.J., Wilson, J.C., 2006. Observations of Mercury-Containing Aerosols. Environ. Sci. Technol. 40, 3163–3167. https://doi.org/10.1021/es052385x

Murphy, D.M., Thomson, D.S., 1995. Laser Ionization Mass Spectroscopy of Single Aerosol Particles. Aerosol Sci. Technol. 22, 237–249. https://doi.org/10.1080/02786829408959743

Muwanguzi, A.J.B., Karasev, A. V., Byaruhanga, J.K., Jönsson, P.G., 2012. Characterization of Chemical Composition and Microstructure of Natural Iron Ore from Muko Deposits. ISRN Mater. Sci. 2012, 9.

Nair, P.R., George, S.K., Sunilkumar, S. V, Parameswaran, K., Jacob, S., Abraham, A., 2006. Chemical composition of aerosols over peninsular India during winter. Atmos. Environ. 40, 6477–6493. https://doi.org/http://dx.doi.org/10.1016/j.atmosenv.2006.02.031

Nash, D.G., 2006. Aerosol mass spectrometry: An introductory review. Int. J. Mass Spectrom. 258, 2–12. https://doi.org/10.1016/J.IJMS.2006.09.017

Nayak, P.K., Vijayan, V., 2006. Complementary PIGE, PIXE, EDXRF and γ-ray spectroscopic investigation on natural chromites. Nucl. Instruments Methods Phys. Res. Sect. B Beam Interact. with Mater. Atoms 245, 505–510. https://doi.org/http://dx.doi.org/10.1016/j.nimb.2005.11.150

Niehaus, R., Sperling, M., Karst, U., 2015. Study on aerosol characteristics and fractionation effects of organic standard materials for bioimaging by means of LA-ICP-MS. J. Anal. At. Spectrom. 30, 2056–2065. https://doi.org/10.1039/C5JA00221D

Niu, S., Dong, L., Zhang, L., Zhu, C., Hai, R., Huang, Y., 2017. Temporal and spatial distribution, sources, and potential health risks of ambient polycyclic aromatic hydrocarbons in the Yangtze River Delta (YRD) of eastern China. Chemosphere 172, 72–79. https://doi.org/10.1016/J.CHEMOSPHERE.2016.12.108

Niu, X., Cao, J., Shen, Z., Ho, S.S.H., Tie, X., Zhao, S., Xu, H., Zhang, T., Huang, R., 2016. PM2.5 from the Guanzhong Plain: Chemical composition and implications for emission reductions. Atmos. Environ. 147, 458–469. https://doi.org/http://dx.doi.org/10.1016/j.atmosenv.2016.10.029

Norris, G., Duvall, R., Brown, S., Bai, S., 2014. EPA Positive Matrix Factorization (PMF) 5.0 Fundamentals and User Guide. Washington, DC. EPA/600/R-14/108 (NTIS PB2015-105147).

Novaes, C.G., Bezerra, M.A., da Silva, E.G.P., Santos, A.M.P. dos, Romão, I.L. da S., Santos Neto, J.H., 2016. A review of multivariate designs applied to the optimization of methods based on inductively coupled plasma optical emission spectrometry (ICP OES). Microchem. J. 128, 331–346. https://doi.org/http://dx.doi.org/10.1016/j.microc.2016.05.015

Okuda, T., Schauer, J.J., Shafer, M.M., 2014. Improved methods for elemental analysis of atmospheric aerosols for evaluating human health impacts of aerosols in East Asia. Atmos. Environ. 97, 552–555. https://doi.org/http://dx.doi.org/10.1016/j.atmosenv.2014.01.043

Omidvarborna, H., Kumar, A., Kim, D.-S., 2014. Characterization of particulate matter emitted from transit buses fueled with B20 in idle modes. J. Environ. Chem. Eng. 2, 2335–2342. https://doi.org/http://dx.doi.org/10.1016/j.jece.2014.09.020

Owoade, K.O., Hopke, P.K., Olise, F.S., Adewole, O.O., Ogundele, L.T., Fawole, O.G., 2016. Source apportionment analyses for fine (PM2.5) and coarse (PM2.5–10) mode particulate matter (PM) measured in an urban area in southwestern Nigeria. Atmos. Pollut. Res. 7, 843–857. https://doi.org/10.1016/J.APR.2016.04.006

Owoade, K.O., Hopke, P.K., Olise, F.S., Ogundele, L.T., Fawole, O.G., Olaniyi, B.H., Jegede, O.O., Ayoola, M.A., Bashiru, M.I., 2015. Chemical compositions and source identification of particulate matter (PM2.5 and PM2.5–10) from a scrap iron and steel smelting industry along the Ife–Ibadan highway, Nigeria. Atmos. Pollut. Res. 6, 107–119. https://doi.org/http://dx.doi.org/10.5094/APR.2015.013

Paatero, P., 1997. Least squares formulation of robust non-negative factor analysis. Chemom. Intell. Lab. Syst. 37, 23–35. https://doi.org/10.1016/S0169-7439(96)00044-5

Pacáková, V., Štulík, K., 2005. CAPILLARY ELECTROPHORESIS | Low-Molecular-Weight Ions A2 - Worsfold, Paul, in: Townshend, A., Poole, C.B.T.-E. of A.S. (Second E. (Eds.), .

Elsevier, Oxford, pp. 354–361. https://doi.org/https://doi.org/10.1016/B0-12-369397-7/00752-4

Pachauri, T., Singla, V., Satsangi, A., Lakhani, A., Maharaj Kumari, K., 2013. SEM-EDX characterization of individual coarse particles in Agra, India. Aerosol Air Qual. Res. 13, 523–536. https://doi.org/10.4209/aaqr.2012.04.0095

Pallozzi, E., Guidolotti, G., Ciccioli, P., Brilli, F., Feil, S., Calfapietra, C., 2016. Does the novel fast-GC coupled with PTR-TOF-MS allow a significant advancement in detecting VOC emissions from plants? Agric. For. Meteorol. 216, 232–240. https://doi.org/10.1016/J.AGRFORMET.2015.10.016

Pan, Y., Tian, S., Li, X., Sun, Y., Li, Y., Wentworth, G.R., Wang, Y., 2015. Trace elements in particulate matter from metropolitan regions of Northern China: Sources, concentrations and size distributions. Sci. Total Environ. 537, 9–22. https://doi.org/https://doi.org/10.1016/j.scitotenv.2015.07.060

Pandey, S.K., Kim, K.-H., Brown, R.J.C., 2011. A review of techniques for the determination of polycyclic aromatic hydrocarbons in air. TrAC Trends Anal. Chem. 30, 1716–1739. https://doi.org/https://doi.org/10.1016/j.trac.2011.06.017

Pant, P., Yin, J., Harrison, R.M., 2014. Sensitivity of a Chemical Mass Balance model to different molecular marker traffic source profiles. Atmos. Environ. 82, 238–249. https://doi.org/10.1016/J.ATMOSENV.2013.10.005

Papp, C., Steinrück, H.-P., 2013. In situ high-resolution X-ray photoelectron spectroscopy – Fundamental insights in surface reactions. Surf. Sci. Rep. 68, 446–487. https://doi.org/https://doi.org/10.1016/j.surfrep.2013.10.003

Pickhardt, C., Dietze, H.-J., Becker, J.S., 2005. Laser ablation inductively coupled plasma mass spectrometry for direct isotope ratio measurements on solid samples. Int. J. Mass Spectrom. 242, 273–280. https://doi.org/https://doi.org/10.1016/j.ijms.2004.12.014

Poster, D.L., Schantz, M.M., Sander, L.C., Wise, S.A., 2006. Analysis of polycyclic aromatic hydrocarbons (PAHs) in environmental samples: a critical review of gas chromatographic (GC) methods. Anal. Bioanal. Chem. 386, 859–881. https://doi.org/10.1007/s00216-006-0771-0

Prather, K.A., Nordmeyer, T., Salt, K., 1994. Real-time characterization of individual aerosol

particles using time-of-flight mass spectrometry. Anal. Chem. 66, 1403–1407. https://doi.org/10.1021/ac00081a007

Qadir, R.M., Schnelle-Kreis, J., Abbaszade, G., Arteaga-Salas, J.M., Diemer, J., Zimmermann, R., 2014. Spatial and temporal variability of source contributions to ambient PM10 during winter in Augsburg, Germany using organic and inorganic tracers. Chemosphere 103, 263–273. https://doi.org/10.1016/J.CHEMOSPHERE.2013.12.015

Qian, G., Li, Y., Gerson, A.R., 2015. Applications of surface analytical techniques in Earth Sciences. Surf. Sci. Rep. 70, 86–133. https://doi.org/http://dx.doi.org/10.1016/j.surfrep.2015.02.001

Rastogi, N., Sarin, M.M., 2009. Quantitative chemical composition and characteristics of aerosols over western India: One-year record of temporal variability. Atmos. Environ. 43, 3481–3488. https://doi.org/10.1016/J.ATMOSENV.2009.04.030

Ravindra, K., Sokhi, R., Van Grieken, R., 2008. Atmospheric polycyclic aromatic hydrocarbons: Source attribution, emission factors and regulation. Atmos. Environ. 42, 2895–2921. https://doi.org/10.1016/J.ATMOSENV.2007.12.010

Revuelta, M.A., McIntosh, G., Pey, J., Perez, N., Querol, X., Alastuey, A., 2014. Partitioning of magnetic particles in PM10, PM2.5 and PM1 aerosols in the urban atmosphere of Barcelona (Spain). Environ. Pollut. 188, 109–117. https://doi.org/10.1016/j.envpol.2014.01.025

Reyes-Herrera, J., Miranda, J., de Lucio, O.G., 2015. Simultaneous PIXE and XRF elemental analysis of atmospheric aerosols. Microchem. J. 120, 40–44. https://doi.org/http://dx.doi.org/10.1016/j.microc.2015.01.004

Rizzio, E., Giaveri, G., Gallorini, M., 2000. Some analytical problems encountered for trace elements determination in the airborne particulate matter of urban and rural areas. Sci. Total Environ. 256, 11–22. https://doi.org/http://dx.doi.org/10.1016/S0048-9697(00)00432-0

Rodríguez, S., Alastuey, A., Querol, X., 2012. A review of methods for long term in situ characterization of aerosol dust. Aeolian Res. 6, 55–74. https://doi.org/10.1016/J.AEOLIA.2012.07.004

Rohr, A.C., Wyzga, R.E., 2012. Attributing health effects to individual particulate matter constituents. Atmos. Environ. 62, 130–152. https://doi.org/http://dx.doi.org/10.1016/j.atmosenv.2012.07.036

Rosière, C.A., Chemale Jr, F., 2000. Itabiritos e minérios de ferro de alto teor do Quadrilátero ferrífero - uma visão geral e discussão. Geonomos 8, 27–43.

Roy, A.A., Wagstrom, K.M., Adams, P.J., Pandis, S.N., Robinson, A.L., 2011. Quantification of the effects of molecular marker oxidation on source apportionment estimates for motor vehicles. Atmos. Environ. 45, 3132–3140. https://doi.org/http://dx.doi.org/10.1016/j.atmosenv.2011.03.020

Roy, A.A., Wagstrom, K.M., Adams, P.J., Pandis, S.N., Robinson, A.L., 2011. Quantification of the effects of molecular marker oxidation on source apportionment estimates for motor vehicles. Atmos. Environ. 45, 3132–3140. https://doi.org/10.1016/J.ATMOSENV.2011.03.020

Saarnio, K., Sillanpää, M., Hillamo, R., Sandell, E., Pennanen, A.S., Salonen, R.O., 2008. Polycyclic aromatic hydrocarbons in size-segregated particulate matter from six urban sites in Europe. Atmos. Environ. 42, 9087–9097. https://doi.org/http://dx.doi.org/10.1016/j.atmosenv.2008.09.022

Saisho, H., 1989. X-ray fluorescence analysis using synchrotron radiation. TrAC Trends Anal. Chem. 8, 209–214. https://doi.org/http://dx.doi.org/10.1016/0165-9936(89)87004-9

Salvador, C.M., Ho, T.-T., Chou, C.C.-K., Chen, M.-J., Huang, W.-R., Huang, S.-H., 2016. Characterization of the organic matter in submicron urban aerosols using a Thermo-Desorption Proton-Transfer-Reaction Time-of-Flight Mass Spectrometer (TD-PTR-TOF-MS). Atmos. Environ. 140, 565–575. https://doi.org/10.1016/J.ATMOSENV.2016.06.029

Sánchez-Rodas, D., de la Campa, A.M.S., Alsioufi, L., 2015. Analytical approaches for arsenic determination in air: A critical review. Anal. Chim. Acta 898, 1–18. https://doi.org/http://dx.doi.org/10.1016/j.aca.2015.09.043

Santos, J.M., Reis, N.C., Galvão, E.S., Silveira, A., Goulart, E.V., Lima, A.T., 2017. Source apportionment of settleable particles in an impacted urban and industrialized region in Brazil. Environ. Sci. Pollut. Res. 24. https://doi.org/10.1007/s11356-017-9677-y

Sarzanini, C., 2002. Recent developments in ion chromatography. J. Chromatogr. A 956, 3–13. https://doi.org/http://dx.doi.org/10.1016/S0021-9673(02)00147-4

Satsangi, P.G., Yadav, S., 2014. Characterization of PM2.5 by X-ray diffraction and scanning electron microscopy–energy dispersive spectrometer: its relation with different pollution

sources. Int. J. Environ. Sci. Technol. 11, 217–232. https://doi.org/10.1007/s13762-012-0173-0

Schauer, C., Niessner, R., Pöschl, U., 2003. Polycyclic Aromatic Hydrocarbons in Urban Air Particulate Matter: Decadal and Seasonal Trends, Chemical Degradation, and Sampling Artifacts. Environ. Sci. Technol. 37, 2861–2868. https://doi.org/10.1021/es034059s

Schauer, J.J., Lough, G.C., Shafer, M.M., Christensen, W.F., Arndt, M.F., DeMinter, J.T., Park, J.-S., 2006. Characterization of metals emitted from motor vehicles. Res. Rep. Health. Eff. Inst. 1–88.

Schmeling, M., 2004. Characterization of urban air pollution by total reflection X-ray fluorescence. Spectrochim. Acta Part B At. Spectrosc. 59, 1165–1171. https://doi.org/http://dx.doi.org/10.1016/j.sab.2004.01.009

Schmeling, M., Klockenkämper, R., Klockow, D., 1997. Application of total-reflection X-ray fluorescence spectrometry to the analysis of airborne particulate matter1This paper was presented at the 6th Conference on "Total Reflection X-Ray Fluorescence Analysis and Related Methods" (TXRF '96) held in two part. Spectrochim. Acta Part B At. Spectrosc. 52, 985–994. https://doi.org/http://dx.doi.org/10.1016/S0584-8547(96)01673-4

Schmid-Beurmann, P., Lottermoser, W., 1993. 57Fe-Moessbauer spectra, electronic and crystal structure of members of the CuS2-FeS2 solid solution series. Phys. Chem. Miner. 19, 571–577. https://doi.org/10.1007/BF00203056

Seebauer, E.G., Barlaz, D.E., 2016. SIMS for analysis of nanostructures. Curr. Opin. Chem. Eng. 12, 8–13. https://doi.org/http://dx.doi.org/10.1016/j.coche.2016.01.007

Seinfeld, J.H., Pandis, S.N., 2006. Atmospheric Chemistry and Physics From Air Pollution to Climate Change, 2nd ed. John Wiley & Sons, Inc., New Jersey.

Sharma, H., Jain, V.K., Khan, Z.H., 2007. Identification of polycyclic aromatic hydrocarbons (PAHs) in suspended particulate matter by synchronous fluorescence spectroscopic technique. Spectrochim. Acta Part A Mol. Biomol. Spectrosc. 68, 43–49. https://doi.org/http://dx.doi.org/10.1016/j.saa.2006.10.054

Shaw, M.J., Haddad, P.R., 2004. The determination of trace metal pollutants in environmental matrices using ion chromatography. Environ. Int. 30, 403–431. https://doi.org/http://dx.doi.org/10.1016/j.envint.2003.09.009

Shi, G.-L., Feng, Y.-C., Zeng, F., Li, X., Zhang, Y.-F., Wang, Y.-Q., Zhu, T., 2009. Use of a Nonnegative Constrained Principal Component Regression Chemical Mass Balance Model to Study the Contributions of Nearly Collinear Sources. Environ. Sci. Technol. 43, 8867–8873. https://doi.org/10.1021/es902785c

Shi, G.-L., Liu, G.-R., Peng, X., Wang, Y.-N., Tian, Y.-Z., Wang, W., Feng, Y.-C., 2014a. A Comparison of Multiple Combined Models for Source Apportionment, Including the PCA/MLR-CMB, Unmix-CMB and PMF-CMB Models. Aerosol Air Qual. Res. 14, 2040–2050. https://doi.org/10.4209/aaqr.2014.01.0024

Shi, G.-L., Liu, G.-R., Peng, X., Wang, Y.-N., Tian, Y.-Z., Wang, W., Feng, Y.-C., 2014b. A Comparison of Multiple Combined Models for Source Apportionment, Including the PCA/MLR-CMB, Unmix-CMB and PMF-CMB Models. Aerosol Air Qual. Res. 14, 2040–2050. https://doi.org/10.4209/aaqr.2014.01.0024

Shi, G.-L., Zeng, F., Li, X., Feng, Y.-C., Wang, Y.-Q., Liu, G.-X., Zhu, T., 2011. Estimated contributions and uncertainties of PCA/MLR–CMB results: Source apportionment for synthetic and ambient datasets. Atmos. Environ. 45, 2811–2819. https://doi.org/http://dx.doi.org/10.1016/j.atmosenv.2011.03.007

Siefert, R.L., Pehkonen, S.O., Erel, Y., Hoffmann, M.R., 1994. Iron photochemistry of aqueous suspensions of ambient aerosol with added organic acids. Geochim. Cosmochim. Acta 58, 3271–3279. https://doi.org/10.1016/0016-7037(94)90055-8

Sitko, R., 2009. Quantitative X-ray fluorescence analysis of samples of less than 'infinite thickness': Difficulties and possibilities. Spectrochim. Acta Part B At. Spectrosc. 64, 1161–1172. https://doi.org/http://dx.doi.org/10.1016/j.sab.2009.09.005

Slezakova, K., Pires, J.C.M., Pereira, M.C., Martins, F.G., Alvim-Ferraz, M.C., 2008. Influence of traffic emissions on the composition of atmospheric particles of different sizes—Part 2: SEM–EDS characterization. J. Atmos. Chem. 60, 221–236. https://doi.org/10.1007/s10874-008-9117-y

Sobanska, S., Coeur, C., Maenhaut, W., Adams, F., 2003. SEM-EDX Characterisation of Tropospheric Aerosols in the Negev Desert (Israel). J. Atmos. Chem. 44, 299–322. https://doi.org/10.1023/A:1022969302107

Song, X., Shao, L., Zheng, Q., Yang, S., 2014. Mineralogical and geochemical composition of

particulate matter (PM10) in coal and non-coal industrial cities of Henan Province, North China. Atmos. Res. 143, 462–472. https://doi.org/https://doi.org/10.1016/j.atmosres.2014.03.015

Song, Y., Zhang, Y., Xie, S., Zeng, L., Zheng, M., Salmon, L.G., Shao, M., Slanina, S., 2006. Source apportionment of PM2.5 in Beijing by positive matrix factorization. Atmos. Environ. 40, 1526–1537. https://doi.org/10.1016/J.ATMOSENV.2005.10.039

Srimuruganandam, B., Shiva Nagendra, S.M., 2012. Source characterization of PM10 and PM2.5 mass using a chemical mass balance model at urban roadside. Sci. Total Environ. 433, 8–19. https://doi.org/10.1016/J.SCITOTENV.2012.05.082

Srivastava, A., Gupta, S., Jain, V.K., 2008. Source Apportionment of Total Suspended Particulate Matter in Coarse and Fine Size Ranges Over Delhi. Aerosol Air Qual. Res. 8, 188–200. https://doi.org/10.4209/aaqr.2007.09.0040

Strezov, V., 2006. Iron ore reduction using sawdust: Experimental analysis and kinetic modelling. Renew. Energy 31, 1892–1905. https://doi.org/10.1016/J.RENENE.2005.08.032

Sunder Raman, R., Hopke, P.K., 2007. Source apportionment of fine particles utilizing partially speciated carbonaceous aerosol data at two rural locations in New York State. Atmos. Environ. 41, 7923–7939. https://doi.org/10.1016/J.ATMOSENV.2007.06.066

Szidat, S., Jenk, T.., Gäggeler, H.., Synal, H.-A., Fisseha, R., Baltensperger, U., Kalberer, M., Samburova, V., Reimann, S., Kasper-Giebl, A., Hajdas, I., 2004. Radiocarbon (14C)-deduced biogenic and anthropogenic contributions to organic carbon (OC) of urban aerosols from Zürich, Switzerland. Atmos. Environ. 38, 4035–4044. https://doi.org/10.1016/J.ATMOSENV.2004.03.066

Szigeti, T., Óvári, M., Dunster, C., Kelly, F.J., Lucarelli, F., Záray, G., 2015. Changes in chemical composition and oxidative potential of urban PM2.5 between 2010 and 2013 in Hungary. Sci. Total Environ. 518–519, 534–544. https://doi.org/10.1016/J.SCITOTENV.2015.03.025

Taioli, S., Simonucci, S., Calliari, L., Dapor, M., 2010. Electron spectroscopies and inelastic processes in nanoclusters and solids: Theory and experiment. Phys. Rep. 493, 237–319. https://doi.org/http://dx.doi.org/10.1016/j.physrep.2010.04.003

Taiwo, A.M., Harrison, R.M., Shi, Z., 2014. A review of receptor modelling of industrially emitted particulate matter. Atmos. Environ. 97, 109–120.

https://doi.org/10.1016/J.ATMOSENV.2014.07.051

Tauler, R., Viana, M., Querol, X., Alastuey, A., Flight, R.M., Wentzell, P.D., Hopke, P.K., 2009. Comparison of the results obtained by four receptor modelling methods in aerosol source apportionment studies. Atmos. Environ. 43, 3989–3997. https://doi.org/10.1016/J.ATMOSENV.2009.05.018

Tecer, L.H., Tuncel, G., Karaca, F., Alagha, O., Süren, P., Zararsız, A., Kırmaz, R., 2012. Metallic composition and source apportionment of fine and coarse particles using positive matrix factorization in the southern Black Sea atmosphere. Atmos. Res. 118, 153–169. https://doi.org/https://doi.org/10.1016/j.atmosres.2012.06.016

Theriault, G.E., Barry, T.L., Thomas, M.J.B., 1975. Technique of preparing powder samples for AES [Auger electron spectroscopy] and/or ESCA analysis. Anal. Chem. 47, 1492–1493. https://doi.org/10.1021/ac60358a042

Thorpe, A., Harrison, R.M., 2008. Sources and properties of non-exhaust particulate matter from road traffic: A review. Sci. Total Environ. 400, 270–282. https://doi.org/10.1016/J.SCITOTENV.2008.06.007

Thurston, G.D., Lioy, P.J., 1987. Receptor modeling and aerosol transport. Atmos. Environ. 21, 687–698. https://doi.org/http://dx.doi.org/10.1016/0004-6981(87)90050-3

Tian, Y.-Z., Liu, G.-R., Zhang, C.-Y., Wu, J.-Y., Zeng, F., Shi, G.-L., Feng, Y.-C., 2013. Effects of collinearity, unknown source and removed factors on the NCPCRCMB receptor model solution. Atmos. Environ. 81, 76–83. https://doi.org/http://dx.doi.org/10.1016/j.atmosenv.2013.08.052

Timkovsky, J., Dusek, U., Henzing, J.S., Kuipers, T.L., Röckmann, T., Holzinger, R., 2015. Offline thermal-desorption proton-transfer-reaction mass spectrometry to study composition of organic aerosol. J. Aerosol Sci. 79, 1–14. https://doi.org/10.1016/J.JAEROSCI.2014.08.010

Tomiyasu, B., Suzuki, K., Gotoh, T., Owari, M., Nihei, Y., 2004. TOF-SIMS measurement for the complex particulate matter in urban air environment. Appl. Surf. Sci. 231, 515–519. https://doi.org/http://dx.doi.org/10.1016/j.apsusc.2004.03.042

Trejos, T., Almirall, J.R., 2004. Effect of Fractionation on the Forensic Elemental Analysis of Glass Using Laser Ablation Inductively Coupled Plasma Mass Spectrometry. Anal. Chem.

76, 1236–1242. https://doi.org/10.1021/ac0349330

Trompetter, W.J., Reyes, A.G., Kennedy, J., Markwitz, A., 2013. Use of micro-proton elastic scattering analysis to determine water content in geological powders. Nucl. Instruments Methods Phys. Res. Sect. B Beam Interact. with Mater. Atoms 306, 257–260. https://doi.org/http://dx.doi.org/10.1016/j.nimb.2012.11.037

Tsai, J.-H., Lin, K.-H., Chen, C.-Y., Ding, J.-Y., Choa, C.-G., Chiang, H.-L., 2007. Chemical constituents in particulate emissions from an integrated iron and steel facility. J. Hazard. Mater. 147, 111–119. https://doi.org/10.1016/J.JHAZMAT.2006.12.054

Tugrul, N., Derun, E.M., Pişkin, M.B., Ekerim, A., 2009. A study on the structural behavior of reduced pyrite ash pellets by XRD and XRF analysis. Waste Manag. Res. 27, 281–287. https://doi.org/10.1177/0734242X08090404

USEPA, 1999. Particulate Matter (PM2.5) Speciation Guidance: Final Draft (Edition 1).

USEPA, 1986. AP-42: Compilation of Air Emission Factors, Fifth Edition, Volumi I, Chapter 12: Metallurgical Industry.

Vale, 2018. Relatório anual, Formulário 20-F.

Vale, 2017a. Produção da Vale no 1T17.

Vale, 2017b. Relatório anual, Formulário 20-F.

Vale, 2016. Produção da Vale no 4T16.

van Drooge, B.L., Crusack, M., Reche, C., Mohr, C., Alastuey, A., Querol, X., Prevot, A., Day, D.A., Jimenez, J.L., Grimalt, J.O., 2012. Molecular marker characterization of the organic composition of submicron aerosols from Mediterranean urban and rural environments under contrasting meteorological conditions. Atmos. Environ. 61, 482–489. https://doi.org/http://dx.doi.org/10.1016/j.atmosenv.2012.07.039

van Drooge, B.L., Nikolova, I., Ballesta, P.P., 2009. Thermal desorption gas chromatography–mass spectrometry as an enhanced method for the quantification of polycyclic aromatic hydrocarbons from ambient air particulate matter. J. Chromatogr. A 1216, 4030–4039. https://doi.org/10.1016/J.CHROMA.2009.02.043

Vander Wal, R.L., Bryg, V.M., Huang, C.-H., 2016. Chemistry characterization of jet aircraft

engine particulate matter by XPS: Results from APEX III. Atmos. Environ. 140, 623–629. https://doi.org/http://dx.doi.org/10.1016/j.atmosenv.2016.05.039

Venkataraman, C., Friedlander, S.K., 1994. Source Resolution of Fine Particulate Polycyclic Aromatic Hydrocarbons Using a Receptor Model Modified for Reactivity. Air Waste 44, 1103–1108. https://doi.org/10.1080/10473289.1994.10467306

Viana, M., Kuhlbusch, T.A.J., Querol, X., Alastuey, A., Harrison, R.M., Hopke, P.K., Winiwarter, W., Vallius, M., Szidat, S., Prévôt, A.S.H., Hueglin, C., Bloemen, H., Wåhlin, P., Vecchi, R., Miranda, A.I., Kasper-Giebl, A., Maenhaut, W., Hitzenberger, R., 2008a. Source apportionment of particulate matter in Europe: A review of methods and results. J. Aerosol Sci. 39, 827–849. https://doi.org/10.1016/J.JAEROSCI.2008.05.007

Viana, M., Pandolfi, M., Minguillón, M.C., Querol, X., Alastuey, A., Monfort, E., Celades, I., 2008b. Inter-comparison of receptor models for PM source apportionment: Case study in an industrial area. Atmos. Environ. 42, 3820–3832. https://doi.org/10.1016/J.ATMOSENV.2007.12.056

Voss, M., Nunes, M.A.G., Corazza, G., Flores, E.M.M., Müller, E.I., Dressler, V.L., 2017. A new approach to calibration and determination of selected trace elements in food contact polymers by LA-ICP-MS. Talanta 170, 488–495. https://doi.org/https://doi.org/10.1016/j.talanta.2017.04.048

Vossler, T., Černikovský, L., Novák, J., Williams, R., 2016. Source apportionment with uncertainty estimates of fine particulate matter in Ostrava, Czech Republic using Positive Matrix Factorization. Atmos. Pollut. Res. 7, 503–512. https://doi.org/https://doi.org/10.1016/j.apr.2015.12.004

Voutsa, D., Samara, C., Kouimtzis, T., Ochsenkühn, K., 2002. Elemental composition of airborne particulate matter in the multi-impacted urban area of Thessaloniki, Greece. Atmos. Environ. 36, 4453–4462. https://doi.org/10.1016/S1352-2310(02)00411-9

Wagner, A., Boman, J., Gatari, M.J., 2008. Elemental analysis of size-fractionated particulate matter sampled in Göteborg, Sweden. Spectrochim. Acta Part B At. Spectrosc. 63, 1426–1431. https://doi.org/http://dx.doi.org/10.1016/j.sab.2008.10.010

Wagner, A., Mages, M., 2010. Total-Reflection X-ray fluorescence analysis of elements in size-fractionated particulate matter sampled on polycarbonate filters — Composition and sources

of aerosol particles in Göteborg, Sweden. Spectrochim. Acta Part B At. Spectrosc. 65, 471–477. https://doi.org/http://dx.doi.org/10.1016/j.sab.2010.02.007

Walkner, C., Gratzer, R., Meisel, T., Bokhari, S.N.H., 2017. Multi-element analysis of crude oils using ICP-QQQ-MS. Org. Geochem. 103, 22–30. https://doi.org/http://dx.doi.org/10.1016/j.orggeochem.2016.10.009

Wallace, H.W., Sanchez, N.P., Flynn, J.H., Erickson, M.H., Lefer, B.L., Griffin, R.J., 2018. Source apportionment of particulate matter and trace gases near a major refinery near the Houston Ship Channel. Atmos. Environ. 173, 16–29. https://doi.org/10.1016/J.ATMOSENV.2017.10.049

Wang, F., Chen, Y., Meng, X., Fu, J., Wang, B., 2016. The contribution of anthropogenic sources to the aerosols over East China Sea. Atmos. Environ. 127, 22–33. https://doi.org/http://dx.doi.org/10.1016/j.atmosenv.2015.12.002

Wang, J., Hu, Z., Chen, Y., Chen, Z., Xu, S., 2013. Contamination characteristics and possible sources of PM10 and PM2.5 in different functional areas of Shanghai, China. Atmos. Environ. 68, 221–229. https://doi.org/http://dx.doi.org/10.1016/j.atmosenv.2012.10.070

Wang, J., Zhang, J., Liu, Z., Wu, J., Zhang, Y., Han, S., Zheng, X., Zhou, L., Feng, Y., Zhu, T., 2017. Characterization of chemical compositions in size-segregated atmospheric particles during severe haze episodes in three mega-cities of China. Atmos. Res. 187, 138–146. https://doi.org/http://dx.doi.org/10.1016/j.atmosres.2016.12.004

Wang, J., Zhou, M., Liu, B., Wu, J., Peng, X., Zhang, Y., Han, S., Feng, Y., Zhu, T., 2016. Characterization and source apportionment of size-segregated atmospheric particulate matter collected at ground level and from the urban canopy in Tianjin. Environ. Pollut. 219, 982–992. https://doi.org/http://dx.doi.org/10.1016/j.envpol.2016.10.069

Wang, Q.Q., Huang, X.H.H., Zhang, T., Zhang, Q., Feng, Y., Yuan, Z., Wu, D., Lau, A.K.H., Yu, J.Z., 2015. Organic tracer-based source analysis of PM2.5 organic and elemental carbon: A case study at Dongguan in the Pearl River Delta, China. Atmos. Environ. 118, 164–175. https://doi.org/10.1016/J.ATMOSENV.2015.07.033

Watson, J.G., Zhu, T., Chow, J.C., Engelbrecht, J., Fujita, E.M., Wilson, W.E., 2002. Receptor modeling application framework for particle source apportionment. Chemosphere 49, 1093–1136. https://doi.org/10.1016/S0045-6535(02)00243-6

WHO, 2005. Air quality guidelines for particulate matter, ozone, nitrogen dioxide and sulfur dioxide. Geneva, Switzerland.

Wieser, P., Wurster, R., Seiler, H., 1980. Identification of airborne particles by laser induced mass spectroscopy. Atmos. Environ. 14, 485–494. https://doi.org/10.1016/0004-6981(80)90214-0

Wilson, W.E., Chow, J.C., Claiborn, C., Fusheng, W., Engelbrecht, J., Watson, J.G., 2002. Monitoring of particulate matter outdoors. Chemosphere 49, 1009–1043. https://doi.org/http://dx.doi.org/10.1016/S0045-6535(02)00270-9

Wittig, A.E. (Beth), Allen, D.T., 2008. Improvement of the Chemical Mass Balance model for apportioning—sources of non-methane hydrocarbons using composite aged source profiles. Atmos. Environ. 42, 1319–1337. https://doi.org/http://dx.doi.org/10.1016/j.atmosenv.2007.10.072

Wnorowski, A., 2017. Characterization of the ambient air content of parent polycyclic aromatic hydrocarbons in the Fort McKay region (Canada). Chemosphere 174, 371–379. https://doi.org/10.1016/J.CHEMOSPHERE.2017.01.114

Wojdyr, M., 2010. Fityk: a general-purpose peak fitting program. J. Appl. Crystallogr. 43, 1126–1128. https://doi.org/10.1107/S0021889810030499

Wonglee, S., Tada, T., Fukuda, H., Hasegawa, J., Oguri, Y., 2011. Chemical speciation of chlorine in particulate matter by wavelength-dispersive PIXE technique. Nucl. Instruments Methods Phys. Res. Sect. B Beam Interact. with Mater. Atoms 269, 3111–3114. https://doi.org/http://dx.doi.org/10.1016/j.nimb.2011.04.083

Wu, D., Zhang, F., Lou, W., Li, D., Chen, J., 2017. Chemical characterization and toxicity assessment of fine particulate matters emitted from the combustion of petrol and diesel fuels. Sci. Total Environ. 605, 172–179. https://doi.org/http://dx.doi.org/10.1016/j.scitotenv.2017.06.058

Wu, Y., Yang, L., Zheng, X., Zhang, S., Song, S., Li, J., Hao, J., 2014. Characterization and source apportionment of particulate PAHs in the roadside environment in Beijing. Sci. Total Environ. 470–471, 76–83. https://doi.org/10.1016/J.SCITOTENV.2013.09.066

Xiu, G.L., Jin, Q., Zhang, D., Shi, S., Huang, X., Zhang, W., Bao, L., Gao, P., Chen, B., 2005. Characterization of size-fractionated particulate mercury in Shanghai ambient air. Atmos. Environ. 39, 419–427. https://doi.org/10.1016/J.ATMOSENV.2004.09.046

Yadav, S., Tandon, A., Attri, A.K., 2013. Characterization of aerosol associated non-polar organic compounds using TD-GC-MS: A four year study from Delhi, India. J. Hazard. Mater. 252–253, 29–44. https://doi.org/10.1016/J.JHAZMAT.2013.02.024

Yang, H.-H., Lee, K.-T., Hsieh, Y.-S., Luo, S.-W., Huang, R.-J., 2015. Emission Characteristics and Chemical Compositions of both Filterable and Condensable Fine Particulate from Steel Plants. Aerosol Air Qual. Res. 15, 1672–1680. https://doi.org/10.4209/aaqr.2015.06.0398

Yatkin, S., Gerboles, M., 2017. Evaluation of EDXRF results from PM10 using standardless analysis and external calibration. Microchem. J. 133, 423–430. https://doi.org/http://dx.doi.org/10.1016/j.microc.2017.04.003

Yatkin, S., Gerboles, M., Borowiak, A., 2012. Evaluation of standardless EDXRF analysis for the determination of elements on PM10 loaded filters. Atmos. Environ. 54, 568–582. https://doi.org/http://dx.doi.org/10.1016/j.atmosenv.2012.02.062

Yin, J., Allen, A.G., Harrison, R.M., Jennings, S.G., Wright, E., Fitzpatrick, M., Healy, T., Barry, E., Ceburnis, D., McCusker, D., 2005. Major component composition of urban PM10 and PM2.5 in Ireland. Atmos. Res. 78, 149–165. https://doi.org/10.1016/J.ATMOSRES.2005.03.006

Yin, J., Harrison, R.M., Chen, Q., Rutter, A., Schauer, J.J., 2010. Source apportionment of fine particles at urban background and rural sites in the UK atmosphere. Atmos. Environ. 44, 841–851. https://doi.org/10.1016/J.ATMOSENV.2009.11.026

Zeng, J., Zhang, G., Bao, L., Long, S., Tan, M., Li, Y., Ma, C., Zhao, Y., 2013. Sulfur speciation and bioaccumulation in camphor tree leaves as atmospheric sulfur indicator analyzed by synchrotron radiation XRF and XANES. J. Environ. Sci. 25, 605–612. https://doi.org/http://dx.doi.org/10.1016/S1001-0742(12)60056-4

Zhang, N., Li, Z., Zheng, J., Yang, X., Shen, K., Zhou, T., Zhang, Y., 2017. Multielemental analysis of botanical samples by ICP-OES and ICP-MS with focused infrared lightwave ashing for sample preparation. Microchem. J. 134, 68–77. https://doi.org/http://dx.doi.org/10.1016/j.microc.2017.05.006

Zhang, Y., Cai, J., Wang, S., He, K., Zheng, M., 2017. Review of receptor-based source apportionment research of fine particulate matter and its challenges in China. Sci. Total Environ. 586, 917–929. https://doi.org/10.1016/J.SCITOTENV.2017.02.071

Zhang, Y., Seigneur, C., Seinfeld, J.H., Jacobson, M., Clegg, S.L., Binkowski, F.S., 2000. A comparative review of inorganic aerosol thermodynamic equilibrium modules: similarities, differences, and their likely causes. Atmos. Environ. 34, 117–137. https://doi.org/10.1016/S1352-2310(99)00236-8

Zhang, Z.-H., Khlystov, A., Norford, L.K., Tan, Z.-K., Balasubramanian, R., 2017. Characterization of traffic-related ambient fine particulate matter (PM2.5) in an Asian city: Environmental and health implications. Atmos. Environ. 161, 132–143. https://doi.org/10.1016/J.ATMOSENV.2017.04.040

Zhang, Z., Li, H., Liu, H., Ni, R., Li, J., Deng, L., Lu, D., Cheng, X., Duan, P., Li, W., 2016. A preliminary analysis of the surface chemistry of atmospheric aerosol particles in a typical urban area of Beijing. J. Environ. Sci. 47, 71–81. https://doi.org/http://dx.doi.org/10.1016/j.jes.2016.01.025

Zhou, L., Dong, L., Huang, Y., Shi, S., Zhang, L., Zhang, X., Yang, W., Li, L., 2014. Spatial distribution and source apportionment of polycyclic aromatic hydrocarbons (PAHs) in Camphor (Cinnamomum camphora) tree bark from Southern Jiangsu, China. Chemosphere 107, 297–303. https://doi.org/10.1016/J.CHEMOSPHERE.2013.12.070

Zou, B.-B., Huang, X.-F., Zhang, B., Dai, J., Zeng, L.-W., Feng, N., He, L.-Y., 2017. Source apportionment of PM2.5 pollution in an industrial city in southern China. Atmos. Pollut. Res. 8, 1193–1202. https://doi.org/10.1016/J.APR.2017.05.001

Zucchiatti, A., Redondo-Cubero, A., 2014. Ion beam analysis: New trends and challenges. Nucl. Instruments Methods Phys. Res. Sect. B Beam Interact. with Mater. Atoms 331, 48–54. https://doi.org/http://dx.doi.org/10.1016/j.nimb.2014.02.013

Zuo, Y., Deng, Y., 1997. Iron(II)-catalyzed photochemical decomposition of oxalic acid and generation of H2O2 in atmospheric liquid phases. Chemosphere 35, 2051–2058. https://doi.org/10.1016/S0045-6535(97)00228-2

8. APPENDIX A

Trends in Analytical Techniques Applied to Particulate Matter Characterization: A Critical Review of Fundaments and Applications

The search was conducted on the main databases using the terms "Analytical technique (e.g. EDXRF, PIXE, ICP-OES, etc.)" AND "aerosol" OR "particulate matter", using no filters, and considering all publication titles.

An evident trend regarding atomic spectrometry over the last 20 years (Figure S1a). The use of techniques based on atomic spectrometry is dominant over all others techniques with about 12200 works (~71%) against about 4000 works (~26%) that used X-ray based techniques followed by activation analysis with 570 works (~3%).
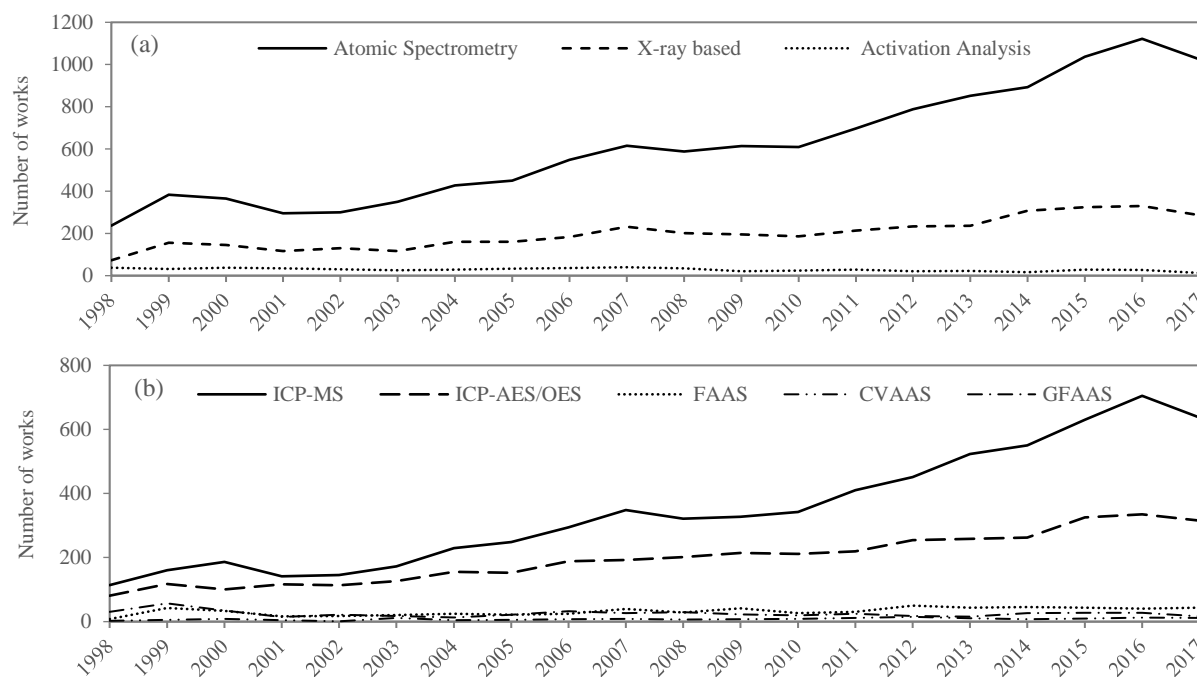
Figure S1. Trends of published works on analytical techniques over the last 20 years (**Using no filters**): (a) General techniques; (b) X-ray related techniques; (c) Atomic spectrometry related techniques. Searching terms: "Analytical technique (e.g: EDXRF, PIXE, ICP-OES, etc.)" AND "aerosol" OR "particulate matter".

Table S1. Trends of published works on analytical techniques over the last 20 years (**Using no filters**): (a) General techniques; (b) X-ray related techniques; (c) Atomic spectrometry related techniques. Searching terms: "Analytical technique (e.g: EDXRF, PIXE, ICP-OES, etc.)" AND "aerosol" OR "particulate matter".

Year	X-ray based								Activation Analysis	Atomic Spectrometry						
	EDXRF	TXRF	WDXRF	SR-XRF	PIXE	PESA	XPS	Total	INAA	CVAAS	FAAS	GFAAS	ICP-AES/OES	ICP-MS	Total
1998		11		4	56	2		**73**	37	3	8	31	81	114	**237**
1999	44	14	2	1	91	4	54	**156**	32	6	43	57	118	160	**384**
2000	66	14	1	4	55	6	47	**146**	38	9	34	35	101	186	**365**
2001	58	9	1	3	39	7	50	**117**	34	5	17	15	117	142	**296**
2002	52	6	3	0	65	4	44	**130**	30	1	18	22	114	145	**300**
2003	73	9	1	0	32	2	67	**117**	26	12	21	18	127	172	**350**
2004	93	10	0	0	52	6	50	**161**	29	5	25	13	155	229	**427**
2005	91	13	0	1	54	2	78	**161**	33	6	22	22	152	248	**450**
2006	93	13	4	1	65	7	95	**183**	36	8	25	33	188	294	**548**
2007	149	12	3	4	57	7	99	**232**	40	9	40	27	192	348	**616**
2008	128	25	1	4	41	2	103	**201**	34	7	29	30	201	321	**588**
2009	132	9	5	1	46	2	115	**195**	21	8	42	23	214	327	**614**
2010	135	11	1	1	35	3	146	**186**	24	9	27	20	211	342	**609**
2011	146	10	6	3	46	2	118	**213**	28	12	31	25	219	410	**697**
2012	163	11	3	3	48	6	163	**234**	21	15	50	18	254	451	**788**
2013	182	11	6	1	34	3	171	**237**	23	11	44	16	258	523	**852**
2014	224	13	4	0	57	9	178	**307**	16	8	46	27	262	550	**893**
2015	243	13	6	2	57	4	225	**325**	28	10	44	28	325	630	**1037**
2016	260	14	10	2	42	2	243	**330**	27	13	41	28	335	705	**1122**
2017	238	6	4	1	35	2	273	**286**	13	12	44	17	315	637	**1025**
TOTAL	2570	234	61	36	1007	82	2319	**3990**	570	169	651	505	3939	6934	**12198**

A refinement on articles' search to atmospheric related publication titles by using the terms "Analytical technique (e.g. EDXRF, PIXE, ICP-OES, etc.)" AND "aerosol" OR "particulate matter", narrowing publication titles to journals including studies on atmospheric composition and its impacts, like as Atmospheric Environment, Science of the Total Environment, Journal of Aerosol Science, Atmospheric Research, Chemosphere, Environmental Pollution, etc. (Table S2 and Figure S2).
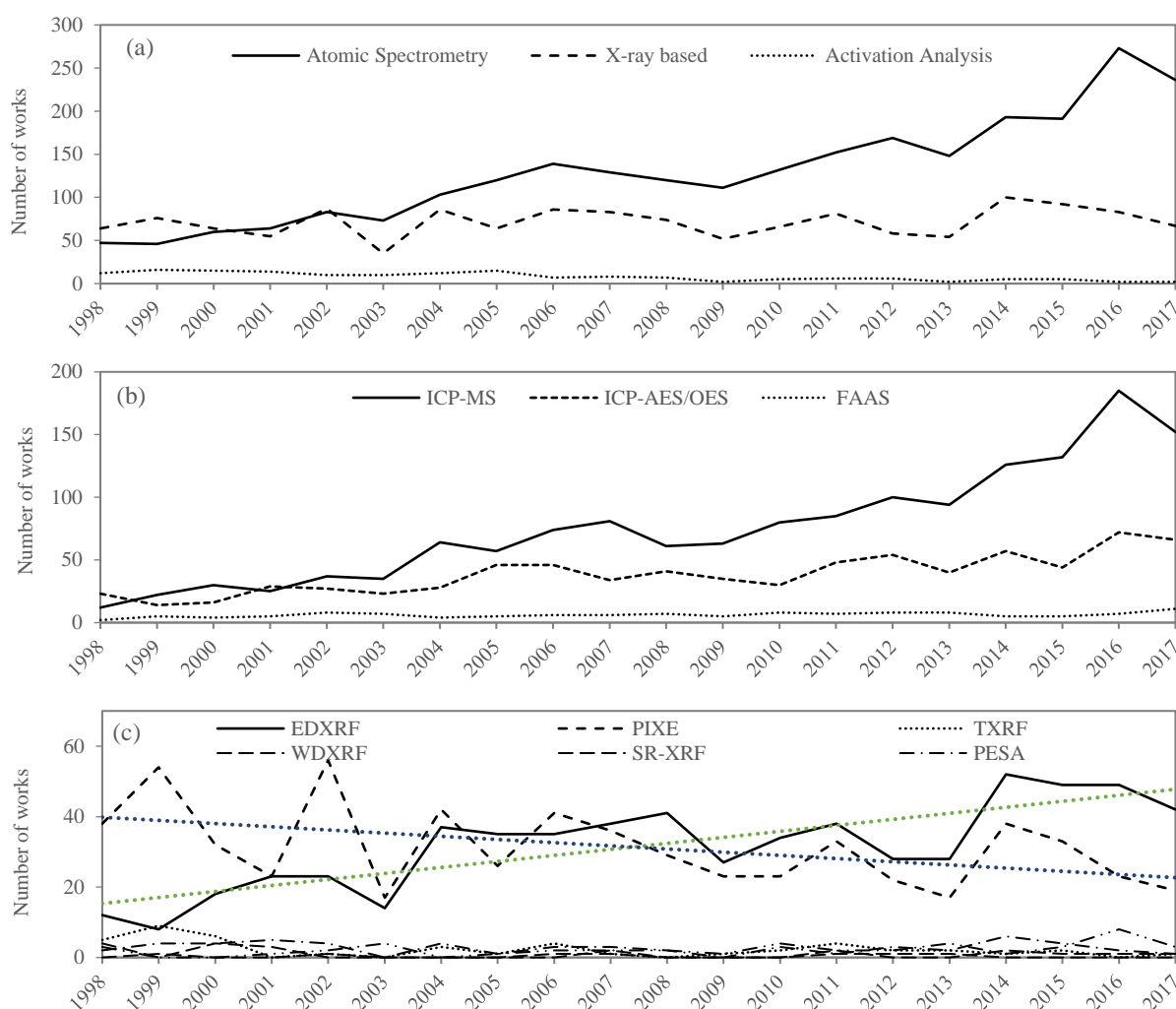
Legend: * Dashed line on graph 2c represent the tendency line for: EDXRF (yellow) and PIXE (blue).

Figure S2. Trends of published articles on analytical techniques over the last 20 years (**Using filter applied for atmospheric related publication titles**): (a) General techniques; (b) X-ray related techniques; (c) Atomic spectrometry related techniques. Searching therm: "Analytical technique (e.g: EDXRF, PIXE, ICP-OES, etc.)" AND "aerosol" OR "particulate matter".

Figure S2a shows that the use of atomic spectrometry for elemental analysis for measurements of atmospheric particles has increased significantly since 2002, although the difference between the number of publications using atomic spectrometry and X-ray based techniques is lower than considering publication titles non related to atmospheric particles. Figure 2a indicates that the use

of atomic spectrometry based techniques like as ICP-MS, ICP-OES, FAAS, GFAAS and CVAAS are reported in 60% of all works published. X-ray based techniques are reported in about 35%, mainly due to the use of EDXRF, and Activation Analysis (INAA) is the technique of choice in less than 5 % of all works.

Table S2. Trends of published articles on analytical techniques over the last 20 years (**Using filter applied for atmospheric related publication titles**): (a) General techniques; (b) X-ray related techniques; (c) Atomic spectrometry related techniques. Searching therm: "Analytical technique (e.g: EDXRF, PIXE, ICP-OES, etc.)" AND "aerosol" OR "particulate matter".

Year	X-ray based								Activation Analysis	Atomic Spectrometry						
	EDXRF	TXRF	WDXRF	SR-XRF	PIXE	PESA	XPS	Total	INAA	CVAAS	FAAS	GFAAS	ICP-AES/OES	ICP-MS	Total
1998	12	5	0	4	38	2	3	64	12	1	2	9	23	12	47
1999	8	9	1	0	54	4	0	76	16	0	5	5	14	22	46
2000	18	6	0	4	32	4	0	64	15	2	4	8	16	30	60
2001	23	0	0	3	23	5	1	55	14	1	5	4	29	25	64
2002	23	1	1	0	56	4	2	87	10	0	8	11	27	37	83
2003	14	0	0	0	17	0	4	35	10	4	7	4	23	35	73
2004	37	3	0	0	42	4	0	86	12	1	4	6	28	64	103
2005	35	1	0	0	26	1	1	64	15	4	5	8	46	57	120
2006	35	4	1	0	41	3	2	86	7	4	6	9	46	74	139
2007	38	1	1	2	36	3	2	83	8	2	6	6	34	81	129
2008	41	0	0	0	29	2	2	74	7	0	7	11	41	61	120
2009	27	1	0	0	23	0	1	52	2	2	5	6	35	63	111
2010	34	2	0	0	23	3	4	66	5	6	8	8	30	80	132
2011	38	4	2	1	33	1	2	81	6	6	7	6	48	85	152
2012	28	2	0	1	22	3	2	58	6	3	8	4	54	100	169
2013	28	2	0	1	17	2	4	54	2	1	8	5	40	94	148
2014	52	1	2	0	38	6	1	100	5	3	5	2	57	126	193
2015	49	2	1	0	33	4	3	92	5	4	5	6	44	132	191
2016	49	0	1	0	23	2	8	83	2	4	7	5	72	185	273
2017	42	1	1	0	19	1	3	67	2	3	11	4	66	152	236
TOTAL	631	45	11	16	625	54	45	1427	161	51	123	127	773	1515	2589

9. APPENDIX B

The Determination of Markers for Iron-Rich Particles by Resonant Synchrotron X-Ray Diffraction

S1. Wind roses

18-20 Oct 2016	20-22 Oct 2016	22-24 Oct 2016	24-26 Oct 2016	26-28 Oct 2016	28-30 Oct 2016
01-03 Nov 2016	03-05 Nov 2016	05-07 Nov 2016	07-09 Nov 2016	09-11 Nov 2016	11-13 Nov 2016
13-15 Nov 2016	15-17 Nov 2016	17-19 Nov 2016	19-21 Nov 2016	21-23 Nov 2016	23-25 Nov 2016
25-27 Nov 2016	27-29 Nov 2016	29-31 Nov 2016	01-03 Dec 2016	03-05 Dec 2016	05-07 Dec 2016
07-09 Dec 2016	09-11 Dec 2016	11-13 Dec 2016	13-15 Dec 2016	15-17 Dec 2016	17-19 Dec 2016

Figure S1. Wind roses for the sampling period between October-18, 2016 and December-19, 2016.

| 16-18 Jan 2017 | 18-20 Jan 2017 | 20-22 Jan 2017 | 22-24 Jan 2017 | 24-26 Jan 2017 | 26-28 Jan 2017 |

| 28-30 Jan 2017 | 30-01 Jan 2017 | 01-03 Feb 2017 | 03-05 Feb 2017 | 05-07 Feb 2017 | 07-09 Feb 2017 |

| 09-11 Feb 2017 | 11-13 Feb 2017 | 13-15 Feb 2017 | 15-17 Feb 2017 | 17-19 Feb 2017 | 19-21 Feb 2017 |

| 21-23 Feb 2017 | 23-25 Feb 2017 | 25-27 Feb 2017 | 27-29 Feb 2017 | 01-03 Mar 2017 | 03-05 Mar 2017 |

| 05-07 Mar 2017 | 07-09 Mar 2017 | 09-11 Mar 2017 | 11-13 Mar 2017 | 13-15 Mar 2017 | 15-17 Mar 2017 |

Figure S2. Wind roses for the sampling period between January-16, 2016 and March-17, 2017.

S2. X-ray Fluorescence Results

Table S1. Quantitative analysis by XRF for TSP, PM2, and PM$_{2.5}$ at Ilha do Boi (M2) and Enseada do Suá (M1), including mean, standard deviation and detection limits in µg m^{-3}.

Element	TSP - M1		TSP - M2		PM10 - M1		PM10 - M2		PM2.5 - M1		PM2.5 - M2		DL's
	Average	St. Dev.	Average	St. Dev.	Average	St. Dev.	Average	St. Dev.	Average	St. Dev.	Average	St. Dev.	
Concentration in µg m^{-3}													
Cl	5.33	2.50	11.62	7.58	4.45	2.31	7.78	2.94	1.25	0.94	1.85	0.99	0.074
Na	0.99	0.29	2.55	1.12	0.80	0.25	2.10	0.67	0.30	0.07	0.54	0.20	0.013
Fe	2.77	1.58	1.31	0.90	0.95	0.40	0.70	0.43	0.14	0.05	0.25	0.51	0.003
S	1.18	0.24	1.95	0.53	0.92	0.23	1.65	0.40	0.64	0.18	1.05	0.50	0.105

Element	TSP - M1		TSP - M2		PM10 - M1		PM10 - M2		PM2.5 - M1		PM2.5 - M2		DL's
	Average	St. Dev.	Average	St. Dev.	Average	St. Dev.	Average	St. Dev.	Average	St. Dev.	Average	St. Dev.	
	Concentration in µg m^{-3}												
Al	0.29	0.13	0.14	0.08	0.14	0.06	0.10	0.06	0.03	0.01	0.04	0.05	0.01
Si	0.89	0.39	0.42	0.21	0.38	0.19	0.29	0.16	0.06	0.03	0.11	0.17	0.006
K	0.20	0.07	0.26	0.09	0.14	0.06	0.20	0.09	0.09	0.07	0.10	0.11	0.019
Ca	0.73	0.31	0.45	0.23	0.35	0.18	0.32	0.18	0.07	0.10	0.09	0.20	0.01
Mg	0.13	0.03	0.31	0.14	0.09	0.03	0.24	0.08	0.03	0.01	0.08	0.08	0.007
Mn	0.02	0.01	0.01	0.01	0.01	0.00	0.01	0.00	0.00	nd	0.01	0.00	0.003
Ag	0.04	nd	0.05	0.04	0.05	0.04	0.05	0.02	0.03	nd	0.04	0.02	0.011
Au	0.00	nd	0.01	0.00	0.01	0.00	0.01	0.00	0.01	nd	0.01	nd	0.024
Ba	0.08	0.04	0.05	0.02	0.05	0.01	0.04	0.02	0.02	nd	0.02	0.00	0.021
Br	0.01	0.00	0.02	0.01	0.01	0.00	0.01	0.01	0.01	0.00	0.01	0.01	0.037
Cu	0.02	0.01	0.01	0.00	0.02	0.01	0.01	0.00	0.01	0.01	0.01	0.00	0.003
Ce	0.00	nd	0.01	0.01	0.00	nd	0.00	nd	0.01	nd	0.00	0.00	0.003
Cr	0.01	0.01	0.02	0.01	0.01	0.00	0.02	0.01	0.00	nd	0.01	0.01	0.003
Cd	0.00	nd	0.01	0.00	0.00	nd	0.01	0.01	0.00	nd	0.01	0.00	
Cs	0.03	nd	0.05	0.02	0.04	nd	0.02	0.00	0.04	0.00	0.06	0.02	0.037
Ge	0.00	nd	0.00	nd	0.00	0.00	0.00	0.00	0.00	nd	0.00	0.00	0.003
Ga	0.00	nd	0.00	0.00	0.01	0.00	0.01	0.00	0.00	0.00	0.02	0.02	
Hg	0.00	nd	0.01	0.01	0.00	0.00	0.00	0.00	0.00	0.00	0.01	0.00	
Hf	0.00	nd	0.00	nd	0.00	nd	0.00	0.00	0.01	nd	0.02	nd	
I	0.00	0.00	0.01	0.01	0.00	0.00	0.01	0.00	0.00	nd	0.01	nd	0.019
Ir	0.00	nd	0.01	0.01	0.00	nd	0.00	0.00	0.00	nd	0.01	0.01	
La	0.00	nd	0.00	nd	0.00	nd	0.00	0.00	0.02	0.01	0.00	nd	0.013
Lu	0.00	nd	0.01	0.00	0.00	nd	0.01	0.00	0.00	nd	0.00	0.00	
Mo	0.00	nd	0.01	0.00	0.00	0.00	0.01	0.00	0.00	0.00	0.01	0.01	0.003
Ni	0.00	nd	0.01	0.01	0.00	0.00	0.01	0.00	0.00	0.00	0.01	0.00	0.003
Nb	0.00	nd	0.01	0.00	0.00	nd	0.01	0.00	0.01	0.00	0.01	0.00	0.001
P	0.06	0.03	0.13	0.06	0.05	0.02	0.09	0.05	0.03	0.01	0.05	0.04	0.009
Pb	0.00	nd	0.01	nd	0.01	0.00	0.02	0.01	0.02	nd	0.02	0.02	0.01
Pd	0.01	0.01	0.01	0.00	0.01	0.01	0.01	0.00	0.01	0.01	0.01	0.00	0.001
Rb	0.00	nd	0.00	0.00	0.01	nd	0.00	0.00	0.00	nd	0.00	0.00	
Sn	0.07	nd	0.08	0.04	0.04	0.01	0.07	0.02	0.00	nd	0.06	0.01	0.02
Sb	0.08	nd	0.10	0.05	0.04	nd	0.09	0.04	0.05	nd	0.12	0.09	0.097
Sr	0.01	0.00	0.01	0.00	0.01	0.00	0.01	0.00	0.01	0.00	0.01	0.00	0.003
Se	0.00	nd	0.01	0.00	0.00	0.00	0.00	0.00	0.00	0.00	0.01	0.01	0.003
Ti	0.06	0.02	0.02	0.01	0.02	0.01	0.01	0.01	0.01	nd	0.03	0.03	0.004
Th	0.00	nd	0.01	0.00	0.00	nd	0.01	0.00	0.00	nd	0.01	0.00	
Tl	0.00	nd	0.01	0.01	0.00	0.00	0.00	nd	0.00	nd	0.00	0.00	
U	0.00	nd	0.00	0.00	0.00	nd	0.01	0.00	0.00	nd	0.01	0.00	
V	0.01	nd	0.00	0.00	0.01	0.01	0.00	nd	0.01	0.01	0.01	0.00	0.005
W	0.00	nd	0.01	nd	0.00	nd	0.01	0.01	0.00	nd	0.04	0.05	
Y	0.00	nd	0.00	0.00	0.00	0.00	0.00	0.00	0.00	0.00	0.01	0.01	0.008
Zn	0.03	0.02	0.02	0.00	0.02	0.01	0.01	0.00	0.01	0.00	0.01	0.01	0.006
Zr	0.01	0.00	0.01	0.00	0.01	0.00	0.01	0.00	0.00	0.00	0.00	0.00	
EC	2.01	1.78	1.03	0.99	2.14	0.98	1.17	0.68	1.33	0.74	0.83	0.53	0.02
OC	1.68	1.78	1.45	1.28	1.73	1.24	1.31	0.83	1.16	1.10	1.15	1.19	0.02

nd: Element not detected

S3. Resonant Synchrotron X-Ray Diffraction

Figure S3 shows the test conducted at LNLS adjusting the energy at 6.5 and 7.0 keV. Resonant Sr-XRD analysis shows that at 7 keV, energy close to absorption edge of iron (7.112 keV), peaks associated to Fe2O3 show a decrease in intensity (Figure S3a). However, as expected, setting the energy at 6.5 keV, away from the absorption edge of Fe, there is an increasing in the intensity of the peak due to larger scattering (Figure S3b), resulting in better resolution and intensity. This is an unequivocal proof we identify the Fe_2O_3 compound. It is clearly noted the same behavior in Figures S3(c and d). In this case, the compound $BaTiO_3$ show better resolution of the major peaks at 2.81 Å and 2.82 Å when energy was set at 7.0 keV (Figure S3c), energy further away from the absorption K-edge of Ti (4.9664 keV), and the L-edge of Ba (5.2 to 6.0 keV). Indeed, at 6.5 keV, there is only one peak at 2.818 Å, in which can be mistakenly attributed to carbon (PDF – 46-943).
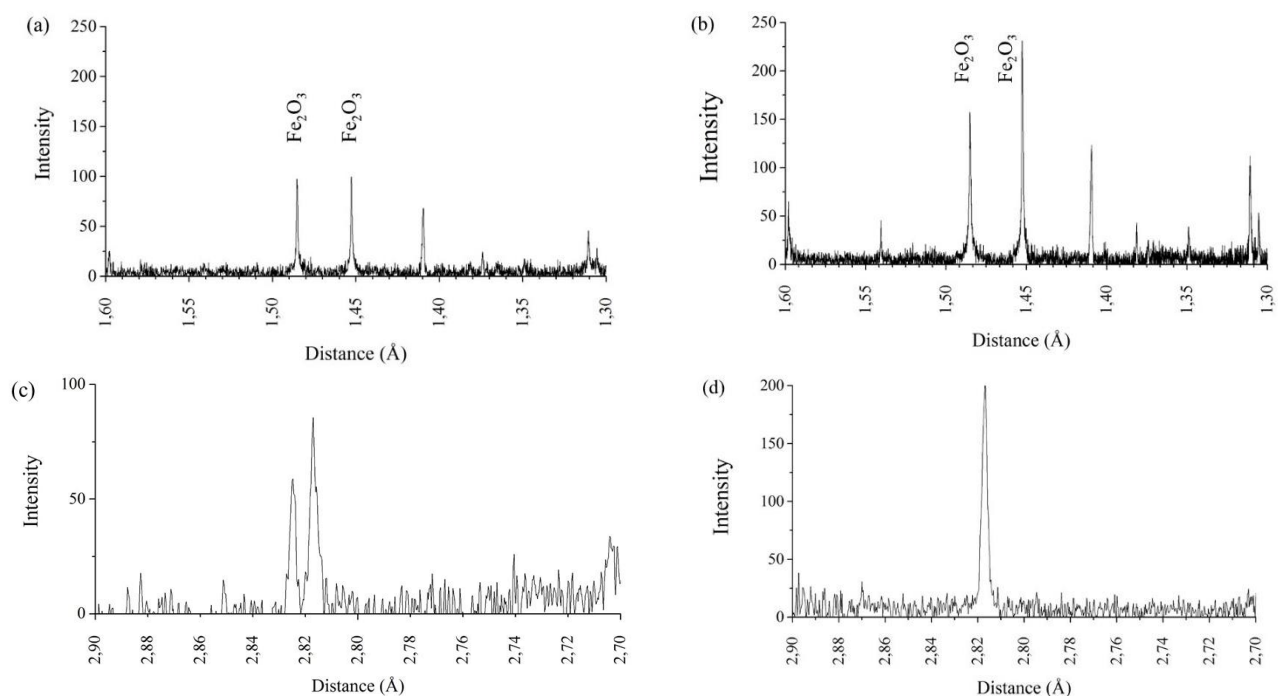
Figure S3. RSr-XRD spectra of: (a) Fe_2O_3 spectra with energy at 7 keV; (b) Fe_2O_3 spectra with energy at 6.5 keV; (c) BaTiO3 spectra with energy at 7 keV; (d) BaTiO3 spectra with energy at 6.5 keV.

S4. PM Mass Concentration

Figure S1 shows the average mass concentration at M1 and M2. At M2 (Figure S1a,b,c), the average mass concentration of TSP, PM_{10} and $PM_{2.5}$ are, respectively, 50.9, 32.8, and 12.2 µg m^{-3}. The average maximum values are always associated to NNE winds with values of 61.5, 39.8, and 13.9 µg m^{-3},

respectively for TSP, PM$_{10}$ and PM$_{2.5}$. From NNE of RGV is located the Tubarão Complex, as shown in Figure 1a (red rings S1 to S7) and in Figure S1b (red dots as point sources), that can be contributing for the increase in PM mass concentrations at M2. At M1 (Figure S1d,e,f). the average mass concentration of TSP, PM$_{10}$ and PM$_{2.5}$ are, respectively, 44.0, 21.5, and 8.9 µg m^{-3}. Opposite to M2, the maximum values at M1 show distinct behavior related to the diameter of the PM. At M1, TSP shows higher average concentration associated to NNE winds with value of 65.5 µg m^{-3}), and NNW winds with value of 61.1 µg m^{-3}. PM$_{10}$ and PM$_{2.5}$ show higher average mass concentration associated to NNW winds with values of 31.6 and 14.9 µg m^{-3}, respectively. From NNW are the main traffic roads in RGV (Figure 1c) with large vehicular flux. Another significant contributor during the sampling period located NNW of M4 was a sanitation and paving working site at Leitão da Silva Avenue. The results indicate that M1 and M2 are distinctly affected by different predominant sources of PM. M2 area is predominantly affected by industrial activities from Tubarão Complex, while M1 area is affected by both industrial and vehicular sources for TSP and PM$_{10}$. Although, PM$_{2.5}$ seems to be more affected by vehicular emissions from NNW.

Ilha do Boi station (M2)
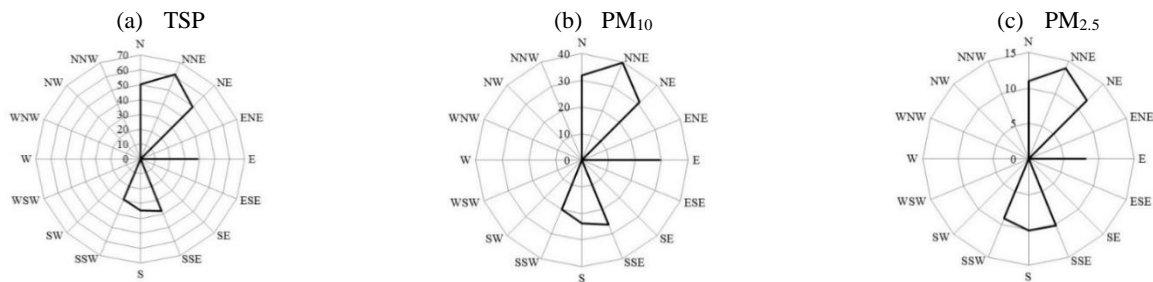
Enseada do Suá station (M1)
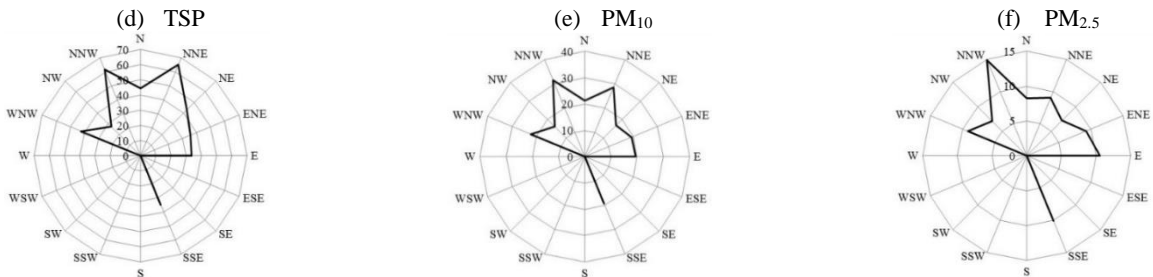
Figure S3. Average concentration by prevailing winds for TSP, PM10 and PM2.5 at Ilha do Boi and Enseada do Suá stations.

Table S2. Specific markers of TSP, PM10 and PM2.5 samples at M1, including their intensities by wind speed.

Crystalline Phase	Sr-XRD Peaks		TSP Intensity (%)				PM10 Intensity (%)				PM2.5 Intensity (%)			
M1 - Enseada do Suá station														
	(Å)	(2θ)	N	ENE	SSE	NW	N	ENE	SSE	NW	N	ENE	SSE	NW
α-Fe$_2$O$_3$	1.48	73.2	30.5	66.1	10.8	21.5	16.9	13.9	4.5	12.1	15.3	13.6	-	-
	1.45	75.1	35.2	26.1	11.4	27.9	16.6	13.8	4.1	12.7	12.5	12.9	-	-
Metallic Fe	1.97	53.4	11.0	12.1	-	6.8	4.4	4.9	-	-	-	-	-	7.9
	1.84	57.5	16.2	18.5	-	12.3	8.0	10.6	-	-	-	-	-	14.6
FeS$_2$	2.45	42.2	9.6	8.6	6.1	-	-	7.2	15.1	5.6	-	7.7	6.1	-
BaTiO$_3$	2.83	36.5	24.1	15.6	21.3	15.8	8.6	13.3	21.9	19.9	-	-	-	-
	2.82	36.6	29.6	32.4	24.1	41.5	37.0	38.0	35.4	36.9	-	-	-	-
EC (Graphite)	3.35	30.6	12.9	12.4	22.3	17.0	-	-	6.3	7.2	-	-	-	-

Table S3. Specific markers of TSP, PM10 and PM2.5 samples at M2, including their intensities by wind speed.

Crystalline Phase	Sr-XRD Peaks		TSP Intensity (%)			PM10 Intensity (%)			PM2.5 Intensity (%)		
M2 - Ilha do Boi station											
	(Å)	(2θ)	N	NE	S	N	NE	S	N	NE	S
α-Fe$_2$O$_3$	1.48	73.2	8.4	11.0	4.3	7.7	4.7	3.7	11.8	8.7	-
	1.45	75.1	6.3	13.4	4.3	5.6	5.0	3.8	12.1	6.7	-
Metallic Fe	1.97	53.4	3.4	3.9	-	3.8	2.9	-	7.6	3.9	-
	1.84	57.5	6.5	4.6	-	4.1	4.1	-	12.1	5.6	-
FeS$_2$	2.45	42.2	3.6	6.6	3.1	3.0	6.6	7.6	13.2	-	-
BaTiO$_3$	2.83	36.5	8.3	9.8	28.7	10.6	24.0	21.5	-	-	-
	2.82	36.6	70.1	31.9	26.9	22.9	54.2	30.6	-	-	-
EC (Graphite)	3.35	30.6	-	-	-	-	-	-	-	-	-

RSr-XRD analysis identified NaCl, iron-based compounds, oxides, silicates, nitrates, chlorides, sulfates, phosphates, organics and carbonaceous compounds. NaCl and iron-based compounds are the most abundant among all crystalline compounds (Figure S4a, b). Among the Fe crystalline phases were found hematite (α-Fe$_2$O$_3$), maghemite (γ-Fe$_2$O$_3$), goethite (FeOOH), magnetite (Fe$_3$O$_4$), CaFe$_2$O$_4$, FeMnO$_3$, metallic iron (Fe°), FeS$_2$, FeSi, FeTi, and K$_2$Fe$_2$O$_4$. Among the iron-based compounds, hematite (α-Fe$_2$O$_3$) was found to have the highest concentration, followed by Fe$_3$O$_4$. BaTiO$_3$ appears consistently in all PM classes indicating a non-directional source. Sulfates, (NH$_4$)$_3$Fe(SO$_4$)$_3$ and FeAl$_2$(SO$_4$)$_4$, phosphates such as NH$_4$Ca$_2$P$_3$O$_{10}$ and a few species of nitrates (KNO$_3$, NH$_4$NO$_3$, and Na$_2$N$_2$O$_2$), and

chlorides as NH_4ClO_4 are also present in PM, and this group comprehends the secondary particles (Figure S4a, b). EC is present in all PM classes, although other carbonaceous species such as $CaCO_3$ was also found. SiO_2, $K_4Ca(SiO_3)_3$, $CaMgSiO_4$, $Fe_2(SiO_4)$, and $Al_2(SiO_4)O$ (Figure S4a, b) were the identified silicates, all associated with crustal sources (Niu et al., 2016; Owoade et al., 2015).
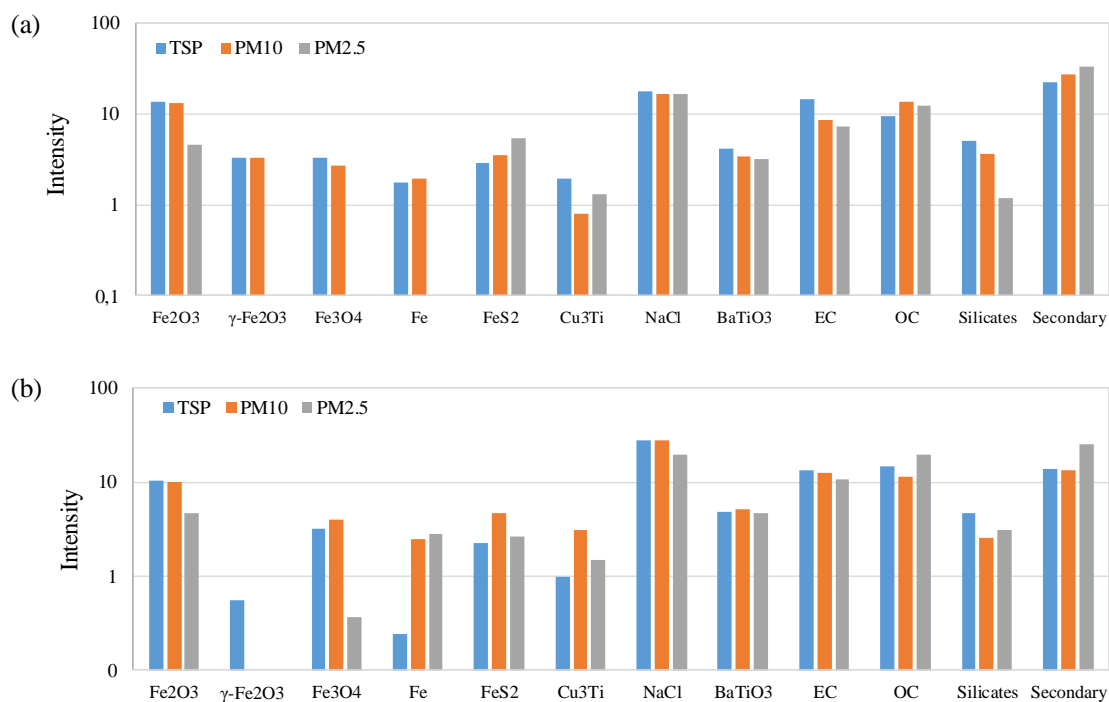
Figure S4. Quantification of crystalline phases at (a) M1 and (b) M2.

S6. Other Fe-rich Markers

Goethite (FEOOH) and magnetite (Fe_3O_4) are iron oxides referred to as constituents of red soils (Fabris et al., 1997). Fe_3O_4 presented concentrations below 2% at both M2 and M1. Despite previous studies reporting the presence of FeOOH in TSP associated to soil and industrial sources in the RGV (de Souza et al., 2002, 2000, 1998), no evidence was found suggesting the presence of FeOOH in PM at both M1 and M2. Powder X-ray diffraction patterns of FeOOH (PDF#29-713) show the most intense peak at 4.1830 Å, which was not found in all PM RSr-XRD spectra (Tables S2 and S3 in Supplementary Material). This might be due to the concentrations been below the detection limit, or the absence of this iron oxide phase in PM. The latter hypothesis is likely since the predominant mineralogical constituents of iron ores are $\alpha\text{-}Fe_2O_3$, martite and kenomagnetite (Rosière and Chemale Jr, 2000).

TSP and PM_{10} RSr-XRD spectra suggest the presence of maghemite ($\gamma\text{-}Fe_2O_3$) with the three major peaks at distance of 2.52 Å, 1.48 Å and 1.61 Å (PDF#24-0081). Either $\gamma\text{-}Fe_2O_3$ and Fe_3O_4 have the same three

major peaks, therefore, the attribution of γ-Fe_2O_3 as a PM component must be treated with caution. In Brazil, γ-Fe_2O_3 is reported to be a constituent of *Itabirito* amphybolytic iron ore, a type of iron ore from *Sistema Sudeste* mines (Rosière and Chemale Jr, 2000). Besides, γ-Fe_2O_3 can be produced during oxidative reactions by the decomposition of both Fe_3O_4 (Jiang et al., 2008), and pyrite (Linak et al., 2007). Such oxidative processes are found in pelletizing, sintering, and coke plants as intermediary phases of steel and pellets production. γ-Fe_2O_3 is also described as a constituent of PM from exhaust pipes (Revuelta et al., 2014), its presence in the RGV was only associated to prevailing winds from NE quadrant (industrial park direction). The absence of γ-Fe_2O_3 in PM associated to NW and S winds is an indicator that vehicular sources are not a representative source of γ-Fe_2O_3 in the RGV since the main traffic roads in the RGV are located in the NW and S quadrant of the sampling sites (Figure 1a, c). The results suggest that all contribution of γ-Fe_2O_3 can be account for the main chimneys of pelletizing, sintering, coke plants, and iron ore stockpiles of the Tubarão Complex.

The oxide $K_2Fe_2O_4$ was identified in all PM classes (TSP, PM_{10} and $PM_{2.5}$). The two major peaks related to $K_2Fe_2O_4$ are 2.81 Å and 1.62 Å. Those two $K_2Fe_2O_4$ major peaks are overlapped by NaCl, which has the most intense peak at 2.81 Å and the third more intense peak at 1.62 Å. The presence of NaCl in large scale in RGV make it impossible to use those peaks as markers of biomass burning. However, in cities far from the contributions of marine source, perhaps its use may be considered. The presence of $K_2Fe_2O_4$ was considered in this work due to the significant concentration of potassium in RGV (see Table 1). Furthermore, the combustion of biomass can lead to reaction between KCl and Fe_2O_3 forming $K_2Fe_2O_4$ and Cl_2 (Cha and Spiegel, 2004), which can also explain the high Cl/Na ratio in RGV. Sintering is another process that can lead to the formation of $K_2Fe_2O_4$, since that process is rich in K and Cl, as reported by Guo et al. (2017).

S7. Non-markers identified crystals

S7.1. Si-Rich Markers

Silicates found by Sr-XRD spectra are composed by SiO_2, $K_4Ca(SiO_3)_3$, $MgSiO_3$, and $Fe_2(SiO_4)$. Among them, $K_4Ca(SiO_3)_3$, $MgSiO_3$ are predominant, indicating that clay minerals (soil) are dominant over quartz (beach sand). Due to many possible combinations among crustal elements and the uncountable variation in stoichiometry, there was not a single peak or group of peaks that could be used as markers for this group of sources.

10.APPENDIX C

Inorganic and Organic Markers for the Apportionment of Highly Correlated Sources of Particulate Matter

S1. Chemical analysis

Table S1. Average concentration ($\mu g\ m^{-3}$) of elemental analysis by X-ray fluorescence of PM_{10} and $PM_{2.5}$ at M1 and M2, including the standard deviation ($\mu g\ m^{-3}$) and the respective limits of detection.

Element	PM10 - M1		PM10 - M2		PM2.5 - M1		PM2.5 - M2		DL's
	Average	St. Dev.	Average	St. Dev.	Average	St. Dev.	Average	St. Dev.	
					$\mu g\ m^{-3}$				
Cl	4.448	2.310	7.784	2.940	1.252	0.935	1.852	0.989	0.074
EC	2.141	0.975	1.174	0.683	1.334	0.739	0.832	0.533	0.120
OC	1.734	1.244	1.311	0.826	1.157	1.097	1.150	1.189	0.095
Na	0.798	0.250	2.105	0.673	0.298	0.071	0.544	0.197	0.013
Fe	0.954	0.402	0.699	0.429	0.145	0.053	0.247	0.514	0.003
S	0.916	0.233	1.651	0.405	0.640	0.184	1.046	0.500	0.105
Al	0.137	0.062	0.103	0.060	0.026	0.011	0.037	0.055	0.010
Si	0.384	0.186	0.287	0.162	0.064	0.028	0.106	0.172	0.006
K	0.138	0.063	0.202	0.089	0.095	0.070	0.101	0.111	0.019
Ca	0.347	0.178	0.317	0.177	0.074	0.103	0.086	0.198	0.010
Mg	0.094	0.029	0.242	0.078	0.030	0.009	0.084	0.082	0.007
Mn	0.012	0.004	0.008	0.003	0.001	0.000	0.005	0.004	0.003
Ag	0.052	0.039	0.046	0.019	0.032	0.017	0.036	0.019	0.011
Ba	0.050	0.011	0.044	0.017	0.019	0.029	0.018	0.001	0.021
Br	0.006	0.002	0.013	0.007	0.005	0.003	0.008	0.008	0.037
Cu	0.016	0.007	0.007	0.005	0.013	0.008	0.006	0.004	0.003
Ce	0.000	0.000	0.005	0.008	0.006	0.014	0.003	0.001	0.003
Cr	0.014	0.004	0.018	0.008	0.001	0.003	0.011	0.012	0.003
Cs	0.045	0.023	0.021	0.005	0.042	0.005	0.063	0.020	0.037
I	0.005	0.000	0.013	0.004	0.005	0.002	0.006	0.002	0.019
Ir	0.000	0.000	0.004	0.002	0.003	0.009	0.008	0.010	
La	0.000	0.000	0.005	0.001	0.018	0.005	0.000	0.000	0.013
Ni	0.003	0.000	0.005	0.000	0.004	0.002	0.007	0.004	0.003
P	0.049	0.017	0.092	0.052	0.027	0.011	0.053	0.039	0.009
Pd	0.012	0.006	0.008	0.003	0.012	0.010	0.011	0.003	0.001
Sn	0.044	0.015	0.067	0.019	0.000	0.000	0.061	0.010	0.020
Sb	0.041	0.011	0.093	0.044	0.048	0.017	0.120	0.091	0.097
Sr	0.006	0.004	0.009	0.003	0.006	0.002	0.006	0.004	0.003
Ti	0.024	0.009	0.014	0.008	0.009	0.005	0.027	0.030	0.004
V	0.010	0.008	0.000	0.000	0.006	0.008	0.006	0.004	0.005
Zn	0.017	0.008	0.009	0.004	0.009	0.004	0.010	0.009	0.006

Table S2. Average concentration (pg m^{-3}) of PAHs by GC-MS of PM$_{2.5}$ and PM$_{10}$ at M1 and M2.

	M1		M2	
	PM$_{2.5}$	PM$_{2.5-10}$	PM$_{2.5}$	PM$_{2.5-10}$
Nap	35.48	5.31	34.61	1.32
Acy	77.41	1.19	91.37	2.71
Ace	6.59	2.22	57.72	20.80
Flu	23.53	4.36	175.14	1.31
Phe	20.55	3.06	146.60	2.49
Ant	2.66	1.22	189.30	4.11
Flt	22.47	5.38	41.52	2.41
Pyr	4.93	1.45	2.96	0.56
BaA	0.61	0.15	6.29	0.35
Chr	1.23	0.35	32.23	1.91
BbF	1.82	5.42	22.64	2.33
BkF	0.87	0.17	1.72	0.88
BaP	1.61	0.54	2.81	<LQ
DahA	<LQ	<LQ	<LQ	<LQ
IcdP	<LQ	<LQ	<LQ	<LQ
BghiP	<LQ	<LQ	30.57	<LQ
Total	199.76	30.81	835.49	41.17
% Total PAHs	86.6	13.4	95.3	4.7

LQ: Limit of Quantification

S2. Pollutant Roses

S2.1. EC and OC Pollutant Roses

In fact, higher contribution of EC is associated to NE quadrant winds at M2 (Figures S2b and S2d), where a coke plant is found. Figures S2a and S2c show high contribution of EC associated to NNE winds, although, EC associated to NW quadrant and South-southeast (SSE) winds are slightly larger. The results infer that the likely sources of EC at M2 is a coke plant located NE of RGV, while M1 receive similar contributions of EC from industrial and vehicular/resuspension sources.

In Figure S2, higher OC concentrations in PM$_{10}$ and PM$_{2.5}$ at M1, ranges from 2 µg m^{-3} to 4.5 µg m^{-3}, always associated to NW quadrant winds. This finding suggests vehicles as the predominant source of OC at M1 for both PM$_{10}$ and PM$_{2.5}$, which is in agreement with the literature (Cheng et al., 2015; Kim and Hopke, 2008; Owoade et al., 2016; Thorpe and Harrison, 2008). The exception is at M2, in which OC in PM$_{10}$ and PM$_{2.5}$ show similar concentrations associate to winds from NE and S quadrant (1.1 µg m^{-3} to 1.6 µg m^{-3}), and lower concentrations associated to winds from NW quadrant. This suggests that M2 is affected by OC emissions from S quadrant of RGV, and by emissions from NE quadrant of RGV. South of M2 is Vila Velha, a city with a fleet of 200 thousand vehicles, which is the likely source of OC from S of M2. OC is also reported in the literature as marker of coal burning and sintering (Y. Guo et al.,

2017; Vossler et al., 2016). Northeast of M2 is located steel industry with units of coke and sinter production, in which is the likely source contributing for the OC at M2.
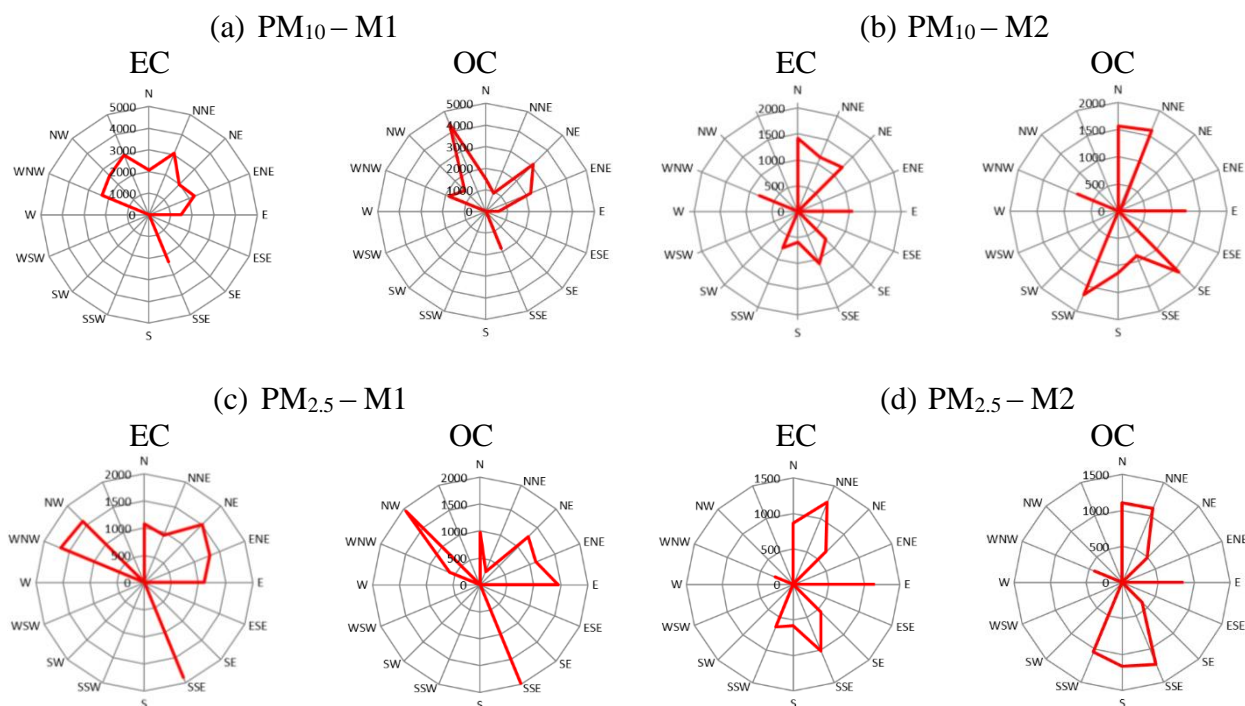
Figure S2. Pollutant roses of EC and OC in ng m^{-3}: (a) PM$_{10}$ at M1; (b) PM$_{10}$ at M2; (c) PM$_{2.5}$ at M1; and (d) PM$_{2.5}$ at M2.

S2.2   Fe Pollutant Roses

Figure S3 shows that Fe in both PM$_{10}$ and PM$_{2.5}$ is predominantly associated to winds from NE quadrant at both M1 and M2. At M1, PM$_{10}$ show higher Fe concentration (about 1.1 µg m^{-3}) associated to N-NNE and E winds (Figure S2a), while at M2, higher Fe concentration is associated to N-NNE-NE winds (Figure S3b). Lower Fe concentrations in PM$_{10}$ are associated to West-Northwest (WNW) and South-southeast (SSE) winds. PM$_{2.5}$ and PM$_{10}$ shows similar behavior regarding the directionality of the Fe, although, at M2, Fe concentrations associated to winds from NE quadrant are doubled compared to M1. Fe is reported in the literature as marker for different sources, such as crustal (Harrison and Smith, 1992; Tecer et al., 2012; J. Wang et al., 2016), industrial, including sintering, pelletizing and steelmaking (Y. Guo et al., 2017; Owoade et al., 2016, 2015), sea port (Choi et al., 2013), and vehicular - exhaust and break abrasion (Karnae and John, 2011; Thorpe and Harrison, 2008; Viana et al., 2008a) (See Table S1).

PM$_{10}$ PM$_{2.5}$

(a) Fe – M1   (b) Fe – M2   (c) Fe – M1   (d) Fe – M2
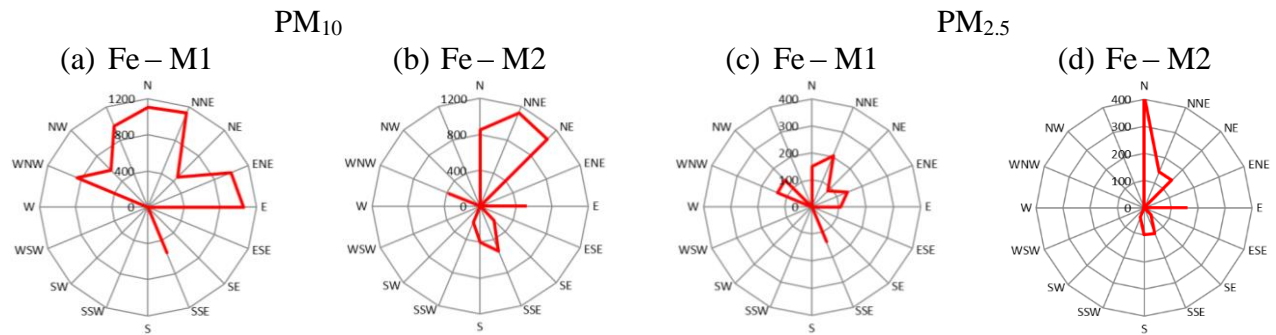
Figure S3. Pollutant roses of iron (Fe) in ng m^{-3}: (a) PM$_{10}$ at M1; (b) PM$_{10}$ at M2; (c) PM$_{2.5}$ at M1; and (d) PM$_{2.5}$ at M2.

Due to generalized presence of Fe as constituent of several process and sources, attributing Fe based only in the literature without a previous study of the directionality can lead to wrong interpretation of the predominant source in the region. The results suggest large contribution of Fe from sources N-NE of M1 and M2. The pelletizing and steel industries are located N-NE of the sampling sites, these industries handle large daily amounts of iron ore, pellets, sinter, pig iron, and steel. Therefore, those activities are likely to be the predominant source of Fe at both M1 and M2.

The pollutant roses show that despite the fact that M1 and M2 are closely located (less than 1.5 km) (Figure 1a), the sources affecting each location are well distinct. While M1 is predominantly affected by both industrial and vehicular/resuspension sources, M2 is predominantly affected by emissions only from the industries.

S3. PMF Factors - PM10 at M1
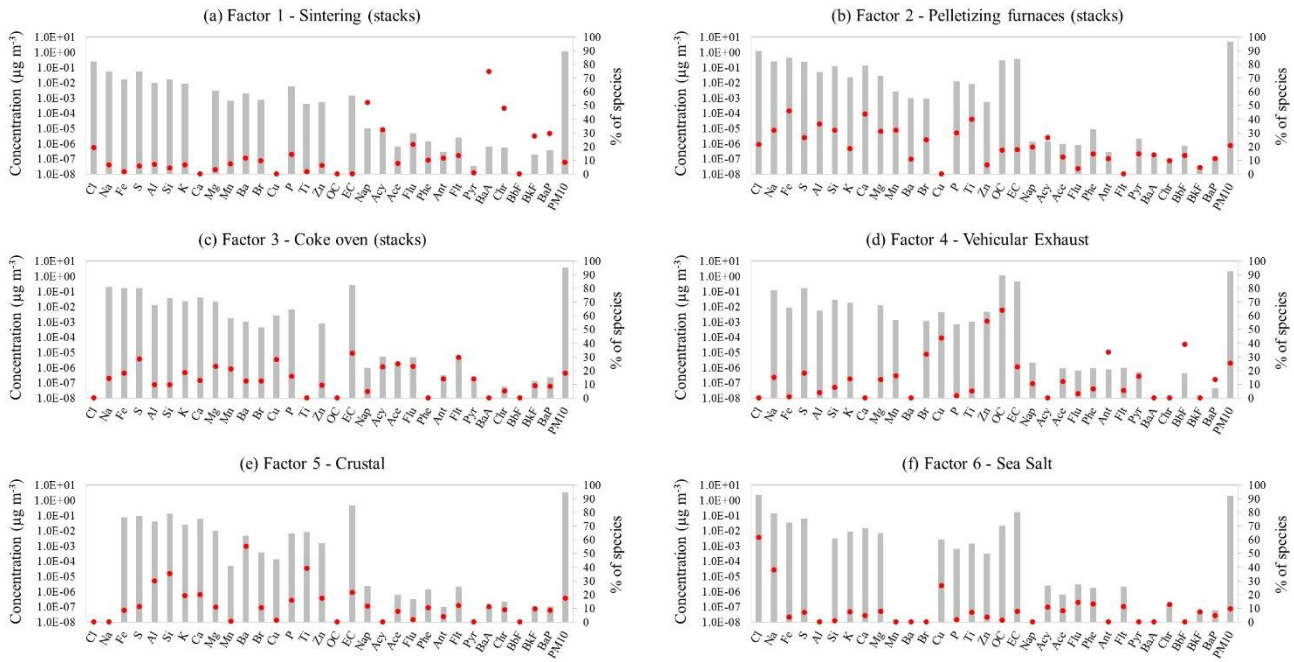
Figure S4. Source apportionment of PM_{10} at M1 by PMF.
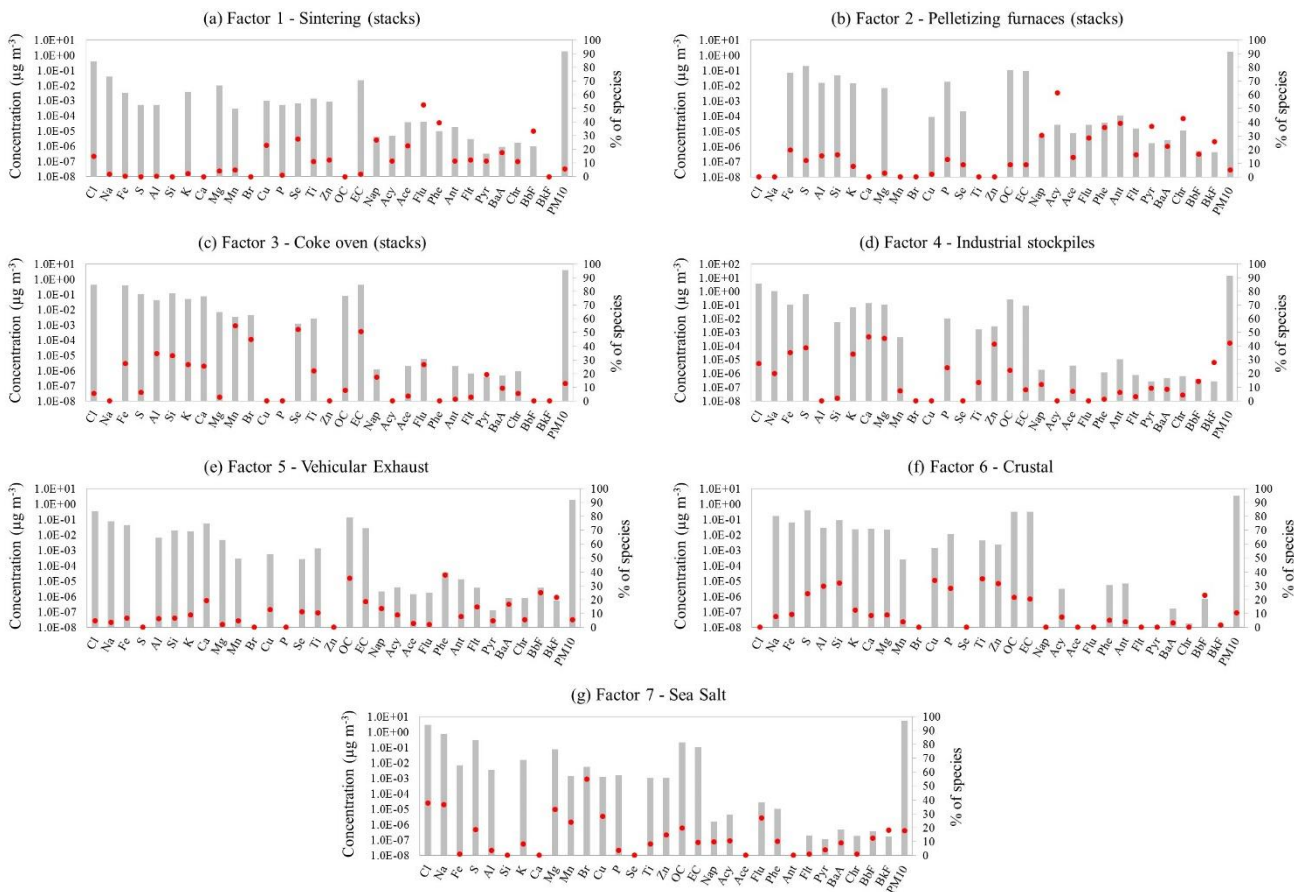
Figure S5. Source apportionment of PM_{10} at M2 by PMF.

S4. Literature review of chemical markers for Receptor Models

Table S3. List of more recent articles on source apportionment using PMF as a receptor model. including the main chemical species used in factors interpretation.

Sources	Na	Ca	Al	Si	Mg	Mn	K	Cl	P	Ba	Br	Fe	S	Cu	Sn	Zn	Ti	As	Se	Mo	Cd	Pb	Ni	Sb	Sr	Cr	V	Ce	NO3	SO4	NH4	EC	OC	Location	PM Classes	References
Crustal (fugitive dust/Soil/Road traffic)			■	■	■																													China	PM$_{2.5}$	Zou et al., 2017
		■		■													■																	Czech Rep.	PM$_{2.5}$	Vossler et al., 2016
		■	■									■																■						China	TSP	Wang et al., 2016
					■																													China	PM$_{2.5}$	Niu et al., 2016
	■	■	■	■								■					■																	Nigeria	PM$_{10-2.5}$|PM$_{2.5}$	Owoade et al., 2016
		■	■	■																														USA	PM$_{2.5}$	Kotchenruther 2016
		■	■		■																													Hong Kong	PM$_{10-2.5}$|PM$_{2.5}$	Cheng et al., 2015
		■	■	■								■		■																				Turkey	PM$_{10-2.5}$|PM$_{2.5}$	Tecer et al., 2012
		■	■														■																	Texas	PM$_{2.5}$	Karnae 2011
		■	■																															U.K.	PM	Harrison e Smith, 1992
		■	■		■																													Review	Review	Viana et al., 2008
		■														■																		Croatia	PM$_{2.5}$	Ivosevic et al., 2015
Sea/Mixed Salt	■			■																														China	TSP	Wang et al., 2016
	■	■	■																															USA	PM$_{2.5}$	Kotchenruther 2016
								■								■																		Nigeria	PM$_{10-2.5}$|PM$_{2.5}$	Owoade et al., 2016
	■									■			■													■								Texas	PM$_{2.5}$	Karnae 2011
	■							■																										Review	Review	Viana et al., 2008
Secondary Aerosol																													■	■	■		■	China	PM$_{2.5}$	Zou et al., 2017
																													■	■	■			USA	PM$_{2.5}$	Kotchenruther 2016
																													■	■				China	TSP	Wang et al., 2016
																													■	■	■			Hong Kong	PM$_{10-2.5}$|PM$_{2.5}$	Cheng et al., 2015
SOA																													■	■	■			Texas	PM$_{2.5}$	Karnae 2011
Coal Burning								■																									■	China	PM$_{2.5}$	Zou et al., 2017
														■				■			■													China	TSP	Wang et al., 2016
							■							■		■		■							■									China	PM$_{2.5}$	Niu et al., 2016
	■												■					■				■						■						Czech Rep.	PM$_{2.5}$	Vossler et al., 2016
						■	■					■		■		■		■			■	■	■		■									Nigeria	PM$_{2.5}$	Owoade et al., 2015
																		■																Turkey	PM$_{10-2.5}$|PM$_{2.5}$	Tecer et al., 2012
																												■						Review	Review	Viana et al., 2008
Biomass Combustion							■									■					■												■	China	PM$_{2.5}$	Zou et al., 2017
				■																													■	USA	PM$_{2.5}$	Kotchenruther 2016
							■																											Czech Rep.	PM$_{2.5}$	Vossler et al., 2016
										■		■				■											■						■	Nigeria	PM$_{10-2.5}$|PM$_{2.5}$	Owoade et al., 2016
																																		Hong Kong	PM$_{10-2.5}$|PM$_{2.5}$	Cheng et al., 2015
	■						■	■																					■			■		Korea	PM$_{2.5}$	Choi et al., 2013
							■																											Turkey	PM$_{10-2.5}$|PM$_{2.5}$	Tecer et al., 2012
																																■		Texas	PM$_{2.5}$	Karnae 2011
																																		China	PM$_{2.5}$	Zou et al., 2017

Sources	Na	Ca	Al	Si	Mg	Mn	K	Cl	P	Ba	Br	Fe	S	Cu	Sn	Zn	Ti	As	Se	Mo	Cd	Pb	Ni	Sb	Sr	Cr	V	Ce	NO3	SO4	NH4	EC	OC	Location	PM Classes	References
Fuel oil combustion (ship/marine vessels)																							X				X							China	TSP	Wang et al., 2016
																							X				X							USA	PM2.5	Kotchenruther 2016
																							X				X							Hong Kong	PM10-2.5|PM2.5	Cheng et al., 2015
																							X				X							Korea	PM2.5	Choi et al., 2013
																							X				X							Texas	PM2.5	Karnae 2011
																											X							U.K.	PM	Harrison e Smith, 1992
Industrial (generalized)		X																										X						China	PM2.5	Zou et al., 2017
						X																X												Nigeria	PM10-2.5|PM2.5	Owoade et al., 2016
						X								X								X												Czech Rep.	PM2.5	Vossler et al., 2016
						X																												USA	PM2.5	Kotchenruther 2016
																				X														China	TSP	Wang et al., 2016
Pigment production																				X	X													China	TSP	Wang et al., 2016
Non-ferrous metal																X																		China	TSP	Wang et al., 2016
						X										X																		Nigeria	PM2.5	Owoade et al., 2015
																		X				X												Hong Kong	PM2.5	Ho et al., 2006
Metal extraction																																		U.K.	PM	Harrison e Smith, 1992
Sintering		X					X	X				X														X	X							China	TSP	Guo et al., 2017
																																		Czech Rep.	PM2.5	Vossler et al., 2016
Pelletizing			X	X								X														X	X							China	TSP	Guo et al., 2017
Iron steelmaking		X		X																						X								China	TSP	Guo et al., 2017
						X										X						X		X										Nigeria	PM10-2.5|PM2.5	Owoade et al., 2016, 2015
Smelting furnace														X																				China	TSP	Wang et al., 2016
Scrap					X							X										X						X						Nigeria	PM10-2.5|PM2.5	Owoade et al., 2016, 2015
Ceramic				X																														Brazil	SPM	Santos et al., 2017
Construction																			X			X												Algeria	TSP	Bouhila et al., 2015
		X			X																													Argentina	PM2.5	Achad et al., 2014
Cement																											X							USA	PM2.5	Kotchenruther 2016
Sea Port	X											X														X								Korea	PM2.5	Choi et al., 2013
Vehicular (generalized)														X												X						X	X	China	PM2.5	Zou et al., 2017
														X		X																		China	TSP	Wang et al., 2016
														X															X	X				USA	PM2.5	Kotchenruther 2016
		X																												X				Korea	PM2.5	Choi et al., 2013
														X							X													Review	Review	Duan et al., 2013
																X																		Turkey	PM10-2.5|PM2.5	Tecer et al., 2012
																																	X	Texas	PM2.5	Karnae 2011
		X	X	X						X											X												X	Review	Review	Viana et al., 2008
										X											X					X								Hong Kong	PM2.5	Ho et al., 2006
											X																							U.K.	PM	Harrison e Smith, 1992
										X		X														X								Argentina	PM2.5	Achad et al., 2014
Fuel additives						X																												Review	Review	Duan et al., 2013
Lubrificating oil		X																																Korea	PM2.5	Choi et al., 2013
		X														X																		India	PM10|PM2.5	Srimuruganandam e Nagendra 2012
		X		X	X				X							X							X	X			X							Croatia	PM2.5	Ivosevic et al., 2015

Sources	Na	Ca	Al	Si	Mg	Mn	K	Cl	P	Ba	Br	Fe	S	Cu	Sn	Zn	Ti	As	Se	Mo	Cd	Pb	Ni	Sb	Sr	Cr	V	Ce	NO3	SO4	NH4	EC	OC	Location	PM Classes	References
Diesel exhausts																■					■													Review	Review	Duan et al., 2013
	■	■			■				■	■		■		■		■							■	■								■		Hong Kong	PM$_{10-2.5}$|PM$_{2.5}$	Cheng et al., 2015
																																■		Nigeria	PM$_{10-2.5}$|PM$_{2.5}$	Owoade et al., 2016
	■	■	■			■				■		■				■																				Srimuruganandam e Nagendra 2012
Rubber																■						■										■	■	Nigeria	PM$_{10-2.5}$|PM$_{2.5}$	Owoade et al., 2016
Brakes												■		■		■						■												Nigeria	PM$_{10-2.5}$|PM$_{2.5}$	Owoade et al., 2016
														■							■	■												Review	Review	Duan et al., 2013
										■		■		■								■		■										Review	Review	Thorpe e Harrison, 2008
Tire wear										■			■			■																		Nigeria	PM$_{10-2.5}$|PM$_{2.5}$	Owoade et al., 2016
																■																		Hong Kong	PM$_{2.5}$	Ho et al., 2006
														■		■					■	■												Review	Review	Duan et al., 2013
										■				■		■																■	■	Review	Review	Viana et al., 2008
																■																		Review	Review	Thorpe e Harrison, 2008